University of Alberta

# ADHESION, INSTABILITY AND PARAMETRIC

# RESONANCE OF MICROBEAM ARRAYS

By

**Jian Zhu** (C)

A thesis submitted to the Faculty of Graduate Studies and Research in partial fulfillment

of the requirements for the degree of

Doctor of Philosophy

Department of Mechanical Engineering

Edmonton, Alberta

Spring 2008

Library and
Archives Canada

Published Heritage
Branch

395 Wellington Street
Ottawa ON K1A 0N4
Canada

Bibliothèque et
Archives Canada

Direction du
Patrimoine de l'édition

395, rue Wellington
Ottawa ON K1A 0N4
Canada

# Canada

University of Alberta

Library Release Form

Name of Author: **Jian Zhu**

Title of Thesis: **Adhesion, Instability and Parametric Resonance of Microbeam Arrays**

Degree: **Doctor of Philosophy**

Year this Degree Granted: **2008**

Permission is hereby granted to the University of Alberta Library to reproduce single copies of this thesis and to lend or sell such copies for private, scholarly or scientific research purposes only.

The author reserves all other publication and other rights in association with the copyright in the thesis, and except as herein before provided, neither the thesis nor any substantial portion thereof may be printed or otherwise reproduced in any material form whatsoever without the author's prior written permission.

Jian Zhu

Date: Dec 17 2007

# Abstract

Microbeam arrays, especially comb drive structures of two opposing arrays of microcantilevers, are commonly employed in many designs of MEMS. This thesis studies some unexplored problems on adhesion, structural instability, and parametric resonance of mutually attracting microbeam arrays.

First, we study surface energy-driven adhesion of two opposing microcantilevers in comb drive structures. For the first time in the literature, our results show that the critical values of surface energy for initial adhesion and full adhesion increase monotonically with increasing overlap length. Therefore, the strength against adhesion can be enhanced by increasing (rather than decreasing) the overlap length. These new results could have significant consequences to MEMS designs in avoiding adhesion failure.

Next, we analyze structural instability of a parallel array of identical microbeams and comb drive microcantilevers. With a simplified spring model, it is verified that equilibrium deflections of intermediate beams would be negligibly small, while the end beams have an important end-effect on instability of the parallel arrays. Based on this concept, some novel methods are proposed to analyze instability of the parallel arrays, in order to obtain the critical value for instability. These methods are justified by good agreement between our results and the exact analysis given for the simplified spring model and some known data in the literature. These results provide simple design criteria for pull-in instability of the parallel array of identical microbeams or comb drive

microcantilevers. To the best of our knowledge, no such simple criteria have been available in the literature.

Finally, we investigate parametric resonance of comb drive microbeam arrays under periodically varying beam-beam interaction. It is found that high-order subharmonic parametric resonance exists due to nonlinear coupling between adjacent oscillators. This remarkable new phenomenon does not appear in the linearly coupled micromechanical oscillators studied in previous related works. Furthermore, the effects of the dc and ac voltages, the nonlinear elasticity coefficient, and the linear damping coefficient, on high-order subharmonics are investigated in this thesis. It is believed that these results offer new and useful insights into the ongoing research on nonlinear dynamics of coupled microbeams or nanobeams in MEMS or NEMS.

This Dissertation is dedicated to
my parents and to my wife.

# Acknowledgements

I would like to extend my deepest gratitude and appreciation to Drs Chongqing Ru and Andrew Mioduchowski for their invaluable guidance, support and encouragement throughout my graduate years.

I am also grateful to my parents and my wife for their patience, love and support throughout my studies.

Jian Zhu

Edmonton, Alberta

October 2007

# Table of Contents

# 4 Instability of mutually attracting comb drive microcantilevers...77

# List of Tables

# List of Figures

# List of Symbols

Chapter 2 (Adhesion of two opposing microcantilevers):

$E$: Young's modulus of the microbeam

$I$: Moment of inertia of the cross section of the microbeam

$L$: Length of the microbeam

$E_1$: Young's modulus of the microbeam on the upper side in the comb drive structure

$I_1$: Moment of inertia of the cross section of the microbeam on the upper side in the comb drive structure

$L_1$: Length of the microbeam on the upper side in the comb drive structure

$E_2$: Young's modulus of the microbeam on the lower side in the comb drive structure

$I_2$: Moment of inertia of the cross section of the microbeam on the lower side in the comb drive structure

$L_2$: Length of the microbeam on the lower side in the comb drive structure

$d$: Gap between two adjacent microbeams

$\delta$: Overlap length between two adjacent microbeams

$\gamma$: Increase in surface energy per unit area due to separation of two surfaces

$U$: Total elastic strain energies of two opposing microcantilevers

$U_1$: Elastic strain energy of the first microcantilever

$U_2$: Elastic strain energy of the second microcantilever

$V$: Total energy of the system consisting of surface energy and elastic strain energy

$w$: Width of the interacting area of the two microbeams

$t$: Attached length of the two microbeams

$x_1$: $x$ coordinate axis for the first microbeam

$y_1$: $y$ coordinate axis for the first microbeam

$x_2$: $x$ coordinate axis for the second microbeam

$y_2$: $y$ coordinate axis for the second microbeam

$s_1$: $x$ coordinate of the adhesion point in the first microbeam

$h_1$: $y$ coordinate of the adhesion point in the first microbeam

$\theta_1$: Slope of the adhesion point in the first microbeam

$s_2$: $x$ coordinate of the adhesion point in the second microbeam

$h_2$: $y$ coordinate of the adhesion point in the second microbeam

$\theta_2$: Slope of the adhesion point in the second microbeam

$\theta$: Slope of the adhesion part between two opposing microcantilevers

$\Delta_1$: Shortenings of the first microbeam in the longitudinal direction due to transverse bending

$\Delta_2$: Shortenings of the second microbeam in the longitudinal direction due to transverse bending

$e$: Critical value of the surface energy for adhesion

$e_1$: Critical value of the surface energy for initial adhesion

$e_2$: Critical value of the surface energy for full adhesion

Chapters 3-5 (structural instability of microbeam arrays):

$F$: Attractive force per unit area between two parallel flat surfaces at any point

$c$: Constant depending on the nature of the interacting force and the materials

$d$: Distance between the two flat surfaces at that point

$n$: Power index for surface attractive forces

$b$: Width of the interacting area of the two microbeams

$C$: Constant defined *as C=cb*

$N$: Total number of the microbeams in the parallel array

$x$: $x$ coordinate axis for the microbeam

$y$: $y$ coordinate axis for the microbeam

$x_1$: $x$ coordinate axis for the microbeam on the upper side in the comb drive structure

$y_1$: $y$ coordinate axis for the microbeam on the upper side in the comb drive structure

$x_2$: $x$ coordinate axis for the microbeam on the lower side in the comb drive structure

$y_2$: $y$ coordinate axis for the microbeam on the lower side in the comb drive structure

$E$: Young's modulus of the microbeam

$I$: Moment of inertia of the cross section of the microbeam

$L$: Length of the microbeam

$E_1$: Young's modulus of the microbeam on the upper side in the comb drive structure

$I_1$: Moment of inertia of the cross section of the microbeam on the upper side in the comb drive structure

$L_1$: Length of the microbeam on the upper side in the comb drive structure

$E_2$: Young's modulus of the microbeam on the lower side in the comb drive structure

$I_2$: Moment of inertia of the cross section of the microbeam on the lower side in the comb drive structure

$L_2$: Length of the microbeam on the lower side in the comb drive structure

$d_0$: Initial separation between the surfaces of two adjacent microbeams.

$\delta$: Overlap length between two adjacent microcantilevers in the comb drive structure

$Y_k$: Equilibrium deflection of microbeam (spring) $k$

$P_k$: Pressure applied on microbeam (spring) $k$

$y_k$: Infinitesimal deviation from the equilibrium deflection $Y_k(x)$

$p_k$: Additional pressure acted on microbeam $k$ due to the deviation deflections

$A_{k,k+1}$: Interaction coefficient between microbeams $k$ and $(k+1)$

$q$: Spring constant

$q_1$: Spring constant of the springs with $k$ as an odd number

$q_2$: Spring constant of the springs with $k$ as an even number

$\beta$: Ratio of spring constants ($\beta = q_1 / q_2$)

$f$: Attractive force applied on adjacent springs

$M$: Constant depending on the nature of the attractive force

$B$: Loading parameter defined based on the initial distance $d_0$ ($B = \dfrac{M}{qd_0^{n+1}}$)

$A_0$: Constant interaction coefficient defined based on the initial separation $d_0$

$$(A_0 = \frac{nC}{d_0^{n+1}})$$

$A_1$: Critical value of the interaction coefficient for instability of a microbeam attracted by a rigid substrate

$A_2$: Critical value of the interaction coefficient for instability of two microbeams

$A_\infty$: Critical value of the interaction coefficient for instability of a large microbeam array

$\alpha$ : Amplified factor

$\varepsilon$ : End-effect factor

$N^*$ : Number of the microbeams (springs) in the small array for instability analysis, where

the $N^*$-th microbeam (spring) is assumed to be fixed


## Chapters 6-7 (Parametric resonance of nonlinearly coupled oscillators):

$N$: Number of the flexible oscillators in the oscillator array

$X_k$ : Displacement of the $k$-th oscillator

$d_0$ : Initial distance between adjacent oscillators

$x_k$ : Dimensionless displacement of the $k$-th spring ( $x_k = \dfrac{X_k}{d_0}$ )

$f$: Attractive force applied on adjacent oscillators

$M$: Amplitude of the attractive force

$d$: Distance between two adjacent oscillators

$n$: Power index for attractive forces

$m$: Mass of the oscillators

$q$: Spring constant of the oscillators

$t$: Time

$\omega_0$ : Frequency of a single isolated oscillator ( $\omega_0 = \sqrt{\dfrac{q}{m}}$ )

$\tau$ : Scaled time ( $\tau = \omega_0 t$ )

$\omega_i$ : Natural frequencies of the oscillator system ($i$=1,2,..., $N$)

$j$: Positive integer

$c$: Linear viscous coefficient

$b$: Cubic nonlinear elasticity coefficient

$V$: Voltage applied

$V_{dc}$ : Dc voltage

$\varepsilon_0$ : Permittivity of the medium between adjacent microbeams

$S$: Area exposed to the electrostatic field

$Q$: Loading parameter ( $Q = \dfrac{\varepsilon_0 S V_{dc}^2}{2 d_0^3 q}$ )

$V_{ac}$ : Ac voltage

$\Omega$ : Frequency of ac voltage

$\omega$ : Frequency of parametric resonance

$\lambda$ : Ratio of the frequency of the ac voltage to the frequency of the parametric resonance

( $\lambda = \Omega / \omega$ )

$A_m$ : Amplitude of the oscillation

$\psi$ : Phase of the oscillation

$\theta$ : Parameter defined as $\theta = (\omega t - \psi)$

$A_{m1}$ : Amplitude of the first oscillation

$A_{m2}$ : Amplitude of the second oscillation

$A_{m3}$ : Amplitude of the third oscillation

$a_{lowest}$ : Smallest amplitude in the solution curve

$F_{electric}$ : Electrostatic force applied on the oscillator

$F_{elastic}$ : Elastic force acting on the oscillator

$\varepsilon$ : Infinitesimal disturbance of the amplitude

$\eta$ : Infinitesimal disturbance of the phase

# Chapter 1

# Introduction

## 1.1 MEMS (Micro-Electro-Mechanical Systems)

Due to growing commercial applications, MEMS have been studied with increasing interest by the researchers in the fields of physics [1-4], chemistry [5-8], mechanics [9-10], and biology [11-12], etc. The development and deployment of MEMS are thought to be critical to the economy and society, as micro engineering and science will lead to major breakthroughs in information technology, computers, medicine, health, manufacturing, transportation, energy, avionics, security, and so on [13-16].

## 1.1.1 Definition, fabrication, and materials

"Microelectromechanical systems (MEMS)" takes a position: "micro" establishes a dimensional scale, "electro" suggests either electricity or electronics (or both), and "mechanical" suggests moving parts of some kind [17-18]. In general, MEMS are defined as the batch-fabricated integrated microscale systems (motion, electromagnetic, radiating energy and optical microdevices/microstructures - driving/sensing circuitry - controlling/processing ICs) that:

1) Convert physical stimuli, events, and parameters to electrical, mechanical, and optical signals and vice versa;

2) Perform actuation, sensing, and other functions;

3) Comprise control (intelligence, decision-making, evolutionary learning, adaptation, self-organization, etc.), diagnostics, signal processing, and data acquisition features;

1

and microscale features of electromechanical, electronic, optical, and biological components (structures, devices, and subsystems), architectures, and operating principle are basics of the MEMS operation, design, analysis, and fabrications [19-20].

MEMS represent the marriage of semiconductor processing to mechanical engineering – at a very small scale [21], and may be fabricated by techniques used for integrated circuit manufacturing [22-25]. It is expected that these techniques will allow miniaturization and mass production of electro-mechanical components in a fashion similar to what has been done with integrated circuits. Most MEMS devices and systems involve fabrication of micromachining [26-29]. The batch fabrication that is characteristic of the microelectronics industry offers the potential for great cost reduction when manufacturing in high volume.

The most common materials for MEMS are inorganic, such as silicon [30-31], silicon dioxide [32-33], silicon nitride [34-35], aluminum [36], and tungsten [37], although certain polymers [38-39] are used as well. Microfabrication that extends beyond conventional microelectronics opens up a much broader range of materials, which offers many choices for design of microsystems [17].

## 1.1.2 Applications

MEMS are being devised and used in a variety of applications, such as electronics [40-43], medicine [44], metrology [45] and so on. An important, commercially successful MEMS device in widespread use today is the automotive airbag sensor [46-47], which measures rapid deceleration of a car and triggers the explosive filling of an airbag. Prior to the use of a MEMS device in this application, airbags were typically triggered by an electromechanical device with a size of a can of soda, weight of several pounds, and cost of about $15. Now the same function is accomplished with this MEMS device that costs just a few dollars and with the size of a small cube of sugar. The smaller size of the MEMS device allows it to respond more quickly to rapid deceleration. As a consequence,

it is now practical to have airbags in car doors to protect occupants against side impacts. MEMS airbag sensors have an additional important advantage over their macromechanical predecessors - integrated electronics that allows for self-testing. The test is initiated whenever a driver turns on the ignition, and its successful conclusion is indicated by an illuminated dashboard light. Other applications for MEMS in daily use include arrays of micromechanical mirrors for projection displays [48], ink-jet printers using control of fluid jets [49], and micro-microphones for hand-held phones [50]. In the future, more and more MEMS will be widely used in heath and medicine [19]. Among possible applications are drug synthesis, drug delivery, nanosurgery, nanotherapy, genome synthesis, diagnostics, novel actuators and sensors, disease diagnosis and prevention, nonrejectable artificial organs design and implant, biocompatible materials and structures, etc. For example, the therapeutic potential will be enormously enhanced due to a direct effective delivery of new types of drugs to the specified body sites [19].

## 1.2 Surface attractive forces of microstructures in MEMS

Mechanics is quite different at the microscopic scale from what we experience at the macroscopic scale in daily life, and one has to develop a whole new intuition about mechanical things [47]. Typical microstructures in current MEMS range from 0.1 to a few μm in thickness, with lateral dimensions of 10-500 μm and gap between adjacent microstructures around 1 μm [51-52]. The surface area to volume ratio in the microworld is much bigger than that for mechanical devices in the macroworld. Surface attractive forces, such as van der Waals force, electrostatic force, capillary force or Casimir force are usually negligible in conventional structures at the macroscale. However, these attractive forces play a dominant role in mechanical deformation of MEMS and could lead to the unwanted adhesion of adjacent surface structures, due to drastic increase of the surface area to volume ratio and reduction in thickness, size and gap between adjacent structures [53]. In what follows, we introduce several important attractive forces for two

flat parallel surfaces, since parallel flat microstructures are popularly used in MEMS (for example, parallel microbeam arrays in comb drive technology).

## i) Electrostatic force

Electrostatic attractive force arises from electrostatic charging of parallel surfaces (or from a difference in work functions) [54]. With a voltage difference $V$ applied, the force per unit area acting between surfaces separated by an air gap $d$ with permittivity $\varepsilon_0$ is given by

$$F(d) = \frac{\varepsilon_0 V^2}{2d^2} \qquad (1.1)$$

## ii) van der Waals force

The van der Waals (vdW) attraction results from the interaction between instantaneous dipole moments of atoms. For two flat parallel surfaces with a separation $d$ less than a characteristic distance, say, $z_0 = 20$ nm (nonretarded regime), the attractive force per unit area is given by [55-56]

$$F(d) = \frac{H_a}{6\pi d^3} \qquad (1.2)$$

where $H_a$ is the Hamaker constant and lies in the range $0.4 - 4 \times 10^{-19} J$ for most solids (and liquids). When the separation is close to or more than $z_0$, the attraction is retarded, and the interaction is called Casimir force or retarded van der Waals force.

INTRODUCTION

### iii) Casimir force

The Casimir force acting on two flat parallel surfaces per unit area is given by [57-58]

$$F(d) = \frac{\pi p_l c}{480 d^4} \qquad (1.3)$$

where $p_l$ is the Planck's constant (= $6.6261 \times 10^{-34}$ m$^2$ kg / s), and $c$ is the light speed ($= 2.9979 \times 10^8$ m/s).

### iv) Capillary force

A thin liquid layer between two solid plates can work as an adhesive. If the contact angle $\theta_c$ between liquid and solid is less than $90^0$, the pressure inside the liquid drop will be lower than outside and a net attractive force between the plates exists. The attractive capillary force between two flat parallel plates with a separation $d$ is given by [59-60]

$$F = \frac{2A\gamma_{la} \cos\theta_c}{d} \qquad (1.4)$$

where $\gamma_{la}$ is the surface tension of the liquid-air interface, and $A$ is the wetted area.

## 1.3 Comb drive microbeam arrays

A comb drive structure consisting of two opposing parallel arrays of microcantilevers [61], as shown in Fig.1.1, is commonly adopted in many designs of

MEMS. This structure takes this name from the similarity in structure to a pair of combs arranged with interwoven tines. One comb support structure is anchored in place and does not move. The second comb support structure is attached to a spring or folded beam and is free to move in order to change the overlap between two comb structures.

Comb-drive microbeam arrays have become extremely popular in MEMS due to their design simplicity and performance capabilities. In addition, their fabrication process is still quite simple, which leads to a high device yield and low production costs [62].

## 1.3.1 Comb drive structures as sensors

The adjacent microbeams in the comb drive structure can be approximately modeled as a lateral variable-capacitance structure as shown in Fig.1.2-$a$) [62-63], where the upper electrode or plate is shifted over to the right by a distance $x$ but the gap is maintained at $d_0$. Neglecting the fringing fields at the edges of the plates, the capacitance will be a function of the overlap ($L$-$x$) and given by

$$C(x) = \frac{\varepsilon_0 b(L - x)}{d_0} \qquad (1.5)$$

where $b$ is the width of the plates, $\varepsilon_0$ is the permittivity of the medium between the two plates, and $x$ ranges from 0 to $L$. By detecting the capacitance between two plates, we can use the comb drive structure as a microsensor to measure the displacement of the upper electrode in the $x$-direction.

The examples of microsensor application that make use of the comb drive structure are too numerous to list. Chu and Gianchandani [64] used this comb drive structure to measure the displacement along the direction of the fingers. They demonstrated this precision integrated positioner for scanning microscopy, and their device utilized V-beam

thermal actuators and a capacitive feedback and was fabricated via deep reactive ion etching using Silicon-On-Insulator (SOI) wafers.

## 1.3.2 Comb drive structures as actuators

Comb drive structures can also act as microactuators. The actuation method of these structures is described in [62, 65]. If $I_c$ is the current supplied through the terminals when the electrodes are biased to a voltage $V$, the electrical energy supplied in a time interval $dt$ is given by $P_e dt = I_c V dt$. The (varying) charge on the electrodes is $CV$, where $C$ is the capacitance, and the change in this charge is $I_c dt = d(CV) = CdV + VdC$, so that $P_e dt = CVdV + V^2 dC$. Part of this energy is stored in the electric field. The instantaneous field energy $W_e$ is $CV^2/2$, and this increases in the time $dt$ by an amount $dW_e = CVdV + 0.5V^2 dC$. The rest of the energy supplied, $P_e dt - dW_e = 0.5V^2 dC$, is delivered as mechanical energy $P_m dt$. Thus, the mechanical power is $P_m = 0.5V^2 dC/dt$. If this comb drive structure is a constant-voltage system, the force in the $x$-direction as shown in Fig.1.2-$b$) is given by $F_x = 0.5V^2 dC/dx$. Based on Eqn (1.5), we can obtain

$$F_x = -\varepsilon_0 b V^2 /(2d_0) \tag{1.6}$$

and this force provides a $x$-direction actuation. Note that this actuation is not a function of position, displacement, or overlap (i.e., the force is constant with respect to $x$), but it is proportional to voltage squared and inversely proportional to the electrode separation $d_0$. In addition, the force generated by this comb drive actuator increases linearly with the

number of comb fingers [62]. Therefore, the comb drive structure always increases the number of electrodes that overlap, in order to increase the actuation force. For example, for a typical comb drive with $d_0 = 2\ \mu m$, $b = 2\ \mu m$, and $V = 100V$, the force generated per finger is 0.044 $\mu N$. With 100 fingers, the force becomes 4.4 $\mu N$, a respectable but not tremendously large value for microactuators, e.g., for a typical microflexure stiffness of $1N/m$, this force would generate a displacement of 4.4 $\mu m$.

Microactuators based on this approach were first demonstrated by Tang [66-68], but have now been very widely used for many different applications. One of the most dramatic microactuator examples is Sandia National Laboratories microengines [69-70], in which comb drive structures that have fifty 6-$\mu$ m-tall fingers separated by 1-$\mu$ m-wide gaps and operated with a voltage of 100 $V$ generate a force of 13.3 $\mu N$. Sandia has used these comb drive structures in a reciprocating manner to drive around a microgear with tremendous speed, and the microgear is linked to other larger structures to result in macroscale motion. Besides this application, comb drive actuators are also used as resonators [71], electromechanical filters [72], optical shutters [73], microgrippers [74] and voltmeters [75]. Sometimes they are even used as the driving element in, e.g. vibromotors [76] and micromechanical gears [77].

## 1.4 Recent studies on mechanics of MEMS

For microstructures in MEMS, the large surface area and small separation between adjacent surfaces make them especially vulnerable to adhesion upon contact. As an example, the "pull-off" force of a displaced surface microstructure in contact with an adjacent surface ranges from a few μN for an airbag accelerometer sense element to nN for a highly compliant microstructure with submicron flexure widths [78]. These forces are considerably weaker than interfacial forces, and hence, permanent adhesion results

upon contact. Adhesion of microstructures has become a research topic of central importance in MEMS design, since it will influence the performance and reliability of MEMS.

## 1.4.1 Adhesion of microstructures in MEMS

Adhesion is an important issue not only in the macroworld [79-81], but also in the microworld [51-59]. Recently, many researchers did extensive theoretical and experimental works on adhesion between microstructures in MEMS due to surface attractive forces (such as van der Waals force, electrostatic force, capillary force or Casimir force) [82-95], in order to find out feasible methods to overcome this annoying problem. In what follows, we introduce several well-known studies on adhesion of microstructures in MEMS.

## i) Adhesion between a microcantilever and a substrate due to capillary forces

Mastrangelo [53, 82-83] presented the physical mechanisms responsible for the adhesion between a microcantilevers and a substrate due to capillary forces as shown in Fig.1.3-$a$), and proposed a theoretical and experimental method for measuring surface energy of micromachined cantilevers. He modeled the role of capillary forces in bringing a microbeam into contact with a substrate and then determined the critical beam length for the beam collapse. Adhesion of the cantilever was predicted by considering the elastic energy which is attempting to pull the beam up off the substrate, and the surface energy that is promoting continued adhesion. As shown in Fig.1.3-$a$), the beam is adhering to the substrate a distance $d=(l-s)$ from its tip. The bending energy stored in the deformed beam

is $U_E = \dfrac{EI}{2}\int_0^s (\dfrac{d^2u}{dx^2})^2 dx = \dfrac{6EIh^2}{s^3}$, where $E$ is the elastic modulus of the beam, $I$ is the

moment of inertia, and $h$ is the height. The interfacial adhesion energy stored in $s \leq x \leq l$ is simply the surface energy per unit area of the bond $\gamma_s$ times the area of contact $U_S = -\gamma_s w(l-s)$, where $w$ is the width of the beam. Thus, the total energy of the system is the sum of the elastic plus surface energies

$$U_T = U_E + U_S = \frac{6EIh^2}{s^3} - \gamma_s w(l-s) \qquad (1.7)$$

The total energy has a single minimum corresponding to the equilibrium length $s^*$. This is found by setting $dU_T / ds = 0$ to obtain $s^* = (\frac{3}{2} \frac{Et^3 h^2}{\gamma_s})^{1/4}$. The beam adheres to the substrate if $s^* < l$, and is free if $s^* > l$.

## ii) Adhesion between a microcantilever and a substrate due to combined electrostatic and adhesive forces

Knapp and de Boer [84] developed modeling approaches for studying adhesion (i.e. stiction) of microcantilevers subject to electrostatic and adhesive forces, as shown in Fig.1.3-$b$). They measured the energy of adhesion using the observed shape of microcantilevers, and showed the relative sensitivities of the cantilever deflections to adhesion versus the applied load. Their modeling and experimental methods can be used to evaluate the performance of microsystems.

## iii) Adhesion between a microcantilever and a substrate due to mechanical point loading

Jones et al. [85] studied the mechanics of adhered microcantilevers subject to point

loading, and investigated several cyclic loading scenarios in the context of adhesion energy and energy dissipation. A compressive point load is applied to the beam in the unstuck region of the cantilever, as shown in Fig.1.3-c). They used the resulting load-displacement relationship along with mechanics models to infer the adhesion energy. Their experiments shed new light on adhesion by characterizing changes during transitions in adhered states, differences between loading and unloading, and energy dissipated during cyclic loading, and the accompanying theoretical framework was used both to interpret experiments and to estimate other important quantities, such as the force and energy required to detach a stiction-failed device.

## iv) Adhesion between a microcantilever and a substrate due to acceleration, Casimir and electrostatic forces

Johnstone and Parameswaran [86] provided a theoretical analysis of three important forces: acceleration (for example, gravity), Casimir and electrostatic forces, which can create an attraction between the microcantilever and the substrate surface. They determined the maximum free standing length of microstructures that would offer reliable operation with in-use stiction. Their analysis offers an insight into the problem of in-use stiction in microstructures, which is a major source of functional failure in dynamic micromechanical systems.

## v) Adhesion between two clamped microbeams due to capillary forces

Wu et al. [87] analyzed the adhesion of two clamped microbeams. Actually, due to the symmetry, this case is equivalent to adhesion between two parallel identical microcantilevers or between a microcantilever and a substrate. They determined the adhesion force between two parallel clamped beams by measuring the relationship between the adhesion length and the geometry of the beams. Their simple method and the

determined adhesion force provide useful data for design of reliable MEMS in preventing the stiction problem.

## 1.4.2 Structural instability of microstructures in MEMS

Structural instability is another important issue for design of MEMS, because it can cause adhesion and stiction of adjacent microstructures and thus malfunction of microdevices [96-101]. For example, for capacitive sensors which are popularly employed in MEMS, when the applied voltage is too strong or the gap between two electrodes is too small, the strong electrostatic force can cause adhesion of the two electrodes, and short-circuit and failure of the microdevices will occur. Some recent studies on structural instability of microstructures in MEMS are as follows.

## i) Pull-in instability of a microbeam attracted by a substrate due to electrostatic forces

Pamidighantam et al. [96] proposed a close-form expression for the critical pull-in voltage between a fixed-fixed or fixed-free beam and a substrate due to electrostatic forces. This expression is obtained based on a model of simple lumped spring-mass system, as shown in Fig.1.4-$a$). Two parallel conductive plates form a capacitor with an effective overlap area $A_{eff}$ and a gap spacing $d$. The bottom plate is fixed and the top plate is suspended by a spring with stiffness $K_{eff}$. By applying a dc voltage $V_{dc}$ across the two plates, and electrostatic attractive force $F_{el}$ is induced which leads to a decrease of the gap spacing, thereby stretching the spring. This results in an increase of the spring force $F_s$ to counteract the electrostatic force. Pull-in instability occurs as a result of the fact that the electrostatic force increases nonlinearly with decreasing gap spacing ($F_{el} \sim d^{-2}$), whereas the spring force is a linear function of the change in the gap spacing

($F_s \sim d_0 - d$). When the restoring spring force can no longer balance the attractive electrostatic force, pull-in instability occurs. In Pamidighantam's expression for the critical pull-in voltage, the effects of axial stress, charge-redistribution, and nonlinear stiffening are taken into account.

In addition, Chowdhury et al. [97] developed another simple computationally efficient closed-form model to determine the pull-in voltage of a cantilever actuated by electrostatic forces. Their results are verified by existing experimental results.

## ii) Structural instability of comb drive microbeam arrays

Hirano et al. [98] analyzed structural instability of a comb drive microbeam array, and modeled the microbeams as several stationary and moving electrodes as shown in Fig.1.4-*b*), where *V* is the applied voltage across the electrodes, *g* is the gap between two electrode surfaces, *t* is the width of the electrodes, and *l* is the length of the overlap of the electrodes. The moving electrode is suspended by two mechanical springs with spring constants of $k_y$ in the direction perpendicular to the stroke and $k_x$ in the direction of the stroke. Based on Hirano's analysis, the following condition should be satisfied in order to keep the system stable

$$k_y > \frac{2\varepsilon_0 t l V^2}{g^3} \qquad (1.8)$$

where $\varepsilon_0$ is the permittivity of the medium between two adjacent microbeams.

With the similar method, Zhou and Dowd [99] investigated the electromechanical structural instability of a comb drive microbeam array with a large travel range.

## 1.4.3 Parametric resonance of comb drive microbeam arrays

Parametric resonance of microstructures in MEMS has attracted more and more attention recently [102-122]. Several interesting examples on parametric resonance of coupled comb drive microbeam arrays are as follows.

## i) Parametric resonance of 67 coupled comb drive microbeams

Buks and Roukes [102-103] fabricated a device which is composed of 67 doubly clamped beam resonators. The microbeams oriented from one side are electrically connected to one electrode while the microbeams oriented from the other side to the other electrode. An electrical voltage applied between the two electrodes induces attracting electrostatic coupling forces between any two adjacent beams. This coupled microbeam system was driven parametrically by applying a periodically varying ac voltage to the two electrodes.

Buks and Roukes investigated parametric resonance of this coupled microbeam array based a simple one-dimensional pendulum model. Applying a voltage $V$ gives rise to an attractive interaction $F = \varepsilon_0 A V^2 /(2d^2)$ between each pendulum and its nearest neighbors, where $\varepsilon_0$ is the permittivity of the medium between two adjacent oscillators, $A$ is the area exposed to the electrostatic field, and $d$ is the distance between two adjacent pendulums. Neglecting coupling between nonneighboring pendulums, and assuming small oscillations (thus the coupling is linearized), they obtained the following equations of motion

$$m\ddot{x}_n = -m\omega_0^2 x_n + \frac{\varepsilon_0 A V^2}{d_0^3}(2x_n - x_{n-1} - x_{n+1}), \quad (n = 2, 3, \ldots, N\text{-}1) \qquad (1.9)$$

where $\omega_0$ is the natural frequency of each pendulum in the absence of any coupling.

With an ac voltage to the dc bias $V = V_{dc} + V_{ac}\cos(\lambda t)$, where $\lambda$ is the frequency of the ac voltage, Eqn (1.9) can be transformed to be a linear Mathieu equation as $\ddot{v}_i = -\omega_i^2(1 - h_i\cos(\lambda t))v_i$, where $v_i$ ($i$= 2, 3, ..., $N$-1) is the transformed displacement, $\omega_i$ is one of the natural frequencies of the oscillator system, which is related to $V_{dc}$, and the amplitude $h_i$ is related to $V_{ac}$.

Based on the theory of linear Mathieu equations, parametric resonance of the comb drive array occurs when the frequency of the ac voltage $\lambda$ is close to $2\omega_i / j$, where $j$ is an integer that labels the so-called instability tongues of the system [123-124]. Note that the frequency of parametric resonance is $\omega = \dfrac{j}{2}\lambda$, thus parametric resonance is superharmonic when $j>2$ ($\omega > \lambda$), harmonic when $j$=2 ($\omega = \lambda$), low-order subharmonic when $j$=1 ($\omega = \lambda/2$), and high-order subharmonic when $j<1$ ($\omega = \lambda/3, \lambda/4, ...$).

Buks and Roukes focused on the low-order subharmonic parametric resonance with $\omega = \lambda/2$. In their experiment, some surprising nonlinear phenomena, which can not be explained by the linear Mathieu equation, were found as follows:

1) instead of showing a band consisting of a sequence of resonance peaks at 67 normal frequencies of the array, the typical response as the frequency was swept up showed a small number of wide peaks where the response gradually increased and very abruptly decreased; and

2) the array responded at frequencies beyond the expect top edge of the band.

## ii) Analysis of nonlinear phenomena in Buk and Roukes' experiment

Lifshitz and Cross [104] thought that both these phenomena are a direct result of the fact that the restoring forces acting on the resonators as well as the damping that they undergo are both nonlinear. Employing a Duffing oscillator model, and considering the nonlinear damping, they obtained

$$\ddot{x}_n + x_n + x_n^3 + \frac{1}{2}\Delta^2[1 + H\cos(2\omega_p t)] \times (x_{n+1} - 2x_n + x_{n-1}) - \frac{1}{2}\Gamma(\dot{x}_{n+1} - 2\dot{x}_n + \dot{x}_{n-1})$$

$$-\frac{1}{2}\eta[(x_{n+1} - x_n)^2(\dot{x}_{n+1} - \dot{x}_n) - (x_n - x_{n-1})^2)(\dot{x}_n - \dot{x}_{n-1})] = 0 \qquad (1.10)$$

This equation includes a cubic nonlinear elastic restoring force (whose coefficient is scaled to 1), a linearized dc electrostatic nearest-neighbor coupling term with a small ac component responsible for the parametric excitation (with coefficients $\Delta^2$ and $\Delta^2 H$ respectively), and linear as well as cubic nonlinear damping terms (with coefficient $\Gamma$ and $\eta$ respectively). Based on this model, Lifshitz and Cross calculated the low-order subharmonic parametric resonance with $\omega = \lambda/2$, which agree qualitatively with the experimental results of Buks and Roukes.

## iii) Multiscale analysis of parametric resonance of coupled nonlinear oscillators

Bromberg et al. [105] studied the low-order subharmonic parametric resonance (with $\omega = \lambda/2$) of coupled nonlinear oscillators with a multiscale analysis. They derived amplitude equations describing the response of a large array of oscillators to parametric excitation, directly from the equations of motion yielding exact expressions for all the coefficients. They showed that interesting response of coupled nonlinear oscillators excited parametrically can also be obtained for quasistatic driving amplitude sweeps, rather than the frequency sweeps that usually performed in experiments. The results obtained by the numerical integration of the equations of motion agreed with their analysis, supporting the validity of the derived amplitude equation.

## iv) Five parametric resonances in a microelectromechanical system

Turner et al. [106-107] reported parametrically excited torsional oscillations in a

microelectromechanical system which is mainly composed by microcantilevers, comb actuators, and torsion bars. Based on a damping Mathieu equation

$$\ddot{x} + a\dot{x} + (b + d\cos\tau)x = 0 \qquad (1.11)$$

where $a$ is the coefficient related to the damping, $b$ is the coefficient related to the dc voltage, and $d$ is the coefficient related to the ac voltage, they measured parametric resonance in five instability tongues (with $j=$ 1, 2, ..., 5), due to the low damping, stability and precise frequency control achievable in this system. The center frequencies of these instability tongues agreed with theoretical predictions. Their results suggested that microelectromechanical systems can provide a unique testing ground for dynamical phenomena that are difficult to detect in macroscopic systems (only the first instability tongue can typically be observed in macroscopic systems). Different from other researchers such as Buks, Roukes, Turner et al. studied the superharmonic (with $\omega > \lambda$), harmonic (with $\omega = \lambda$), and low-order subharmonic (with $\omega = \lambda/2$) parametric resonances in a microelectromechanical system.

## v) Parametric resonance of a nonlinearly coupled oscillator

Zhang et al. [108-109] studied the low-order subharmonic parametric resonance of a microelectromechanical oscillator with cubic mechanical and electrostatic force terms. With a particular design of the electrostatic drive combs and mechanical springs, they demonstrated how to tune the effective cubic stiffness, in order to obtain a wide range of qualitatively varying frequency responses. When the frequency of the ac voltage is close to twice the natural frequency of the oscillator, the resonance in the first instability tongue can be generated with time-varying effective stiffness. The dynamic response of the oscillator can be understood to a good degree when modeled with a nonlinear Mathieu equation

$$\ddot{x} + \alpha\dot{x} + (\beta + 2\delta\cos 2\tau)x + (\delta_3 + \delta_3^{'}\cos 2\tau)x^3 = 0 \qquad (1.12)$$

where $\alpha$ is the coefficient related to the damping, $\beta$ and $\delta$ are the coefficients related to the linear elastic and electrostatic forces, $\delta_3$ and $\delta_3^{'}$ are the coefficients related to the nonlinear (cubic) elastic and electrostatic force. They showed that the effective cubic nonlinearity, along with contributions from the mechanical constraints and electrostatic field, plays an important role in the dynamic response of the oscillator.

## vi) Parametric resonance of a nonlinearly coupled oscillator array

Following Zhang and Turner, Rhoads et al [110-112] investigated the low-order subharmonic parametric resonance of an array of electrostatically driven microelectromechanical oscillators, and provided a complete description of the dynamic response and its dependence on the system parameters. The oscillator systems they considered are capable of displaying not only typical hardening or softening nonlinear characteristics, but also mixed nonlinear characteristics wherein the principal response branches bend toward or away from one another near resonance. These systems were shown to transition between various qualitatively different nonlinear regimes as the excitation amplitude is varied. Experimental results are in good agreement with their analytical predictions.

## 1.4.4 Some unexplored problems of major concerns

In spite of many endeavors made in the mechanics research of MEMS, there are still some important problems unexplored, which include adhesion, structural instability (based on the elastic beam/cantilever model), and high-order subharmonic parametric resonance of comb drive microbeam arrays. These important issues will be discussed in this thesis.

## i) Adhesion of comb drive microbeam arrays

Comb drive structures are usually driven and controlled by electric voltages and electrostatic forces [61-64, 66-77, 98-99, 101]. Adhesion of two adjacent microbeams/electrodes in comb drive structures can cause short circuit and failure of microdevices. As described above, many researchers focused on adhesion between a cantilever and a rigid substrate or between two clamped beams [51-59, 82-95]. However, to the best of our knowledge, little attention was paid to adhesion of two opposing microcantilevers in comb drive microbeam arrays. It is practically significant to study adhesion of comb drive structures and the effects of the overlap length, since these structures are widely employed as sensors and actuators in MEMS.

## ii) Structural instability of large microbeam arrays based on the elastic beam model

Compared to structural instability of a microbeam attracted by a rigid substrate, structural instability of a mutually attracting microbeam array is much more complicated to analyze, especially when the number of the microbeam in the array is very large. Hirano et al. [98] made the instability analysis of a comb drive structure, based on a model of a moving electrode attracted by two stationary electrodes. Hirano's method is effective in predicting the occurrence of instability of comb drive structures, and is also employed by some other researchers [99, 101]. However, Hirano's spring model only considered the average deflection of the microbeam, but ignored the deflection difference with the different points in the microbeam. Actually, in order to analyze structural instability of a microbeam array, it is important to obtain the realistic and accurate deflections of different points in the microbeams. No doubt, the elastic beam model can provide more reliable and realistic results, compared to the simplified spring model, although it also involves more complicated analysis. However, few analysis is made for

structural instability of mutually attracting microbeam arrays based on the elastic beam model.

### iii) High-order subharmonic parametric resonance of comb drive microbeam arrays

Based on linear or nonlinear Mathieu equations, many researchers studied low-order subharmonic parametric resonance of comb drive microbeam arrays [102-112], with the resonance frequency equal to half of the exciting ac voltage frequency. By now, few result has been available in the literature on high-order subharmonic parametric resonance of comb drive structures. Whether high-order subharmonic parametric resonance exists or not is a very interesting issue for dynamics of comb drive structures, because it is related to the issue whether the range of exciting resonance frequencies can be expanded to $3\omega_0$, $4\omega_0$, ..., even infinity, where $\omega_0$ is one of the natural frequencies of the comb drive microbeam array.

## 1.5 Contributions of the present work [125-131]

In this thesis, we will focus on adhesion, structural instability, and high-order subharmonic parametric resonance of comb drive microbeam arrays.

Chapter 2 studies surface energy-driven adhesion of two opposing microcantilevers in comb drive structures [125]. We propose an analytic model by considering the elastic strain and surface energies. Based on this model, adhesion becomes possible when an attached state of the two opposing cantilevers becomes an equilibrium state at which the release rate of the strain energy with respect to the attached length is equal to the surface energy per unit length. It is found that the strength of two opposing cantilevers against adhesion can be enhanced by increasing (rather than decreasing) the overlap length, and these results could have significant consequences to comb drive design in avoiding

adhesion failure.

In Chapters 3-5, we analyze structural instability of mutually attracting microbeam arrays based on the elastic beam model. Chapter 3 studies structural instability of a parallel array of identical microbeams each of which interacts with two neighboring microbeams through distance-dependent surface attractive forces (such as electrostatic, van der Waals, or Casimir forces) [126]. Based on a simplified spring model, it is verified that equilibrium deflections of intermediate beams (except the beams at the two ends of parallel array) would be negligibly small. However, the end beam at each of the two ends usually has a big deflection because it is attracted by its adjacent beam from one side only. These big deflections with the end beams have an important end effect on the instability of the microbeam array. When the end-effect is neglected, exact analysis of parallel beams shows that the critical value of the beam-beam interaction coefficient for instability of the parallel array, defined on the initial distance between adjacent beams, is exactly a half of the critical value of the interaction coefficient for instability of two mutually attracting beams, or equivalently a quarter of the critical value of the interaction coefficient for instability of a single beam attracted by a rigid body. With the end-effect, the critical interaction coefficient for instability of the parallel array will be reduced by 20%-35%, and therefore the actual critical value can be given, conservatively, by 60% of the critical value without the end-effect. These results provide a simple design criterion for pull-in instability of a parallel array of identical microbeams.

In Chapter 4, we study structural instability of mutually attracting comb-drive microcantilevers [127-128]. Without the end-effect, the critical value of the beam-beam interaction coefficient for instability of a large comb drive microcantilever array is found to be exactly a half of the critical value of the interaction coefficient for instability of a pair of opposing microcantilevers, and this conclusion is valid for all other combinations of the geometrical and material parameters of the microcantilevers. Furthermore, the end-effect on the critical value for instability of the comb-drive microcantilevers is

examined by quantifying the effect on instability of the amplified interaction coefficients between neighboring beams at the two ends. With the end-effect, for two opposing microcantilever array with the same bending rigidity ( $E_1I_1 = E_2I_2$ , $L_1 = L_2$ ), the end-effect is found to lower the critical value for instability by 25-40%, insensitive to the overlap length [127]. For two opposing arrays with different bending rigidities, the end-effect is found to lower the critical interaction coefficient for instability, and the reduction in the critical value for instability increases with decreasing bending rigidities of the end microcantilevers [128]. These results indicate the significance of the end design on the instability of comb-drive structures.

Structural instability of a large coupled microbeam array is usually initialized at its ends, due to unbalanced attraction from one side only. In Chapter 5, a simplified approximate method is developed to analyze instability of a large parallel microbeam array, based on instability analysis of a small array of only a few microbeams at the ends of the original large array [129]. The critical value for instability of the original large array is determined by the critical value for instability of a small array of only a few microbeams at the two ends, and the results based on this simplified substitution method are found to be good agreement with those obtained by other methods based on the instability analysis of the original large array which contains a large number of microbeams. It is believed that this simplified substitution method can reduce the instability analysis of a large array of microbeams to a much simpler problem of a small array of only a few microbeams.

In Chapters 6-7, we study high-order subharmonic parametric resonance of comb drive microbeam arrays. Chapter 6 analyzes parametric response of a nonlinearly coupled micromechanical oscillator model under periodically varying nonlinear coupling forces [130]. Similar to most of previous related works in which the periodically varying coupling forces between adjacent oscillators are linearized [102-105], our analytic model predicts superharmonic, harmonic, and low-order subharmonic parametric resonance.

Different from previous related works, our present work focuses on new physical phenomena caused by the nonlinear coupling. For example, our results shows that periodically varying nonlinear coupling considered in this present model does lead to the appearance of high-order subharmonic parametric resonance when the external excitation frequency is a multiple or nearly a multiple ($\geq 3$) of one of the natural frequencies of the oscillator system. This remarkable new phenomenon does not appear in the linearly coupled micromechanical oscillators studied previously, and makes the range of exciting resonance frequencies expanded to infinity.

Chapter 7 studies high-order subharmonic parametric resonance of a nonlinearly coupled oscillator array, in which these are three oscillators with elastic geometrical nonlinearity [131]. The effects of the dc and ac voltages, the nonlinear elastic geometrical coefficient, and the linear damping coefficient on high-order subharmonic responses of a nonlinear oscillator array are investigated in detail in this chapter. It is believed that these results offer new and useful insights into the ongoing research on nonlinear dynamics of coupled microbeams or nanobeams in MEMS or NEMS.
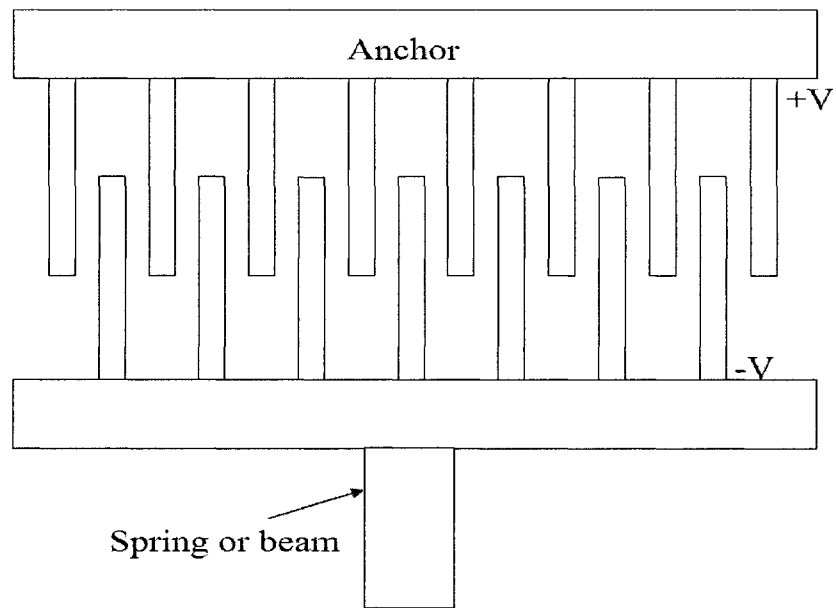
Fig.1.1 A comb drive structure.
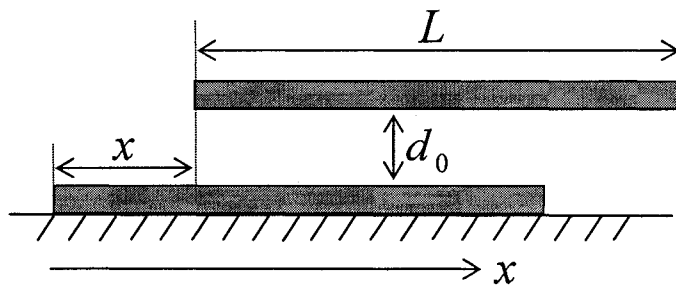


*a*) Model of comb drive sensors.
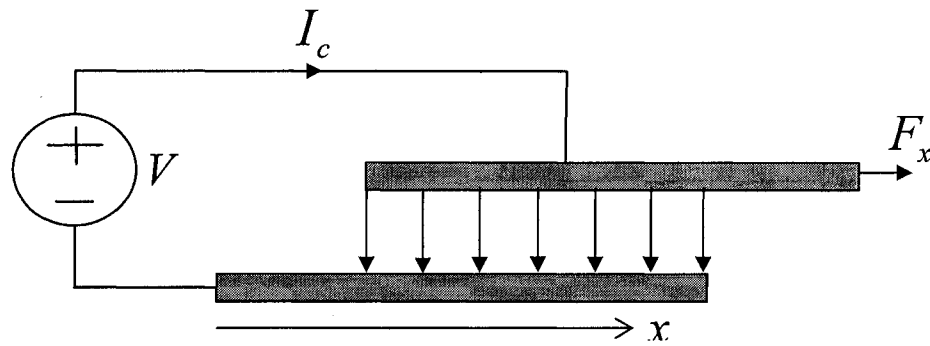


*b*) Model of comb drive actuators.

Fig.1.2 Models of comb drive sensors and actuators.
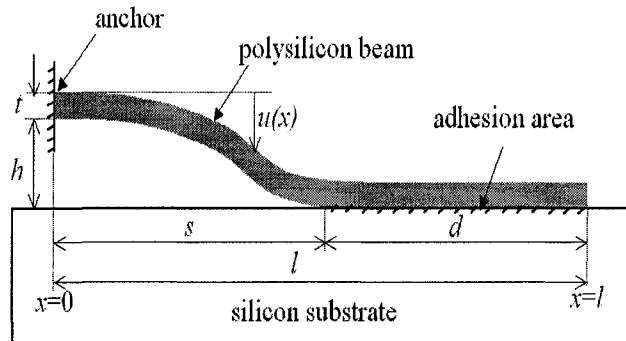
*a)* Adhesion due to capillary forces.
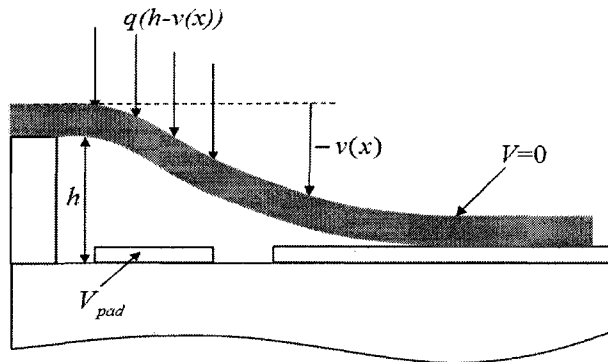


*b)* Adhesion due to electrostatic and adhesive forces.
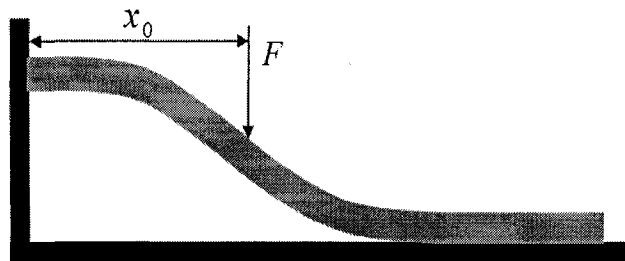


*c)* Adhesion due to point loading.

Fig.1.3 Adhesion of microstructures in MEMS.
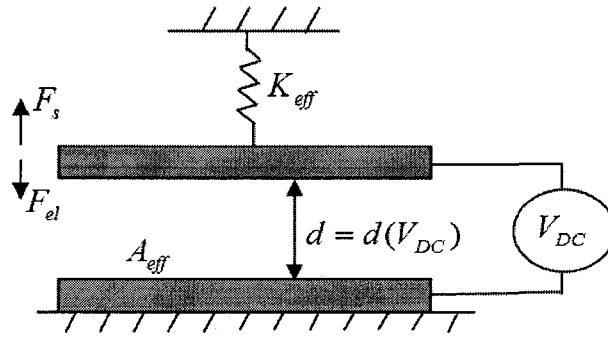
*a*) Model of a lumped spring-mass system.
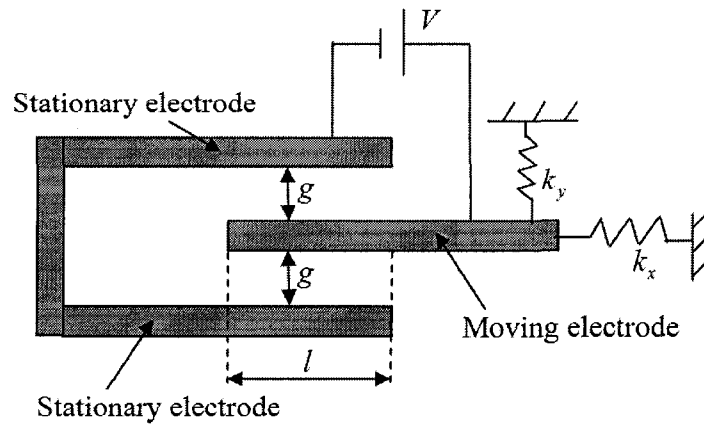


*b*) Model of stationary and moving electrodes.

Fig.1.4 Models of structural instability of microstructure in MEMS.

# Chapter 2

# Adhesion of Two Opposing Microcantilevers

## 2.1 Introduction

Adhesion and stiction of densely assembled surface microstructures have raised a major concern in the design of MEMS (microelectromechanical systems). Owing to drastic increase of the surface area-to-volume ratio in microstructures, surface attractive forces, such as van der Waals force, electrostatic force, capillary force or Casimir force [51-59, 82-95], are dominant in determining mechanical deformation of microstructures and even lead to adhesion, stiction, and failure of microsystems. Therefore, surface forces-driven adhesion of surface microstructures has become a research topic of central importance in MEMS design.

Exact deformation analysis of complex surface microstructures under distance-dependent surface attractive forces raises a challenging problem. Because surface forces are usually rapidly decreasing functions of the distance and significant only for extremely short distances, a simplified yet effective method has been suggested based on the concept of surface energy. With this method, the change of the attractive energy between any two surfaces is neglected as long as they are not brought in actual contact. On the other hand, if two surfaces are brought into physical contact, the change of the attractive energy is set to be equal to the surface energy reduction due to the contact area. Thus, equilibrium of the whole system is determined by the total energy, defined as the sum of elastic strain energy and the surface energy reduction of the attached area of attracting structures. A classical example is the well-known JKR theory

of contacting bodies with adhesion [132]. Similar concept and method have been used to study adhesion of surface microstructures in MEMS. For example, Mastrangelo & Hsu [53, 82-83] considered a cantilever beam attracted by a parallel rigid substrate due to capillary forces. Their method has been extended to other similar adhesion problems, such as adhesion of cantilever beams with non-zero free end slope [85, 94-95], adhesion of cantilever beams with elastic constraint at the clamped end [89], symmetric adhesion of two parallel identical microcantilevers clamped on the same side [87], and adhesion of plate-like microstructures [93].

In many designs of MEMS, however, one has to consider two opposing parallel arrays of microcantilevers oriented in opposite directions, as shown in Fig.2.1. This structure is a common building block in MEMS. For example, such structures enjoy widespread use in comb drive technology [61-64, 66-77, 98-99, 101], where "side-to-side" instability due to jump-to-together of adjacent microcantilevers, or called "side snap over", has been a design concept of major concern especially with continuing scale-down of MEMS. In spite of above-mentioned extensive studies on adhesion of a cantilever attracted by a rigid substrate or two parallel identical microcantilevers clamped on the same side, to our knowledge, no analysis has been made for side-to-side adhesion of two parallel opposing microcantilevers shown in Fig.2.2. It is anticipated that, due to the free end flexibility of microcantilevers, sidewall adhesion of two opposing cantilevers shown in Fig.2.2 would occur much more easily than two parallel cantilevers clamped on the same side [87] under otherwise similar conditions. No doubt, sidewall adhesion of two opposing microcantilevers, as shown in Fig.2.2, is of practical significance for many MEMS designs and deserves a thorough study. This chapter aims to develop a simplified analytical model for such an adhesion problem. As will be shown in this chapter, adhesion of two opposing microcantilevers, as shown in Fig.2.2, exhibits many interesting new features as compared to the cantilever-substrate system or two parallel identical microcantilevers oriented in the same direction studied extensively in the

literature [82-95].

## 2.2 An analytical model

Because adhesion of two opposing parallel arrays of microcantilever beams shown in Fig.2.1 is essentially determined by adhesion of two adjacent opposing beams, we consider two opposing microcantilevers, of lengths $L_1$, $L_2$ and bending rigidities $E_1 I_1$ and $E_2 I_2$, respectively, as shown in Fig.2.2, where the two opposing beams have an overlap length $\delta$, and their surfaces are apart by a small gap $d$.

Adhesion of the two beams is determined by the competition between the surface energy reduction (as the driving force) and the elastic strain energy (as the resistant force). Let $\gamma$ be the increase in surface energy due to separation of two surfaces per unit area of the attached interface (which is equal to the surface energy of two separate surfaces minus the interface energy of the attached surfaces). Here, $\gamma$ depends on the nature of the surface attractive force, and detailed calculation of the surface energy for various surface attractive forces can be found in the literature (see [51-59] and [82-95]), with or without considering roughness or other conditions of surfaces. Let that the elastic strain energies of the two beams be $U_1$ and $U_2$, the width of the interacting area of the two beams (which is the dimension of the two cantilevers in the direction perpendicular to the plane of Fig.2.2) be $w$, and the attached length of the two beams be $t$, the total energy of the system $V$ is given by

$$V = U - \gamma w t, \quad U = U_1 + U_2 \tag{2.1}$$

The equilibrium state of the system is defined by local minimum of the total energy (2.1). If the unbent configuration of two separate straight beams (with $t$=0 and $V$=0) is the only

local minimum of the total energy (2.1), the two beams will remain undeflected and adhesion will never occur. On the other hand, if there exists at least one local minimum of the total energy (2.1) with the attached length $t>0$, adhesion of the two beams can occur and thus the configuration of two separate straight beams will be no longer the only possible equilibrium state. In other words, whether adhesion would occur or not is determined by whether an equilibrium state of two attached beams with $t>0$ exists. It is in this sense that adhesion instability of MEMS has been studied in the literature [82-95]. It turns out that when $\gamma$ is sufficiently small, as will be shown later, the configuration of two separate straight beams (with $t=0$) is the only local minimum of the system (2.1) and thus adhesion will not occur. However, non-trivial equilibrium state of two bent beams with the attached length $t>0$ does exist when $\gamma$ is sufficiently large. One of the main goals of the present study is to determine the minimum value of $\gamma$ for adhesion, and its dependence on varying geometrical and material parameters. In particular, it is of interest to compare the ciritcal values of $\gamma$ for adhesion of two opposing cantilevers with the known critical values for cantilever-substrate system or two parallel identical cantilevers oriented in the same direction studied extensively in the literature [82-95].

In this chapter, because the total bending strain energy of two attached beams is mainly contributed from bending of the unattached suspended parts of the two beams, we assume that the strain energy of the attached portion is negligible. Consequently, the curvature of the attached part of the two beams can be neglected and therefore the attached part can be assumed to be straight. Although accuracy of this assumption needs to be justified with a more refined model, it seems reasonable especially when the attached length $t$ is small compared to the lengths $L_1$ and $L_2$. Based on this assumption, let beam 1 deflect $h_1$ with a slope $\theta_1$ at a point $x_1 = s_1$ measured from its clamped end, and beam 2 deflect $h_2$ with a slope $\theta_2$ at a point $x_2 = s_2$ measured from its clamped

end, as shown in Fig.2.2. Because the attached portion of the two beams is assumed to be straight, we have

$$\theta_1 = \theta_2 = \theta \tag{2.2}$$

$$h_1 + h_2 + t\theta = d \tag{2.3}$$

where $\theta$ is so small in the present problem that $\sin\theta = \theta$. Unlike the existing models [82-95] where the attached portion is known to be always horizontal, the slope of the attached portion for the present problem, $\theta$, is unknown and will be determined as part of the solution.

Furthermore, the shortenings of beam 1 and beam 2 in the longitudinal direction due to transverse bending are given approximately by [125]

$$\Delta_1 = \frac{3h_1^2}{5s_1}, \quad \Delta_2 = \frac{3h_2^2}{5s_2} \tag{2.4}$$

Thus, it is seen from Fig.2.2 that

$$s_1 - \Delta_1 + s_2 - \Delta_2 + t = L_1 + L_2 - \delta \tag{2.5}$$

where $\theta$ is so small in the present problem that $\cos\theta = 1$. Thus, the attached length $t$ and the unknown slope $\theta$ can be expressed through (2.5) and (2.3) as

$$t = L_1 + L_2 - \delta - s_1 + \Delta_1 - s_2 + \Delta_2, \quad \theta = \frac{d - h_1 - h_2}{L_1 + L_2 - \delta - s_1 + \Delta_1 - s_2 + \Delta_2} \tag{2.6}$$

31

Consequently, the equilibrium states are defined by four independent variables $h_1$, $h_2$, $s_1$ and $s_2$. Here, it should be stated that the longitudinal shortenings of the two cantilevers due to transverse bending are essential for condition (2.5). It can be verified that removal of the two longitudinal shortening terms from (2.5) will lead a substantially different critical value of the surface energy for initial adhesion.

The strain energy of beam 1 may include two parts. The first part is due to bending of the suspended length $[0, \ s_1]$. In addition, unattached part of the beam 1 at its free end shown in Fig.2.2, of length $(L_1 - s_1 - t)$, may or may not be bent. In fact, if the slope of the beam 2 decreases at the point $x_2 = s_2$, we have

$$s_2\theta < 3h_2 / 2 \qquad (2.7)$$

and thus the unattached free end of beam 1 keeps straight and has no strain energy, as shown in Fig.2.2(a). On the other hand, if the slope of beam 2 increases at the point $x_2 = s_2$, we have

$$s_2\theta > 3h_2 / 2 \qquad (2.8)$$

and thus the unattached free end portion of beam 1, of length $(L_1 - s_1 - t)$, must be bent, as shown in Fig.2.2(b), in contact with beam 2 at a point $x_2 = s_2 - (L_1 - s_1 - t)$ measured from the clamped end of beam 2. Since the slope of the attached part is $\theta$, it follows from (2.7, 2.8) that the additional slope of the unattached free end portion of beam 1, relative to the (straight) attached part, is estimated by $3h_2 /(2s_2)$. Thus, the end deflection of the unattached free end portion of beam 1, measured from the straight

attached part, is given by

$$(L_1 - s_1 - t)(\theta - 3h_2/(2s_2)) \qquad (2.9)$$

Therefore, if the end moment of the unattached free end portion of beam 1 is neglected, the strain energy of the unattached free end portion of beam 1 is given approximately by [125]

$$\frac{3}{2} \frac{E_1 I_1 (\theta - \frac{3h_2}{2s_2})^2}{(L_1 - s_1 - t)} \qquad (2.10)$$

Hence, the total strain energy of beam 1 is given by

$$U_1 = \frac{E_1 I_1 (2s_1{}^2 \theta^2 - 6s_1 h_1 \theta + 6h_1{}^2)}{s_1{}^3}, \quad \text{if } s_2 \theta \leq 3h_2/2 \text{ or } (L_1 - s_1 - t) = 0$$

$$U_1 = \frac{E_1 I_1 (2s_1{}^2 \theta^2 - 6s_1 h_1 \theta + 6h_1{}^2)}{s_1{}^3} + \frac{3}{2} \frac{E_1 I_1 (\theta - \frac{3h_2}{2s_2})^2}{(L_1 - s_1 - t)},$$

$$\text{if } s_2 \theta > 3h_2/2 \text{ and } (L_1 - s_1 - t) > 0 \qquad (2.11)$$

Similarly, the strain energy of beam 2 is given by

$$U_2 = \frac{E_2 I_2 (2s_2{}^2 \theta^2 - 6s_2 h_2 \theta + 6h_2{}^2)}{s_2{}^3}, \quad \text{if } s_1 \theta \leq 3h_1/2 \text{ or } (L_2 - s_2 - t) = 0$$

$$U_2 = \frac{E_2 I_2 (2s_2{}^2 \theta^2 - 6s_2 h_2 \theta + 6h_2{}^2)}{s_2{}^3} + \frac{3}{2} \frac{E_2 I_2 (\theta - \frac{3h_1}{2s_1})^2}{(L_2 - s_2 - t)},$$

33

$$\text{if } s_1\theta > 3h_1/2 \text{ and} (L_2 - s_2 - t) > 0 \qquad (2.12)$$

Here, it should be stated that the additional strain energy (2.10) for the unattached free end portion is relevant when the full adhesion is approached, but not important for initial adhesion.

Therefore, substituting (2.6) into (2.11, 2.12) and eventually into (2.1), the total energy $V$ can be expressed as a function of four variables $h_1$, $h_2$, $s_1$ and $s_2$. Thus the equilibrium states, defined by local minimums of the total energy $V$, can be determined by $dV=0$ which gives

$$\frac{\partial V}{\partial h_1} = 0, \quad \frac{\partial V}{\partial s_1} = 0, \quad \frac{\partial V}{\partial h_2} = 0, \quad \frac{\partial V}{\partial s_2} = 0 \qquad (2.13)$$

The surface energy-driven adhesion of the two opposing cantilever beams is determined by the existence of at least one local minimum of (2.1) meeting three obvious geometric restrictions

$$t > 0, \quad t \le (L_1 - s_1), \quad t \le (L_2 - s_2) \qquad (2.14)$$

As will be shown later, local minimum of (2.1) meeting the restrictions (2.14) with $t>0$ will not exist when $\gamma$ is sufficiently small. When $\gamma$ increases, local minimum of (2.1) meeting the restrictions (2.14) with $t>0$ will eventually emerge after $\gamma$ exceeds a certain critical value. The critical value of $\gamma$ beyond which a local minimum meeting the restrictions (2.14) with $t>0$ exists, labeled by $\gamma_1$, corresponds to the minimum surface energy for initial adhesion of the two beams. When $\gamma$ exceeds $\gamma_1$ and further

increases, the attached length $t$ increases until it reaches the maximum attached length defined by $t = (L_1 - s_1)$ and $t = (L_2 - s_2)$. The minimum value of $\gamma$ for the existence of a local minimum with $t>0$ and $t = (L_1 - s_1)$ and $t = (L_2 - s_2)$, labeled by $\gamma_2$, corresponds to the minimum surface energy for full adhesion of the two beams from one of the two free ends to the other. In what follows, we shall study the dependence of the two critical values on varying geometric parameters, as well as the geometric characteristics of two attached beams.

## 2.3 Results and discussions

In almost all practical examples of comb drive technology [61-64, 66-77, 98-99, 101], microcantilevers of two opposing arrays have exactly the same material and geometric characteristics. Hence, we assume here $E_1 I_1 = E_2 I_2 = EI$, $L_1 = L_2 = L$, and thus we have $s_1 = s_2 = s$ and $h_1 = h_2 = h$. In addition, in view of typical data of surface microstructures in MEMS mentioned before, we consider $d/L$=0.1, 0.01 or 0.001, and $\delta/L$=0.2, 0.5 or 0.8. Numerical results obtained by the present model for all cases are shown in Figs 2.3-2.7.

## 2.3.1 Critical values of surface energy for initial or full adhesion

As explained before, the attached equilibrium state of the two cantilevers is defined by a stationary point of the total energy $V$ determined by $dV$=0, or equivalently by (see (2.1))

$$\frac{dU}{dt} = \gamma w \tag{2.15}$$

where $U$ is the total strain energy of the two cantilevers. This means that the variation of

35

the strain energy, $dU$, must vanish at the attached equilibrium state when $dt=0$. If the release rate of the strain energy of the attached state $dU/dt$ is greater than $\gamma w$, the attached state is not an equilibrium state and detachment of the attached part, defined by decreasing attached length $dt<0$, will continue until an equilibrium state is reached. On the other hand, if the release rate of the strain energy of the attached state $dU/dt$ is smaller than $\gamma w$, the attached state is not an equilibrium state and adhesion of the two cantilevers, defined by increasing attached length $dt>0$, will grow until an equilibrium state is reached. In particular, this indicates that the release rate of the strain energy, $dU/dt$, should be an increasing function of the attached length $t$, or a decreasing function of the unattached suspended length of the cantilevers. In what follows, for convenience, let us define a dimensionless parameter $e$ through the surface energy $\gamma$ by

$$e = \frac{\gamma w L^4}{EId^2} \qquad (2.16)$$

The lowest value of $e$ for initial adhesion with $t>0$ is labeled by $e_1$, while the lowest value of $e$ for full adhesion (that is, the two beams are attached from one of the two free ends to the other) is labeled by $e_2$. These two critical values of $e$ are shown in Fig.2.3, as a function of the overlap length. It is seen from Fig.2.3 that, for given cantilever length $L$ and the gap $d/L$, both the critical values $e_1$ and $e_2$ are monotonically increasing functions of the overlap length $\delta$. This can be explained by the fact that the release rate of the strain energy $dU/dt$, with respect to the change of the attached length, increases with decreasing suspended length of the cantilevers (that is, the suspended length $s$ between the clamped end and the attached end, as shown in Fig.2.2). Consequently, increasing the overlap length leads to a decrease in the suspended length of the

cantilevers and then an increase in the release rate of the bending strain energy, and therefore a higher surface energy is required for adhesion of the two cantilevers. To our knowledge, this nontrivial conclusion remains unknown in the literature. It implies that, in contrast to someone's intuition, the strength of two opposing identical beams against initial adhesion and full adhesion can be promoted by increasing, rather than decreasing, the overlap length $\delta$. For example, when the gap $d$=0.01$L$, the critical value $e_1$ for initial adhesion increases almost one order of magnitude, from about 0.0001 to almost 0.001, when the overlap length increases from 0.3$L$ to 0.8$L$. In addition, it is seen from Fig.2.3 that the critical value $e_2$ for full adhesion is almost independent of the gap $d$, while the critical value $e_1$ for initial adhesion increases significantly with increasing gap $d$. Indeed, the value $e_2$ is almost the same for $d$=0.1$L$, 0.01$L$ and 0.001$L$, over the whole range of the overlap length $\delta$.

It is of interest to compare the critical values $e_1$ for initial adhesion of two opposing cantilevers obtained here, with the critical value for adhesion of a single cantilever beam, of bending rigidity $EI$ and length $L$, attracted by a rigid substrate at a separation $d$. When the cantilever beam is attached to the rigid substrate with a suspended length $s$, the attached length is $(L$-$s)$ and the total energy is (see e.g. [53])

$$V = \frac{6EId^2}{s^3} - \gamma w(L - s)$$
(2.17)

It is easily verified that, in the present notations, the cantilever beam would be attached to the rigid substrate (as a local minimum of the total energy (2.17)) with $s$<$L$ only if $e$>18. It is seen from Fig.2.3 that, for arbitrary overlap length $\delta$, the critical value $e_1$ for initial adhesion of two opposing cantilevers with separation $d$≤0.1$L$ is very much lower

than the critical value ($e$=18) for initial adhesion of a single cantilever attached to a rigid substrate. This indicates that the critical value of surface energy for initial adhesion of two opposing cantilevers is much lower than the critical value of surface energy for adhesion of a single cantilever attracted by a rigid substrate or two parallel identical cantilevers clamped on the same side [87]. To our knowledge, no similar quantitative analysis has been made in the literature before.

## 2.3.2 Geometric characteristics of two attached beams

To examine geometric characteristics (such as the attached length $t$) of the attached beams when the surface energy is beyond the critical value $e_1$ for initial adhesion but below the critical value $e_2$ for full adhesion, geometric parameters of two attached beams are shown in Figs 2.4-2.6 for $\delta$ =0.2$L$, 0.5$L$ and 0.8$L$, respectively. Because two beams are identical, we have $s_1 = s_2 = s$ and $h_1 = h_2 = h$. First of all, it is seen from these figures that ($2\theta s/3h$ ) is always between 1 and 1.1, which implies that each of the two beams is only slightly deflected at the free-end, as the case b) shown in Fig.2.2.

In addition, for all cases shown in these figures, when the surface energy parameter $e$ increases from the critical value $e_1$ to the critical value $e_2$, the attached length $t/L$ always increases, first very quickly and then slowly. In particular, when the parameter $e$ approaches the critical value $e_2$ for full adhesion, the attached length $t/L$ is very close to the overlap length $\delta/L$. These results show how the adhesion of two opposing cantilevers develops when the surface energy parameter $e$ is larger than the critical value $e_1$ for initial adhesion. The cases beyond the critical value $e_2$ for full adhesion are of less interest and will not be discussed in this chapter.

## 2.3.3 Energy comparison between attached and unattached states

The attached equilibrium states of two beams studied here correspond to local minimums of the total energy defined by (2.1), but not necessarily have a negative total energy lower than the unattached straight beams (the latter has $V=0$). In spite of this, the lowest critical value of surface energy for the existence of at least one attached equilibrium state has been widely used to define the critical condition against adhesion, and therefore is of fundamental importance for MEMS design. For example, for the classic case of a single cantilever beam attracted by a rigid substrate [53], it can be easily verified from (2.17) that although adhesion occurs when the attached length $(L\text{-}s)>0$, the total energy of the attached single cantilever beam is negative only if the attached length $(L\text{-}s)$ is longer than $L/4$ (that is, $3L/4>s$). In other words, all attached equilibrium states with $3L/4<s<L$ have a positive total energy, which is higher than the total energy ($V=0$) of the unattached straight single beam. In spite of this, the critical value for adhesion is still defined by $(L\text{-}s)>0$, but not by $(L\text{-}s)>L/4$, because the former makes possible that the unattached state could jump to the attached state of higher energy due to any external energy disturbance.

Clearly, the total energy $V(= U - \gamma wt)$ of the attached state of two opposing cantilevers will be lower than the total energy of the unattached state (with $V=0$) if and only if $U/(\gamma wt)<1$. In order to see when the total energy of the attached equilibrium state is negative and thus smaller than the total energy of the unattached state, the ratio $U/(\gamma wt)$ is shown in Fig.2.7 for $\delta=0.2L$, $0.5L$ and $0.8L$. It is expected that this ratio $U/(\gamma wt)$ could be less than unity only if the surface energy $\gamma$ or/and the attached length $t$ is sufficiently large. This could happen more likely for opposing cantilevers of larger overlap length. In fact, it is seen from Fig.2.7 that for smaller or moderate overlap length, such as $\delta/L=0.2$ or $0.5$, the surface energy reduction ($\gamma wt$) is always smaller

than the elastic bending energy of two attached beams ($U_1 + U_2$), even up to the critical value $e_2$ for full adhesion. This is attributed to lower surface energy and smaller attached length. Indeed, up to the critical value $e_2$ for full adhesion, the elastic bending energy of the attached two beams of smaller or moderate overlap length ($\delta / L = 0.2$ or $0.5$) is at least a few times larger than the associated surface energy reduction. This indicates that for small or moderate overlap length $\delta / L \leq 0.5$, the attached state of two beams is only metastable when the value of $e$ is between $e_1$ and $e_2$, because it has a positive total energy higher than the total energy ($V = 0$) of the unattached straight state of two beams. Here, it should be pointed out that even for smaller or moderate overlap lengths, of course, the total energy of the attached state of two beams would become negative and then lower than the total energy ($V = 0$) of the unattached straight state when the surface energy parameter $e$ is sufficiently large and much beyond the critical value $e_2$.

For large overlap length such as $\delta / L = 0.8$, however, as marked in Fig.2.7, the surface energy reduction ($\gamma w t$) can be larger than the elastic bending energy of the attached two beams even before the surface energy parameter $e$ reaches the critical value $e_2$ for full adhesion. This is attributed to higher surface energy for adhesion and larger attached length when the full adhesion is approached. It follows that for large overlap lengths such as $\delta / L = 0.8$, the attached state of two beams could be stable for the value of $e$ even smaller than $e_2$, in the sense that the attached state has a negative total energy lower than that of the unattached straight state of two beams (with $V = 0$). Here, it should be reminded that unlike the total energy discussed here, the critical value of surface energy for adhesion discussed in Section 2.3.1 are determined by the rate of change of the total energy rather than by the total energy itself, and the results obtained here are consistent with the results obtained in Section 2.3.1. In fact, cantilevers of smaller or moderate overlap length have smaller release rate of the strain energy and would be

attached at a lower surface energy, and therefore the surface energy reduction is smaller than the strain energy before the full adhesion is reached, because of lower surface energy and shorter attached length. On the other hand, cantilevers of large overlap length have larger release rate of the strain energy and would be attached only at a higher surface energy, and therefore the surface energy reduction is larger than the strain energy when the full adhesion is approached, because of higher surface energy and longer attached length.

Finally, for attached state of two cantilevers of large overlap length, it is seen from Fig.2.7 that the critical value of surface energy parameter $e$ for surface energy reduction larger than elastic bending energy is almost independent of the gap $d/L$. In fact, for $\delta/L$=0.8 and $d/L$=0.1, 0.01 and 0.001, the critical value of $e$ for $(U_1+U_2)/(\gamma wt)<1$ is 6.888, 6.912 and 6.912, respectively, while the associated attached length is always about $t/L$=0.7. We notice that these values of $e$ are even much lower than $e$=18 for initial adhesion of a single cantilever beam attracted by a rigid substrate mentioned above. Again, this result confirms that, compared to a single cantilever attracted by a rigid substrate under otherwise similar conditions, two opposing cantilevers not only request a much lower critical value of surface energy for adhesion, but also have an energetically more stable attached equilibrium state than a single cantilever attached on a rigid substrate.

It should be stated that the analytical models on adhesion [125] suggested in this chapter and the other models on structural instability [126-129] and parametric resonance [130-131] suggested in the following chapters 3-7 would be applicable not only to microbeams but also to nanobeams [133-134]. In particular, it has been well established that attractive van der Waals forces between parallel carbon nanotubes often become the single dominant force in carbon nanotube-based NEMS (nanoelectromechanical systems), and mechanical behavior of carbon nanotubes can be well described by elastic beam models [135-139].

## 2.4 Conclusions

An analytical model is developed for adhesion of two opposing microcantilever beams based on an assumption that elastic bending energy of the attached portion of two beams is negligible. Detailed numerical results are shown for two opposing cantilever beams of equal bending rigidity and length. The present model predicts that the critical values of the surface energy for initial adhesion and full adhesion increase monotonically with increasing overlap length, which suggests that the strength of two opposing cantilevers against adhesion can be enhanced by increasing rather than decreasing the overlap length. In addition, when the surface energy increases from the critical value for initial adhesion to the critical value for full adhesion, the attached length of the two beams increases monotonically and eventually approaches the overlap length. On the other hand, because the adhesion of two beams of large overlap length occurs at higher surface energy and has larger maximum attached length, it can have a lower total energy than an attached state of two beams of small or moderate overlap length as the full adhesion is approached. In particular, the former can be energetically stable while the latter is usually only metastable before the full adhesion is reached. For the first time to our knowledge, the present results show that the critical values for adhesion of two opposing microcantilevers are much lower than the critical values for adhesion of a single microcantilever attracted by a rigid substrate or other similar problems studied in the literature. These results could have relevant consequences to MEMS especially for comb drive design.
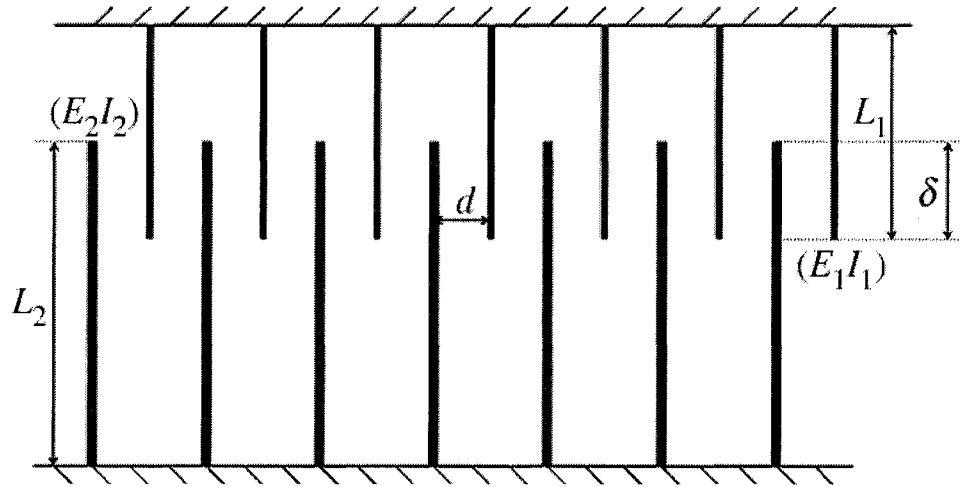
Fig.2.1 Two parallel arrays of microcantilever beams oriented in opposite directions.
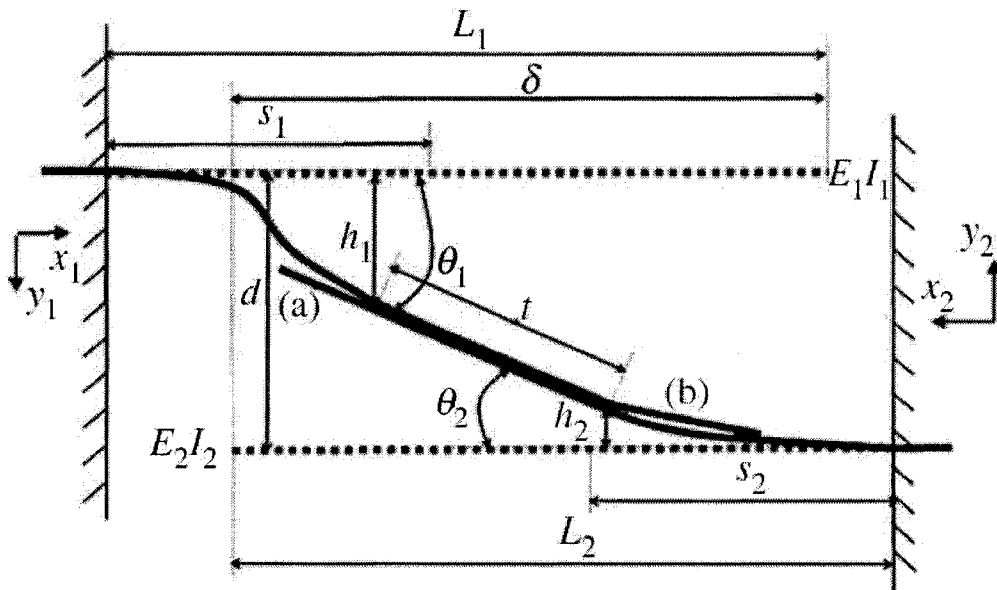


Fig.2.2 Surface energy-driven adhesion of two opposing microcantilever beams.

$$e\left(=\frac{\gamma w L^4}{EId^2}\right)$$
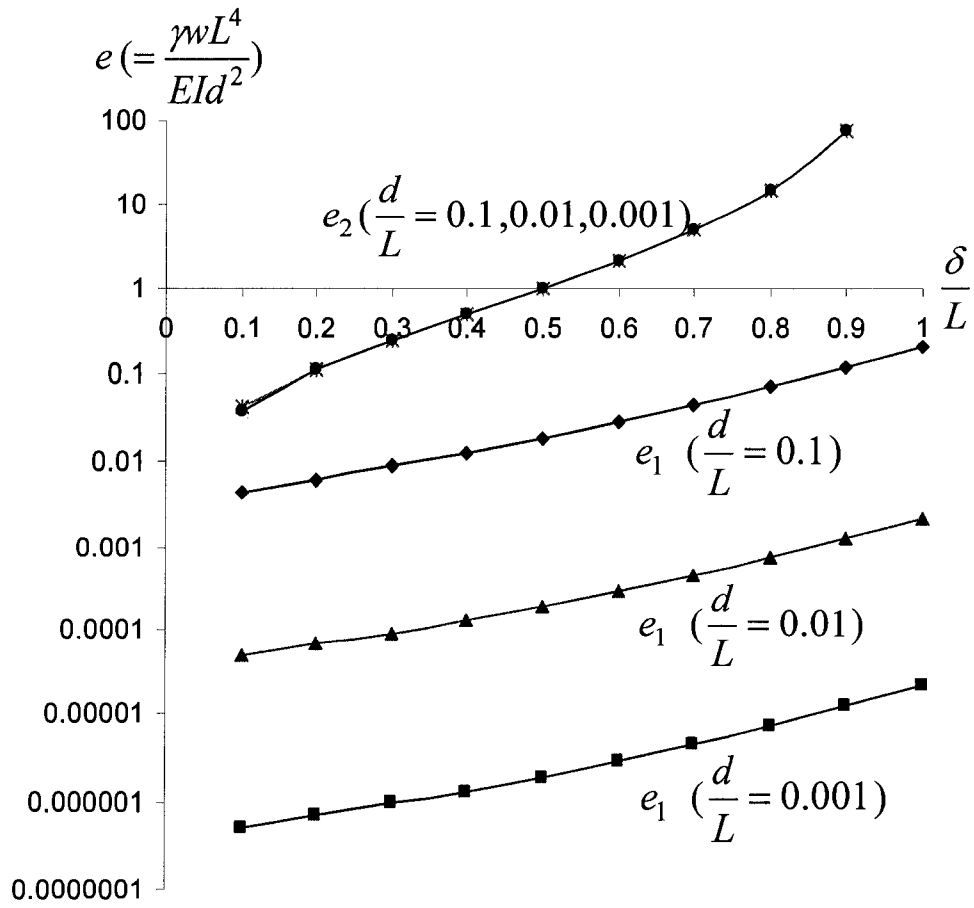
Fig.2.3 Critical values of the surface energy parameter $e$ defined by (2.16) for initial adhesion and full adhesion of two identical beams.
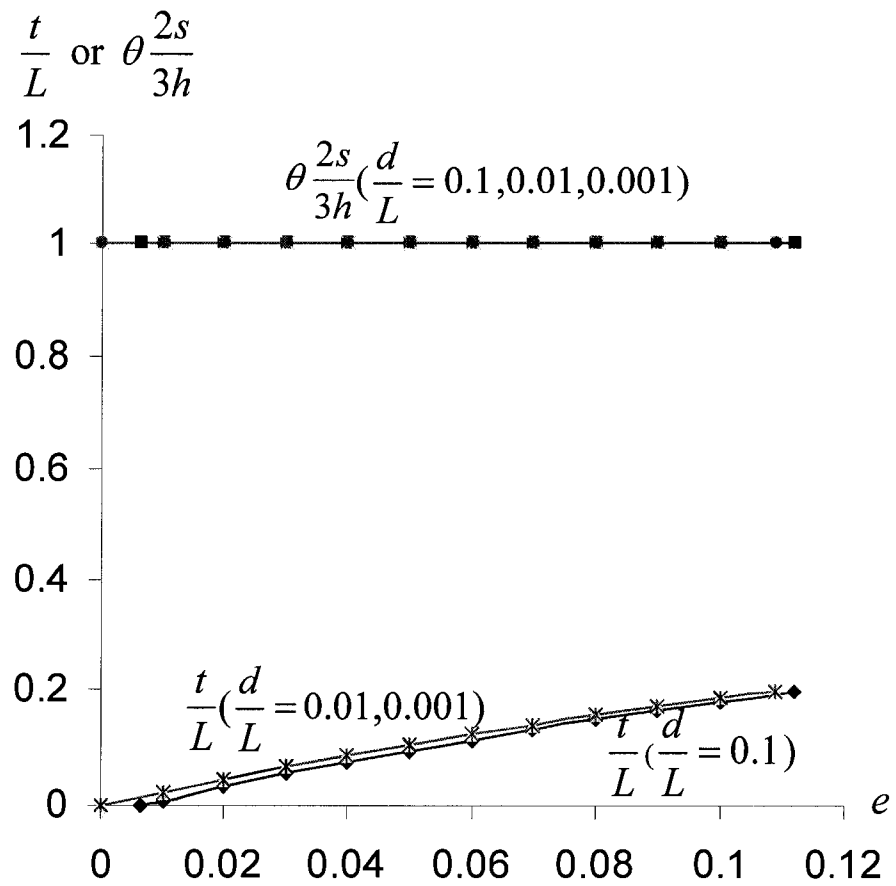
Fig.2.4 Geometric parameters of two attached identical beams when $\delta/L = 0.2$ and $d/L = 0.1$ ( $e_1 = 0.0063$, $e_2 = 0.112$), $d/L = 0.01$ ( $e_1 = 0.00007$, $e_2 = 0.109$), or $d/L = 0.001$ ($e_1 = 0.0000007$, $e_2 = 0.109$).
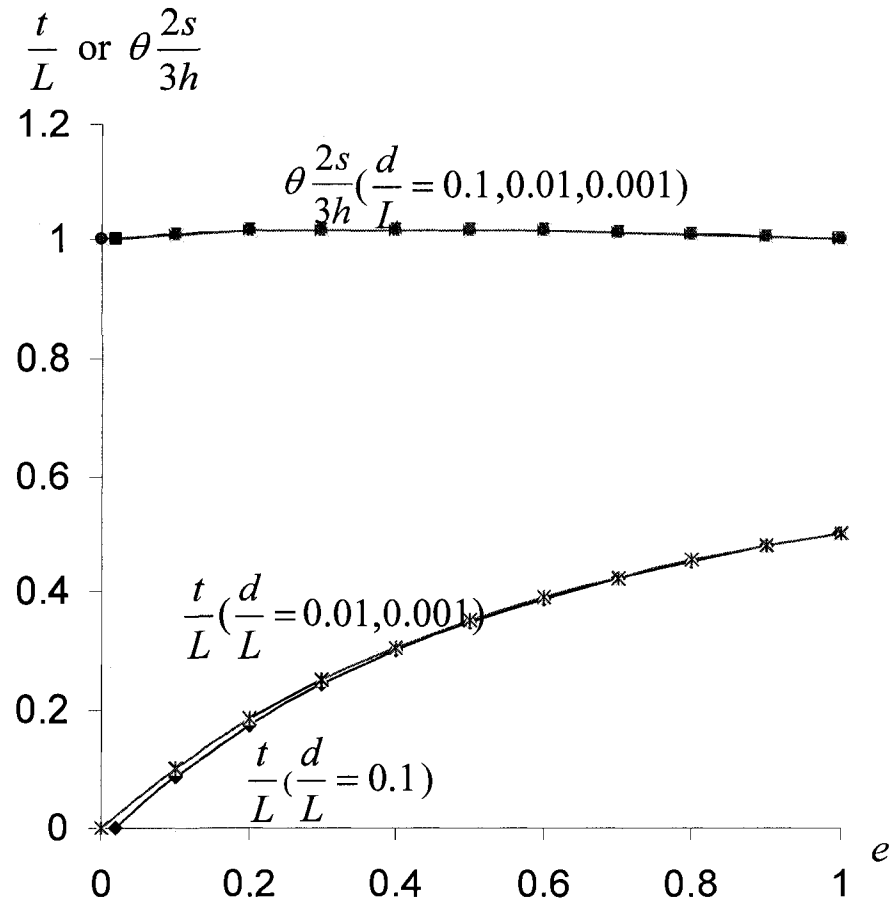
Fig.2.5 Geometric parameters of two attached identical beams when $\delta/L$ =0.5 and $d/L = 0.1$ ( $e_1$ =0.019, $e_2$ =0.996), $d/L$ =0.01 ( $e_1$ =0.00019, $e_2$ =0.999), or $d/L$ =0.001 ($e_1$=0.0000019, $e_2$=0.999).
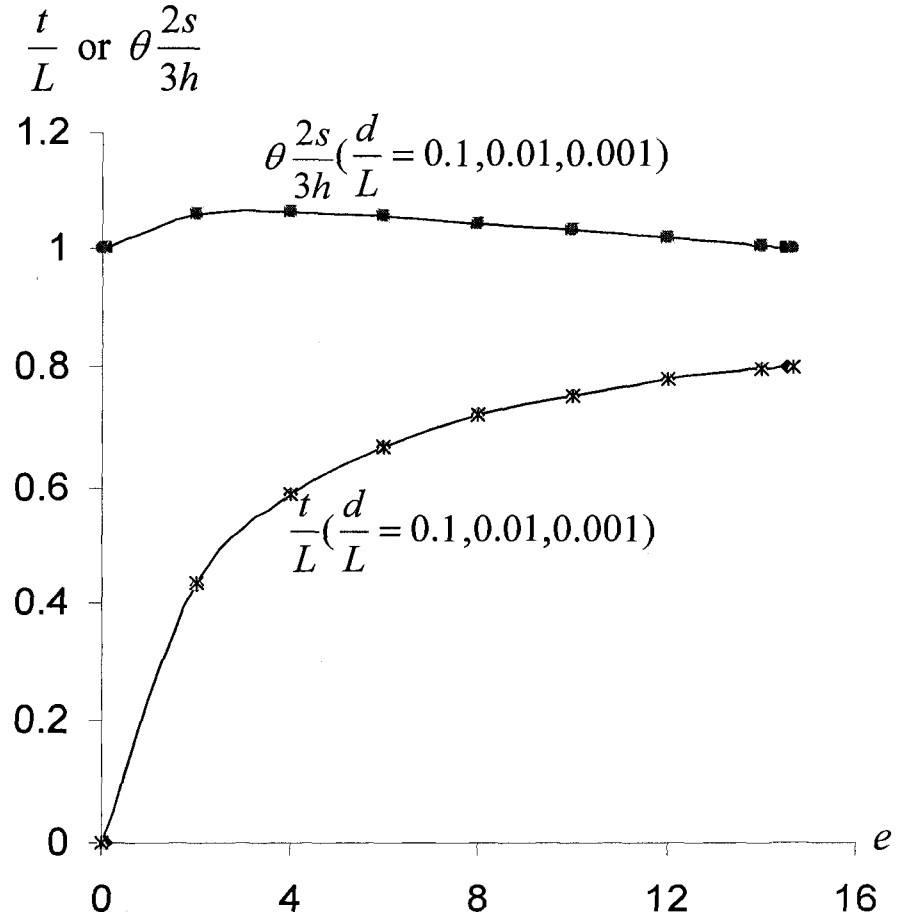
Fig.2.6 Geometric parameters of two attached identical beams when $\delta/L$ =0.8 and $d/L = 0.1$ ( $e_1$ =0.071, $e_2$ =14.508), $d/L$ =0.01 ( $e_1$ =0.00073, $e_2$ =14.647), or $d/L$ =0.001 ($e_1$=0.0000072, $e_2$=14.648).
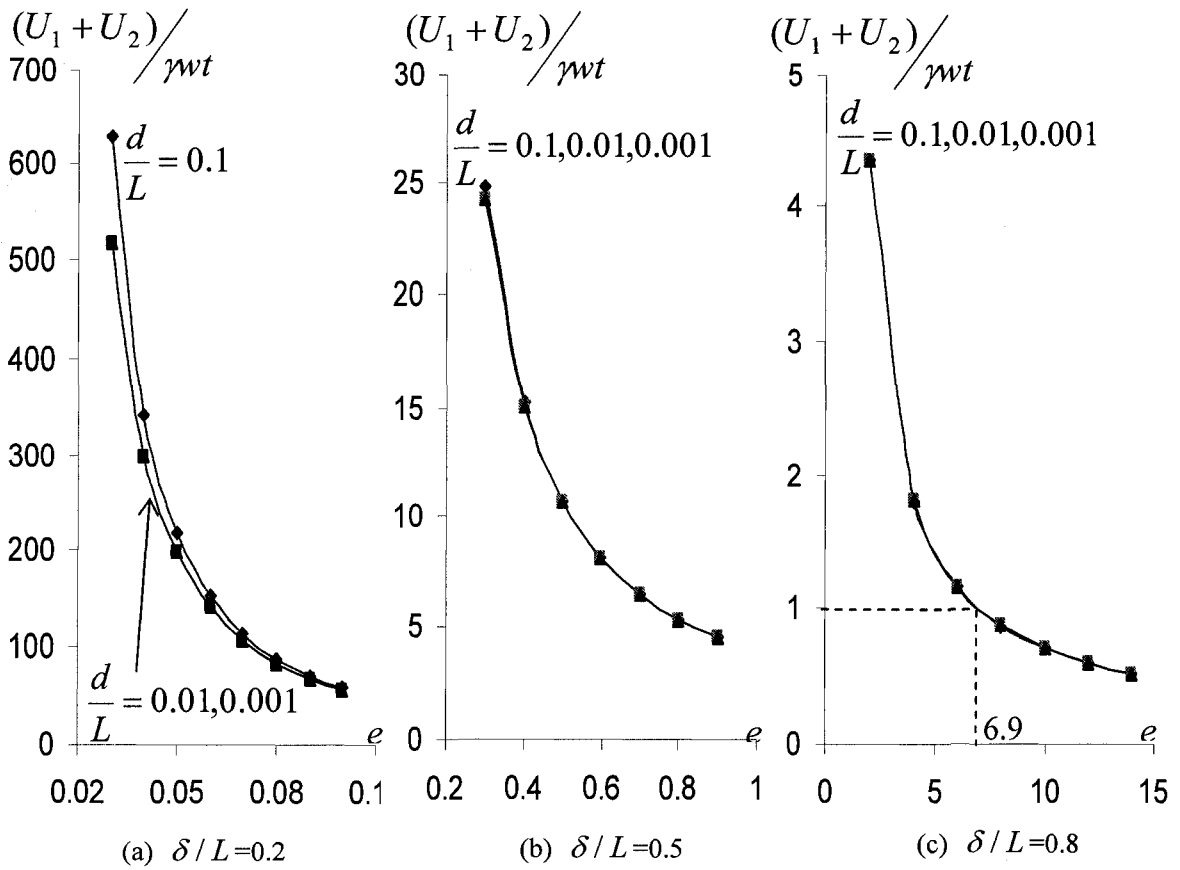
Fig.2.7 The ratio of elastic strain energy to surface energy reduction for two attached identical beams when $d/L$=0.1, 0.01 or 0.001, and $\delta/L$=0.2, 0.5, or 0.8.

# Chapter 3

# Instability of a Parallel Array of Mutually Attracting Identical Microbeams

## 3.1 Introduction

Structural instability of a parallel array of microbeams is an important issue in MEMS design, because it can cause adhesion of adjacent microbeams and even failure of microsystems. Surface attractive forces, such as van der Waals force, electrostatic force, capillary force or Casimir force [51-59, 82-95], play a dominant role in mechanical deformation of microsystems, although they are always ignored in macrosystems. This chapter studies surface forces-driven structural instability of a parallel array of mutually attracting identical microbeams.

Exact structural instability analysis of parallel microbeams under distance-dependent surface attractive forces, as formulated in Section 3.2, raises a challenging nonlinear problem especially when the number of microbeams in the array is large. This probably can explain why, to our best knowledge, this problem has not been studied in detail in the literature. In an attempt to study this problem, we noticed that because the beam-beam interaction is essentially limited to immediately adjacent beams only, each of intermediate beams is attracted by two almost equal but opposite attractions from two neighboring beams. Hence, equilibrium deflections of intermediate beams could be expected to be vanishingly small except the beams at the ends of the parallel array. Although the large deflections of the two beams at the ends of the parallel array, caused by one-side attraction from the adjacent beam, have a non-negligible effect on instability of the parallel array, it is expected that this effect would be relatively small and could be estimated easily when the number $N$ is large. Actually, all of these intuitive ideas are well confirmed by an exact analysis given in Section 3.3 for a simplified yet essentially

similar $N$-spring system.

Based on these concepts, a simple method is developed in this chapter to analyze structural instability of a parallel array of mutually attracting identical microbeams. This method is applied to a few cases of practical significance in Section 3.4, where the end-effect of the beams at the ends of the parallel array is neglected. In section 3.5, the end-effect on the critical interaction coefficient for instability, defined on the initial distance between adjacent beams, is estimated. Finally, in Section 3.6, the results obtained by the present methods are compared to exact results obtained in Section 3.3 for a simplified spring model and some known data available in the literature for a few special cases. All results are summarized in Section 3.7.

## 3.2 Formulation of instability analysis

Consider a parallel array of $N$ mutually interacting identical beams of equal bending rigidity $EI$ and length $L$, as shown in Fig.3.1. Let adjacent beams interact with each other through their interacting area of width $b$. Generally, we assume that the attractive force per unit area between two parallel flat surfaces at any point is a power function of the distance between the two flat surfaces at that point

$$F = c / d^n \tag{3.1}$$

where $c$ is a constant depending on the nature of the interacting force and the materials, $d$ is the distance between the two flat surfaces at that point, and the index $n$ can be 2 (such as electrostatic force), 3 (such as van der Waals force), or 4 (such as Casimir force or retarded van der Waals force) [51-59]. In this chapter, we consider the case in which one of the surface forces is dominant over the others, and thus $n=2$, 3 or 4. In other words, combined effects of more than one type of the surface forces will not be examined in this chapter. Thus, the interacting force per unit axial length between any two adjacent beams is given by

$$f = Fb = C / d^n, \, C=cb \tag{3.2}$$

50

Here, we assume that the distance between the microbeams and other possible surrounding materials (such as a ground plane) is so large that the associated interaction forces can be neglected as compared to the beam-beam interaction. The smallest distance $d$ beyond which the beam-beam interaction can be neglected depends on the index $n$ and the beam material. For example, for van der Waals force ($n=3$), the interaction is usually negligible for most materials when $d$ is larger than 100 nm. In addition, the width $b$ and the length $L$ are assumed to be much larger than the gap $d$ so that the non-uniform interaction effect (such as fringing field, see p1068 [90]) is negligible and the uniform parallel plate model (3.1, 3.2) works well for the beam-beam interaction.

Now, let us consider $N$ parallel mutually interacting beams as shown in Fig.3.1, where $d_0$ is the initial distance between the two flat surfaces of adjacent beams. Assume that $Y_k(x)$ be the equilibrium deflection of beam $k$ ($k=1,2...N$), defined downward positive, under the beam-beam interaction described by (3.2), thus we have

$$EI\frac{d^4Y_k}{dx^4} = P_k \tag{3.3}$$

where $P_k$ is the resultant force per unit axial length acted on beam $k$ due to the interactions with two adjacent beams ($k$-$1$) and ($k$+$1$), given by

$$P_k = \frac{-C}{(d_0 + Y_k - Y_{k-1})^n} + \frac{C}{(d_0 + Y_{k+1} - Y_k)^n} \tag{3.4}$$

where $P_k$ is defined positive along the deflection direction, and $d_0$ is the initial (constant) separation between the surfaces of any two adjacent beams.

Since the equilibrium of $N$ mutually interacting beams leads to a conservative stability problem, pull-in instability of the equilibrium state can be studied by the equilibrium method [140-141]. Thus, an equilibrium state becomes unstable when there exists any adjacent equilibrium state characterized by infinitesimal non-zero deviations

$y_k(x)$ from the equilibrium deflections $Y_k(x)$ ($k$=1,2...$N$). With the infinitesimal deviation $y_k(x)$, the total deflection of beam $k$ is ($Y_k + y_k$) and governed by

$$EI \frac{d^4(Y_k + y_k)}{dx^4} = P_k + p_k \qquad (3.5)$$

where $p_k$ is the additional resultant force per unit axial length acted on beam $k$ due to the deviation deflections of beam $k$ and two adjacent beams ($k$-$1$) and ($k$+$1$), given by

$$p_k = \frac{-C}{(d_0 + Y_k - Y_{k-1} + y_k - y_{k-1})^n} + \frac{C}{(d_0 + Y_{k+1} - Y_k + y_{k+1} - y_k)^n} - P_k \qquad (3.6)$$

Because the deviations $y_k(x)$ are infinitesimal, $p_k$ ($k$=1,2...$N$) given by (3.6) can be expanded in $y_k$. Noticing (3.4) and neglecting all nonlinear terms, we have

$$p_k = A_{k-1,k}(y_k - y_{k-1}) - A_{k,k+1}(y_{k+1} - y_k) \qquad (3.7)$$

where $A_{k-1,k}$, the interaction coefficient between beams ($k$-$1$) and $k$, and $A_{k,k+1}$, the interaction coefficient between beams $k$ and ($k$+$1$), are defined by

$$A_{k-1,k} = \frac{nC}{(d_0 + Y_k - Y_{k-1})^{n+1}}$$

$$A_{k,k+1} = \frac{nC}{(d_0 + Y_{k+1} - Y_k)^{n+1}} \qquad (3.8)$$

Obviously, these interaction coefficients depend on the changed distance between two adjacent beams and thus are usually $x$-dependent. Thus, subtracting (3.5) by (3.3), we obtain the equations for $N$ deviations $y_k(x)$ ($k$=1,2...$N$) as

$$EI\frac{d^4y_k}{dx^4} = A_{k-1,k}(y_k - y_{k-1}) - A_{k,k+1}(y_{k+1} - y_k) \qquad (3.9)$$

Thus, instability of the $N$ parallel beams is defined by the existence of any non-zero solutions $y_k$ of linear equations (3.9) under the associated boundary conditions for beams [140-141]. In general, $N$ coupled nonlinear equations (3.3, 3.4) have to be solved first, to get the equilibrium deflections $Y_k(x)$ ($k=1,2...N$). In addition, because $Y_k(x)$ are $x$-dependent, the interaction coefficients given by (3.8) are $x$-dependent and thus (3.9) becomes variable-coefficient equations for $y_k$ ($k=1,2...N$), which makes the existence of non-zero solutions of (3.9) a technically difficult problem especially when the number $N$ is large.

In this chapter, a novel approximate method is developed based on a simple observation. In many MEMS problems, the number $N$ of parallel microbeams is usually large. In this case, because the beam-beam interaction defined by (3.2) is essentially limited to immediately adjacent beams only, for each of intermediate beams, the two interactions from two adjacent beams on opposite sides would be almost equal but opposite and thus could cancel each other. Hence, it is expected that equilibrium deflections of all intermediate beams would be negligibly small except the two beams at the ends of the parallel array ($k=1$ and $k=N$). Because exact analysis of mutually attracting parallel beams is technically difficult especially when the number $N$ is large, this intuitive idea will be studied in detail for a simplified yet essentially similar system of $N$ mutually attracting springs.

## 3.3 Instability of a simplified $N$-Spring system

To confirm the above idea, let us consider $N$ equally spaced and mutually attracting springs of identical spring constant $q$, shown in Fig.3.2. Let all springs be arranged along a straight line from $k=1$ (left end) to $k=N$ (right end), the displacement of the $k$-th spring is $Y_k$ (defined right positive), and any two adjacent springs are attracted each other through the force $f = M/d^n$, where $M$ is a constant and $d$ is the distance between the two springs. Equilibrium of the $N$ mutually attracting springs under spring-spring

attraction is governed by $N$ dimensionless nonlinear equations for $N$ unknowns $Y_k / d_0$ ($k$=1,2...$N$)

$$-\frac{Y_1}{d_0} + \frac{B}{(1 + \frac{Y_2}{d_0} - \frac{Y_1}{d_0})^n} = 0 , \ k=1, \tag{3.10}$$

$$-\frac{Y_k}{d_0} + \frac{B}{(1 + \frac{Y_{k+1}}{d_0} - \frac{Y_k}{d_0})^n} - \frac{B}{(1 + \frac{Y_k}{d_0} - \frac{Y_{k-1}}{d_0})^n} = 0 , \ k=2,...,N\text{-}1, \tag{3.11}$$

$$-\frac{Y_N}{d_0} - \frac{B}{(1 + \frac{Y_N}{d_0} - \frac{Y_{N-1}}{d_0})^n} = 0 , \ k=N, \tag{3.12}$$

where the constant $B = \dfrac{M}{qd_0^{n+1}}$ is the interaction coefficient defined by the initial

distance $d_0$ between adjacent springs, which represents the intensity of the interaction between neighboring springs. The displacements of the springs increase gradually with the value of $B$ when $B$ is sufficiently small. On the other hand, when $B$ reaches a certain critical value, an instability occurs and then the displacements of the springs suffer a jump and lead to a collision of some adjacent springs. This critical value of $B$ depends on the index $n$. For example, prior to the instability, the displacements $Y_k / d_0$ ($k$=1,2...$N$) determined by nonlinear equations (3.10-3.12), obtained by iteration method, are shown in Fig.3.3 for $N$=20 with $n$=2 and $B$=1/12, $n$=3 and $B$=1/22, and $n$=4 and $B$=1/28, respectively. As expected, it is seen from Fig.3.3 that accurate equilibrium displacements of almost all intermediate springs are negligibly small, and even the two springs ($k$=2 and $k$=$N$-1) adjacent to the end spring have a relatively small displacement compared to the displacement of the end springs (k=$1$ and k=$N$). Similar results can be obtained for larger number $N$. This result for the $N$-spring system suggests that equilibrium displacements of all intermediate beams of a parallel array of mutually attracting microbeams should be negligibly small because the two attractions from two adjacent beams on opposite sides are almost equal but opposite and thus cancel each other.

This simple observation can be used to largely simplify the analysis of instability and achieve a simple approximate instability criterion with reasonable accuracy. To see this, let us consider infinitesimal deviations $y_k$ of $N$ springs from their equilibrium positions defined by $Y_k$ and study the existence of equilibrium non-zero deviations $y_k$ ($k$=1,2...$N$). First, let us neglect the end effect and then $Y_k$=0 for $k$=1,2...$N$, and thus expand equilibrium equations (3.10-3.12) at the zero-displacement position, the equilibrium equations for infinitesimal deviations $y_k$ ($k$=1,2...$N$) are obtained as

$$-\frac{y_1}{d_0} - nB(\frac{y_2}{d_0} - \frac{y_1}{d_0}) = 0 \, , \, k\text{=}1, \tag{3.13}$$

$$-\frac{y_k}{d_0} - nB(\frac{y_{k+1}}{d_0} - \frac{y_k}{d_0}) + nB(\frac{y_k}{d_0} - \frac{y_{k-1}}{d_0}) = 0 \, , \, k\text{=}2,\ldots, N\text{-}1, \tag{3.14}$$

$$-\frac{y_N}{d_0} + nB(\frac{y_N}{d_0} - \frac{y_{N-1}}{d_0}) = 0 \, , \, k\text{=}N, \tag{3.15}$$

The minimum value of ($nB$) for the existence of non-zero solutions $y_k$ ($k$=1,2...$N$) of (3.13-3.15) is shown in Fig.3.4 for increasing number $N$. It is seen from Fig.3.4 that non-zero solutions of (3.13-3.15) exist for sufficiently large number $N$ when ($nB$) is bigger than ¼. This means that when the end-effect is neglected, $1/(4n)$ is the approximate critical value of $B$ for instability of the equilibrium position of the $N$-spring system, characterized by vanishingly small displacements of intermediate springs such as those shown in Fig.3.3. This approximate instability criterion, which is based on (3.13-3.15) and neglects the end-effect of the beams at the two ends of the parallel springs, gives $B$=1/8 for $n$=2, $B$=1/12 for $n$=3, and $B$=1/16 for $n$=4.

For the actual spring system described by nonlinear equations (3.10-3.12) with the end-effect, however, our numerical results (not shown here) based on exact nonlinear equations (3.10-3.12) show that the accurate critical value of $B$ for instability of the equilibrium position of the $N$-spring system, characterized by vanishingly small displacements of intermediate springs such as those shown in Fig.3.3, is very close to $B$=1/11 for $n$=2, $B$=1/15.8 for $n$=3, and $B$=1/20.6 for $n$=4, which are about 22%-27%

lower than the values given by the above approximate instability criterion without considering the end-effect. This is due apparently to the fact that the above approximate criterion, based on equations (3.13-3.15), neglects the large displacements of the two springs at the two ends of the $N$-spring system. In other words, although neglecting vanishingly small displacements of intermediate springs will not lead to significant errors, neglecting the large displacements of the two springs ($k$=1 and k=$N$) at the ends of the $N$-spring system, each of which is attracted by its adjacent spring from one side only, will lead to a higher critical value for instability. Indeed, as will be shown in Section 3.6, including the end-effect of the two springs at the two ends of the $N$-spring system will lower the critical value and lead to a critical value of $B$ which is very close to the exact numerical result obtained for the $N$-spring system.

## 3.4 Instability of parallel microbeams without the end-effect

Now let us return to the parallel microbeams problem. The above exact analysis for a simplified yet similar $N$-spring system suggests that equilibrium deflections of all intermediate beams, except the beams at the two ends of the parallel array, can be assumed to be negligibly small. Based on this idea, in this section, we shall first neglect the end-effect of the beams at the two ends and assume that equilibrium deflections of all beams ($k$=1,2...$N$) are neglected. Thus, it is seen from (3.8) that all beam-beam interaction coefficients are equal and constant, that is $A_{1,2} = A_{2,3} = ... = A_{N-1,N} = A_0$, where

$A_0$ is a constant defined based on the initial separation $d_0$ as follow

$$A_0 = \frac{nC}{d_0^{n+1}} \tag{3.16}$$

Throughout the chapter, the constant $A_0$ defined by (3.16) represents the intensity of the beam-beam interaction, and thus the onset of instability will be defined by a critical value of $A_0$. With $A_{1,2} = A_{2,3} = ... = A_{N-1,N} = A_0$, equations (3.9) now become

$$EI\frac{d^4 y_k}{dx^4} = A_0(y_k - y_{k-1}) - A_0(y_{k+1} - y_k) = -A_0(y_{k+1} + y_{k-1} - 2y_k) \qquad (3.17)$$

The end-effect on the critical value of $A_0$ for instability of the parallel array of microbeams will be studied in Section 3.5.

## *a)* Hinged beams

Since simple exact formulas are available only for hinged beams, let us begin with the case a) in Fig.3.1. For a single hinged beam ($N$=1) attracted by a rigid beam through an arbitrary constant interaction coefficient $A$, its deflection $y(x)$ is governed by

$$EI\frac{d^4 y}{dx^4} = Ay \qquad (3.18)$$

Let $y = \sin(m\pi x/L)$ ($m$=1,2...), one finds that the (lowest) eignevalue is

$$A = A_1 = EI(\pi/L)^4, N=1 \qquad (3.19)$$

When two mutually attracting beams, through a constant interaction coefficient $A$, are considered ($N$=2), we have

$$EI\frac{d^4 y_1}{dx^4} = A(y_1 - y_2), \quad EI\frac{d^4 y_2}{dx^4} = A(y_2 - y_1) \qquad (3.20)$$

The lowest eigenvalue of $A$ is given by

$$A = A_2 = EI(\pi/L)^4/2, N=2 \qquad (3.21)$$

Similarly, for example, one can consider 3, 4, 5, 10, 20 or 50 beams with an arbitrary constant interaction coefficient $A$ between any two adjacent beams. It is seen from the

results shown in Fig.3.5 $a$) that the critical value of $A$ for instability of $N$ mutually attracting beams decreases with increasing number of beams $N$, and approaches a quarter of the critical value $A_1$ given by (3.19) for a single hinged beam attracted by a rigid body, or a half of the critical value $A_2$ given by (3.21) for two interacting hinged beams. In other words, when the end-effect is neglected, the critical value of the (constant) interaction coefficient for structural instability of a parallel array of identical hinged beams is given by

$$A = A_\infty = A_1 / 4 = A_2 / 2 = EI(\pi / L)^4 / 4 \qquad (3.22)$$

Hence, it is concluded that when the end-effect is neglected and all interaction coefficients are equal to $A_0$ defined by (3.16) based on the initial separation $d_0$, a parallel array of hinged microbeams becomes unstable when the value of $A_0$ reaches the critical value $A_\infty$ given by (3.22), see Fig.3.5. In addition, it is found that the deflections of any two adjacent beams associated with the instability are always equal but opposite when the number $N$ of beams increases infinitely.

## $b$) Clamped beams

Similar results for clamped beams with an arbitrary constant interaction coefficient $A$ when $N=1$ or 2 can be obtained by the Galerkin method (the details are omitted here), with the result

$$A = A_1 = 5.139EI(\pi / L)^4, N=1 \qquad (3.23)$$

$$A = A_2 = 2.569EI(\pi / L)^4, N=2 \qquad (3.24)$$

When $N$ is large, similar results are shown in Fig.3.5 $b$). Again, the critical value of $A$ for instability of $N$ mutually attracting clamped beams decreases with the increasing number of beams $N$, and approaches one quarter of the critical value (3.23) given for a single clamped beam attracted by a rigid body, or a half of the critical value (3.24) given for two

interacting clamped beams. In other words, the critical value of A for instability of $N$ mutually attracting clamped beams is given by

$$A = A_{\infty} = A_1 / 4 = A_2 / 2 = 1.285 EI (\pi / L)^4 \qquad (3.25)$$

Thus, it is concluded that when the end-effect is neglected and all interaction coefficients are equal to $A_0$ defined by (3.16) based on the initial separation $d_0$, a parallel array of clamped microbeams becomes unstable when the value of $A_0$ reaches the critical value $A_{\infty}$ given by (3.25), see Fig.3.5. In addition, the deflections of any two adjacent clamped beams associated with the instability are always equal but opposite when the number $N$ of beams increases infinitely. Here, for clamped beams (and immovable hinged beams), possible initial axial stress (or called "residual stress") and its nonlinear dependence on axial stretching strain (or called "stress stiffening") due to bending deflection are neglected based on the assumption of linearized small deflections. In particular, this assumption is consistent with the small-gap assumption on which the fringing field effect is omitted.

## *c*) **Cantilever beams**

Parallel array of microcantilevers is of major significance compared to hinged or clamped ones, due to its common uses in MEMS. Similar results for cantilever beams with an arbitrary constant interaction coefficient $A$ when $N$=1 or 2 are

$$A = A_1 = 0.127 EI (\pi / L)^4 , N=1 \qquad (3.26)$$

$$A = A_2 = 0.063 EI (\pi / L)^4 , N=2 \qquad (3.27)$$

When $N$ is very large, similar results are shown in Fig.3.5 $c$). Again, the critical value of $A$ for instability of $N$ mutually attracting cantilever beams decreases with the increasing number of beams $N$, and approaches one quarter of the critical value (3.26) given for a single cantilever beam attracted by a rigid body, or a half of the critical value (3.27) given for two interacting cantilever beams. In other words, the critical value of $A$ for instability

of $N$ mutually attracting cantilever beams is

$$A = A_\infty = A_1 / 4 = A_2 / 2 = 0.032 EI (\pi / L)^4 \qquad (3.28)$$

It is concluded that when the end-effect is neglected and all interaction coefficients are equal to $A_0$ defined by (3.16) based on the initial separation $d_0$, a parallel array of microcantilevers becomes unstable when the value of $A_0$ reaches the critical value $A_\infty$ given by (3.28), see Fig.3.5. Similar to hinged and clamped beams, the deflections of any two adjacent beams associated with the instability are always equal but opposite when the number $N$ of cantilever beams increases infinitely.

## 3.5 The end-effect on instability

All results of Section 3.4 are based on a simplification that equilibrium deflections of all beams (including the two end beams) are neglected, which implies that all interaction coefficients defined by (3.8) are given approximately based on the unchanged gap $d_0$ and thus $A_{1,2} = A_{2,3} = ... = A_{N-1,N} = A_0$, where $A_0$ defined by (3.16) represents the intensity of the beam-beam interaction. As shown in Fig.3.3 in Section 3.3 for a simplified $N$-spring system, this assumption is valid for almost all intermediate beams which have two adjacent beams from two opposite sides, but invalid for the beams at the ends of the parallel array especially for the two end beams ($k=1$ and $k=N$). To achieve a more accurate approximate method, therefore, we now consider the end-effect and assume that only the distance change between any two adjacent intermediate beams ($k=2...N$-1) can be neglected, and then $A_{2,3} = A_{3,4} = ... = A_{N-2,N-1} = A_0$, where $A_0$ is a constant defined by (3.16) based on the initial separation $d_0$.

On the other hand, because each of the two end beams at the ends of the parallel array ($k=1$ or $N$) is attracted by its adjacent beam from one side only, it has a non-negligible deflection. In particular, it follows from the symmetry that $Y_1(x) > 0$ and $Y_N(x) = -Y_1(x) < 0$ for sufficiently large $N$. In addition, the non-negligible deflection of the end beam ($k=1$ or $N$) will cause a stronger attraction to its neighboring beam ($k=2$ or

$N$-1) and, consequently, the neighboring beam ($k$=2 or $N$-1) will be attracted to the end beam and thus we have $Y_2(x) < 0$ and $Y_{N-1}(x) = -Y_2(x) > 0$. Therefore, $A_{1,2}$, the interaction coefficients between the end beam ($k$=1) and its neighboring beam ($k$=2), and $A_{N-1,N}$, the interaction coefficients between the end beam ($k$=$N$) and its neighboring beam ($k$=$N$-1), are equal and given by

$$A_{1,2}(x) = A_{N-1,N}(x) = \frac{nC}{(d_0 + Y_2(x) - Y_1(x))^{n+1}} = \frac{nC}{(d_0 + Y_N(x) - Y_{N-1}(x))^{n+1}}, 0 \leq x \leq L \quad (3.29)$$

Obviously, because $Y_1(x) - Y_2(x) > 0$ (or $Y_N(x) - Y_{N-1}(x) < 0$ ), the $x$-dependent interaction coefficient $A_{1,2}(x) = A_{N-1,N}(x)$ for the two beams at each of the ends of the parallel array at the onset of instability depends on the reduction of the distance between the two beams and can be much larger than the constant $A_0$ defined by (3.16) based on the initial separation $d_0$. In this chapter, the $x$-dependent amplified interaction coefficients $A_{1,2}(x) = A_{N-1,N}(x)$, at the onset of instability for the two beams at each of the ends, will be replaced approximately, based on an estimate of the average reduction of the distance over the beams, by a constant amplified factor $\alpha$ defined as

$$A_{1,2} = A_{N-1,N} \approx \alpha A_0, \quad \alpha > 1 \quad (3.30)$$

As shown below, the amplified factor $\alpha$ can be calculated approximately based on an estimated average value of the reduction of the distance between the end beam and its adjacent beam at the onset of instability.

In doing so, the end-effect on instability of a parallel array of microbeams can be studied by examining the dependence on the amplified factor $\alpha$ of the critical value of $A_0$ for the existence of non-zero solutions $y_k$ ($k$=1,2...$N$) of linear constant-coefficient equations (3.9) with the coefficients $A_{2,3} = A_{3,4} = ... = A_{N-2,N-1} = A_0$, where $A_0$ is defined by (3.16) based on the initial separation $d_0$, and the coefficients

$A_{1,2} = A_{N-1,N} = \alpha A_0$, where the amplified factor $\alpha$ is defined by (3.29, 3.30) and will be estimated approximately later.

## 3.5.1 Estimate of the amplified factor $\alpha$

In order to estimate the amplified factor $\alpha$ for the interaction coefficient between the two beams at each of the two ends, we have to estimate the distance reduction between the end beam and its adjacent beam at the onset of instability and the influence of the distance reduction on the amplified factor $\alpha$ defined by (3.29, 3.30). Since the deflection of the beam adjacent to the end beam is relatively small, as a crude estimate, it can be taken as approximately zero. Thus, the deflection of the end beam can be roughly estimated by considering the end beam as a single beam attracted by a rigid body. With this method, the deflection of the end beam can be estimated based on the nonlinear equations (3.3, 3.4). Here, of major concern is the case $c$) of Fig.3.1 (microcantilevers), due to the popularity of microcantilevers in MEMS and the susceptibility of microcantilevers to surface force-driven instability and adhesion.

For a single cantilever beam attracted by a rigid body, Johnstone & Parameswaran [86] have studied the deflection of the cantilever attracted by electrostatic ($n$=2) or Casimir ($n$=4) forces, as a function of an interaction coefficient equivalent to the constant $A_0$ defined by (3.16) in this chapter, see their figures 2 and 4 of [86]. Hence, their numerical results can be used to approximately estimate the amplified factor $\alpha$. For example, Johnstone & Parameswaran showed that the actual maximum deflection of the cantilever beam when instability occurs is about $0.3 d_0$ (for $n$=4) or $0.47 d_0$ (for $n$=2), where $d_0$ is the initial separation between the surfaces of the cantilever beam and the rigid body. Since the deflection of a cantilever at its fixed end is always zero, average value of the deflection could be defined by a half of the free-end maximum deflection. However, because the free-end interaction plays a dominant role in instability of a cantilever, it seems reasonable to assume that the average deflection of a cantilever should be defined by a value that is slightly larger than a half of the free-end deflection, say, by 2/3 of the free-end deflection. In doing so, the average deflection of a single cantilever attracted by a rigid body at the onset of instability should be about $0.2 d_0$ (for

$n$=4) or $0.31d_0$ (for $n$=2). Because $1/(1-0.2)^5 \approx 3.0$ and $1/(1-0.31)^3 \approx 3.1$, it follows from (3.29, 3.30) that the actual interaction coefficient between the single cantilever beam and the rigid substrate at the onset of instability of the single cantilever beam is about three times the constant $A_0$ defined by (3.16) based on the initial separation $d_0$. On the other hand, because the critical value for instability of a parallel array of mutually attracting cantilevers is lower than the critical value for a single cantilever attracted by a rigid body under otherwise identical conditions, the amplified factor $\alpha$ for each of the two end beams when the instability of parallel beams occurs should be smaller than 3. In fact, the results of Section 3.6 shown below for the simplified $N$-spring system indicate that the amplified factor $\alpha$ for the end springs at the onset of instability of the $N$-spring system is about 1.9 to 2.1, depending on the index $n$ and approximate methods. Therefore, it is concluded that the amplified factor $\alpha$ for the end beams at the onset of instability of a large parallel array of microbeams should be not larger than 3.

## 3.5.2 Effect of the amplified factor $\alpha$ on the critical value

Because the end effect actually leads to an amplified interaction coefficient for the two end beams, the approximate critical value given in Section 3.4, which neglects the end-effect, would be higher than the actual critical value for instability. In other words, the actual critical value of $A_0$ for instability of the parallel microbeams with the end-effect will be lower than the approximate critical value of $A_0$ without the end-effect estimated in Section 3.4. Therefore, the actual critical value with the end-effect can be given through an end-effect factor $\varepsilon$ by

$$A_0 = \varepsilon A_\infty, \quad 0 < \varepsilon < 1 \tag{3.31}$$

where $A_\infty$ is the critical value without the end-effect, given by (3.22), (3.25) or (3.28) for case $a$), $b$) or $c$), respectively.

To quantify the dependence of end-effect factor $\varepsilon$ on the amplified factor $\alpha$, we compare the critical value of $A_0$ obtained in Section 3.4 without the end-effect, to the

critical value of $A_0$ for the existence of non-zero solutions $y_k$ ($k=1,2...N$) of equations

(3.9) with $A_{2,3} = A_{3,4} = ... = A_{N-2,N-1} = A_0$ and $A_{1,2} = A_{N-1,N} = \alpha A_0$, where $A_0$ is

defined by (3.16) based on the initial distance $d_0$. The end-effect factor $\varepsilon$ due to the

end-effect, as a function of the amplified factor $\alpha$ (>1), is shown in Fig.3.6 for all three

cases $a$), $b$) and $c$). It is seen from Fig.3.6 that the amplified factor $\alpha$ has a

non-vanishing effect on the critical value of $A_0$ when the number $N$ increases to infinity.

In particular, this effect, represented by the dependency of the end-effect factor $\varepsilon$ on the

amplified factor $\alpha$, is almost identical for three different cases $a$), $b$) and $c$). Thus, with

estimated amplified factor $\alpha$, the actual critical value with the end-effect can be

estimated by Fig.3.6. For instance, if the amplified factor $\alpha$ for the end beams of

parallel microcantilevers is 2, the end-effect factor $\varepsilon$ determined by Fig.3.6 is 0.8,

which implies that the critical value of $A_0$ for the parallel array of microcantilevers with

the end-effect is 20% lower than the approximate critical value of $A_0$ without the

end-effect given by (3.28). On the other hand, if the amplified factor is 3, the end-effect

factor $\varepsilon$ determined by Fig.3.6 is 0.6, which implies that the critical value of $A_0$ with

the end-effect is 40% lower than the approximate value given by (3.28) without the

end-effect. In particular, as explained before, the actual amplified factor is not larger than

3 when the number $N$ is large. Consequently, the actual critical value of $A_0$ for large

parallel arrays is not less than $0.6 A_\infty$, where $A_\infty$ is the critical value without the

end-effect, given by (3.22), (3.25) or (3.28) for case $a$), $b$) or $c$). For example, for a large

cantilever array, the present method predicts that a conservative estimate of the critical

value for instability is given by $0.6 A_\infty = 0.0192 EI(\frac{\pi}{L})^4$.

The approximate method developed here offers a simple design criterion for (static)

pull-in instability of mutually attracting parallel microbeams (such as electrically coupled

array of cantilever or doubly-clamped microbeams recently fabricated in [102-103]), with

controlled errors and acceptable accuracy. For example, when the interaction law (3.1) or

(3.2) is given, the criterion (31) determines a critical separation $d_0$ below which the

instability occurs. On the other hand, when the separation $d_0$ is given, the criterion

(3.31) determines a critical value for the constant $C$ of the power law (3.1) or (3.2) determined by, for example, the Hamaker constant of the van der Waals forces, or the applied electrical voltage for electrostatic forces, beyond which the instability occurs. It is believed that the model for multiple cantilevers is highly relevant for comb structures, which are much applied in MEMS devices for electrostatic actuation and capacitive detection.

## 3.6 Comparisons with exact results and known data

To demonstrate the effectiveness of the present method, an attempt has been made to compare our results with available known data. Unfortunately, to our best knowledge, only few related data are available in the literature, and most of them are limited to a single beam interacting with a rigid substrate. Here, let us first apply the present method to the simple $N$-spring system and compare our results with the exact results obtained by iteration method.

### 3.6.1 Comparison with exact results of the $N$-spring system

First, let us consider a single spring attracted by a fixed point with $n=2$. Thus, with $N=1$ and $Y_2 = 0$, Eqn. (3.10) with $n=2$ gives $B = \frac{Y_1}{d_0}(1 - \frac{Y_1}{d_0})^2$. It can be easily verified that the maximum value of $B$ for $0 \le \frac{Y_1}{d_0} \le 1$ is $B = \frac{4}{27}$, which indicates instability of the spring and is attained at $\frac{Y_1}{d_0} = \frac{1}{3}$. According to the present methods, when the end-effect is neglected and then the change in gap $d$ is neglected, it is seen from Fig.3.4 that the critical value for instability when $N=1$ is $B=1/2$. However, because the gap is reduced by $\frac{d_0}{3}$ at instability, the amplified factor $\alpha$ for the interaction coefficient is

$1 \Big/ (2/3)^3 = \frac{27}{8}$ (see the definition of $B$ based on the gap $d$). Since the end-effect factor $\varepsilon = 1/\alpha$ for the case of single degree of freedom, the actual interaction coefficient for instability is determined by $27B/8=1/2$, which gives $B=4/27$, in perfect agreement with

the above exact value. It can be verified that this result is identical to the well-known formula for instability of a suspended electrode attracted by a fixed electrode (see e.g. [17]). Therefore, in the simplest case of single degree of freedom, the present approximate methods lead to the exact result provided that the exact amplified factor $\alpha$ is known.

For the $N$-spring system, as shown in Fig.3.4, the critical value of $B$ for instability of the spring system without the end-effect, as the lowest eigenvalue of equations (3.13-3.15), is $1/(4n)$ which is about 22%-27% higher than the actual critical value without neglecting the end-effect. To study the end effect, it is noticed from Fig.3.3 that although the displacements of almost all intermediate springs are negligibly small, the spring ($k=2$) adjacent to the end spring ($k=1$) does have a significant (negative) displacement which could affect the distance between spring 1 and spring 2 and thus amplify the interaction coefficient between the two springs.

Thus, to estimate the distance reduction between the two springs at each of the ends, we neglect the deflection of the spring $k=3$ and consider the first two equation of (3.10-3.12) with $Y_3 = 0$. Numerical results indicate that when $B=1/11$ and $n=2$, the distance reduction between spring 1 and spring 2 is estimated by $(Y_1 - Y_2) \approx 0.22$, which leads to an amplified factor $\alpha \approx 2.1$. Similarly, for $B=1/15.8$ and $n=3$, numerical results give $(Y_1 - Y_2) \approx 0.16$, which leads to an amplified factor $\alpha \approx 2.0$, and for $B=1/20.6$ and $n=4$, $(Y_1 - Y_2) \approx 0.12$ which leads to an amplified factor $\alpha \approx 1.9$. In fact, exact iteration method shows that the actual distance reduction between the end spring and its neighboring spring is $0.24 d_0$ for $n=2$ and $B=1/11$, $0.18 d_0$ for $n=3$ and $B=1/15.8$, or $0.14 d_0$ for $n=4$ and $B=1/20.6$, which lead to the amplified factor 2.3, 2.2 or 2.1, respectively. Therefore, the approximate estimate based on the first two equations of (3.10-3.12) with $Y_3 = 0$ leads to relative errors around 10%.

To study the end-effect of the $N$-spring system, we examine the existence of non-zero solutions of (3.13-3.15) with an amplified factor $\alpha$ for the interaction coefficients between the two springs at each of the two ends. Thus, the end-effect factor $\varepsilon$, defined by the ratio of the critical value of $B$ with the end-effect ($\alpha > 1$) to the critical value of $B$ without the end-effect ($\alpha = 1$), is calculated as a function of the amplified

factor $\alpha$. It is found that the dependence of the end-effect factor $\varepsilon$ on the amplified factor $\alpha$ for the $N$-spring system is almost identical to Fig.3.6 obtained for parallel array of mutually attracting microbeams. Hence, Fig.3.6 can also be applied to the $N$-spring system. Thus, because the estimated amplified factor $\alpha$ is about 2.1, 2.0, or 1.9, for $n$=2, 3 or 4, respectively, it follows from Fig.3.6 that the estimated end-effect factor $\varepsilon$ is about 0.78, 0.80, 0.83 for $n$=2, 3, or 4. Thus, the present method predicts that the critical value of $B$ for instability of the $N$-spring system is about 1/10.12, 1/14.64, or 1/18.83 for $n$=2, 3 or 4, respectively. On the other hand, if the accurate amplified factor $\alpha$ =2.3, 2.2 or 2.1 is used to estimate the end-effect factor $\varepsilon$, the present method gives the critical value of $B$ as 1/10.81, 1/15.58 or 1/20.24, which are very close to the exact critical value of $B$ with relative errors less than 2%, as shown in Table 3.1. Therefore, the relative errors of the present method for the spring system are less than 2% or 10%, depending on whether the accurate amplified factor $\alpha$ is known or must be estimated approximately by a simple method based on the first two equations of (3.10-3.12) with $Y_3 = 0$.

## 3.6.2 Comparison with available known data

For a single cantilever beam attracted by a rigid substrate through Casimir force ($n$=4), Johnstone & Parameswaran [86] showed that instability will occur when the free-end (maximum) deflection reaches about $0.3 \, d_0$ (see figure 2 of [86]). As explained above, it seems reasonable to define the average deflection of a single cantilever by 2/3 of its free-end deflection. This means that instability of a single cantilever occurs when its average defelction reaches $0.2 \, d_0$. Thus, because $1/(1-0.2)^5 \approx 3$, the actual interaction coefficient between a single beam and a rigid body is about 3 times the interaction coefficient $A_0 = 4cb/d_0^5$ given by (3.16) based on the initial separation $d_0$. In other words, the amplified factor for the actual interaction coefficient between a single beam and a rigid body when the instability occurs is about 3. According to the present method, instability will occur when the actual interaction coefficient (rather than $A_0$ given by (3.16) based on the initial separation $d_0$) reaches the critical value (3.26) for instability

of a single cantilever beam attracted by a rigid body. This leads to a critical value

$A_0 = 4cb/d_0^5$ =2(0.0635) $[EI(\pi/L)^4]$ /3=0.0423 $[EI(\pi/L)^4]$ , which implies that the corresponding critical value of the force constant Fc defined by Johnstone and Parameswaran should be 0.0036, which is in excellent agreement with the numerical result 0.00356 given by Johnstone & Parameswaran [86].

As another example, let us consider a single cantilever beam attracted by a rigid substrate through electrostatic forces ($n$=2). The cantilever beam will become unstable when the free-end (maximum) deflection reaches about $0.47d_0$ (see Table 2 of [86]), or when the average deflection of the cantilever beam reaches about $0.47d_0 \times (2/3) \approx 0.31d_0$ . Thus, because $1/(1-0.31)^3 \approx 3.1$ , the actual interaction coefficient based on the reduced distance between the cantilever beam and the substrate when the instability occurs is about 3.1 times the value $A_0=2cb/d_0^3$ given by (3.16) based on the initial separation $d_0$. According to the present method, instability will occur when the actual interaction coefficient (rather than $A_0$ given by (3.16) based on the initial separation $d_0$) reaches the critical value (3.26). This gives a critical value

$A_0 = 2cb/d_0^3 = 2(0.0635)[EI(\pi/L)^4]/3.1$ =0.041 $[EI(\pi/L)^4]$ , and thus the corresponding critical value of the force constant Fe defined by Johnstone and Parameswaran should be 0.16, in good agreement with the value 0.15 given by Johnstone & Parameswaran [86].

As stated before, to achieve a simple approximate criterion for the end effect on instability of large parallel arrays, the present methods have employed the concept of a constant amplified factor $\alpha$ defined by (3.30) based on an estimated (weighted) average change in the distance between the end beam and its adjacent beam. Apparently, actual deflection and distance change are always non-uniform over the beams. Therefore, an alternative method, which is more complicated than the present methods, is to assume a reasonable form for the deflection of the end beam. For example, for a cantilever of length $L$, a suggested expression used in [86] for the deflection is $Y(x) = (\frac{x}{L})^2 Y_{max}$ , where $Y_{max}$ represents the maximum end deflection. Thus, if the deflection of the

adjacent beams is much smaller and can be neglected, the interaction coefficient $A_{1,2}$

and $A_{N-1,N}$ can be estimated approximately by

$$A_{1,2}(x) = A_{N-1,N}(x) = \frac{nC}{(d_0 - (\frac{x}{L})^2 Y_{max})^{n+1}} = \alpha(x)A_0, \quad \alpha(x) \equiv \frac{1}{(1 - (\frac{x}{L})^2 \frac{Y_{max}}{d_0})^{n+1}} \quad (3.32)$$

where $\alpha$ given by (3.30) can be understood as a weighted average of $\alpha(x)$ defined by (3.32). Based on (3.32), an alternative approximate method can be developed in which the end effect can be studied by examining the dependence on the maximum deflection $Y_{max}$ of the critical value of $A_0$ for the existence of non-zero solutions $y_k$ ($k$=1,2...$N$) of variable-coefficient equations (3.9), with the constant coefficients $A_{2,3} = A_{3,4} = ... = A_{N-2,N-1} = A_0$ and the two variable coefficients $A_{1,2}$ and $A_{N-1,N}$ given by (3.32), where $Y_{max}$ is the unknown maximum deflection of the end beam at the onset of instability which must be calculated in one way or another or estimated approximately.

For example, for a single cantilever attracted by a rigid body, Johnstone & Parameswaran showed that $Y_{max} = 0.3d_0$ when $n$=4, and $Y_{max} = 0.47d_0$ when $n$=2. Using the Galerkin method with these data, it can be verified that the critical value of $A_0$ for the existence of non-zero solutions $y_1$ of (3.9) when $N$=1, with the variable coefficient $A_{1,2}$ given by (3.32), is $A_0 = 0.0442[EI(\pi/L)^4]$ for $n$=4, or $A_0 = 0.0435[EI(\pi/L)^4]$ for $n$=2, while the methods based on the constant $\alpha$ defined by (3.30) give $A_0 = 0.0423[EI(\pi/L)^4]$ for $n$=4 and $A_0 = 0.041[EI(\pi/L)^4]$ for $n$=2, as stated above. Therefore, the values given by the two methods are quite close to each other with relative errors around 5%. Because the critical values given in [86] are approximate in nature, one cannot seriously comment on which of the two methods gives an better estimate of the critical value for this specific case. Therefore, it is believed that the present methods based on the constant $\alpha$ defined by (3.30) offer a simple yet effective approximate method to predict the critical value for instability.

Now, let us return to the methods based on the constant amplified factor $\alpha$ defined by (3.30). For a large number of mutually attracting parallel cantilevers under electrostatic forces ($n=2$), the maximum deflection of the two end beams at the instability is about 0.25 $d_0$ [142], which corresponds to an average deflection $0.25 d_0 \times (2/3) \approx 0.17 d_0$ and, because $1/(1-0.17)^3 \approx 1.75$, an amplified factor 1.75 for the interaction coefficient between the two beams at each of the ends of the parallel array. On one hand, the relation between the maximum deflection and the loading parameter for a single cantilever attracted by a rigid substrate (see figure 4 of [86]) implied that the critical value of the load parameter at the instability of the parallel cantilevers should be about 0.7 times the critical value for a single cantilever attracted by a rigid body (the latter is the maximum load of figure 4 of [86]). On the other hand, using the present method, because the amplified factor at the instability of parallel beams is about 1.75, it follows from Fig.3.6 that the end-effect factor $\varepsilon$ is about 0.85. Notice that the amplified factor for a single cantilever attracted by a rigid body at its instability is about 3, as explained before, and 3(0.85)/4=0.64, the critical value for instability of parallel cantilevers should be about 0.64 times the critical value for instability of a single cantilever attracted by a rigid body. This result is in good agreement with the above-mentioned 0.7 estimated from figure 4 of [86], with relative error around 10%. This suggests that the present criterion (3.31) offers a useful simple criterion for instability of parallel array of microbeams. To our best knowledge, no such simple criterion is available in the literature.

In conclusion, it should be stated that the present method is subjected to several limitations. For example, combined action of more than one type of surface forces is not considered in the present analysis, although the present method can be extended to this more complicated case without essential technical difficulty. In addition, fringing effect on electrostatic interaction (see e.g. [90, 143-144]) and the role of possible other surrounding materials have been neglected in the present analysis based on the assumption that the gap $d_0$ is small as compared to other dimensions of the beams (such as the beam-width and the distance between the beams and other surrounding materials).

## 3.7 Conclusions

Structural instability of mutually attracting parallel microbeams is studied. Based on a simplified $N$-spring model, it is verified that equilibrium deflections of intermediate beams (except the two beams at each end of the parallel array) are negligible because two attractions from two neighboring beams are almost equal but opposite. When the end-effect of the beams at the ends of the parallel array is neglected, the critical value of the beam-beam interaction coefficient for instability of the parallel array, defined based on initial separation between adjacent beams, is exactly half of the critical value of the interaction coefficient for instability of two mutually attracting beams, or equivalently a quarter of the critical value of the interaction coefficient for instability of a single beam attracted by a rigid body. On the other hand, the end-effect of the beams at the ends of the parallel array lowers the critical value about 20%-35% when the number of beams is sufficiently large, irrespective of the power-index and the boundary conditions of beams. The present method is justified by good agreement between the results obtained by the present method and the exact analysis given for the simplified spring model and some known data available in the literature for a few special cases. It is believed that the method developed here offers a simple design criterion for (static) structural instability of a parallel array of mutually attracting identical microbeams or nanobeams in MEMS or NEMS. To our best knowledge, no such simple criterion has been available in the literature.

Table 3.1 Comparison of the critical value of $B$ predicted by the present methods for the spring system with the exact critical value obtained by iteration numerical method.

| $n$ | Critical value without end effect | Present method based on approximate $\alpha$ | | Present method based on accurate $\alpha$ | | Exact critical value of $B$ |
|---|---|---|---|---|---|---|
| | | $\alpha$ | $B$ | $\alpha$ | $B$ | |
| 2 | 1/8 | 2.1 | 1/10.12 | 2.3 | 1/10.81 | 1/11.0 |
| 3 | 1/12 | 2.0 | 1/14.64 | 2.2 | 1/15.58 | 1/15.8 |
| 4 | 1/16 | 1.9 | 1/18.83 | 2.1 | 1/20.24 | 1/20.6 |

Enlarged cross-section of microbeams
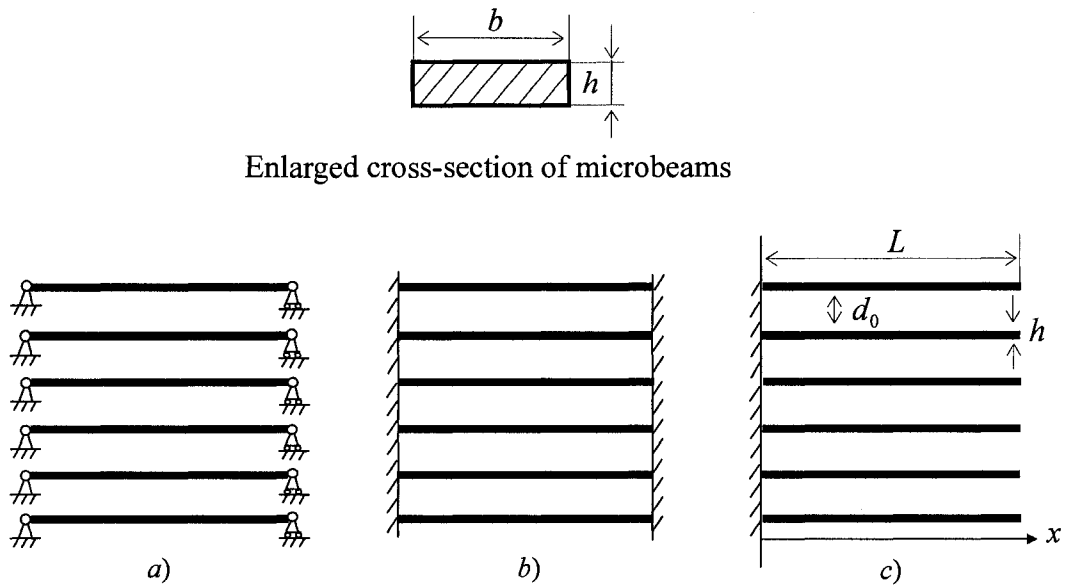


Fig.3.1 Parallel arrays of mutually attracting microbeams.

*a*) hinged; *b*) clamped; *c*) cantilever.
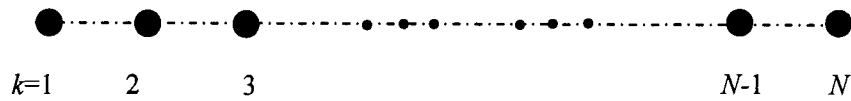


Fig.3.2 The simplified system of $N$ mutually attracting springs of spring constant $q$.
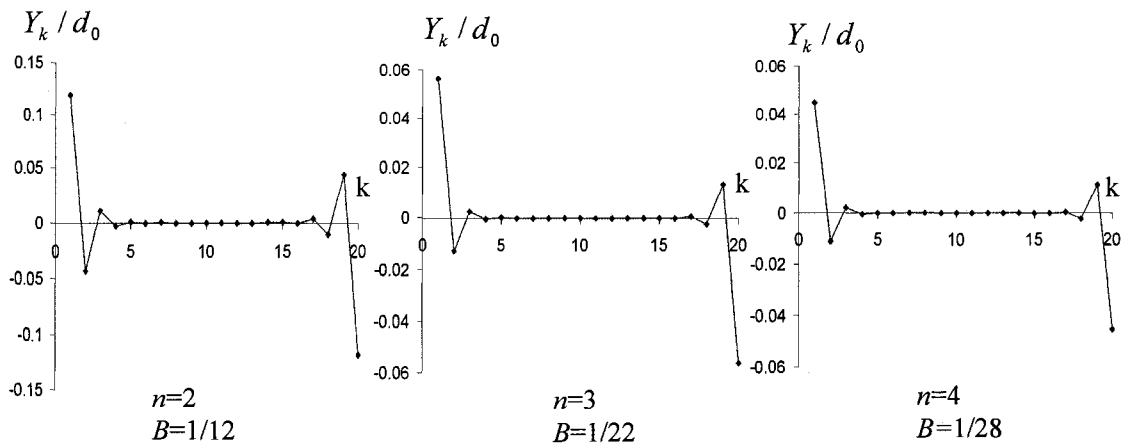
Fig.3.3 Equilibrium displacements of $N$ mutually attracting springs ($N$=20).
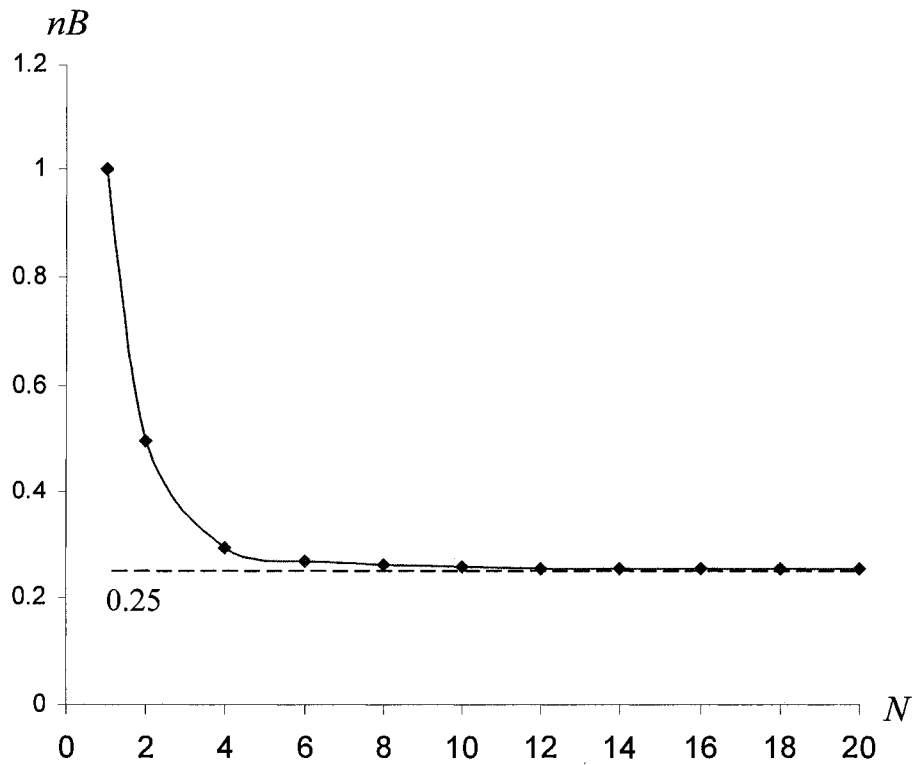


Fig.3.4 Critical value of ($nB$) for instability of the $N$-spring system when the end-effect is neglected.
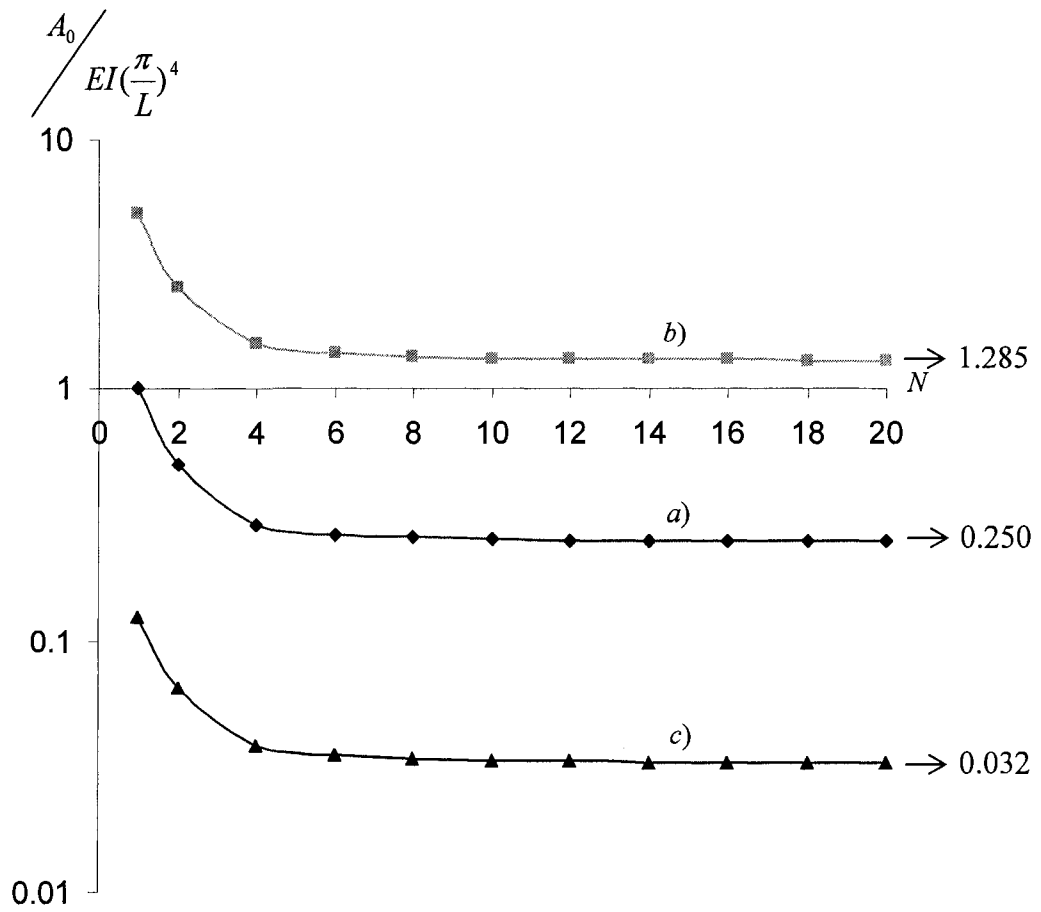
Fig.3.5 Critical value of $A_0$ (defined by (3.16) based on the initial separation $d_0$) for instability of a) hinged, b) clamped, and c) cantilever microbeams, as a function of the number of beams $N$ when the end-effect is neglected.
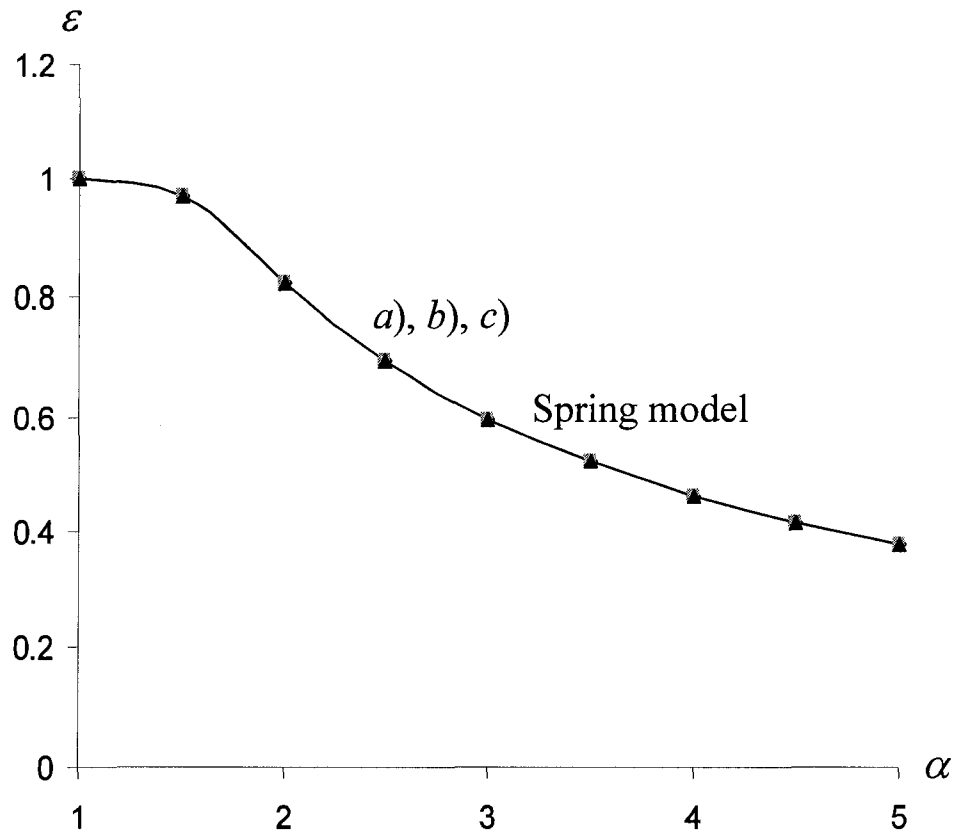
Fig.3.6 End-effect factor $\varepsilon$ defined by (3.31) for the critical value of $A_0$ for instability of a) hinged, b) clamped, and c) cantilever microbeams, as a function of the amplified factor $\alpha > 1$.

# Chapter 4

# Instability of Mutually Attracting Comb Drive Microcantilevers

## 4.1 Introduction

In this chapter, we analyze surface forces-driven instability of a comb-drive structure which consists of two opposing parallel arrays of microcantilevers as shown in Fig.4.1. A simple approximate method is developed based on the concept that the deflections of the intermediate microcantilevers in the comb drive structure are negligibly small, and this concept is well confirmed by exact numerical analysis conducted for a representative $N$-spring system with alternative spring constants $q_1$ and $q_2$, as shown in Fig.4.2.

First, instability analysis of two opposing arrays of microcantilevers is formulated in Section 4.2. An exact instability analysis is given in Section 4.3 for a representative $N$-spring system. When the end-effect at the ends of the array is neglected, the critical value of the beam-beam interaction coefficient for instability is determined in Section 4.4. In Section 4.5, the end-effect on the critical value for instability of the array is examined. The results obtained by the present methods for the spring system are compared to exact data obtained by iteration numerical method in Section 4.6. Finally, all results are summarized in Section 4.7.

## 4.2 Formulation of instability analysis

Let us consider the comb-drive microcantilever array shown in Fig.4.1, where all

77

cantilevers on the upper side, with the bending rigidity $E_1 I_1$, length $L_1$, width $b_1$ and thickness $h_1$, are labeled by odd subscripts (1, 3, 5...) and defined by the axial coordinate $x_1$, while all cantilevers on the lower side, with the bending rigidity $E_2 I_2$, length $L_2$, width $b_2$ and thickness $h_2$, are labeled by even subscripts (2, 4, 6...) and defined by the axial coordinate $x_2$, $\delta$ is the overlap depth of the opposing microcantilevers, and $d_0$ is the initial (constant) separation between the two flat surfaces of any two adjacent cantilevers. Over the overlap domain ($L_1 - \delta \le x_1 \le L_1$, or $L_2 - \delta \le x_2 \le L_2$), adjacent cantilevers interact with each other through the interacting area of width $b$.

Similar to Chapter 3, in this chapter, the attractive force per unit area between two surfaces of any two adjacent microcantilevers at any point is also assumed to be $F = c / d^n$, where $c$ is a constant depending on the nature of the interacting force and the materials, $d$ is the distance between the two surfaces at that point, and the index $n$ is either 2 (such as electrostatic force), 3 (such as unretarded van der Waals force), or 4 (such as Casimir force or retarded van der Waals force) [51-59]. Thus, over the overlap domain ($L_1 - \delta \le x_1 \le L_1$, or $L_2 - \delta \le x_2 \le L_2$), the interacting force per unit axial length between any two adjacent microcantilevers is given by $f = Fb = C / d^n$, where $C=cb$, and $b$ is the width of the interacting area of two adjacent microcantilevers and defined as $\min(b_1, b_2)$. In this chapter, we also only consider the case in which one type of the surface forces is dominant over the others, and thus $n=2$, 3 or 4. In addition, the width ($b_1$ or $b_2$) and length ($L_1$ or $L_2$) are assumed to be much larger than the gap $d$ so that the non-uniform interaction effect (such as fringing field, see p.1068 of [90]) is negligible, and then the uniform parallel plate model described above works well for the beam-beam

interaction.

Let $Y_k(x)$ be the equilibrium deflection (defined right positive in Fig.4.1) of cantilever $k$ under the interaction forces over the overlap domain between adjacent cantilevers. Thus we have

$$E_1 I_1 \frac{d^4 Y_k(x_1)}{dx_1^4} = P_k, \text{ for } k=1, 3, 5\ldots \tag{4.1}$$

$$E_2 I_2 \frac{d^4 Y_k(x_2)}{dx_2^4} = P_k, \text{ for } k=2, 4, 6\ldots \tag{4.2}$$

where $P_k$ is the resultant force (defined right positive in Fig.4.1) per unit axial length acted on cantilever $k$ due to the interactions with two adjacent beams ($k$-1) and ($k$+1), which vanishes outside the overlap domain and is given by

$$P_k = \frac{-C}{(d_0 + Y_k - Y_{k-1})^n} + \frac{C}{(d_0 + Y_{k+1} - Y_k)^n} \quad \text{for} \quad L_1 - \delta \leq x_1 \leq L_1 \quad \text{or} \quad L_2 - \delta \leq x_2 \leq L_2$$

(within the overlap domain).

Structural instability of the equilibrium state can be studied by the equilibrium method [140-141], and an equilibrium state becomes unstable when there exists any adjacent equilibrium state characterized by infinitesimal non-zero deviations $y_k(x)$ from the equilibrium deflections $Y_k(x)$ ($k$=1,2...$N$). With infinitesimal deviation $y_k(x)$, the total deflection of cantilever $k$ is ($Y_k(x) + y_k(x)$) and governed by

$$E_1 I_1 \frac{d^4 (Y_k(x_1) + y_k(x_1))}{dx_1^4} = P_k + p_k, \text{ for } k=1, 3, 5\ldots \tag{4.3}$$

$$E_2 I_2 \frac{d^4 (Y_k(x_2) + y_k(x_2))}{dx_2^4} = P_k + p_k, \text{ for } k=2, 4, 6\ldots \tag{4.4}$$

where $p_k$ is the additional resultant force per unit axial length acted on cantilever $k$ due to the interactions with two adjacent beams ($k$-1) and ($k$+1) over the overlap domain, caused by the deviations of cantilever $k$ and two adjacent cantilevers ($k$-1) and ($k$+1),

given by $p_k = \dfrac{-C}{(d_0 + Y_k - Y_{k-1} + y_k - y_{k-1})^n} + \dfrac{C}{(d_0 + Y_{k+1} - Y_k + y_{k+1} - y_k)^n} - P_k$ for

$L_1 - \delta \le x_1 \le L_1$ or $L_2 - \delta \le x_2 \le L_2$. Because the deviations $y_k(x)$ are infinitesimal, $p_k$ ($k$=1,2...$N$) can be expanded in $y_k$. Neglecting all nonlinear terms of $y_k$, we have

$p_k = A_{k-1,k}(y_k - y_{k-1}) - A_{k,k+1}(y_{k+1} - y_k)$, for $L_1 - \delta \le x_1 \le L_1$ or $L_2 - \delta \le x_2 \le L_2$,

where $A_{k-1,k}$, the interaction coefficient between cantilevers ($k$-1) and $k$, and $A_{k,k+1}$, the interaction coefficient between cantilevers $k$ and ($k$+1), are non-zero only over the overlap domain ($L_1 - \delta \le x_1 \le L_1$ or $L_2 - \delta \le x_2 \le L_2$), where they are defined by

$$A_{k-1,k} = \frac{nC}{(d_0 + Y_k - Y_{k-1})^{n+1}}, \quad A_{k,k+1} = \frac{nC}{(d_0 + Y_{k+1} - Y_k)^{n+1}}$$

$$\text{for } L_1 - \delta \le x_1 \le L_1 \text{ or } L_2 - \delta \le x_2 \le L_2 \qquad (4.5)$$

Thus, subtracting (4.3, 4.4) by (4.1, 4.2), respectively, we obtain the equations for $N$ deviations $y_k(x)$ ($k$=1,2...$N$) as

$$E_1 I_1 \frac{d^4 y_k(x_1)}{dx_1^4} = A_{k-1,k}(y_k - y_{k-1}) - A_{k,k+1}(y_{k+1} - y_k), \text{ for } k=1, 3, 5... \qquad (4.6)$$

$$E_2 I_2 \frac{d^4 y_k(x_2)}{dx_2^4} = A_{k-1,k}(y_k - y_{k-1}) - A_{k,k+1}(y_{k+1} - y_k), \text{ for } k=2, 4, 6... \qquad (4.7)$$

80

In particular, the coefficients $A_{k-1,k}$ and $A_{k,k+1}$ are defined by (4.5) over the overlap domain ( $L_1 - \delta \leq x_1 \leq L_1$ or $L_2 - \delta \leq x_2 \leq L_2$ ), and are identically zero outside the overlap domain.

Thus, instability of the comb-drive microcantilever array is defined by the existence of any non-zero solutions $y_k$ of linear Eqns (4.6, 4.7) under the associated boundary conditions for microcantilevers [140-141]. It is a technically challenging problem to solve Eqns (4.6, 4.7) due to the fact that the coefficients $A_{k-1,k}$ and $A_{k,k+1}$ in Eqns (4.6, 4.7) are $x$-dependent, which are identically zero outside the overlap domain and depend on $Y_k(x_1)$ and $Y_k(x_2)$ (see Eqn (4.5)) within the overlap domain. In this chapter, we employ a simple approximate method to study instability of the com-drive microcantilever array. This method is based on a simple observation that equilibrium deflections $Y_k$ of almost all intermediate cantilevers are negligibly small because the two interactions forces from two adjacent beams on opposite sides are almost equal but opposite and thus cancel each other. In the next section, this intuitive idea will be examined with a spring system consisting of alternating arrays of springs with spring constants $q_1$ and $q_2$, as shown in Fig.4.2. In fact, many of existing related papers have studied large beam arrays entirely based on the simple spring system, because the latter is much simple but yet captures the main features of the beam arrays [102-112].

## 4.3 Instability of a representative *N*-spring system

Let us consider $N$ equally spaced and mutually attracting springs, arranged along a straight line, from $k=1$ (left end) to $k=N$ (right end), as shown in Fig.4.2. Let all springs of odd index ($k=1, 3, 5...$) have the spring constant $q_1$, while all springs of even index ($k=2$, 4, 6...) have the spring constant $q_2$, and any two adjacent springs are attracted to each

other through the force $f = M / d^n$, where $M$ is a constant and $d$ is the distance between the two springs. Under the spring-spring interaction forces, all springs will displace from their original neutral positions. We assume the displacement of the $k$-th spring to be $Y_k$ (defined right positive in Fig.4.2), thus equilibrium of the $N$ mutually attracting springs are governed by $N$ dimensionless nonlinear equations for $N$ unknowns $Y_k / d_0$ ($k$=1, 2, ..., $N$) given by

$$-\frac{Y_1}{d_0} + \frac{B}{(1 + \frac{Y_2}{d_0} - \frac{Y_1}{d_0})^n} = 0, \quad k=1, \tag{4.8}$$

$$-\frac{Y_k}{d_0} + \frac{\beta B}{(1 + \frac{Y_{k+1}}{d_0} - \frac{Y_k}{d_0})^n} - \frac{\beta B}{(1 + \frac{Y_k}{d_0} - \frac{Y_{k-1}}{d_0})^n} = 0, \quad k=2, 4,... \tag{4.9}$$

$$-\frac{Y_k}{d_0} + \frac{B}{(1 + \frac{Y_{k+1}}{d_0} - \frac{Y_k}{d_0})^n} - \frac{B}{(1 + \frac{Y_k}{d_0} - \frac{Y_{k-1}}{d_0})^n} = 0, \quad k=3, 5... \tag{4.10}$$

$$-\frac{Y_N}{d_0} - \frac{B}{(1 + \frac{Y_N}{d_0} - \frac{Y_{N-1}}{d_0})^n} = 0, \quad k=N \text{ is an odd number,} \tag{4.11}$$

$$-\frac{Y_N}{d_0} - \frac{\beta B}{(1 + \frac{Y_N}{d_0} - \frac{Y_{N-1}}{d_0})^n} = 0, \quad k=N \text{ is an even number,} \tag{4.12}$$

where the two constants $B$ and $\beta$ are defined by

$$B = \frac{M}{q_1 d_0^{n+1}}, \quad \beta = \frac{q_1}{q_2} \tag{4.13}$$

In particular, for given ratio $\beta$, the constant $B$ is the interaction coefficient defined on the initial distance $d_0$ between any two adjacent springs, which represents the intensity of the interaction between neighboring springs. In addition, (4.9) is identical to (4.10) and (4.11) is identical to (4.12) when $\beta=1$.

Equilibrium displacements of all springs governed by (4.8-4.12) can be obtained by Newton iteration method. It is found that equilibrium displacements of the springs suffer discontinuity when the loading parameter $B$ reaches a certain critical value. For $B$ smaller than the critical value, equilibrium displacements vary smoothly with the parameter $B$. When the loading parameter $B$ exceeds the critical value, equilibrium displacements of the springs obtained from (4.8-4.12) suffer a jump and lead to collision of some adjacent springs because the distance reduction between them is larger than the initial gap $d_0$. Since comb-drive microbeam arrays are usually electrostatically controlled [61-64, 66-77, 98-99, 101], in what follows, all numerical results for the spring system and comb-drive arrays will focus on the power index $n=2$. For example, when $n=2$, for $\beta = q_1 / q_2 =0.2$ or 1, our numerical results show that equilibrium positions of the spring system are stable when the loading parameter $B$ given by (4.13) is below the critical value $1/7.543$ for $\beta=0.2$, or $1/11$ for $\beta=1$, respectively, regardless of $N$ as an even or odd number. On the other hand, for $q_1 / q_2 =5$, equilibrium positions of the spring system are stable when the loading parameter $B$ is below $1/37.713$ when $N$ is an even number, or when $B$ is below $1/28.1$ when $N$ is an odd number. Here a significant difference exists between the critical value with an even number $N$ and the critical value with an odd number $N$ when $q_1 / q_2 =5$, because the rigidity of the springs of odd indexes (1, 3...) is much larger than the rigidity of the springs of even indexes (2, 4...). Therefore, when $N$ is an even number, the rigidity of the right end spring $k=N$ is smaller, and the spring system has a lower critical value of $B$ for instability. Obviously, when $N$ is an odd number, both the left and

the right end springs ($k=1$ and $k=N$) have the same much larger rigidity and then the critical value of $B$ for instability is much higher. In particular, no such a difference exists for even or odd number $N$ when $\beta=0.2$ because the left end spring $k=1$ always has the smaller rigidity which determines the instability of the spring system, regardless of $N$ as an even or odd number.

Stable equilibrium displacements of all springs of the spring system are shown in Fig.4.3 for a few examples. It is seen from Fig.4.3 that:

1) When the loading parameter $B$ is below the critical value mentioned above, as expected, accurate equilibrium displacements of almost all intermediate springs are negligibly small. In particular, in all cases shown, the displacement of the spring $k=3$ at the left end (or the spring $k=N-2$ at the right end) at the onset of instability is negligibly small (around $0.01/d_0$ or less), compared to the much larger displacements of the end springs ($k=1$ and $k=N$) and their neighboring springs ($k=2$ or $k=N-1$). This implies that Eqns (4.8) and (4.9) (with $k=2$) based on $Y_3=0$ can be employed to approximately determine the displacements $Y_1$ and $Y_2$ at the left end with the specific $B$ and $\beta$ when $B$ is below the critical value. These results for the $N$-spring system suggest that the deflections of the intermediate beams should be negligibly small. A relevant theory should make use of this important feature, in order to achieve a much simple but yet reasonably accurate method. In addition, it is also important to isolate the end phenomena and quantify its effect on the critical value for instability.

2) For most cases shown in Fig.4.3 (except the case when $\beta=5$ and $N$ is an odd number), even the two springs ($k=2$ and $k=N-1$) adjacent to one of the end springs ($k=1$ or $N$) have a very small displacement compared to the largest displacement of the end springs ($k=1$ or $k=N$). In all of theses cases, therefore, the distance change between the springs $k=2$ and $k=3$ or between the springs $k=N-2$ and $k=N-1$ is negligible. This means that the amplified interaction between the end spring and its neighbor would be mainly responsible for the

end-effect, although it may be applied to two ends of a symmetric spring system (Fig.4.3-*b* for $\beta$ =1, or Fig.4.3-*a* when $\beta$ =0.2 and $N$ is an odd number), or to only one end of a non-symmetric spring system (Fig.4.3-*a* when $\beta$ =0.2 and $N$ is an even number, or Fig.4.3-*c* when $\beta$ =5 and $N$ is an even number).

3) When $\beta$ =5 and $N$ is an odd number, it is seen from Fig.4.3-*d* that the displacement of the spring $k$=2 or $k$=$N$-1 is even larger than the displacement of the end spring $k$=1 or $k$=$N$, due to the fact that the rigidity of the end springs $k$=1 and $k$=$N$ is much larger than the rigidity of the springs $k$=2 and $k$=$N$-1. This means that the distance change between the springs $k$=2 and $k$=3 or between the springs $k$=$N$-2 and $k$=$N$-1 can be larger than (or comparable to) the distance change between the end spring and its neighboring spring, as shown in Fig.4.3-*d*. In this case, unlike the cases shown in Fig.4.3-*a, b,* and *c,* the large distance change between the springs $k$=2 and $k$=3 or between the springs $k$=$N$-2 and $k$=$N$-1 would be also responsible for the end-effect and cannot be neglected. On the other hand, even in this case, the displacements $Y_1$ and $Y_2$ at the left end can still be well estimated by using the Eqns (4.8) and (4.9) (with $k$=2) based on $Y_3$=0.

It is found from Fig.4.3 that equilibrium displacements of almost all intermediate springs (from $k$=3 to $k$=$N$-2) are negligibly small. This observation can be used to largely simplify the analysis of instability and achieve a simple approximate instability criterion with reasonable accuracy. To see this, let us consider infinitesimal deviations $y_k$ of $N$ springs from their equilibrium positions defined by $Y_k$ and study the existence of equilibrium non-zero deviations $y_k$ ($k$=1,2...$N$). Firstly let us neglect the end-effect and then $Y_k$ =0 ($k$=1,2...$N$), and thus expand equilibrium Eqns (4.8-4.12) at the zero-displacement position, the resulting equilibrium equations for infinitesimal deviations $y_k$ ($k$=1,2...$N$) are obtained as

$$-\frac{y_1}{d_0} - nB(\frac{y_2}{d_0} - \frac{y_1}{d_0}) = 0 \ , \ k=1, \tag{4.14}$$

$$-\frac{y_k}{d_0} - \beta nB(\frac{y_{k+1}}{d_0} - \frac{y_k}{d_0}) + \beta nB(\frac{y_k}{d_0} - \frac{y_{k-1}}{d_0}) = 0 \ , \ k=2,4,\ldots \tag{4.15}$$

$$-\frac{y_k}{d_0} - nB(\frac{y_{k+1}}{d_0} - \frac{y_k}{d_0}) + nB(\frac{y_k}{d_0} - \frac{y_{k-1}}{d_0}) = 0 \ , \ k=3,5,\ldots \tag{4.16}$$

$$-\frac{y_N}{d_0} + nB(\frac{y_N}{d_0} - \frac{y_{N-1}}{d_0}) = 0 \ , \ k=N \quad \text{is an odd number} \tag{4.17}$$

$$-\frac{y_N}{d_0} + \beta nB(\frac{y_N}{d_0} - \frac{y_{N-1}}{d_0}) = 0 \ , \ k=N \quad \text{is an even number} \tag{4.18}$$

The minimum value of $(nB)$ for the existence of non-zero solutions $y_k$ ($k=1,2\ldots N$) of (4.14-4.18) is shown in Fig.4.4 for $\beta=0.2$, 1 and 5, respectively, as a function of increasing number $N$. It is seen from Fig.4.4 that non-zero solutions of (4.14-4.18) exist for sufficiently large number $N$ when $(nB)$ is bigger than 0.42 when $\beta=0.2$, or bigger than 0.25 when $\beta=1$, or bigger than 0.084 when $\beta=5$. This means that, for $n=2$, the critical value of $B$ for instability of the $N$-spring system without the end-effect is $B=0.21$ when $\beta=0.2$, or $B=0.125$ for $\beta=1$, or $B=0.042$ for $\beta=5$.

As mentioned before, our numerical results for exact nonlinear Eqns (4.8-4.12) show that the accurate critical value for instability of the $N$-spring system (with the end-effect) is about $1/7.543=0.1326$ for $\beta=0.2$, or $1/11=0.0909$ for $\beta=1$, or $1/37.713=0.0265$ when $\beta=5$ and $N$ is an even number, or $1/28.1=0.0356$ when $\beta=5$ and $N$ is an odd number. Obviously, compared to the critical value for instability without the end-effect, the end-effect lowers the actual critical value for instability around 15%-40%, and the

reduction in the critical value for instability is related to the spring coefficient (or the rigidity) of either of the end springs. For example, when $\beta=5$ and $N$ is an odd number (the spring coefficients of the two end springs are big), the end-effect lowers the critical value for instability by 15%. When $\beta=1$ (regardless of $N$ as an odd or even number), the end springs have the same spring coefficient as the other springs, and the end-effect lowers the critical value for instability by 27%. When $\beta=0.2$ (regardless of $N$ as an odd or even number), or when $\beta=5$ and $N$ is an even number, one or two end springs have a small spring coefficient, and the end-effect lowers the critical value for instability by 40%.

## 4.4 Instability of comb drive microcantilevers without the end-effect

In this section, let us first neglect the end-effect of the cantilevers at the two ends and assume that equilibrium deflections of all cantilevers (including those at the ends), $Y_k$ ($k=1, 2...N$), are negligible, and then it follows from (4.5) that all coefficients $A_{k-1,k}$ and $A_{k,k+1}$ over the overlap domain ($L_1-\delta \le x_1 \le L_1$ or $L_2-\delta \le x_2 \le L_2$) are equal and are given by

$$A_{1,2} = A_{2,3} = A_{3,4} = ... = A_{N-2,N-1} = A_{N-1,N} = A_0 = \frac{nC}{d_0^{n+1}} \tag{4.19}$$

where $A_0$ is a constant defined by (4.19) based on the initial separation $d_0$, which represents the intensity of the beam-beam interaction. Thus, the governing equations (4.6, 4.7) for infinitesimal deviations $y_k$ ($k=1,2...N$) become

$$E_1 I_1 \frac{d^4 y_k(x_1)}{dx_1^4} = p_k(x_1), \text{ for } k=1, 3, 5... \tag{4.20}$$

$$E_2 I_2 \frac{d^4 y_k(x_2)}{dx_2^4} = p_k(x_2), \text{ for } k=2, 4, 6... \tag{4.21}$$

where $p_k(x_1)$ ($k$=3,5...) is given by

$$p_k = 0, \quad 0 < x_1 < L_1 - \delta,$$

$$p_k = A_0[2y_k(x_1) - y_{k-1}(x_2) - y_{k+1}(x_2)], \quad L_1 - \delta \leq x_1 \leq L_1, k=3, 5,... \tag{4.22}$$

for the cantilevers on the upper side with odd index $k>1$, and $p_k(x_2)$ ($k$=2,4...) is given by

$$p_k = 0, \quad 0 < x_2 < L_2 - \delta,$$

$$p_k = A_0[2y_k(x_2) - y_{k-1}(x_1) - y_{k+1}(x_1)], \quad L_2 - \delta \leq x_2 \leq L_2, k=2, 4,... \tag{4.23}$$

for the cantilevers on the lower side with even index $k$=2,4..., with $x_2 + x_1 = L_1 + L_2 - \delta$.

The eigenvalue problem of (4.20, 4.21) is complicated by the fact that each beam interacts with two neighboring beams only through the overlap length rather than the entire beam length. To our knowledge, no similar problem has been analyzed in the literature. Here, a procedure is suggested using the Galerkin method. For example, for only two opposing microcantilevers ($N$=2), the deviations $y_1(x_1)$ and $y_2(x_2)$ can be expressed by the respective fundamental modes of cantilevers 1 and 2 as

$$y_1(x_1) = \sum_{i=1}^{m} a_i F_i(x_1), \quad y_2(x_2) = \sum_{i=1}^{m} b_i G_i(x_2) \tag{4.24}$$

where $F_i(x_1)$ $(i=1,2...m)$ are the first $m$ modes of cantilever 1, and $G_i(x_2)$ $(i=1,2...m)$ are the first $m$ modes of cantilever 2, given by [140]

$$F_i(x_1) = \sin \beta_i x_1 - \sinh \beta_i x_1 - c_i (\cos \beta_i x_1 - \cosh \beta_i x_1)$$

$$G_i(x_1) = \sin \gamma_i x_2 - \sinh \gamma_i x_2 - c_i (\cos \gamma_i x_2 - \cosh \gamma_i x_2) \tag{4.25}$$

where

$$\beta_1 l_1 = \gamma_1 l_2 = 1.875 ,$$

$$\beta_2 l_1 = \gamma_2 l_2 = 4.694 ,$$

$$\beta_3 l_1 = \gamma_3 l_2 = 7.855 ,$$

$$\beta_4 l_1 = \gamma_4 l_2 = 10.996 ,$$

$$\beta_5 l_1 = \gamma_5 l_2 = 14.137 ,$$

$$\beta_6 l_1 = \gamma_6 l_2 = 17.279 , \quad ......$$

$$c_i = \frac{\sin \beta_i l_1 + \sinh \beta_i l_1}{\cos \beta_i l_1 + \cosh \beta_i l_1} = \frac{\sin \gamma_i l_2 + \sinh \gamma_i l_2}{\cos \gamma_i l_2 + \cosh \gamma_i l_2} \tag{4.26}$$

To solve the eigenvalue problem, first, one should substitute expansions (4.24) into (4.20, 4.21) for $k=1$ and $k=2$, respectively, and change the variable $x_2$ in (4.21) into $x_1$, and change the variable $x_1$ in (4.20) into $x_2$, on using $x_1 + x_2 = L_1 + L_2 - \delta$. Thus,

multiplying (4.20) by $F_i(x_1)$ ($i$=1,2...$m$) and then integrating over $x_1$=[0, $L_1$], and

multiplying (4.21) by $G_i(x_2)$ ($i$=1,2...$m$) and then integrating over $x_2$=[0, $L_2$], one will

obtain $2m$ equations for $2m$ unknown coefficients $a_i$ and $b_i$ ($i$=1,2...$m$). The critical

value of $A_0$ for instability of the array without the end-effect is determined as the lowest

eigenvalue for the existence of non-zero coefficients $a_i$ and $b_i$ ($i$=1,2...$m$). In this

chapter, we take $m$=3 because relative errors between $m$=3 and $m$= 4 are already less than

1%. Similar procedure can be applied to (4.20, 4.21) for an arbitrary number ($N$) of

microcantilevers with a constant interaction coefficient $A_0$ between any two adjacent

cantilevers.

For a large number ($N$) of microcantilevers, it is found that the critical value of the

interaction coefficient $A_0$, defined by the lowest eigenvalue of (4.20, 4.21), is exactly a

half of the critical value of $A_0$ for two opposing cantilevers ($N$=2). For example, for

$E_2 I_2 = E_1 I_1$, $L_2 = L_1$ and $\delta / L = 0.5$, the critical value of the beam-beam interaction

coefficient $A_0$, as the lowest eigenvalue of (4.20, 4.21), is shown in Fig.4.5 for

increasing number $N$. It is seen from Fig.4.5 that, for example, the critical value of $A_0$

for $N$ cantilevers when $N$=10 is 0.037, which is about 51% of the critical value 0.073 for

two opposing cantilevers with $N$=2. When the number $N$ increases, the critical value for $N$

cantilevers quickly converges to a half of the critical value for two opposing cantilevers.

In fact, for large $N$, the deflections of any two adjacent beams determined by the

instability mode are equal but opposite. Therefore, the interaction force acting on each

beam is doubled, which leads to a doubled equivalent interaction coefficient as compared

to two beams. This conclusion is valid for all other combinations of the geometrical and

material parameters of the microcantilevers. Hence, when the end-effect is neglected, it is

enough to study the critical value of $A_0$ for two opposing microcantilevers ($N$=2) only.

Numerical results obtained for two opposing cantilevers of varying bending rigidity ratio $E_2 I_2 /(E_1 I_1)$, the length ratio $L_2 / L_1$ and the overlap depth $\delta / L_1 (\leq 1)$, are shown in Figs.4.6-4.8. Without loss of generality, we assume that $L_2 \geq L_1$. Thus, for three different bending rigidity ratios $E_2 I_2 /(E_1 I_1)$=1, 0.1 and 10, the dimensionless critical value of $A_0$ is shown in Figs.4.6-4.8 for the length ratio $L_2 / L_1$ between 1 and 3, as a function of the overlap depth $\delta / L_1$. It is seen from Figs.4.6-4.8 that for given bending rigidity ratio and overlap depth $\delta / L_1$, the critical value for instability decreases with increasing length of the longer cantilever ($L_2$). However, for given bending rigidity ratio and length ratio ($L_2 / L_1$), the critical value is not a monotonic function of the overlap depth $\delta / L_1$. For example, when $E_2 I_2 / E_1 I_1$=1 and $L_2 / L_1$=1, it is seen from Fig.4.6 that the critical value of $A_0$ attains the minimum at $\delta / L_1$=0.5. On the other hand, the highest critical value is always associated with the smallest overlap depth $\delta / L_1$=0.1, and the lowest critical value is always associated with a larger overlap depth $\delta / L_1 \geq 0.5$.

The results shown in this section, in which the end-effect is neglected, offer only a crude approximation for the actual critical value for instability of the array shown in Fig.4.1 because, as shown later, the end-effect will lower the critical value for instability (see Section 4.5 and Section 4.6). However, the results given in this section do offer exact critical values for instability when the array of microcantilevers is ended with two rigid walls at the two ends, or in other words, when the two end cantilevers $k$=1 and $k$=$N$ have infinite bending rigidity, such as those shown in figure 1 of [145]. This conclusion is also confirmed by the spring system with two end springs fixed.

# 4.5 Instability of comb drive microcantilevers with the end-effect

The analysis of Section 4.4 is based on the simplifying assumption that equilibrium deflections of all cantilevers (including the two end ones) are neglected, which implies that all interaction coefficients defined by (4.5) are determined by the initial gap $d_0$ and thus $A_{1,2} = A_{2,3} = ... = A_{N-1,N} = A_0$, where $A_0$ is defined by (4.19). As shown in the Section 4.3 for a simplified $N$-spring system, this assumption is valid for almost all intermediate beams (from $k=3$ to $k=N-2$), but is invalid for the two end beams ($k=1$ and $k=N$), due to the unbalanced attraction from one side only. In other words, although neglecting vanishingly small distance change between intermediate beams will not lead to any sensible error, neglecting the large distance change between each of the two end beams and its neighboring beam will lead to a considerable error in the critical value for instability.

Firstly, we will consider the case that microcantilevers of two opposing arrays have the same material and geometrical characteristics ($E_1 I_1 = E_2 I_2 = EI$ and $L_1 = L_2 = L$).

## 4.5.1 Microcantilevers of identical bending rigidities

In order to develop a simple method to quantify the end-effect, we now assume that only the distance change between any two adjacent intermediate beams ($k=2...N-1$) is negligible, and then $A_{2,3} = A_{3,4} = ... = A_{N-2,N-1} = A_0$, where $A_0$ is defined by (4.19) based on the initial separation $d_0$. On the other hand, the large distance change between the end beam and its neighboring beam and its effect on the critical value for instability will be accounted for.

## 4.5.1.1 The end-effect phenomenon

Because each of the two end beams ($k$=1 or $N$) is attracted by its adjacent beam from one side only, it has a large non-zero deflection. In particular, when $E_1 I_1 = E_2 I_2 = EI$ and $L_1 = L_2 = L$, it follows from the symmetry that $Y_1(x) > 0$ and $Y_N(x) = -Y_1(x) < 0$ for sufficiently large $N$. In addition, the large deflection of the end beam ($k$=1 or $N$) will cause a strong attraction to its neighboring beam ($k$=2 or $N$-1). Consequently, the neighboring beam ($k$=2 or $N$-1) will be attracted to the end beam and thus we have $Y_2(x) < 0$ and $Y_{N-1}(x) = -Y_2(x) > 0$. Therefore, $A_{1,2}$, the actual interaction coefficient between the end beam ($k$=1) and its neighboring beam ($k$=2), and $A_{N-1,N}$, the actual interaction coefficient between the end beam ($k$=$N$) and its neighboring beam ($k$=$N$-1), are equal and are given by

$$A_{1,2} = A_{N-1,N} = \frac{nC}{(d_0 + Y_2 - Y_1)^{n+1}} = \frac{nC}{(d_0 + Y_N - Y_{N-1})^{n+1}} \tag{4.27}$$

Obviously, because $Y_1(x) - Y_2(x) > 0$ (or $Y_N(x) - Y_{N-1}(x) < 0$ ), the interaction coefficients $A_{1,2} = A_{N-1,N}$ given by (4.27) for two beams at each of the ends at the onset of instability would be much larger than the interaction coefficient $A_0$ for intermediate beams, defined by (4.19) based on the initial separation $d_0$.

The amplified interaction coefficients $A_{1,2} = A_{N-1,N}$ can be estimated approximately, based on the average value of the distance change over the overlap domain of the two adjacent beams, by a constant amplified factor $\alpha$ ($>1$) as

$$A_{1,2} = A_{N-1,N} = \alpha A_0, \quad \alpha > 1 \tag{4.28}$$

As shown below, the amplified factor $\alpha$ can be calculated approximately based on an estimated distance reduction between the end beam and its adjacent beam at the onset of instability.

Thus, the end-effect on instability can be studied by examining the dependence on the amplified factor $\alpha$ of the critical value for the existence of non-zero solutions $y_k$ ($k=1,2...N$) of linear equations (4.6, 4.7) with the coefficients $A_{2,3} = A_{3,4} = ... = A_{N-2,N-1} = A_0$, where $A_0$ is defined by (4.19) based on the initial separation $d_0$, and the coefficients $A_{1,2} = A_{N-1,N} = \alpha A_0$, where the amplified factor $\alpha$ is defined by (4.27, 4.28). In what follows, because comb-drive microcantilevers in MEMS are usually electrostatically controlled, we shall focus on the power index $n=2$. Similar results can be obtained when $n=3$ or 4 without any difficulty.

## 4.5.1.2 Estimate of the amplified factor $\alpha$

To estimate the amplified factor $\alpha$ for the interaction coefficient between the two beams at each of the two ends, one has to estimate the distance reduction between the end beam and its adjacent beam at the onset of instability and to quantify its influence on the amplified factor $\alpha$ defined by (4.27, 4.28). Since the deflection of the third cantilever ($k=3$, or $k=N-2$) is negligibly small, it can be treated as rigid. Thus, the deflections of the two cantilevers at each of the two ends can be estimated by considering the two cantilevers attracted by a rigid cantilever ($k=3$ or $k=N-2$). For example, the deflections of the end cantilever ($k=1$) and its neighbor cantilever ($k=2$) can be estimated based on the first two of nonlinear equations (4.1 4.2) with $Y_3 = 0$, which give

$$E_1 I_1 \frac{d^4 Y_1(x_1)}{dx_1^4} = P_1, \tag{4.29}$$

$$E_2 I_2 \frac{d^4 Y_2(x_2)}{dx_2^4} = P_2, \tag{4.30}$$

where $P_k$ ($k=1$ or 2) is identically zero outside the overlap domain, and is given by

$$P_1 = \frac{C}{(d_0 + Y_2 - Y_1)^n} \quad \text{for} \quad L_1 - \delta \le x_1 \le L_1 \tag{4.31}$$

$$P_2 = \frac{-C}{(d_0 + Y_2 - Y_1)^n} + \frac{C}{(d_0 - Y_2)^n} \quad \text{for} \quad L_2 - \delta \le x_2 \le L_2 \tag{4.32}$$

within the overlap domain. In this way, the deflections $Y_1(x_1)$ and $Y_2(x_2)$ can be calculated approximately based on the two nonlinear equations (4.29, 4.30) using the Galerkin method described in Section 4.4. Once $Y_1(x_1)$ and $Y_2(x_2)$ are obtained, the average distance reduction between the end beam and its neighboring beam can be estimated by integration of $(Y_1 - Y_2)$ over the overlap domain, and thus the amplified factor defined by (4.27, 4.28) can be estimated. The estimated amplified factor for several specific values of the overlap depth $\delta/L$ is shown in Fig.4.9, as a function of the loading parameter $A_0$ defined by (4.19), where, dashed parts of all curves are obtained by extrapolation method. In particular, the amplified factor for the left end $k=1$ is the same as the amplified factor for the right end $k=N$ when $E_1 I_1 = E_2 I_2$ and $L_1 = L_2 = L$. It is seen from Fig.4.9 that the amplified factor $\alpha$ increases very quickly with increasing loading parameter $A_0$ and approaches a limiting value between 2.3 and 3 when $A_0$ tends to its maximum value. As shown below, the amplified interaction coefficient $\alpha A_0$ ($\alpha > 1$) between the end beam and its neighboring beam is mainly

responsible for the end-effect on instability.

### 4.5.1.3 The critical value for instability with the end-effect

The end-effect leads to an amplified interaction coefficient for the two end beams. Hence, the actual critical value of $A_0$ for instability of the array with the end-effect will be lower than the approximate critical value of $A_0$ estimated in Section 4.4 without considering the end-effect. Therefore, the actual critical value with the end-effect can be expressed by an end-effect factor $\varepsilon$ as

$$A_0 = \varepsilon A_\infty, \quad 0 < \varepsilon < 1 \tag{4.33}$$

where $A_\infty$ is the critical value of $A_0$ without the end-effect, estimated in Section 4.4.

To calculate the dependence of the end-effect factor $\varepsilon$ on the amplified factor $\alpha$, we compare the critical value $A_\infty$ obtained in Section 4.4 without the end-effect, to the critical value of $A_0$ for the existence of non-zero solutions $y_k$ ($k$=1,2...$N$) of equations (4.6, 4.7) with $A_{2,3} = A_{3,4} = ... = A_{N-2,N-1} = A_0$ and $A_{1,2} = A_{N-1,N} = \alpha A_0$. The end-effect factor $\varepsilon$, as a function of the amplified factor $\alpha$ (>1), is shown in Fig.4.10 for several specific values of the overlap depth $\delta / L$. It is seen from Fig.4.10 that the amplified factor $\alpha$ has a significant effect on the end-effect factor $\varepsilon$ and the dependency of $\varepsilon$ on $\alpha$ is insensitive to the overlap depth $\delta / L$. Thus, with estimated amplified factor $\alpha$, the end-effect factor $\varepsilon$ and the actual critical value for instability can be estimated by Fig.4.10. For instance, if the amplified factor $\alpha$ is 2.3, the end-effect factor $\varepsilon$ determined by Fig.4.10 is about 0.75, which implies that the actual critical value of $A_0$ would be about 25% lower than the approximate critical value $A_\infty$ estimated in Section

4.4 without considering the end-effect. On the other hand, if the amplified factor is 3, the end-effect factor $\varepsilon$ determined by Fig.4.10 is about 0.6, which implies that the actual critical value of $A_0$ will be about 40% lower than the approximate critical value $A_\infty$ estimated in Section 4.4 without the end-effect.

Finally, based on the results shown in Fig.4.6 and Figs.4.9-4.10, the critical value of $A_0$ for instability of two opposing arrays of microcantilevers with the end-effect is calculated and shown in Fig.4.11 (with $E_1 I_1 = E_2 I_2 = EI$ and $L_1 = L_2 = L$), as a function of the overlap depth $\delta / L$. It is seen from Fig.4.11 that, similar to the critical value without the end-effect (which is a half of the critical value for two opposing microcantilevers given by Fig.4.6), the critical value with the end-effect is also a non-monotonic function of the overlap depth $\delta / L$ and attains its minimum around $\delta / L = 0.5$. Therefore, when $E_1 I_1 = E_2 I_2$ and $L_1 = L_2$, the lowest critical value of $A_0$ occurs around $\delta / L = 0.5$.

## 4.5.2 Microcantilevers of different bending rigidities

In many cases of practical significance, although the lengths of two opposing arrays are identical or close to each other, differences in other parameters, such as material parameter, width, and thickness (see Fig.4.1), can cause a big difference in bending rigidity of two opposing arrays. Next, we will consider instability of two opposing microcantilever arrays with different bending rigidities, and the following two typical cases will be considered: 1) the bending rigidity of the upper array is more than that of the lower array (for example, $E_2 I_2 = 0.1 E_1 I_1$, $L_1 = L_2$ and $N$ is an odd number); 2) the bending rigidity of the upper array is less than that of the lower array (for example, $E_2 I_2 = 10 E_1 I_1$, $L_1 = L_2$ and $N$ is an odd or even number). The two cases are equivalent only when $N$ is an even number.

Following the similar steps described in Section 4.5.1, the critical value of $A_0$ for instability with the end-effect, as a function of the overlap depth $\delta/L_1$, is shown in Fig.4.12-$a$ when $E_2 I_2 = 0.1 E_1 I_1$, $L_1 = L_2$ and $N$ (=11) is an odd number. It should be noted that for the case with $E_2 I_2 = 0.1 E_1 I_1$, $L_1 = L_2$ and $N$ as an odd number, the rigidity of the second beam $k$=2 (or $N$-1) is much less than the rigidity of the end beam $k$=1 (or $k$=$N$), thus, $|Y_2(x)| > Y_1(x)$ and $Y_{N-1}(x) > |Y_N(x)|$ (as shown in Fig.4.3-$d$ for the similar spring system). Therefore, not only the distance change between the beams $k$=1 and $k$=2 but also that between the beams $k$=2 and $k$=3 accounts for the end-effect. The detailed description can be found in [128]. Based on the critical value for instability without the end-effect shown in Fig.4.8 for $L_1 = L_2$, it is seen from Fig.4.12-$a$ that the end-effect factor $\varepsilon$ is around 0.9-0.95, and the end-effect lowers the critical value for instability by 5%-10%, irrespective of the overlap depth.

Similarly, the critical value for instability with the end-effect when $E_2 I_2 = 10 E_1 I_1$ and $L_1 = L_2$, as a function of the overlap depth $\delta/L_1$, is shown in Fig.4.12-$b$. Similar to the spring system with $q_1 < q_2$ as shown in Fig.4.3-$a$, the deflection of the second beam ($k$=2) is much smaller than the largest deflection of the end beam ($k$=1), therefore, the distance change between the beams $k$=2 and $k$=3 is neglected, and only the distance change between the beams $k$=1 and $k$=2 accounts for the end-effect. Although the end-effect occurs at the left end only when the number $N$ of microcantilevers is an even number, and occurs at both the left and right ends when $N$ is an odd number, the critical values for instability are same, regardless of $N$ as an even or odd number (similar to the spring system with $q_1 < q_2$). Based on the critical value for instability without the end-effect shown in Fig.4.7 for $L_1 = L_2$, it is seen from Fig.4.12-$b$ that the end-effect

factor $\varepsilon$ is around 0.55-0.7, and the end-effect lowers the critical value for instability by 30%-45%, irrespective of the overlap depth. In addition, we should point out that when $N$ is an even number, the case with $E_2I_2 = 0.1E_1I_1$ and $L_1 = L_2$ is equivalent to the case with $E_2I_2 = 10E_1I_1$ and $L_1 = L_2$ if we define the right end beam as the first ($k$=1) and the left end as the last ($k$=$N$). Therefore, the end-effect on instability of the comb-drive array with $E_2I_2 = 0.1E_1I_1$, $L_1 = L_2$ and $N$ as an even number is equivalent to the end-effect on instability for $E_2I_2 = 10E_1I_1$, $L_1 = L_2$ and $N$ as an even number.

Based on Fig.4.11 and Fig.4.12, it is found that the end-effect lowers the critical value for instability, and the reduction in the critical value for instability depends on the rigidities of the end beams at the two ends of the comb-drive array. For example, for the case with $E_2I_2 = 0.1E_1I_1$, $L_1 = L_2$ and $N$ as an odd number, the rigidities of two end beams are big, and the end effect reduces the critical value for instability by 5% or 10%. For the case with $E_1I_1 = E_2I_2$, $L_1 = L_2$ (regardless of $N$ as an odd or even number), the rigidities of the end beams are identical to the rigidities of the other beams in the array, and the end effect reduces the critical value for instability by 25% or 35%. When the rigidity of one of the two end beams is small, such as the case with $E_2I_2 = 10E_1I_1$ and $L_1 = L_2$ (regardless of $N$ as an odd or even number), or the case with $E_2I_2 = 0.1E_1I_1$, $L_1 = L_2$ and $N$ as an even number, the end effect reduces the critical value for instability by 30% or 45%. That is to say, the smaller the rigidity of one of the two end beams, the more the reduction in the critical value for instability with the end-effect. This conclusion is consistent with the results for simplified spring system and confirms that end design could have a significant effect on instability of comb-drive microcantilever arrays.

To demonstrate the effectiveness of the present method, we try to compare our results with experimental data available in the literature. Grade et al. [142] found that for

the comb-drive microcantilevers with similar geometric parameters under electrostatic forces ($n$=2), the maximum deflection of the end beams at the onset of instability is about $0.25\,d_0$. With our present method, we can also approximately determine the distance change between the end beam $k$=1 and its neighbor $k$=2 at the onset of instability by solving Eqns (4.29, 4.30) with $Y_3 = 0$. For example, when $E_1 I_1 = E_2 I_2 = EI$ and $L_1 = L_2 = L$, the results show the average distance change between the end beam and its neighbor at the onset of instability is $0.256\,d_0$ for $\delta/L$=0.2, or $0.249\,d_0$ for $\delta/L$=0.5, or $0.242\,d_0$ for $\delta/L$= 0.8. Thus, with the present method the relative error in the distance change between the first cantilever and its neighbor at the onset of instability is less than 3.2% for $\delta/L$=0.2, 0.5, and 0.8.

In addition, as a special case, it is noted that microcantilevers in the extreme case $\delta/L_1$=0.1 can be approximately described as a parallel array of linear springs. For example, for the microcantilevers in the array with $E_1 I_1 = E_2 I_2 = EI$, $L_1 = L_2 = L$ and $\delta/L$=0.1, the interaction forces between two adjacent cantilevers have their resultant force at the middle point of the overlap domain ($x_1 = x_2$=0.95L). At this point, the deflection is $(P(0.95L)^3/(3EI))$ with application of a concentrated load $P$, and the equivalent spring constant is $(3EI/(0.95L)^3) \approx 3.5 EI/L^3$. Because the exact critical value for a spring system with $q_1 = q_2$ is $B$=1/11, the critical value for $\delta/L$=0.1 should be $(\dfrac{A_0}{EI(\frac{\pi}{L})^4}) \approx 0.0656$. On the other hand, it is seen from Fig.4.11 that the critical value given by the present method is $(\dfrac{A_0}{EI(\frac{\pi}{L})^4}) \approx 0.067$ when $\delta/L$=0.1. Hence, it is concluded that the relative error of the present results given by Fig.4.11 is less than 3% when $\delta/L$=0.1. Comparison for other cases of overlap depth is not available due to a

lack of relevant data.

In next section we shall apply the present method to the spring system described in Section 4.3 to examine the accuracy of the present method.

## 4.6 Comparisons with exact results obtained by iteration method

Let us apply the present method to the spring system and compare the results with exact results obtained by numerical iteration method. Here, it should be stated that the spring system is believed to represent essential features of microbeam arrays. Actually, the comb-drive arrays examined in [102-112] have been studied entirely based on the similar spring systems.

It is found in Section 4.3 that for most cases (except the case when $\beta=5$ and $N$ is an odd number shown in Fig.4.3-$d$), even the second springs at two sides have a very small displacement compared to the largest displacement of the end springs ($k=1$ or $k=N$). Therefore, for these cases, the distance change between the springs $k=2$ and $k=3$ or between the springs $k=N$-2 and $k=N$-1 is negligible, and the amplified interaction between the end spring and its neighbor would be mainly responsible for the end-effect. Thus, for most cases, the end-effect on instability can be analyzed by estimating the amplified factor $\alpha$ between the end spring and its neighbor (for the case when $\beta=5$ and $N$ is an odd number, we have to consider both of the amplified factor $\alpha$ and the modified factor $\lambda$).

### 4.6.1 Estimate of the amplified factor $\alpha$ for the spring system

In order to quantify the end-effect, we have to estimate the distance reduction between the end spring and its neighbor. As explained in Section 4.5, it is a good approximation to neglect the displacement of the spring $k=3$ at the left end (or the spring

$k=N-2$ at the right end) and consider the first two Eqns of (4.8-4.12) with $Y_3 = 0$, which give

$$-\frac{Y_1}{d_0} + \frac{B}{(1+\frac{Y_2}{d_0}-\frac{Y_1}{d_0})^n} = 0 \tag{4.34}$$

$$-\frac{Y_2}{d_0} + \frac{\beta B}{(1-\frac{Y_2}{d_0})^n} - \frac{\beta B}{(1+\frac{Y_2}{d_0}-\frac{Y_1}{d_0})^n} = 0 \tag{4.35}$$

Numerical results of (4.34, 4.35) for $n=2$ indicate that when $\beta=0.2$ and $B=1/7.543$ (the exact critical value), the distance reduction between the springs 1 and 2 obtained from (4.34, 4.35) is $(Y_1-Y_2)/d_0=0.295$, which is very close to the exact value 0.31 obtained from exact Eqns (4.8-4.12). In particular, the approximate amplified factor is then $\alpha \approx 2.86$ which is close to the accurate $\alpha = 3$. Similarly, for $\beta=1$ and $B=1/11$ (the exact critical value), the distance reduction between the springs 1 and 2 obtained from (4.34, 4.35) is $(Y_1-Y_2)/d_0=0.22$, which is very close to exact value 0.24 obtained from exact Eqns (4.8-4.12). The corresponding approximate amplified factor $\alpha \approx 2.1$ which is close to the accurate $\alpha = 2.3$. On the other hand, when $\beta=5$ and $N$ is an even number (say, $N=20$), the end-effect occurs at the right end, and the distance reduction between the springs $N$ and $N-1$ at $B=1/37.713$ (the exact critical value) is $(Y_1-Y_2)/d_0=0.295$, which is very close to the exact value 0.31 obtained from exact Eqns (4.8-4.12). The corresponding approximate amplified factor $\alpha \approx 2.86$ which is close to the accurate $\alpha = 3$. Finally, for $\beta=5$ and $N$ is an odd number (say, $N=21$), the distance reduction between the springs 1 and 2 when $B=1/28.1$ (the exact critical value) obtained from (4.34,

4.35) is $(Y_1 - Y_2)/d_0$ =0.134, which is reasonably close to the exact value 0.173 obtained

from exact Eqns (4.8-4.12). In addition, the distance increase between the springs 2 and 3

obtained from (4.34, 4.35) with $Y_3$ =0 is $Y_2/d_0$ =0.087, which is reasonably close to the

exact value 0.12 obtained from exact Eqns (4.8-4.12). In particular, the approximate

amplified factor for the springs 1 and 2 is $\alpha \approx 1.54$ compared to the accurate $\alpha = 1.78$,

while the modified factor for the interaction coefficient between the springs 2 and 3 is

$\lambda \approx 0.78$ (that is, $A_{2,3} = 0.78 A_0$) compared to the accurate $\lambda = 0.71$. From these

comparisons, it is concluded that the relative errors of the simple estimate of $Y_1$ and $Y_2$

based on the two Eqns (4.34, 4.35) are usually limited to 10% or less for most examples

considered here. Therefore, it does offer an effective simple method to estimate the

distance changes between adjacent springs at each of the two ends and the associated

amplified factors.

The amplified factor for the interaction coefficient between the end spring $k$=1 and

its neighboring spring $k$=2, or between the end spring $k$=$N$ and its neighboring spring

$k$=$N$-1, is estimated based on the approximate method (4.34, 4.35) and demonstrated in

Fig.4.13, as a function of the loading parameter $B$ for $\beta$ =0.2, 1 and 5 ($n$=2). It is seen

that the amplified interaction coefficient between the end spring and its neighboring

spring can be as large as 2-3 times the interaction coefficient for other intermediate

springs defined by (4.13) when the loading parameter approaches the critical value for

instability. As shown below, the amplified interaction coefficient between the end spring

and its neighboring spring is mainly responsible for the end-effect.

## 4.6.2 End-effect on instability of the spring system

Let us now examine the effect of the amplified factor on the critical value for

instability by studying the existence of non-zero solutions of (4.14-4.18) with an

amplified factor $\alpha$ for the interaction coefficient between the two springs at one or both of the two ends. Here, two remarks should be mentioned. First, the amplified factor may be applied to one or both of the two ends, dependent on the ratio $\beta$ and whether $N$ is an odd or even number. For example, when $\beta=0.2$, it is seen from Fig.4.3-$a$ that the distance change between the end spring and its neighbor is significant only at the left end but not at the right end for an even number $N$, while it is significant for both ends for an odd number $N$. Consequently, the amplified factor is applied only to the left end when $N$ is an even number, while the same amplified factor is applied to both ends when $N$ is an odd number. Second, besides the amplified factor for the end spring and its neighbor, the distance change between the springs $k=2$ and $k=3$, or between the springs $k=N-2$ and $k=N-1$, is negligible in most cases, but can be non-negligible in some special cases. For example, when $\beta=5$, it is seen from Fig.4.3-$c,d$ that the distance change between the springs $k=2$ and $k=3$ and between the springs $k=N-2$ and $k=N-1$ is small and negligible for an even number $N$, but comparable to the distance change between the end spring and its neighbor and then non-negligible for an odd number $N$.

When the same amplified factor is applied to both ends and the distance change between the beams $k=2$ and $k=3$ or between the beams $k=N-2$ and $k=N-1$ is negligible (it is the case when $\beta=0.2$ and $N$ is an odd number, or when $\beta=1$ and $N$ is an even or odd number), the end-effect on the critical value for instability can be studied by examining the dependence on the amplified factor $\alpha$ of the lowest eigenvalue of the problem

$$-\frac{y_1}{d_0} - \alpha n B(\frac{y_2}{d_0} - \frac{y_1}{d_0}) = 0, \, k=1, \tag{4.36}$$

$$-\frac{y_2}{d_0} - n\beta B(\frac{y_3}{d_0} - \frac{y_2}{d_0}) + \alpha n\beta B(\frac{y_2}{d_0} - \frac{y_1}{d_0}) = 0, \, k=2, \tag{4.37}$$

$$-\frac{y_k}{d_0} - nB(\frac{y_{k+1}}{d_0} - \frac{y_k}{d_0}) + nB(\frac{y_k}{d_0} - \frac{y_{k-1}}{d_0}) = 0, \; k=3,5,\ldots \tag{4.38}$$

$$-\frac{y_k}{d_0} - n\beta B(\frac{y_{k+1}}{d_0} - \frac{y_k}{d_0}) + n\beta B(\frac{y_k}{d_0} - \frac{y_{k-1}}{d_0}) = 0, \; k=4,6,\ldots \tag{4.39}$$

$$-\frac{y_{N-1}}{d_0} - \alpha n\beta B(\frac{y_N}{d_0} - \frac{y_{N-1}}{d_0}) + n\beta B(\frac{y_{N-1}}{d_0} - \frac{y_{N-2}}{d_0}) = 0, \; k=N\text{-}1, \text{ where } N \text{ is an odd number}$$

$$\tag{4.40}$$

$$-\frac{y_{N-1}}{d_0} - \alpha nB(\frac{y_N}{d_0} - \frac{y_{N-1}}{d_0}) + nB(\frac{y_{N-1}}{d_0} - \frac{y_{N-2}}{d_0}) = 0, \; k=N\text{-}1, \text{where } N \text{ is an even number}$$

$$\tag{4.41}$$

$$-\frac{y_N}{d_0} + \alpha nB(\frac{y_N}{d_0} - \frac{y_{N-1}}{d_0}) = 0, \; k=N \quad \text{is an odd number} \tag{4.42}$$

$$-\frac{y_N}{d_0} + \alpha n\beta B(\frac{y_N}{d_0} - \frac{y_{N-1}}{d_0}) = 0, \; k=N \quad \text{is an even number} \tag{4.43}$$

Obviously, Eqns (4.36-4.43) reduce to (4.14-4.18) when $\alpha=1$. Thus, the end-effect factor $\varepsilon$, defined by the ratio of the critical value of $B$ with the end-effect to the critical value of $B$ without the end-effect, can be calculated as a function of the amplified factor $\alpha$ by solving the eigenvalue problem with Eqns (4.36-4.43).

Here, for all cases in which the small distance change between the beams $k=2$ and $k=3$ or between the beams $k=N$-2 and $k=N$-1 is negligible, the end-effect factor $\varepsilon$ is shown in Fig.4.14, as a function of the amplified factor $\alpha$ applied to one or both of the two ends. On the other hand, when $\beta=5$ and $N$ is an odd number (the only case considered here in which the distance change between the beams $k=2$ and $k=3$ or between the beams $k=N$-2 and $k=N$-1 is large and non-negligible), the end-effect factor $\varepsilon$ is shown in Fig.4.15, as a function of the amplified factor applied to both ends for a varying modified factor $\lambda$ for the interaction coefficients $A_{2,3}$ and $A_{N-2,N-1}$, where $\lambda$ (<1) is

defined by $A_{2,3} = A_{N-2,N-1} = \lambda A_0$. In other words, for the case shown in Fig.4.15, the interaction coefficients with the end-effect are $A_{3,4} = A_{4,5} = ... = A_{N-3,N-2} = A_0$, $A_{2,3} = A_{N-2,N-1} = \lambda A_0$ and $A_{1,2} = A_{N-1,N} = \alpha A_0$, where $A_0$ is defined by (4.19).

We can determine the critical value for instability of the spring system based on Fig.4.13 and Fig.4.14 (or Fig.4.15). For example, it is seen from Fig.4.13 that when $\beta = 0.2$ and $N$ is an even number, the estimated approximate amplified factor for the left end $k=1$ is 2.85 while the accurate $\alpha = 3$. Thus, based on Fig.4.14 (or by solving Eqns (4.36-4.43)), the estimated approximate end-effect factor $\varepsilon$ is found to be 0.67 while the accurate $\varepsilon = 0.63$. Consequently, the approximate critical value of $B$ for instability of the spring system predicted by the present methods is $0.21 \times 0.67 = 0.141$ if the approximate $\alpha$ estimated based on (4.34, 4.35) is used, or is $0.21 \times 0.63 = 0.1323$ if the accurate $\alpha$ is used. Obviously, the formed leads to a relative error less than 10% to the exact critical value $B=0.132$, while the latter is almost coincident with the exact critical value of $B$. Detailed comparison between the approximate critical values given by the present methods and the exact critical values obtained by numerical iteration method is shown in Table 4.1 for all cases considered. It is seen from Table 4.1 that for the $N$-spring system, the critical values of $B$ predicted by the linear instability model are very close to the exact numerical results obtained by solving the nonlinear Eqns (4.8-4.12), with relative errors around or less than 5%. Even when the rude estimate based on (4.34, 4.35) is used, the relative errors of the present methods is less than 10%. This suggests that the present method offers a simple approximate method to determine the critical value for instability of two opposing microcantilever arrays. Although the Ritz method (or the Galerkin method) along with Newton iteration method can be applied to analyze the exact structural instability of two opposing microcantilever arrays, it would be a very challenging nonlinear problem especially when the number of parallel microbeams is large.

## 4.7 Conclusions

Structural instability of two opposing arrays of mutually attracting microcantilevers is studied. When the end-effect of the beams at the ends of the array is neglected, the critical value of the beam-beam interaction coefficient for instability of the array is exactly half of the critical value for instability of two mutually attracting opposing cantilevers. In particular, the role of overlap length over which each beam is attracted by two neighboring opposing beams is examined for variable lengths and bending stiffnesses of microcantilevers. Furthermore, the end-effect is studied by examining the effect on the critical value for instability of the enhanced interaction coefficient between the beams at the ends of the array. It is found that the end-effect lowers the critical interaction coefficient for instability, and the reduction in the critical value for instability increases as bending rigidities of the end beams decrease. The validity of the present method is confirmed by good agreement between the results obtained by the present methods for a representative spring system and the exact results obtained by numerical method.

Table 4.1 Comparison of the critical value of $B$ predicted by the present methods for the spring system with the exact critical value obtained by iteration numerical method.

| | | Critical value without end effect | Present method based on approximate $\alpha$ | | Present method based on accurate $\alpha$ | | Exact critical value of $B$ |
|---|---|---|---|---|---|---|---|
| | | | $\alpha$ | $B$ | $\alpha$ | $B$ | |
| $\beta=0.2$ | $N$=20 | 0.209 | 2.86 | 0.140 | 3 | 0.1317 | 0.1326 |
| | $N$=21 | 0.209 | 2.86 | 0.140 | 3 | 0.1317 | 0.1326 |
| $\beta=1$ | | 0.125 | 2.1 | 0.0975 | 2.3 | 0.0913 | 0.0909 |
| $\beta=5$ | $N$=20 | 0.042 | 2.86 | 0.0281 | 3 | 0.0263 | 0.0265 |
| | $N$=21 | 0.042 | $\alpha=1.54$ $\lambda=0.78$ | 0.0378 | $\alpha=1.78$ $\lambda=0.71$ | 0.0357 | 0.0356 |
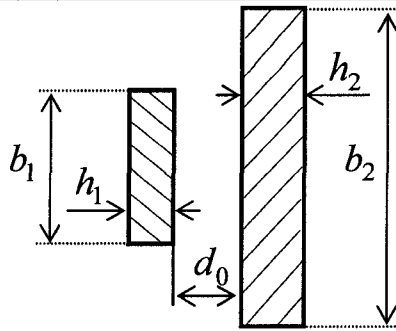
Enlarged cross-sections of microcantilevers
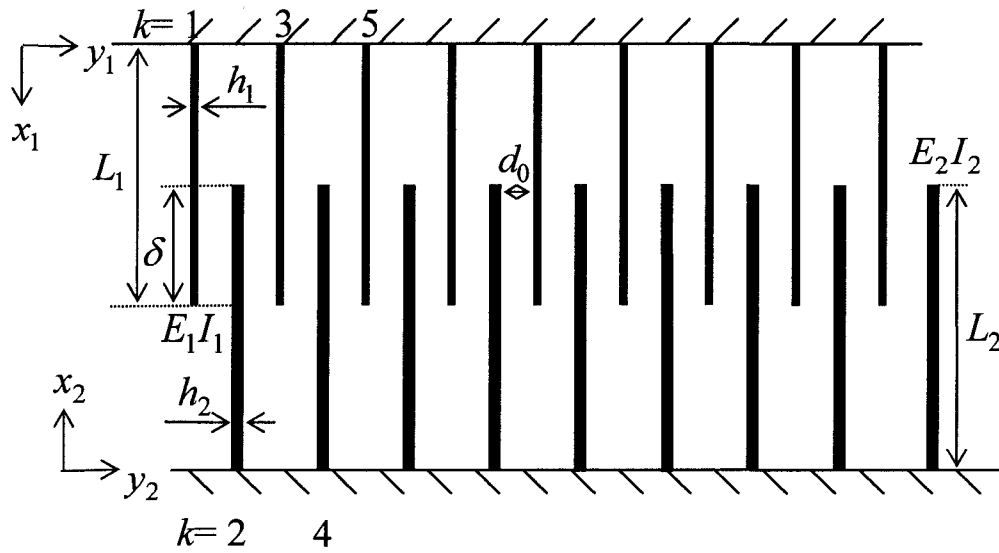


Fig.4.1 A comb-drive microcantilever array.
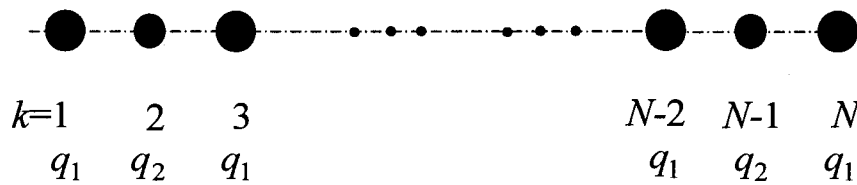


Fig.4.2 A spring system consisting of alternating array of the springs with spring constant $q_1$ and the springs with spring constant $q_2$.
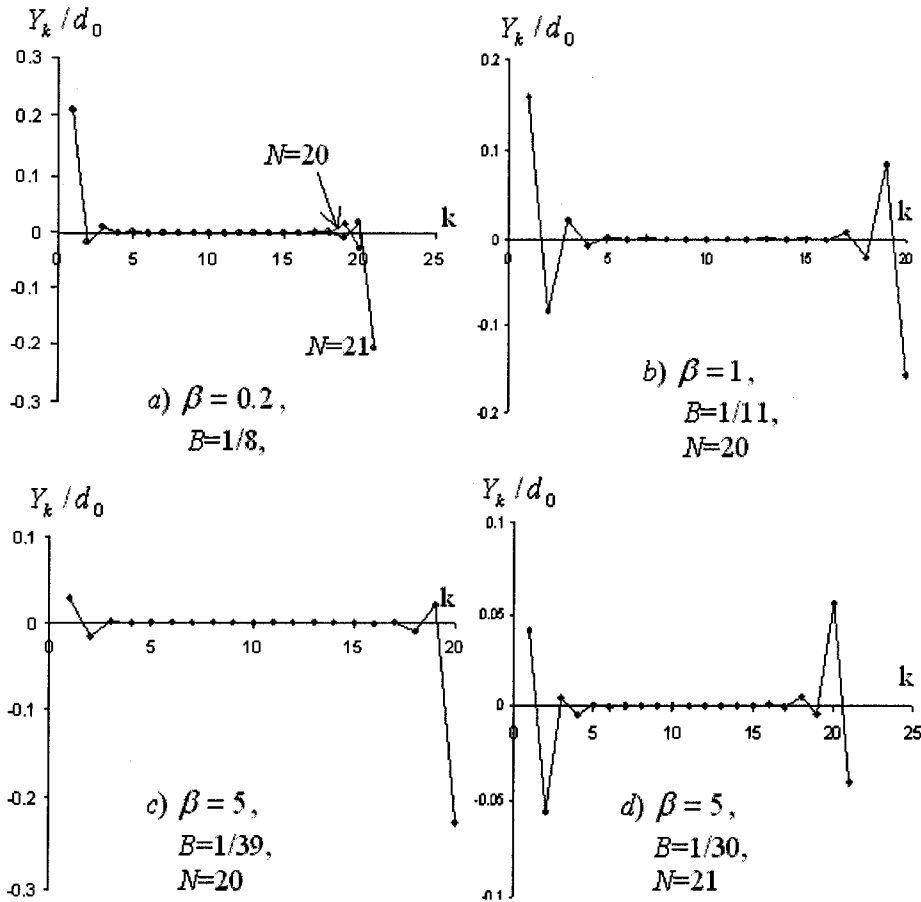
Fig.4.3 Pre-instability equilibrium displacements of $N$ mutually attracting springs for $n=2$ when $N=20$ or 21. $a$) $\beta=0.2$, $B=1/8$; $b$) $\beta=1$, $B=1/11$; $c$) $\beta=5$, $B=1/39$, and $N=20$; $d$) $\beta=5$, $B=1/30$, and $N=21$.
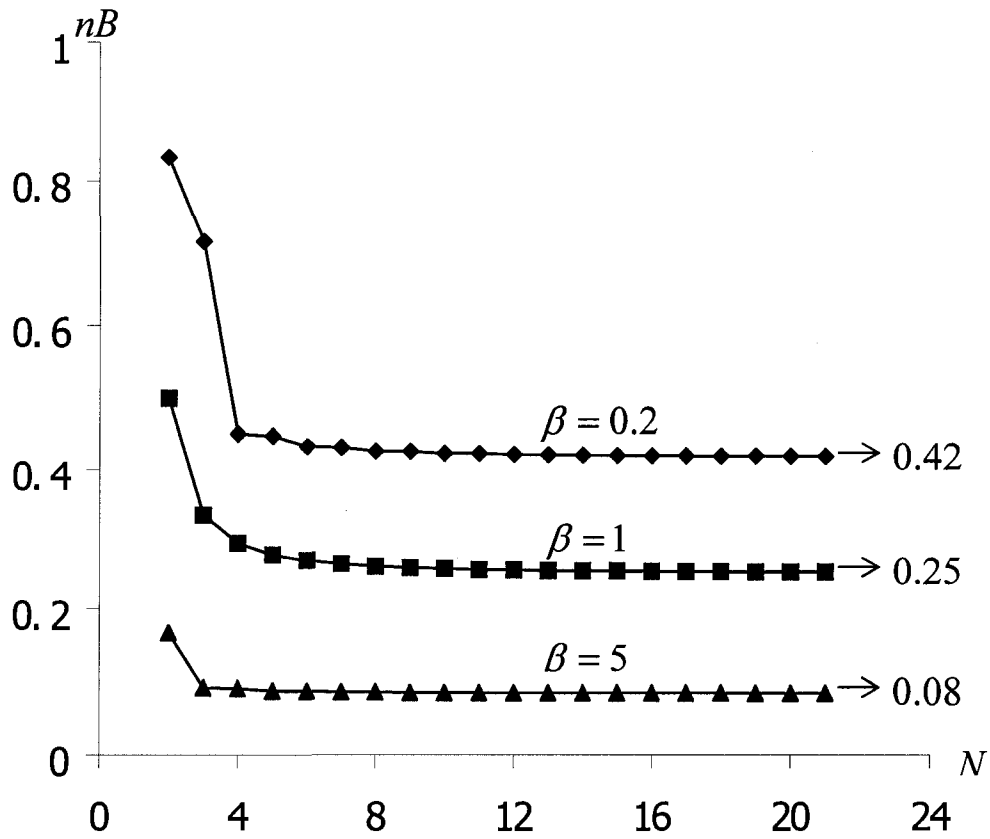
Fig.4.4 Critical value of ($nB$) for instability of the spring system with varying spring-constant ratio $\beta$ when the end-effect is neglected.
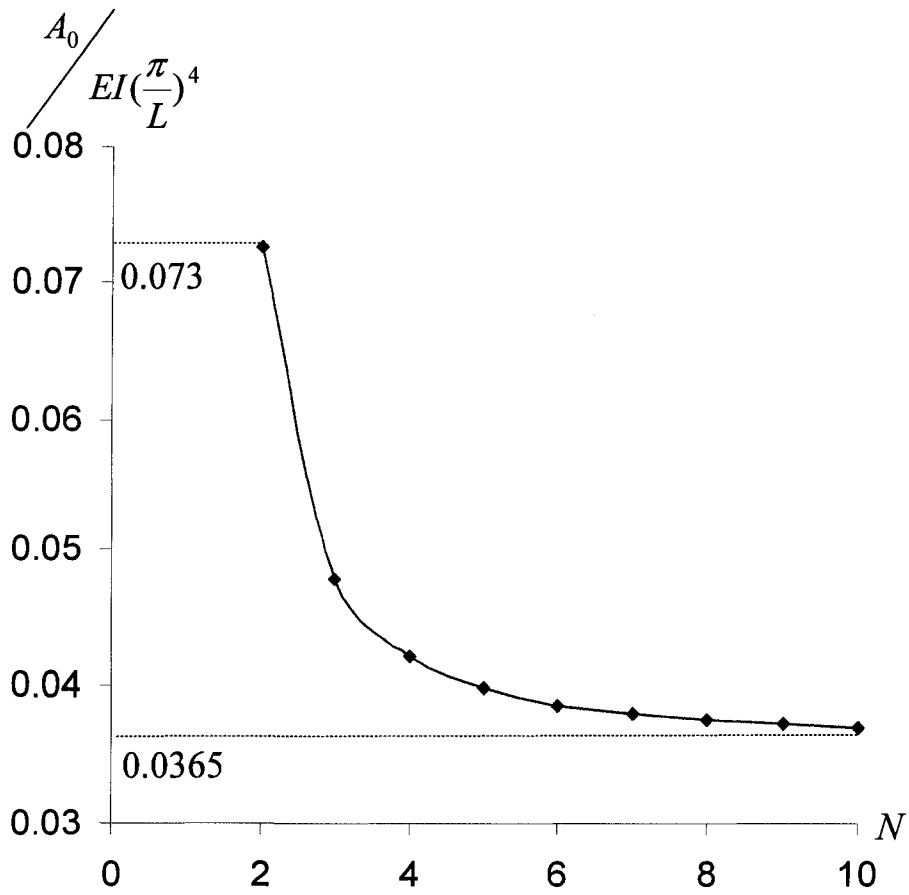
Fig.4.5 Critical value of the beam-beam interaction coefficient $A_0$ for instability of two opposing arrays of microcantilevers without the end-effect, as a function of the number of microcantilevers $N$ (when $L_1 = L_2$ , $E_1 I_1 = E_2 I_2$ , and $\delta / L_1 = 0.5$).
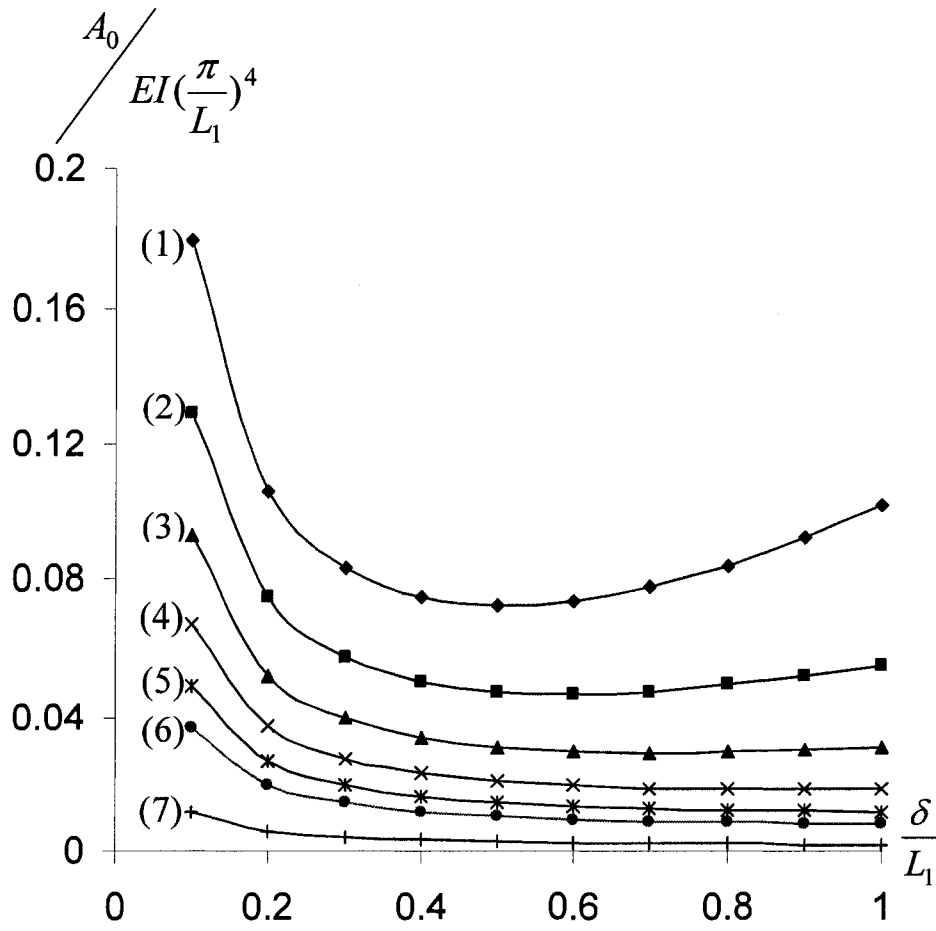
(1): $L_2 / L_1 = 1$; (2): $L_2 / L_1 = 1.2$; (3): $L_2 / L_1 = 1.4$; (4): $L_2 / L_1 = 1.6$;

(5): $L_2 / L_1 = 1.8$;    (6): $L_2 / L_1 = 2$;    (7): $L_2 / L_1 = 3$

Fig.4.6 Critical value of the beam-beam interaction coefficient $A_0$ for two opposing microcantilevers with varying length ratio $L_2 / L_1$, as a function of the overlap depth $\delta / L_1$ when $E_2 I_2 = E_1 I_1$.
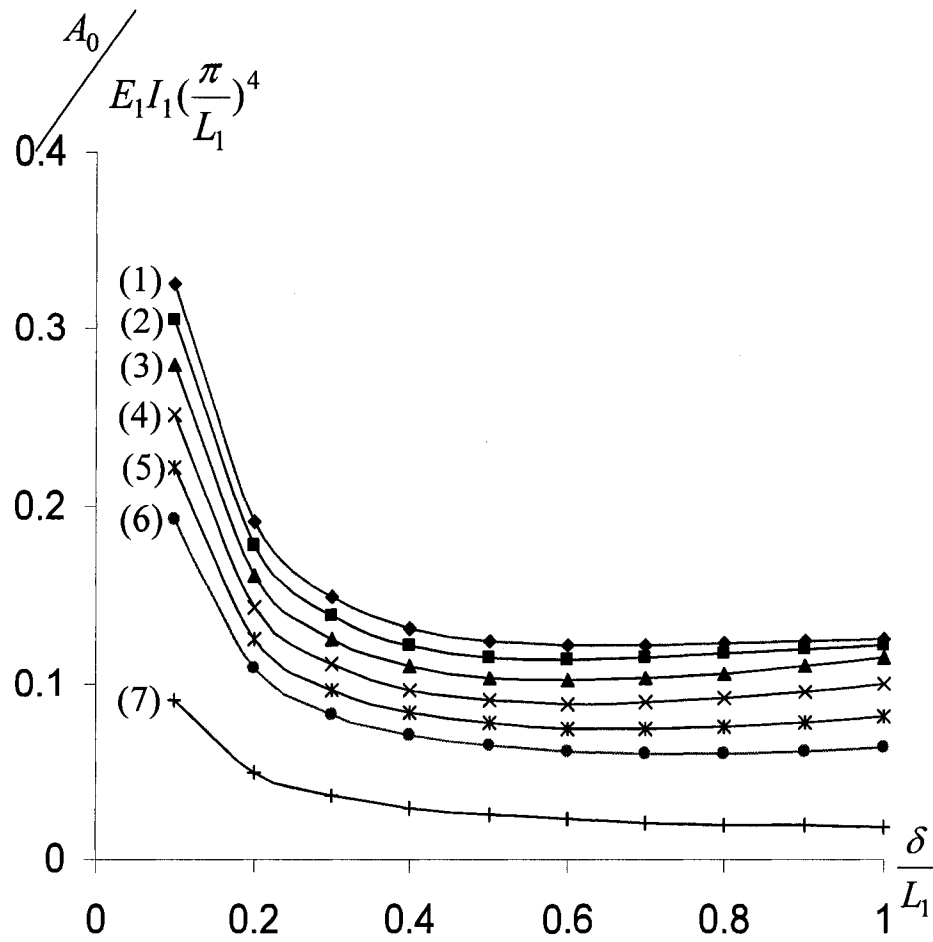
(1): $L_2 / L_1 = 1$; (2): $L_2 / L_1 = 1.2$; (3): $L_2 / L_1 = 1.4$; (4): $L_2 / L_1 = 1.6$;

(5): $L_2 / L_1 = 1.8$;　(6): $L_2 / L_1 = 2$;　(7): $L_2 / L_1 = 3$

Fig.4.7 Critical value of the beam-beam interaction coefficient $A_0$

for two opposing microcantilevers with varying length ratio $L_2 / L_1$,

as a function of the overlap depth $\delta / L_1$ when $E_2 I_2 = 10 E_1 I_1$.
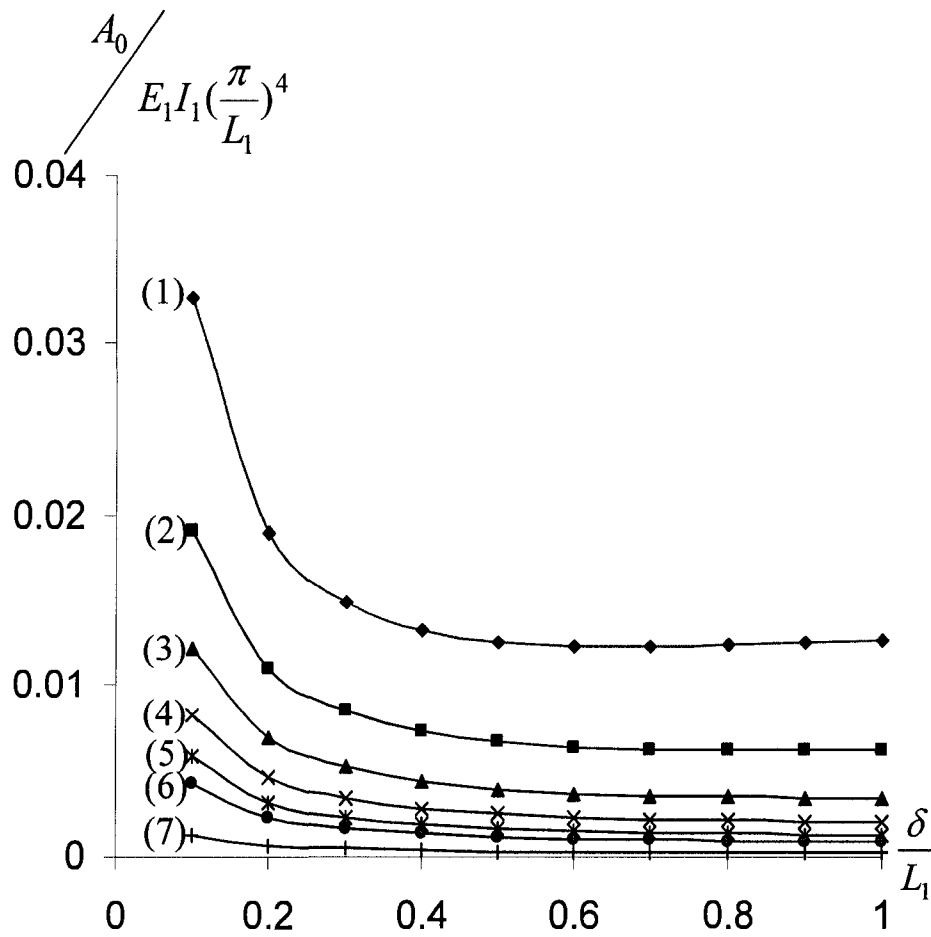
(1): $L_2 / L_1 = 1$; (2): $L_2 / L_1 = 1.2$; (3): $L_2 / L_1 = 1.4$; (4): $L_2 / L_1 = 1.6$;

(5): $L_2 / L_1 = 1.8$;     (6): $L_2 / L_1 = 2$;     (7): $L_2 / L_1 = 3$

Fig.4.8 Critical value of the beam-beam interaction coefficient $A_0$

for two opposing microcantilevers with varying length ratio $L_2 / L_1$,

as a function of the overlap depth $\delta / L_1$ when $E_2 I_2 = 0.1 E_1 I_1$.
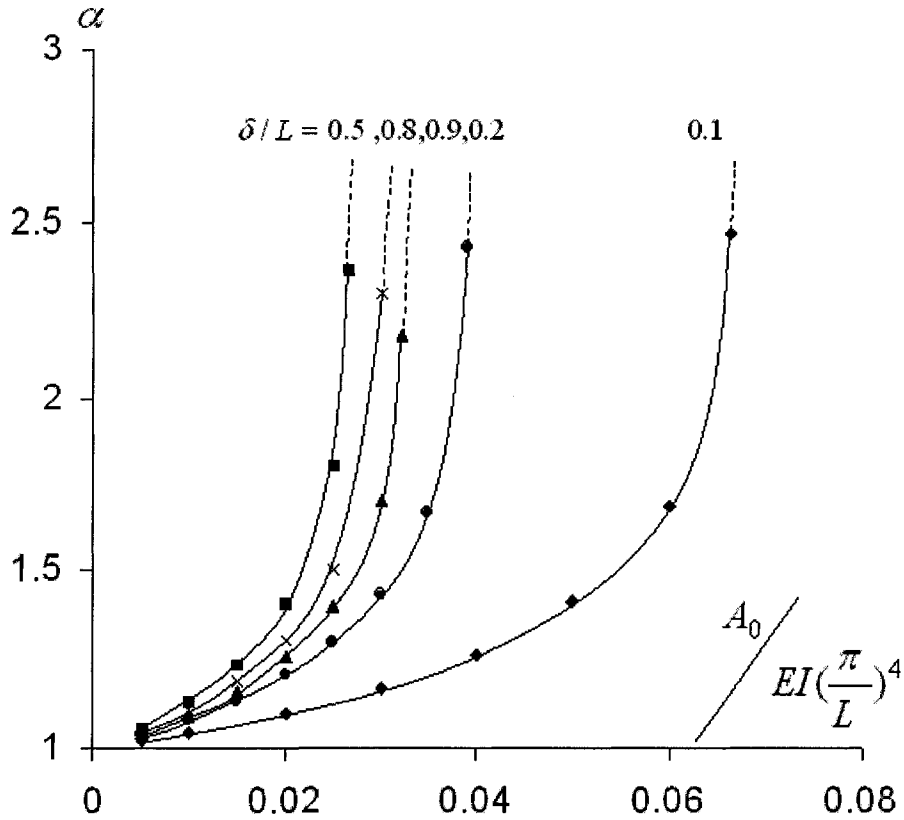
Fig.4.9 Amplified factor $\alpha$ for the interaction coefficient between the end beam and its neighboring beam estimated based on approximate method (4.29, 4.30), as a function of the loading parameter $A_0$ defined by (4.19) based on the initial separation $d_0$, for varying overlap depth $\delta/L$ with $E_1 I_1 = E_2 I_2$, $L_1 = L_2$ and $n=2$.
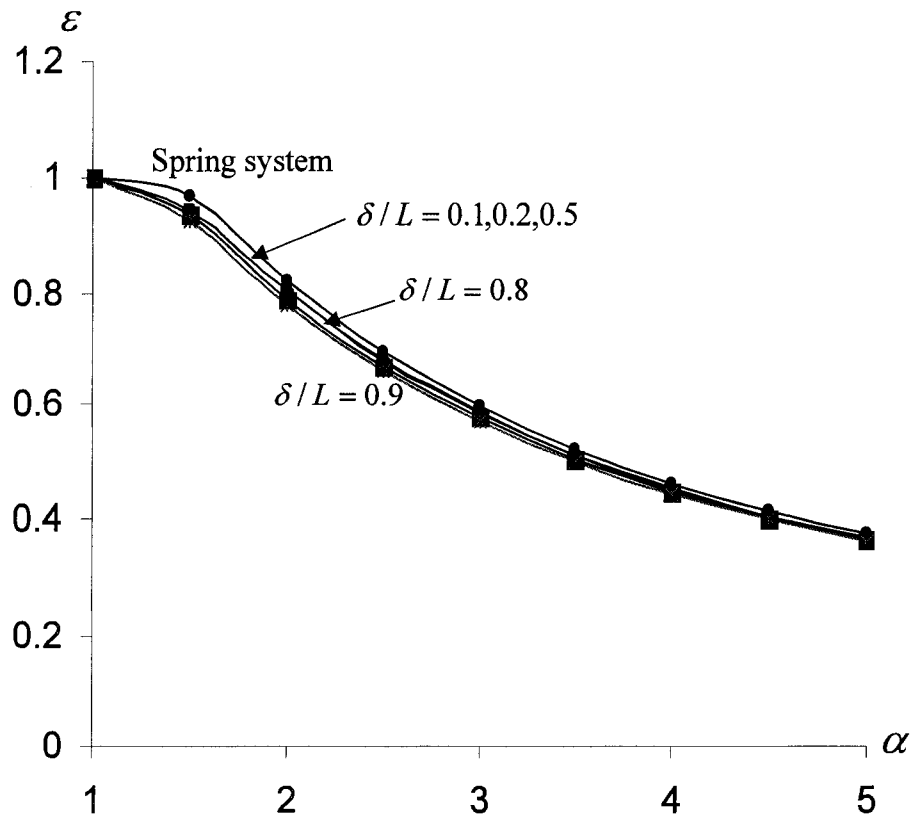
Fig.4.10 End-effect factor $\varepsilon$, defined as the ratio of the critical value with the end-effect to the critical value without the end-effect, as a function of $\alpha$, for two opposing arrays of microcantilevers (when $E_1 I_1 = E_2 I_2$, $L_1 = L_2$) and the spring system when $n=2$.

$$\frac{A_0}{EI(\frac{\pi}{L})^4}$$

0.07

0.06

0.05

0.04

0.03

0.02

0    0.2    0.4    0.6    0.8    1

$$\frac{\delta}{L}$$
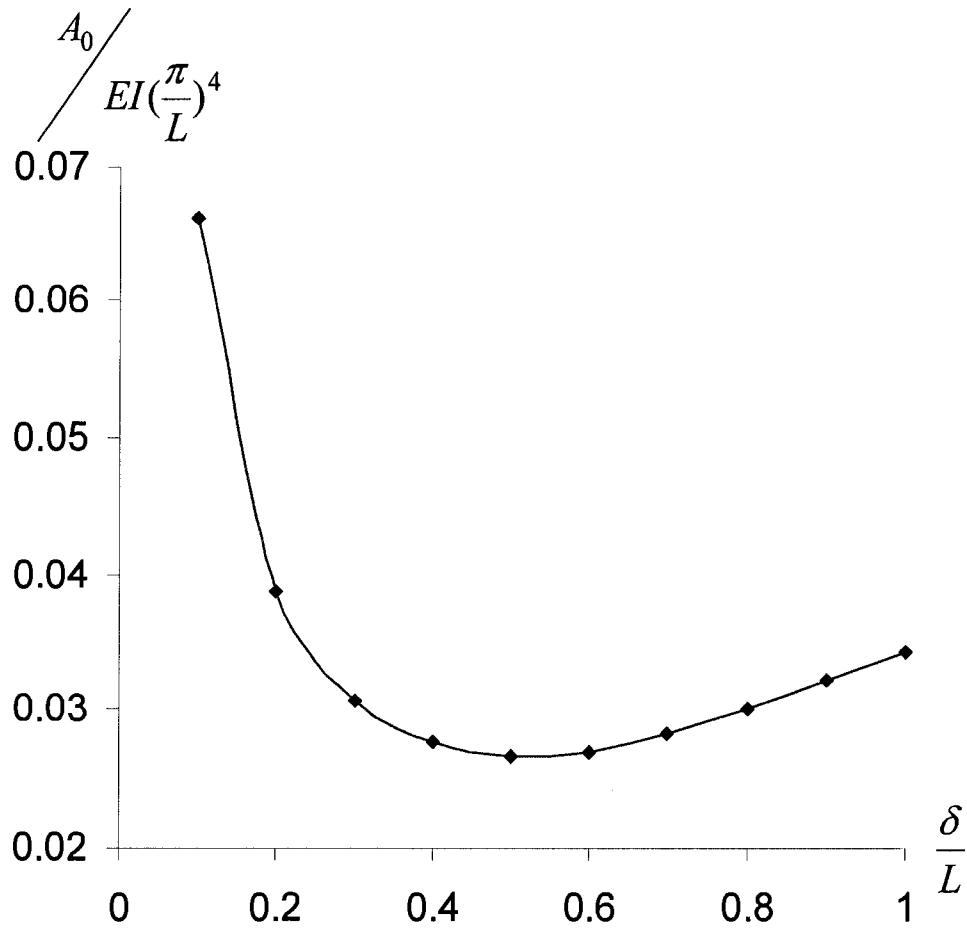
Fig.4.11 Critical value of the loading parameter $A_0$, given by the present method with the end-effect, for instability of two opposing parallel arrays of microcantilevers when $E_1 I_1 = E_2 I_2$, $L_1 = L_2$ and $n=2$.

$(a)$: $E_2 I_2 = 0.1 E_1 I_1$,

$N$ as odd number

$(b)$: $E_2 I_2 = 10 E_1 I_1$,

$N$ as an odd or even number
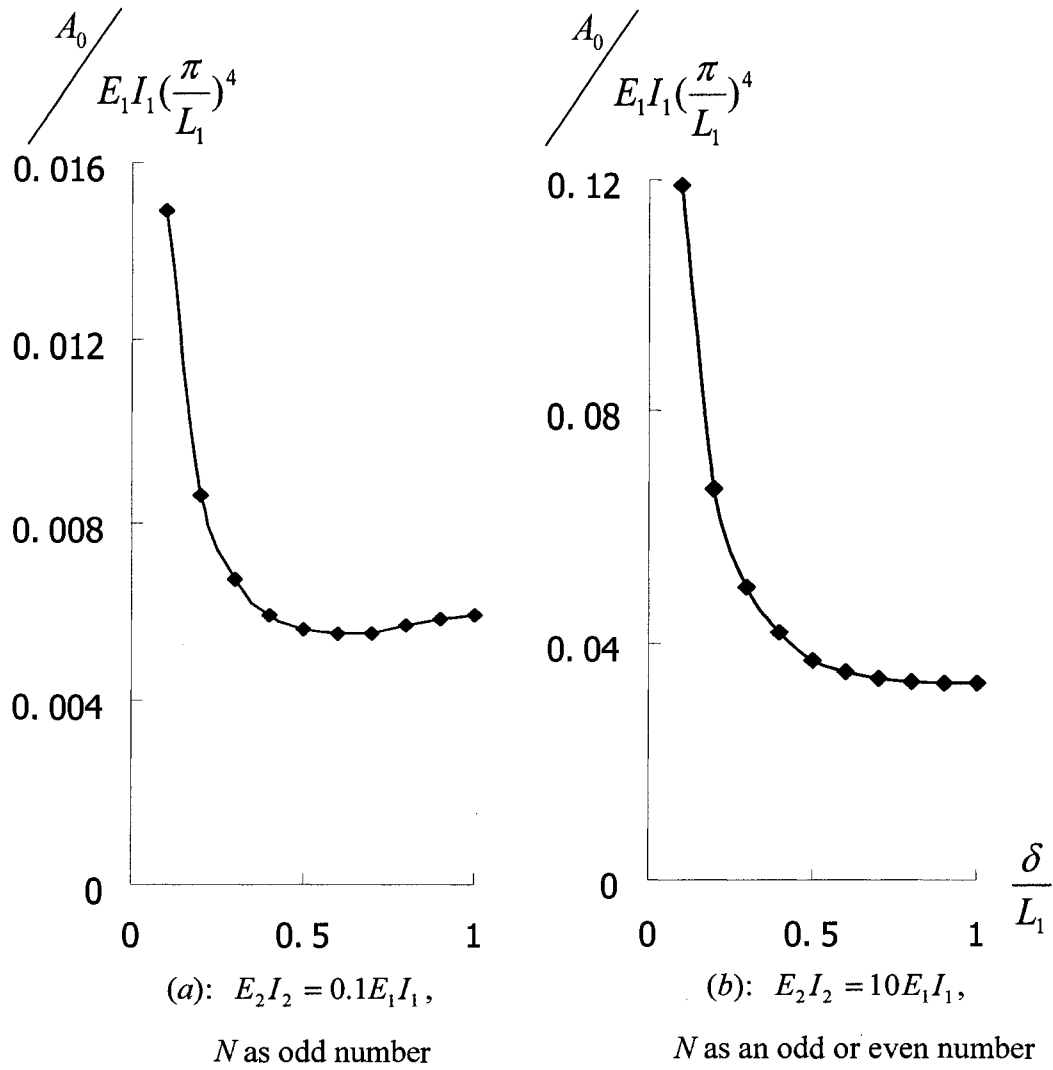
Fig.4.12 Critical value of the loading parameter $A_0$ for instability of comb-drive microcantilever arrays with $L_1 = L_2$, as a function of the depth $\delta / L_1$ when $n=2$.

$\beta = 0.2$        $\beta = 1$        $\beta = 5$
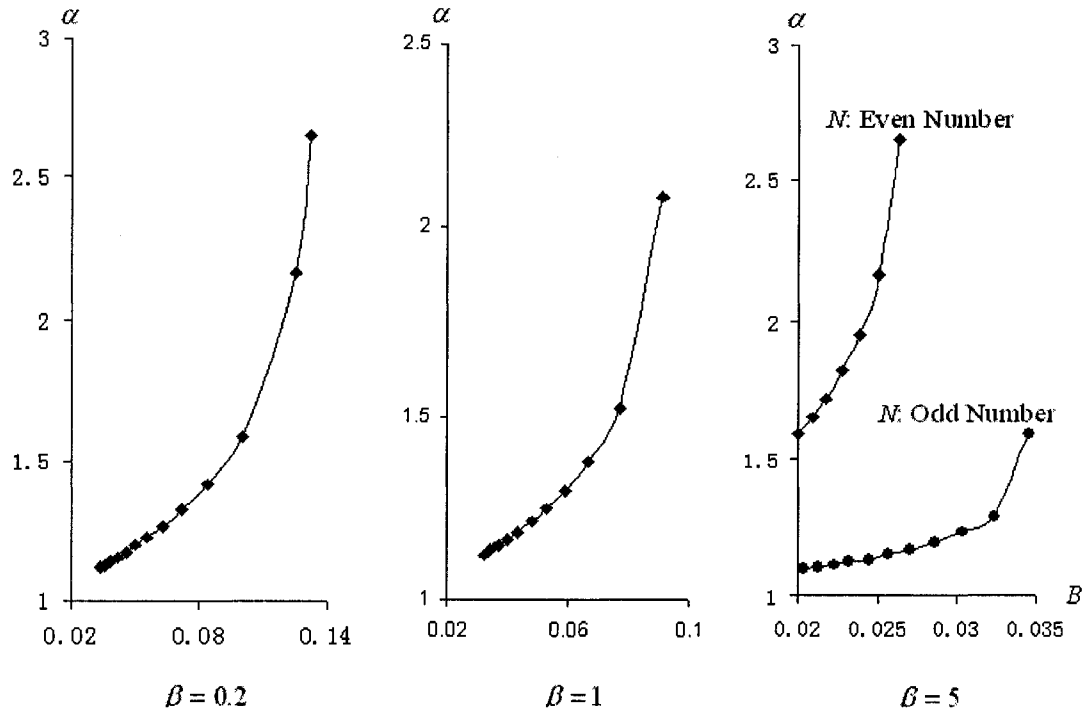
Fig.4.13 Amplified factor for the interaction coefficient between the end spring $k=1$ and its neighbor $k=2$ (or between the end spring $k=N$ and its neighbor $k=N-1$) estimated based on the approximate method (4.34, 4.35), as a function of the loading parameter $B$, for $\beta=0.2$, 1 and 5 ($n=2$).
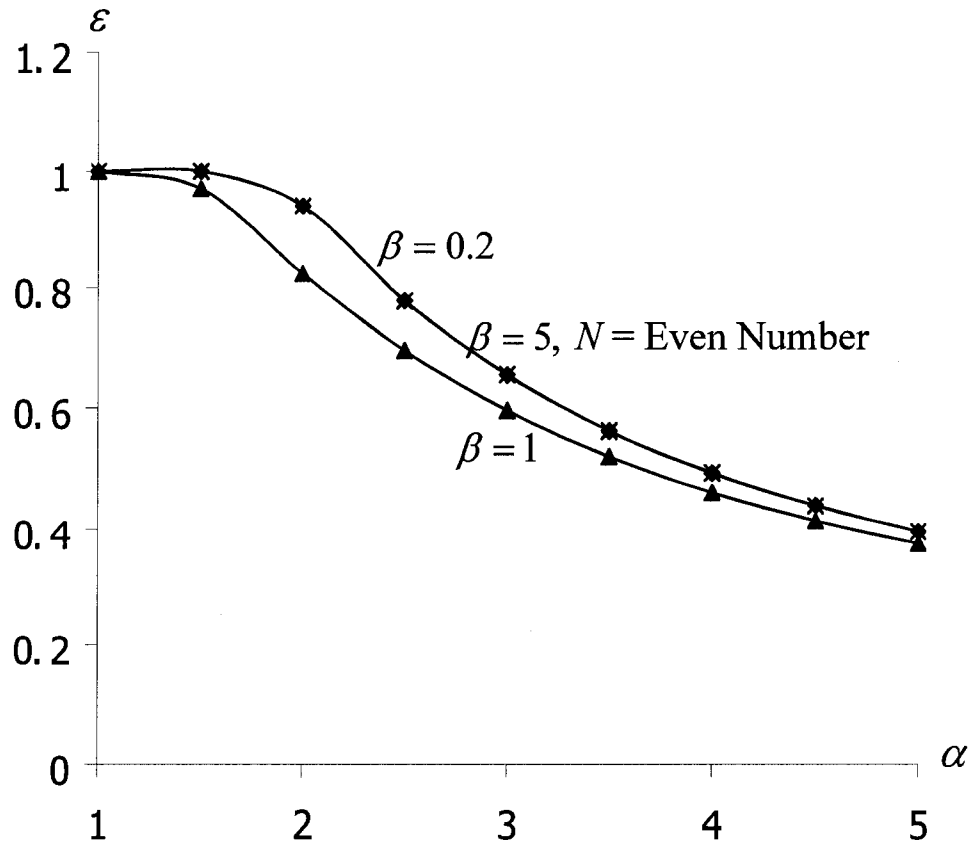
Fig.4.14 End-effect factor $\varepsilon$, defined as the ratio of the critical value with the end-effect to the critical value without the end-effect (when $n=2$), as a function of the amplified factor $\alpha$.

1: $\lambda = 0.3$;   2: $\lambda = 0.5$;   3: $\lambda = 0.7$;   4: $\lambda = 0.8$;   5: $\lambda = 0.9$.
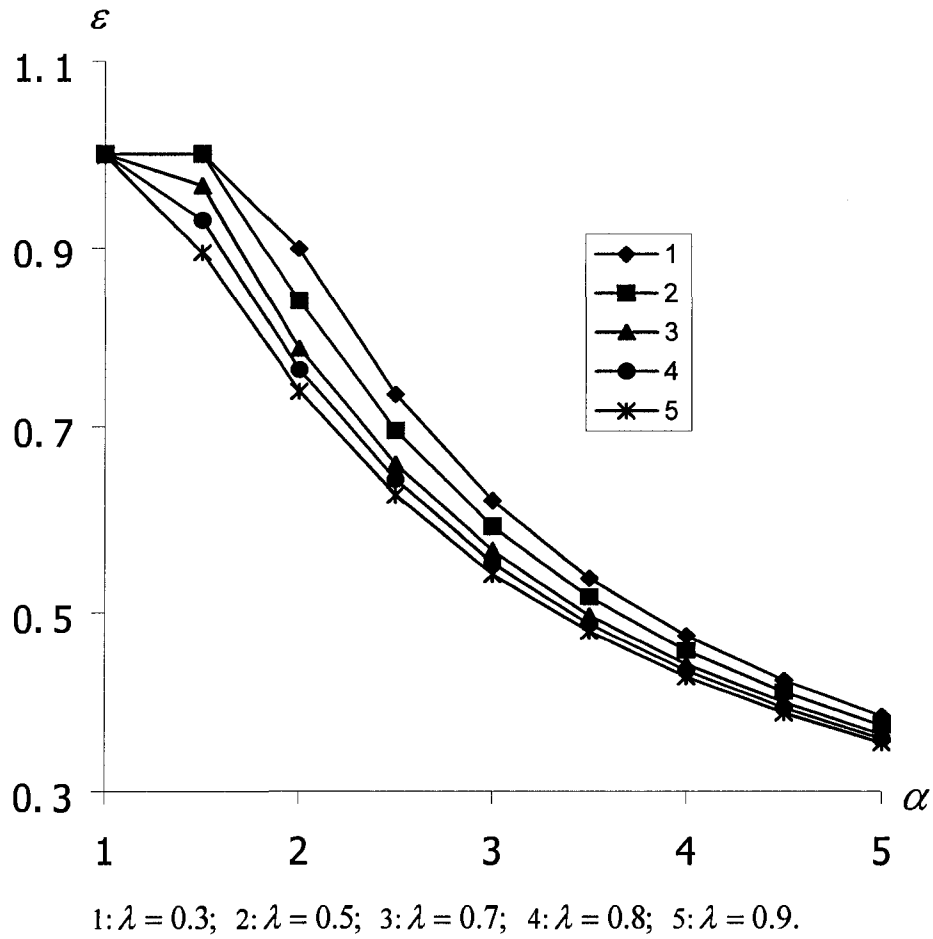
Fig.4.15 End-effect factor $\varepsilon$ when $\beta = 5$ and $N$ is an odd number, as a function of the amplified factor $\alpha$ for varying modified factor $\lambda$, where $\lambda$ is defined by $A_{23} = A_{N-2,N-1} = \lambda A_0$ (with

$A_{3,4} = A_{4,5} = ... = A_{N-3,N-2} = A_0$ , $A_{23} = A_{N-2,N-1} = \lambda A_0$ and

$A_{1,2} = A_{N-1,N} = \alpha A_0$, where $A_0$ is defined by (4.19)).

# Chapter 5

# A Substitution Method to Analyze Instability of Large Microbeam Arrays

## 5.1 Introduction

In Chapters 3 and 4, we developed a method for instability of a large parallel array of mutually attracting microbeams, based on the concept of the end-effect on instability. This method is based on a simplified analysis of the original large microbeam array which contains a large number of microbeams, and still suffers some technical complexity when the number of microbeams is extremely large. Therefore, it is of practical interest to develop an even easier method for the same problem.

In this chapter, a substitution method is proposed to study instability of a large array of mutually attracting microbeams. In Section 5.2, this method is introduced briefly. The effectiveness of this method is examined in Section 5.3 for the spring system. In Sections 5.4 and 5.5, instability of a large array of identical microbeams or opposing microcantilevers is analyzed using this substitution method, with comparison to the results obtained in Chapters 3 and 4. Finally, all results are summarized in Section 5.6.

## 5.2 A substitution method

Let us consider instability of $N$ microbeams as shown in Fig.5.1 $a)$-$d$), which is same as the cases we considered in Chapters 3 and 4.

As shown by the previous works in Chapters 3 and 4, equilibrium deflections of all intermediate beams could be negligibly small because two interactions from two adjacent beams on the opposite sides are almost equal but opposite and thus cancel each other. This means that structural instability of a large array of microbeams will be initialized at the ends of the large array and characterized by collision of adjacent microbeams at its

two ends. Therefore, it is expected that instability of the original large array can be determined by instability of a small array of only a few (3, 4, or more) microbeams at each of the two ends with the innermost microbeam fixed. In this chapter, this idea is explored to develop a substitution method based on instability analysis of a small array of only a few microbeams, and the critical value of interaction coefficient for instability of the original large array can be well estimated by the critical value of interaction coefficient for instability of the substitute small array.

In next section, this method will first be employed to study instability of the $N$-spring system.

## 5.3 Instability of a N-spring system

To illustrate the present substitution method, let us first consider $N$ equally spaced and mutually attracting springs as shown in Fig.5.1 $e$). For this spring system to represent not only the cases Fig.5.1 $a$)-$c$) but also the case Fig.5.1-$d$), we assume that all springs of odd index ($k$=1, 3, 5...) have the spring constant $q_1$, while all springs of even index ($k$=2, 4, 6...) have the spring constant $q_2$. This spring system is same as that we employed in Chapter 4.

The instability of the spring array is defined by a critical value of the spring-spring interaction beyond which some adjacent springs jump together so that the distance reduction between them is larger than the initial separation $d_0$. Equilibrium displacements of all springs can be obtained by solving Eqns (4.8-4.12) with Newton iteration method, and the exact critical values of $B$ (defined in (4.13)) for instability and the equilibrium displacement of the end springs and their neighboring springs at the onset of instability for $\beta$=0.2, 1 and 5, and $n$=2 (for electrostatic force), 3 (for unretarded van der Waals force), and 4 (for Casimir force or retarded van der Waals force), are shown in Table 5.1.

Equilibrium displacements of the spring system prior to instability are shown in Fig.5.2 for a few examples with $n$=2, 3 or 4. It is seen from Fig.5.2 that when the loading parameter $B$ is below the critical value, as expected, accurate equilibrium displacements of almost all intermediate springs are negligibly small. Actually, in all cases shown, the

displacement of the spring $k=3$ at the left end (or the spring $k=N-2$ at the right end) prior to the onset of instability is negligibly small (around $0.02 d_0$ or less), compared to the much larger displacements of the end springs ($k=1$ and $k=N$) and their neighboring springs ($k=2$ or $k=N-1$). For instance, for $n=2$, $B=1/7.6$, $\beta =0.2$, and $N=20$, the displacement of the third spring is $0.014 d_0$, and the displacements of the fourth and fifth springs are $-0.0009 d_0$ and $0.0005 d_0$, respectively. For $n=3$, $B=1/15.9$, $\beta =1$, and $N=20$ or 21, the displacement of the third spring is $0.017 d_0$, and the displacements of the fourth and fifth springs are $-0.0060 d_0$ and $0.0020 d_0$, respectively. For $n=4$, $B=1/54.5$, $\beta =5$, and $N=21$, the displacement of the third spring is $0.0057 d_0$, and the displacements of the fourth and fifth springs are $-0.0096 \ d_0$ and $0.0009 d_0$, respectively.

Based on the fact that equilibrium deflections of all intermediate springs (except those at the ends) are negligibly small, it is anticipated that structural instability of the original large spring array is determined by structural instability of only a few outermost springs (say $N^*$ springs with $N^* <<N$) at each of the two ends of the large array in which the deflection of the innermost spring $k=N^*$ (left end) or $k=(N-N^*+1)$ (right end) can be assumed to be zero. Therefore, in doing so, the critical value for structural instability of the original large array (a much more complicated problem) can be reduced to determining the critical value for structural instability of a small array of only fewer springs at the two ends (a much simpler problem).

It should be stated which of the two ends determines instability of the original large array depends on the parameters $\beta$ and $N$. If $N$ is an even number, for $\beta <1$, the deflection of the spring $k=1$ is bigger than that of the spring $k=N$ because of the smaller rigidity of the spring $k=1$. Thus, instability of the large array will be initialized on the left end, and then instability of the original large array depends on structural behavior of a few ($N^*$) springs at the left end with the innermost spring $k=N^*$ fixed. On the other hand, for $\beta >1$, because the rigidity of the spring $k=N$ is smaller than that of the spring $k=1$, instability of the original large array depends on structural behavior of a few ($N^*$) springs at the right end with the innermost spring $k=(N-N^*+1)$ fixed. When $\beta =1$, all springs are identical and the spring system is symmetric about the two ends. Thus,

structural instability of the array can be determined by a few springs on either of the two ends. Finally, if $N$ is an odd number, because the spring system is symmetric about the two ends, regardless of $\beta >$, $=$ or $<1$, structural instability of the large array can be determined by the behavior of a few springs on either of the two ends.

In what follows, let us consider structural instability of $N^*$ springs at the left end with the innermost spring $k=N^*$ fixed. The critical interaction coefficients for instability of this small array of $N^*$ springs for $\beta=0.2$, 1, or 5 will be compared with the exact critical value for instability of the original large array for $\beta=0.2$ ($N$ is an even or odd number), 1 ($N$ is an even or odd number), or 5 ($N$ is an odd number), obtained with the Newton iteration method shown in Table 5.1. For the case in which $\beta=5$ and $N$ is an even number, we should consider structural instability of $N^*$ springs at the right end with the innermost spring $k=(N-N^*+1)$ fixed. However, this case (with $\beta=5$ and $N$ is an even number) is equivalent to the case in which $\beta=1/5=0.2$ (with an even number $N$) if we define the right end spring as the first ($k=1$) and the left end as the last ($k=N$). Therefore, structural instability for the case $\beta=0.2$ is equivalent to structural instability of the case $\beta=5$ when $N$ is an even number. Thus, without loss of the generality, we shall focus on the instability of $N^*$ springs at the left end of the original large array, for $\beta=0.2$, 1, or 5, respectively.

## 5.3.1 Estimate of the critical value for instability

### i) Estimate of the critical value with $Y_2=0$ ($N^*=2$)

As the simplest approximation, let us first consider only two springs ($N^*=2$) at the left end, with the inner spring $k=N^*=2$ fixed (that is $Y_2=0$). Based on Eqn (4.8) with $Y_2=0$, the deflection of the left end spring is determined by

$$-\frac{Y_1}{d_0} + \frac{B}{(1-\frac{Y_1}{d_0})^n} = 0 \qquad (5.1)$$

The critical value for instability of the small array of only two springs governed by (5.1) is 1/6.75 for $n=2$, or 1/9.482 for $n=3$, or 1/12.208 for $n=4$. In addition, the distance change between the end spring and its neighbor at the onset of instability is $0.3333\,d_0$ for $n=2$, or $0.2477\,d_0$ for $n=3$, or $0.1978\,d_0$ for $n=4$. On the other hand, the exact critical value for instability of the original large array, obtained by the Newton iteration method, is shown in Table 5.1. Thus, the average relative error in the critical value for instability is 130% for $n=2$, or 138% for $n=3$, or 142% for $n=4$. In addition, the average relative error in the distance change between the end spring and its neighbor at the onset of instability is 46% for $n=2$, or 49% for $n=3$, or 45% for $n=4$. Therefore, for the original large array, considering only two springs at its left end will lead to unacceptable large errors in the critical value for instability and the distance change between the end spring and its neighbor at the onset of instability.

## ii) Estimate of the critical value with $Y_3=0$ ($N^*=3$)

Next, let us consider three springs at the left end of the large array, with the innermost spring $k=N^*=3$ fixed (that is $Y_3=0$). It follows from (5.2) and (5.3) that the deflections of the left end spring and the second spring are determined by

$$-\frac{Y_1}{d_0} + \frac{B}{(1+\frac{Y_2}{d_0} - \frac{Y_1}{d_0})^n} = 0 \tag{5.2}$$

$$-\frac{Y_2}{d_0} + \frac{\beta B}{(1-\frac{Y_2}{d_0})^n} - \frac{\beta B}{(1+\frac{Y_2}{d_0} - \frac{Y_1}{d_0})^n} = 0 \tag{5.3}$$

The critical values for instability of the small array of three springs governed by (5.2) and (5.3) for $\beta=0.2$, 1 or 5 and $n=2$, 3, or 4, as well as the corresponding distance changes between the end spring and its neighbor at the onset of instability, are shown in Table 5.2. It is seen from Table 5.2 that considering the small array of only 3 springs at the left end of the large array offers an effective substitution method to estimate the critical value for instability of the original large array, with relative errors less than 2%. In addition, the

average relative error in the distance change between the end spring and its neighbor at the onset of instability is 2.8% for $n=2$, or 5.5% for $n=3$, or 4.7% for $n=4$. Hence, considering only three springs at the end has already led to useful approximate results with small relative errors.

## iii) Estimate of the critical value with $Y_4=0$ ($N^*=4$)

Further, let us consider $N^*=4$ springs at the left end of the large array with $Y_4=0$. It follows from (5.4), (5.5) and (5.6) that the deflections of the first, second, and third springs are determined by

$$-\frac{Y_1}{d_0} + \frac{B}{(1+\frac{Y_2}{d_0}-\frac{Y_1}{d_0})^n} = 0 \qquad (5.4)$$

$$-\frac{Y_2}{d_0} + \frac{\beta B}{(1+\frac{Y_3}{d_0}-\frac{Y_2}{d_0})^n} - \frac{\beta B}{(1+\frac{Y_2}{d_0}-\frac{Y_1}{d_0})^n} = 0 \qquad (5.5)$$

$$-\frac{Y_3}{d_0} + \frac{B}{(1-\frac{Y_3}{d_0})^n} - \frac{B}{(1+\frac{Y_3}{d_0}-\frac{Y_2}{d_0})^n} = 0 \qquad (5.6)$$

Similarly, the critical values for instability and the distance changes between the end spring and its neighbor at the onset of instability for $\beta=0.2$, 1 or 5 and $n=2$, 3, or 4 are shown in Table 5.3. It is seen from Table 5.3 that considering the small array of 4 springs at the left end of the large array offers an almost accurate critical value for instability of the original large array, with relative errors less than 0.5%. The average relative error in the distance change between the end spring and its neighbor at the onset of instability is 2.5% for $n=2$, or 1.1% for $n=3$, or 3.5% for $n=4$.

## 5.3.2 The accuracy of the substitution method for the spring system

Further numerical results are obtained for larger $N^*$ (omitted here). The results show that the difference between the critical value for $N^*=5$ and the critical value for $N^*=4$ is always less than 0.5% for $\beta=0.2$, 1, or 5, and $n=2$, 3, or 4. The estimated critical values of $B$ for $N^*=2$, 3, 4, or 5 are shown in Fig.5.3. It is seen from Fig.5.3 that the relative errors quickly converge to zero when the number $N^*$ of springs considered in the substitute small array increases beyond $N^*=5$. For example, when $N^*=5$, the relative error in the critical value of interaction coefficient obtained by this substitution method is less than 0.1% for $\beta=0.2$, 1, or 5, and $n=2$, 3, or 4. In addition, this substitution method is also good in predicting the distance change between the end spring and its neighbor at the onset of instability, with relative errors around 5% (for $N^*=5$). When $\beta>1$ and $N$ is an even number, similarly, we can consider a few ($N^*$) springs at the right end with the innermost spring $k=(N-N^*+1)$ fixed, in order to predict the structural instability of the original large array.

In conclusion, for a simplified spring system, it is verified that the substitution method suggested here can be used to approximately determine the critical value for instability of the large array, based on an analysis of a substitute small array of only a few springs at its two ends. Clearly, such a substitution method largely simplifies the instability analysis of the original large array of interacting springs.

## 5.4 Instability of a parallel array of identical microbeams

The results obtained for the spring system show that the proposed substitution method can provide reasonably accurate critical values of the interaction coefficient for instability of an original large array of interacting springs. In this section, this method is employed to determine the critical values for instability of a large parallel array of identical microbeams, as shown in Fig.5.1 $a)$-$c)$.

## i) Estimate of the critical value with $Y_2 = 0$ ($N^* = 2$)

First, let us consider two microbeams ($N^* = 2$) with the second microbeam fixed ($Y_2 = 0$). Based on Eqn (3.3) with $Y_2 = 0$, the deflection of the end beam $Y_1(x)$ is determined by

$$EI\frac{d^4 Y_1}{dx^4} = \frac{C}{(d_0 - Y_1)^n} \tag{5.7}$$

Eqn (5.7) can be solved numerically by the Galerkin method, and the critical value of interaction coefficient $A_0$ ($= \frac{nC}{d_0^{n+1}}$, defined in (3.16) and (4.19)) for instability of a large array of microbeams is determined as the lowest interaction coefficient at which the jump-to-together instability occurs. Since parallel arrays of microbeams in MEMS, especially in the comb drive technology, are usually electrostatically controlled [61-64, 66-77, 98-99, 101], we shall focus on the power index $n=2$. For $n=2$, the present method with $N^* = 2$ predicts that the critical value of $A_0 \big/ EI(\frac{\pi}{L})^4$ for instability of the two microbeams is 0.283 for hinged beams, or 1.449 for clamped beams, or 0.0345 for cantilevers. In addition, the maximum deflection of the end beam at the onset of instability, predicted by the present method ($N^* = 2$), is $0.3854 d_0$ for hinged beams, or $0.3943 d_0$ for clamped beams, or $0.4477 d_0$ for cantilevers. On the other hand, the critical value of $A_0 \big/ EI(\frac{\pi}{L})^4$ for $n=2$ predicted by the method suggested in Chapter 3 [126], based on instability analysis of the original large array of $N$ microbeams, is 0.185 for hinged beams, or 0.923 for clamped beams, or 0.0229 for cantilevers. Thus, the relative error in the critical value of the interaction coefficient for instability is 53% for hinged beams, or 57% for clamped beams, or 51% for cantilevers. Therefore, for the large array of identical microbeams, considering only two microbeams at the ends will lead to large relative errors in the critical value of interaction coefficient for instability.

## ii) Estimate of the critical value with $Y_3$=0 ($N^*$=3)

Let us further analyze instability of three microbeams ($N^*$=3) at the end of the original large array shown in Fig.5.1 $a$)-$c$), with the third microbeam fixed ($Y_3 = 0$). It follows from (5.8) and (5.9) that the deflections of the end beam and its neighbor are determined by

$$EI\frac{d^4 Y_1}{dx^4} = \frac{C}{(d_0 + Y_2 - Y_1)^n} \tag{5.8}$$

$$EI\frac{d^4 Y_2}{dx^4} = \frac{C}{(d_0 - Y_2)^n} + \frac{-C}{(d_0 + Y_2 - Y_1)^n} \tag{5.9}$$

Numerical results based on the Galerkin method showed that when $n$=2 and $N^*$=3, the critical value of $\left. A_0 \middle/ EI(\frac{\pi}{L})^4 \right.$ for instability of the three microbeams predicted by the present method is 0.178 for hinged beams, or 0.915 for clamped beams, or 0.022 for cantilevers. In addition, the maximum distance change between the first and second beams at the onset of instability, predicted by the present method ($N^*$=3), is $0.2820 d_0$ for hinged beams, or $0.3122 d_0$ for clamped beams, or $0.3294 d_0$ for cantilevers. Compared to the results given in Chapter 3 [126], the relative error in the critical value of the interaction coefficient for instability of the present method ($N^*$=3) is 3.8% for hinged beams, or 0.9% for clamped beams, or 3.9% for cantilevers. Thus, considering only 3 microbeams ($N^*$=3) at the ends of the original large array can effectively estimate the critical value for instability of the original large array with relative errors less than 4%.

## iii) Estimate of the critical value with $Y_4$=0 ($N^*$=4)

Similarly, let us consider four microbeams ($N^*$=4) at one end of the original array with the fourth microbeam fixed ($Y_4 = 0$). Thus, the deflections of the first, second, and third beams are determined by

$$EI\frac{d^4Y_1}{dx^4} = \frac{C}{(d_0 + Y_2 - Y_1)^n} \tag{5.10}$$

$$EI\frac{d^4Y_2}{dx^4} = \frac{C}{(d_0 + Y_3 - Y_2)^n} + \frac{-C}{(d_0 + Y_2 - Y_1)^n} \tag{5.11}$$

$$EI\frac{d^4Y_3}{dx^4} = \frac{C}{(d_0 - Y_3)^n} + \frac{-C}{(d_0 + Y_3 - Y_2)^n} \tag{5.12}$$

Using the Galerkin method, it is showed that when $n=2$ and $N^*=4$, the critical value of $A_0 \Big/ EI(\frac{\pi}{L})^4$ for instability of the four microbeams predicted by the present method is 0.176 for hinged beams, or 0.904 for clamped beams, or 0.0218 for cantilevers. In addition, the maximum distance change between the first and second beams at the onset of instability is $0.2829\, d_0$ for hinged beams, or $0.3058\, d_0$ for clamped beams, or $0.3358\, d_0$ for cantilevers. Thus, as compared to the results given in Chapter 3 [126], the relative error in the critical value of interaction coefficient for instability of the present method ($N^*=4$) is 4.9% for hinged beams, or 2.1% for clamped beams, or 4.8% for cantilevers. Here, it should be pointed out that the critical values for instability given by the previous method in Chapter 3 [126] are approximate in nature, and cannot be used as the exact critical values. This can explain why the relative errors with $N^*=4$ are even larger than the relative errors with $N^*=3$. In fact, it is expected that the results given by the present substitution method quickly converge to the exact values when the number $N^*$ increases.

The critical values, as a function of the number ($N^*$) of microbeams considered in the substitute small array, are shown in Fig.5.4, where the dash lines represent the critical values for instability given by the previous approximate method in Chapter 3 [126] for hinged, fixed beams, and cantilevers. Indeed, the difference between the critical value for instability with $N^*=5$ and that with $N^*=4$ is always less than 0.2% for hinged, fixed beams or cantilevers. Since the critical value for instability decreases monotonically with

increasing the number ($N^*$) of microbeams considered in the substitute small array, it is believed that the present substitution method offers an accurate prediction in the critical value for instability of the large array when the number $N^*$ increases.

## 5.5 Instability of comb drive microcantilevers

Let us now use the substitution method to predict the critical value for instability of comb drive microcantilevers, shown in Fig.5.1 $d$). Because in almost all practical examples of comb drive technology, such as those reported in [61-64, 66-81, 98-99, 101], comb drive microcantilevers have the same material and geometrical characteristics, we shall assume in this section that $E_1I_1 = E_2I_2 = EI$ and $L_1 = L_2 = L$.

## i) Estimate of the critical value with $Y_2 = 0$ ($N^* = 2$)

Let us first consider two opposing microcantilevers ($N^* = 2$) with the second one fixed ($Y_2 = 0$). Based on (4.1) with $Y_2 = 0$, the deflection $Y_1(x_1)$ of the first cantilever is determined by

$$EI\frac{d^4Y_1}{dx_1^4} = 0 \quad \text{for } 0 \leq x_1 < L - \delta$$

$$EI\frac{d^4Y_1}{dx_1^4} = \frac{C}{(d_0 - Y_1)^n} \quad \text{for } L - \delta \leq x_1 \leq L \tag{5.13}$$

With the Galerkin method, the critical values of $\dfrac{A_0}{EI(\frac{\pi}{L})^4}$ given by the present method when $n=2$ and $N^* = 2$ are shown in Fig.5.5 with respect to the overlap depth $\delta$. It is seen from Fig.5.5 that the critical value of $\dfrac{A_0}{EI(\frac{\pi}{L})^4}$ predicted by the present method with $N^* = 2$ is 0.0616 for $\delta/L = 0.2$, or 0.0379 for $\delta/L = 0.5$, or 0.0346 for $\delta/L = 0.8$. In addition, the average distance change between the first cantilever and its

neighbor at the onset of instability is $0.323 d_0$ for $\delta/L = 0.2$, or $0.273 d_0$ for $\delta/L = 0.5$, or $0.205 d_0$ for $\delta/L = 0.8$. On the other hand, the critical values of the interaction coefficient for instability of the original array of comb drive microcantilevers obtained in the previous work, see Fig.4.11 in Chapter 4 [127], is also shown in Fig.5.5. For example, the critical value in Fig.4.11 is 0.0389 for $\delta/L = 0.2$, or 0.0266 for $\delta/L = 0.5$, or 0.03 for $\delta/L = 0.8$. In addition, Grade et. al. [142] found that for the comb drive microcantilevers under electrostatic forces ($n=2$), the maximum deflection of the end beams at the onset of instability is about $0.25 d_0$. Thus, the present method ($N^* = 2$) lead to relative errors in the critical value of interaction coefficient for instability around 58% for $\delta/L = 0.2$, or 42% for $\delta/L = 0.5$, or 15% for $\delta/L = 0.8$. The average relative error in the distance change between the first cantilever and its neighbor at the onset of instability is 19% for $\delta/L = 0.2$, 0.5, or 0.8. Obviously, for the large comb drive microcantilever array, considering only two cantilevers at its ends leads to substantial errors.

## ii) Estimate of the critical value with $Y_3 = 0$ ($N^* = 3$)

Next, let us consider three cantilevers ($N^* = 3$) with the third one fixed ($Y_3 = 0$). Based on (4.1 ) and (4.2) with $Y_3 = 0$, the deflections of the end beam and its neighbor are determined by

$$EI \frac{d^4 Y_1}{dx_1^4} = 0 \qquad \text{for } 0 \leq x_1 < L - \delta$$

$$EI \frac{d^4 Y_1}{dx_1^4} = \frac{C}{(d_0 + Y_2 - Y_1)^n} \qquad \text{for } L - \delta \leq x_1 \leq L \tag{5.14}$$

$$EI \frac{d^4 Y_2}{dx_2^4} = 0 \qquad \text{for } 0 \leq x_2 < L - \delta$$

$$EI \frac{d^4 Y_2}{dx_2^4} = \frac{C}{(d_0 - Y_2)^n} + \frac{-C}{(d_0 + Y_2 - Y_1)^n} \quad \text{for } L - \delta \leq x_2 \leq L \tag{5.15}$$

With the Galerkin's method, the critical values of $A_0 / EI(\frac{\pi}{L})^4$ given by the present

method when $n=2$ and $N^*=3$, are shown in Fig.5.5, as a function of the overlap depth $\delta$.

It is seen from Fig.5.5 that this curve predicted by the present method with $N^*=3$ is close

to the curve of Fig.4.11 in Chapter 4 [127]. With the present method ($N^*=3$), the critical

value of $A_0 / EI(\frac{\pi}{L})^4$ for instability is 0.039 for $\delta/L=0.2$, or 0.0266 for $\delta/L=0.5$, or

0.03 for $\delta/L=0.8$. In addition, the average distance change between the first cantilever

and its neighbor at the onset of instability is $0.256\,d_0$ for $\delta/L=0.2$, or $0.249\,d_0$ for

$\delta/L=0.5$, or $0.242\,d_0$ for $\delta/L=0.8$. Thus, for $\delta/L=0.2$, or 0.5, or 0.8, the relative

error in the critical value of interaction coefficient for instability is less than 0.3%, and

the relative error in the average distance change between the first cantilever and its

neighbor at the onset of instability is less than 3.2%. Therefore, for the large comb drive

microcantilever array, considering only 3 microcantilevers ($N^*=3$) at its ends of the large

array gives a good estimate of the critical value for instability and the distance change

between the first cantilever and its neighbor at the onset of instability, with reasonably

small relative errors.

### iii) Estimate of the critical value with $Y_4=0$ ($N^*=4$)

Further, if four cantilevers ($N^*=4$) are considered with the fourth one fixed ($Y_4 = 0$),

the deflections of the first, second, and third beams are determined by

$$EI\frac{d^4Y_1}{dx_1^4} = 0 \quad \text{for } 0 \le x_1 < L-\delta$$

$$EI\frac{d^4Y_1}{dx_1^4} = \frac{C}{(d_0 + Y_2 - Y_1)^n} \quad \text{for } L-\delta \le x_1 \le L \tag{5.16}$$

$$EI\frac{d^4 Y_2}{dx_2^4} = 0 \quad \text{for } 0 \le x_2 < L - \delta$$

$$EI\frac{d^4 Y_2}{dx_2^4} = \frac{C}{(d_0 + Y_3 - Y_2)^n} + \frac{-C}{(d_0 + Y_2 - Y_1)^n} \quad \text{for } L - \delta \le x_2 \le L \quad (5.17)$$

$$EI\frac{d^4 Y_3}{dx_1^4} = 0 \quad \text{for } 0 \le x_1 < L - \delta$$

$$EI\frac{d^4 Y_3}{dx_1^4} = \frac{C}{(d_0 - Y_3)^n} + \frac{-C}{(d_0 + Y_3 - Y_2)^n} \quad \text{for } L - \delta \le x_1 \le L \quad (5.18)$$

With the Galerkin method, the critical values of $A_0 / EI(\frac{\pi}{L})^4$ given by the present method when $n=2$ and $N^*=4$ are shown in Fig.5.5 with respect to the overlap depth $\delta$. It is seen from Fig.5.5 that this curve is also close to the curve of Fig.4.11 in Chapter 4 [127]. With the present method ($N^*=4$), the critical value of $A_0 / EI(\frac{\pi}{L})^4$ for instability is 0.0385 for $\delta / L = 0.2$, or 0.0263 for $\delta / L = 0.5$, or 0.0298 for $\delta / L = 0.8$. In addition, the average distance change between the first cantilever and its neighbor at the onset of instability is 0.253 $d_0$ for $\delta / L = 0.2$, or 0.247 $d_0$ for $\delta / L = 0.5$, or 0.236 $d_0$ for $\delta / L = 0.8$. Thus, compared to the results of Fig.4.11 in Chapter 4 [127] for $\delta / L = 0.2$, 0.5, or 0.8, the relative error in the critical value for instability is less than 1.1%, and the relative error in the average distance change between the first cantilever and its neighbor at the onset of instability is less than 5.6%.

Furthermore, the critical values of $A_0 / EI(\frac{\pi}{L})^4$ for $N^*=5$ are also shown in Fig.5.5, which are very close to those for $N^*=4$. For example, with the present method ($N^*=5$), the critical value of $A_0 / EI(\frac{\pi}{L})^4$ is 0.0384 for $\delta / L = 0.2$ (0.3% less than that for $N^*=4$), or 0.0263 for $\delta / L = 0.5$ (almost identical to that for $N^*=4$), or 0.0298 for $\delta / L = 0.8$

(almost identical to that for $N^*=4$). In addition, the average distance change between the first microcantilever and its neighbor at the onset of instability is $0.246\,d_0$ for $\delta/L=0.2$, or $0.252\,d_0$ for $\delta/L=0.5$, or $0.238\,d_0$ for $\delta/L=0.8$. Thus, compared to the results of Fig.4.11 in Chapter 4 [127] for $\delta/L=0.2$, 0.5, or 0.8, the relative error in the critical value for instability is less than 1.3%, and the relative error in the average distance change between the first cantilever and its neighbor at the onset of instability is less than 4.8%.

In order to demonstrate the dependence of the predicted critical value on the number $N^*$, the critical values of $\dfrac{A_0}{EI(\dfrac{\pi}{L})^4}$ given by the present method for $\delta/L=0.2$, 0.5, or 0.8 are shown in Fig.5.6, as a function of the number $N^*$, where the dash lines represent the corresponding critical values in Fig.4.11 in Chapter 4 [127]. Here, it should be pointed out that the critical values for instability given by the previous method in Chapter 4 [127] are approximate in nature, and cannot be used as the exact critical values. This can explain why the relative errors with $N^*=4$ are even larger than the relative errors with $N^*=3$. In fact, it is expected that the results given by the present substitution method quickly converge to the exact values when the number $N^*$ increases.

These results shown in Sections 5.4 and 5.5 justify that the substitution method suggested here offers an alternative design criterion for structural stability of large arrays of microbeams, which is simpler than the procedure developed previously in Chapters 3 and 4 [126-127] and could be more easily applied to practical problems in MEMS. Although vibration of a coupled array of microbeams has been recently studied [102-112] using a spring model with linearized interaction, structural instability of a large and nonlinearly coupled microbeam array and the associated end-phenomena have not been studied in the literature at all.

In concluding our discussion, it should be stated that the present method is subjected to a few limitations. First, the beam-beam interaction is restricted to only single type of attractive forces ($n=2$, or 3, or 4) between the nearest adjacent beams, possible repulsive interaction (for example, between similarly charged adjacent microbeams) and combined interaction of more than one type of surface forces are not considered. Second, the so-

called "fringing filed effect" of electrostatic interaction has been neglected based on the present assumption that the gap between adjacent beams is small compared to other dimensions of the microbeams. We believe that the methods developed here can be extended to most of the mentioned more general cases without essential technical difficulties, although the extension to some cases would require a more complicated analysis. Here, it should also be stated that the present substitution method is developed only for static instability of large coupled microbeam arrays, but not necessarily applicable to their nonlinear dynamics. To what degree the present ideas and methods can be extended to nonlinear dynamics of large coupled microbeam arrays requests a detailed separate study, which constitutes one interesting subject for future work.

## 5.6 Conclusions

A substitution method is suggested to study structural instability of a large array of mutually attracting microbeams, based on instability analysis of a small array of only a few microbeams at the ends of the original large array with its innermost microbeam fixed. An exact analysis of the $N$-spring system confirms the accuracy of this substitution method. Further, this substitution method is used to study instability of a large array of identical microbeams and comb drive microcantilevers. Our results show that the present substitution method can predict the critical value for instability of the original large array of microbeams with reasonable relative errors (typically less than 5%), even when a small array of only 4 or 5 microbeams at the ends of the original large array are considered. In addition, the present method also predicts the distance change between the end microbeam and its neighbor at the onset of instability for the original large array. It is believed that this substitution method reveals an essential feature of the instability of a large coupled microbeam array initialized at its two ends, and offers a useful approximate criterion for structural instability of a large parallel array of mutually attracting microbeams or nanobeams in MEMS or NEMS.

Table 5.1 Critical values of $B$ for instability and equilibrium displacement change between the end spring and its neighbor at the onset of instability for $\beta$ =0.2, 1 and 5, $n$=2, 3, and 4.

| $\beta$ | $n$ | $N$ | Exact Critical Value of $B$ | $(Y_1 - Y_2)/d_0$ | $(Y_{N-1} - Y_N)/d_0$ |
|---|---|---|---|---|---|
| | 2 | 20 | 1/7.543 | 0.3115 | 0.0482 |
| | | 21 | 1/7.543 | 0.3115 | 0.3115 |
| 0.2 | 3 | 20 | 1/10.651 | 0.2333 | 0.0367 |
| | | 21 | 1/10.651 | 0.2333 | 0.2333 |
| | 4 | 20 | 1/13.753 | 0.1869 | 0.0297 |
| | | 21 | 1/13.753 | 0.1869 | 0.1869 |
| | 2 | 20 | 1/11 | 0.2439 | 0.2439 |
| | | 21 | 1/11 | 0.2439 | 0.2439 |
| 1 | 3 | 20 | 1/15.8 | 0.1781 | 0.1781 |
| | | 21 | 1/15.8 | 0.1781 | 0.1781 |
| | 4 | 20 | 1/20.6 | 0.1398 | 0.1398 |
| | | 21 | 1/20.6 | 0.1398 | 0.1398 |
| | 2 | 20 | 1/37.713 | 0.0482 | 0.3134 |
| | | 21 | 1/28.1 | 0.1705 | 0.1705 |
| | 3 | 20 | 1/53.254 | 0.0367 | 0.2339 |
| 5 | | 21 | 1/41.3 | 0.1221 | 0.1221 |
| | 4 | 20 | 1/68.765 | 0.0297 | 0.1869 |
| | | 21 | 1/54.4 | 0.1050 | 0.1050 |

Table 5.2 Critical values of $B$ for instability and distance change between the end spring and its neighbor at the onset of instability for $\beta=0.2$, 1 and 5, $n=2$, 3, 4 when $N^*(=3)$ springs at the left end of the original array are considered and the displacement of the third spring is assumed to be zero ($Y_{N^*}=0$).

| $\beta$ | $n$ | Critical Value of $B$ | Relative error of $B$ | $(Y_1-Y_2)/d_0$ | Relative error of $(Y_1-Y_2)/d_0$ |
|---|---|---|---|---|---|
| 0.2 | 2 | 1/7.523 | 0.266% | 0.3109 | 0.193% |
|  | 3 | 1/10.613 | 0.358% | 0.2186 | 6.301% |
|  | 4 | 1/13.701 | 0.380% | 0.1856 | 0.696% |
| 1 | 2 | 1/10.9 | 0.917% | 0.2312 | 5.207% |
|  | 3 | 1/15.5 | 1.936% | 0.1870 | 4.997% |
|  | 4 | 1/20.2 | 1.980% | 0.1432 | 2.432% |
| 5 | 2 | 1/27.6 | 1.812% | 0.1655 | 2.933% |
|  | 3 | 1/40.7 | 1.474% | 0.1159 | 5.078% |
|  | 4 | 1/53.6 | 1.493% | 0.0935 | 10.952% |

Table 5.3 Critical values of $B$ for instability and distance change between the end spring and its neighbor at the onset of instability for $\beta$=0.2, 1 and 5, $n$=2, 3, 4 when $N^*$(=4) springs at the left end of the original array are considered and the displacement of the fourth spring is assumed to be zero ($Y_{N^*}$=0).

| $\beta$ | $n$ | Critical Value of $B$ | Relative error of $B$ | $(Y_1 - Y_2)/d_0$ | Relative error of $(Y_1 - Y_2)/d_0$ |
|---------|-----|-----------------------|-----------------------|-------------------|-------------------------------------|
| 0.2 | 2 | 1/7.542 | 0.013% | 0.3127 | 0.385% |
| | 3 | 1/10.650 | 0.009% | 0.2322 | 0.472% |
| | 4 | 1/13.751 | 0.015% | 0.1858 | 0.589% |
| 1 | 2 | 1/11 | 0 | 0.2398 | 1.681% |
| | 3 | 1/15.8 | 0 | 0.1742 | 2.190% |
| | 4 | 1/20.5 | 0.488% | 0.1460 | 4.435% |
| 5 | 2 | 1/28.1 | 0 | 0.1612 | 5.455% |
| | 3 | 1/41.2 | 0.243% | 0.1230 | 0.737% |
| | 4 | 1/54.3 | 0.184% | 0.0992 | 5.524% |
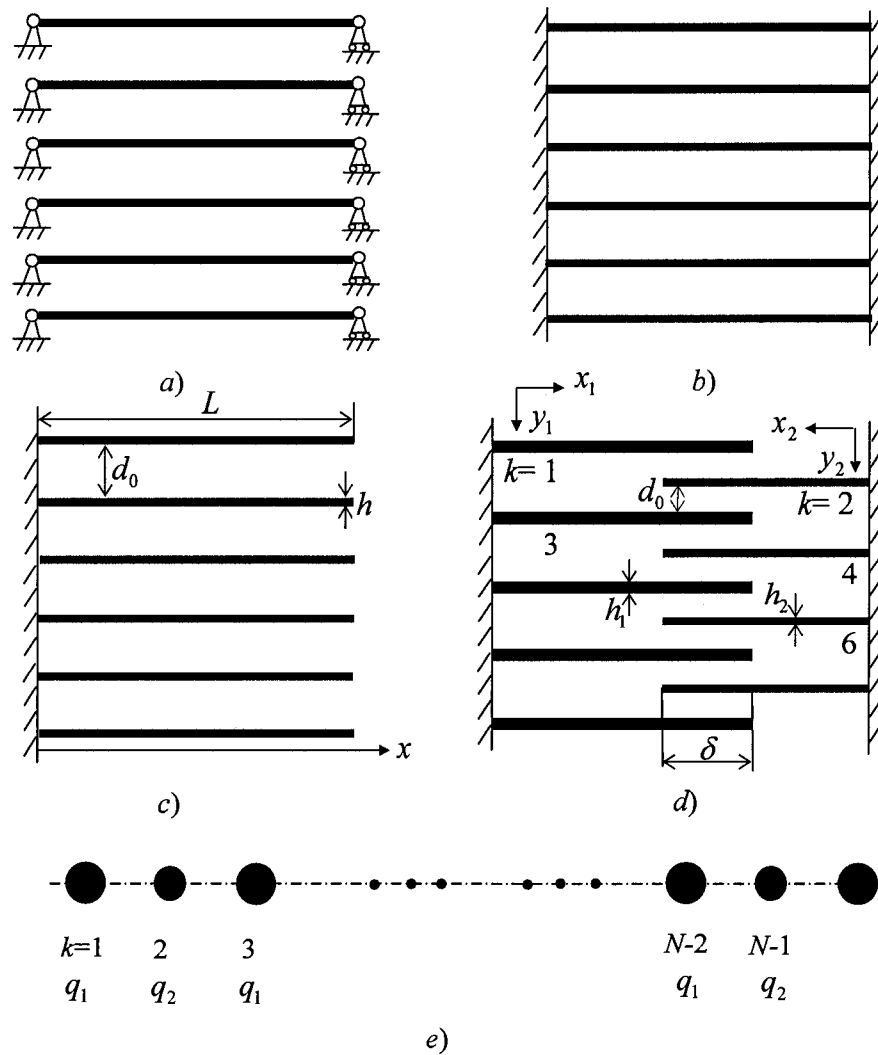
Fig.5.1 A large array of mutually attracting microbeams and springs.

*a*) hinged beams; *b*) clamped beams; *c*) cantilever beams; *d*) comb drive cantilevers; *e*) springs.
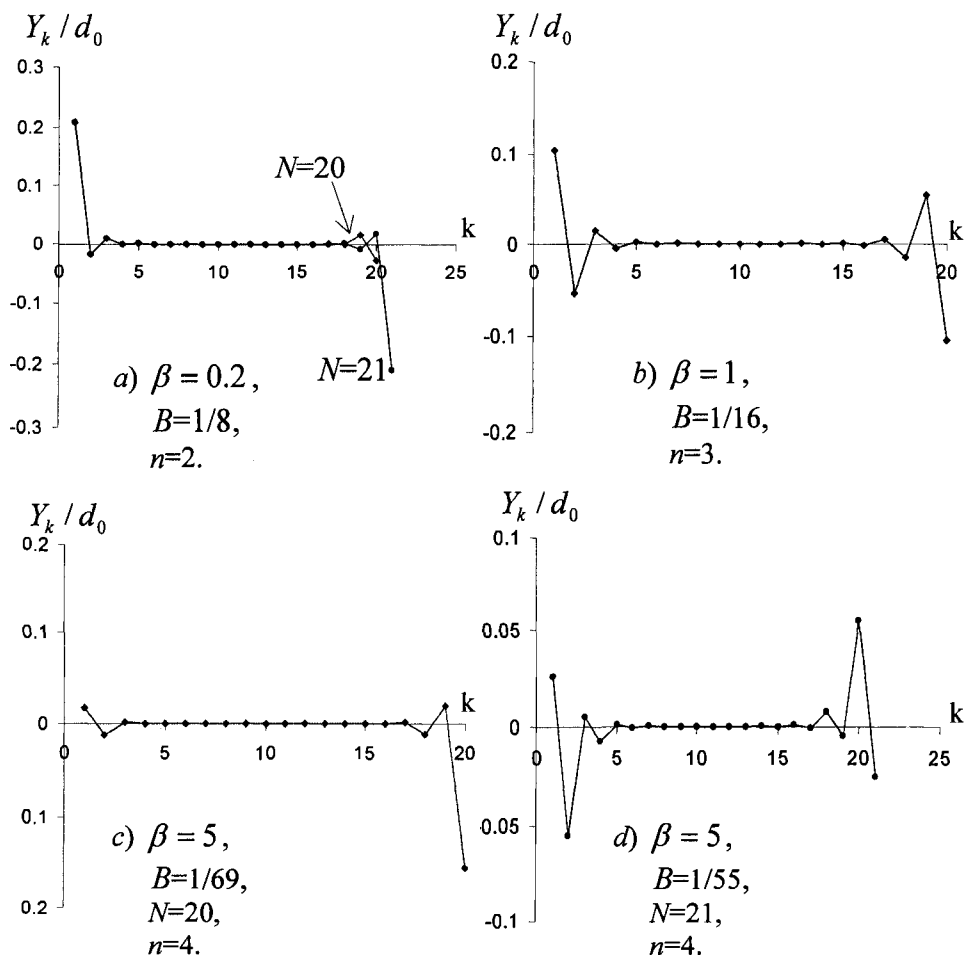
Fig.5.2 Equilibrium displacements of $N$ mutually attracting springs when $N$=20 or 21 prior to instability. $a)$ $\beta$=0.2, $B$=1/8, and $n$=2; $b)$ $\beta$=1, $B$=1/16, and $n$=3; $c)$ $\beta$=5, $B$=1/69, $N$=20, and $n$=4; $d)$ $\beta$=5, $B$=1/55, $N$=21, and $n$=4.

*a)* $\beta = 0.2$          *b)* $\beta = 1$          *c)* $\beta = 5$
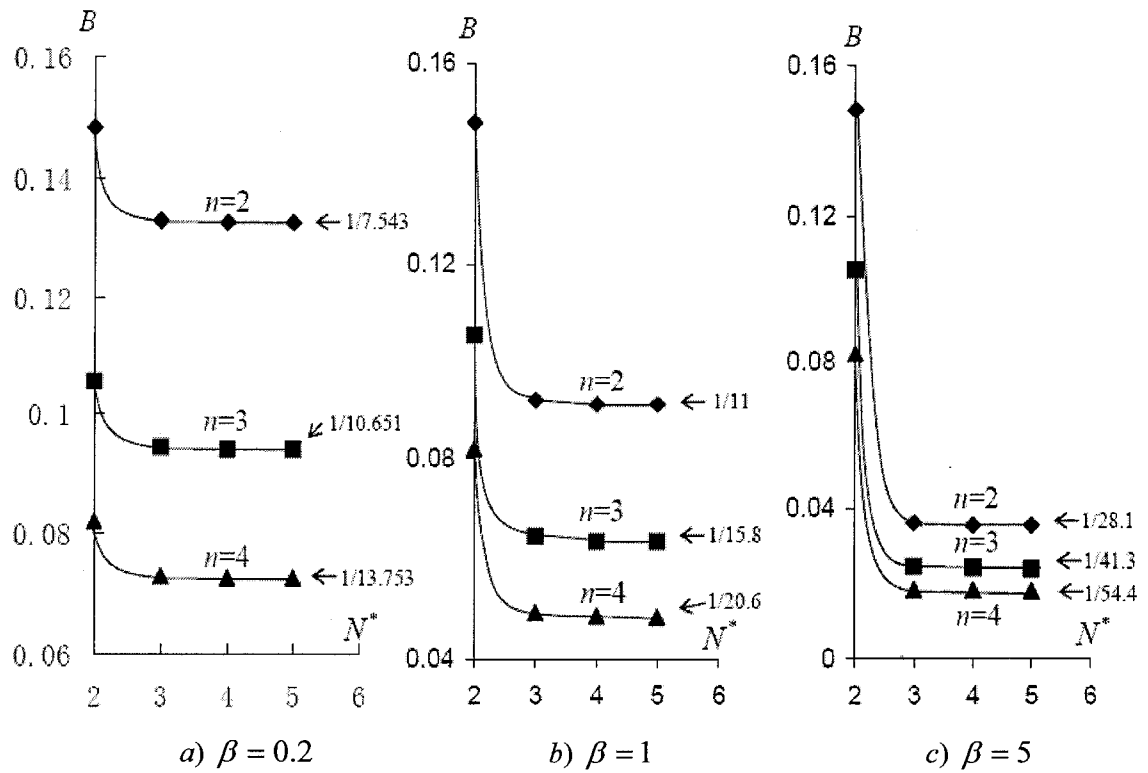
Fig.5.3 Critical values of $B$ for instability of the small array of $N^*$ springs at the left end of the original large spring array when $\beta = 0.2$, 1 or 5, and $n=2$, 3, or 4, where the displacement of the $N^*$-th spring is assumed to be zero ($Y_{N^*} = 0$).
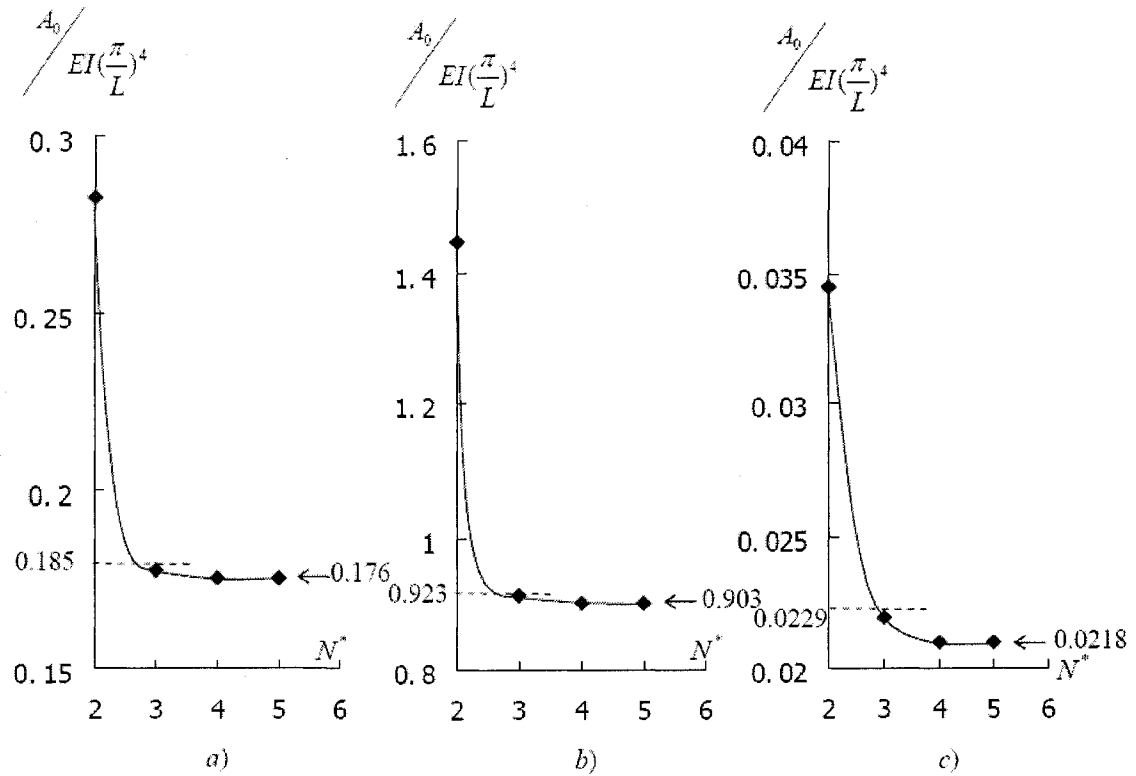
Fig.5.4 Critical value of the interaction coefficient for instability of a small array of $N^*$ microbeams at the end of the original identical microbeam array when $n=2$, where the $N^*$-th microbeam is assumed to be fixed ($Y_{N^*}=0$). $a$) hinged; $b$) clamped; $c$) cantilever.
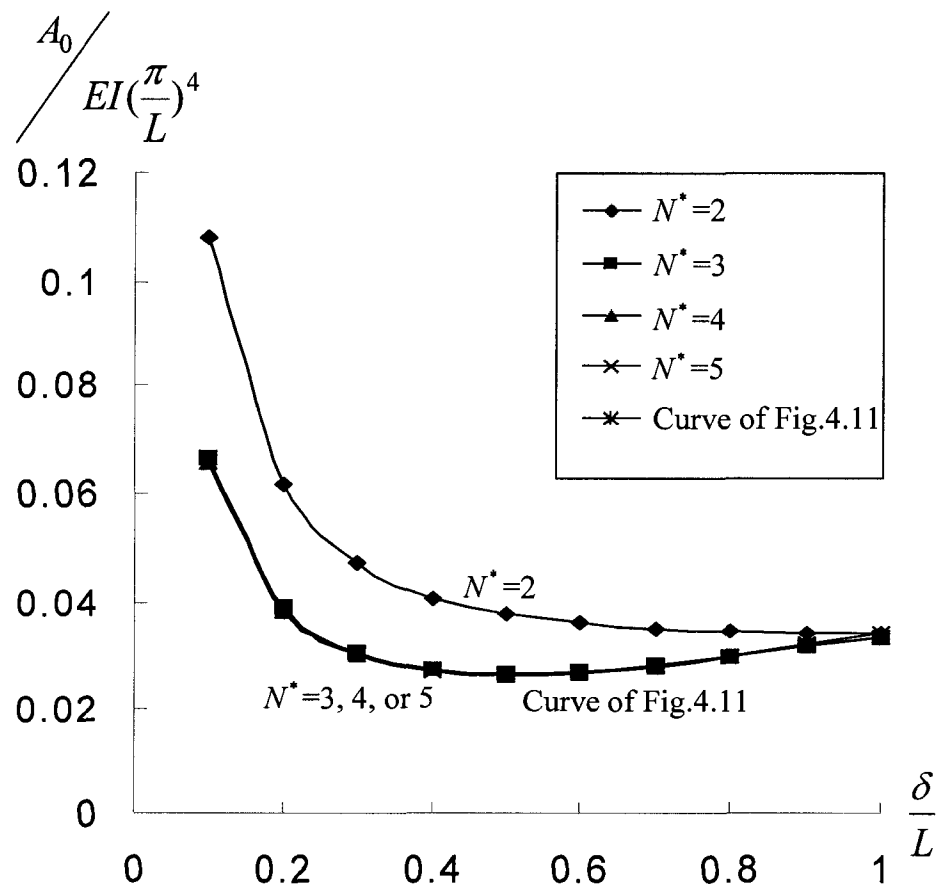
Fig.5.5 Critical value of the interaction coefficient for instability of a small array of $N^*$ microcantilevers at the end of the original comb drive microcantilever array when $n=2$, as a function of the depth $\delta/L$ when $E_1 I_1 = E_2 I_2 = EI$ , $L_1 = L_2 = L$ , where the $N^*$-th microcantilever is assumed to be fixed ($Y_{N^*} = 0$).
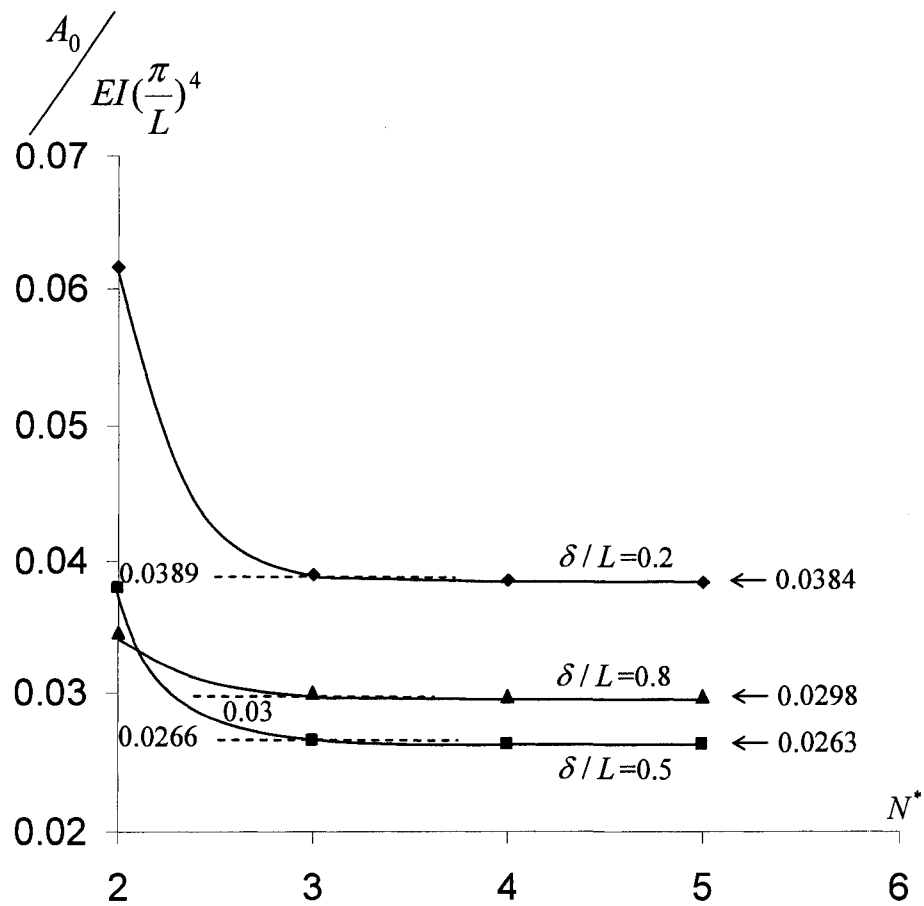
Fig.5.6 Critical value of the interaction coefficient for instability of a small array of $N^*$ microcantilevers at the end of the original large comb drive microcantilever array when $\delta / L$=0.2, 0.5, or 0.8 and $n$=2, where the $N^*$-th microcantilever is assumed to be fixed ($Y_{N^*}$=0).

# Chapter 6

# High-Order Subharmonic Parametric Resonance of a Nonlinearly Coupled Micromechanical Linear Oscillator

## 6.1 Introduction

Earlier researches on MEMS-related mechanics have mainly focused on mechanical behavior of individual components (such as a single microcantilever attracted by a rigid substrate) [82-95]. More recently, considerable attention has turned to collective mechanical behavior of coupled micromechanical systems. Especially, due to their relevance to MEMS/NMES [21, 133-134], growing interest has been attracted to collective nonlinear dynamic behavior of large coupled micromechanical/nanomechanical systems, such as parametric resonance [102-112], and localized modes [146-149] of a coupled large array of interacting microbeams. In particular, Buks & Roukes [102-103] fabricated an array of 67 doubly clamped microbeams, in which all even-numbered beams are electrically connected to one electrode while all odd-numbered beams to another electrode. An electrical voltage applied between the two electrodes induces attracting electrostatic forces between side-faces of any two adjacent beams. This coupled microbeam system was driven parametrically by introducing a periodically varying ac component to the voltage applied between the two electrodes. The response of the microbeam array showed some interesting nonlinear phenomena. For example, as the exciting frequency of the periodically varying ac component was swept up, typical response consisted of a small number of wide peaks, instead of 67 resonance peaks predicted by the linear theory of parametric resonance. Using a perturbation theory, Lifshitz & Cross [104] studied and explained these nonlinear phenomena based on a

model of linearly coupled array of nonlinear oscillators. More recently, Bromberg et al. [105] further studied parametric resonance of a large array of linearly coupled oscillators using a multiscale perturbation analysis.

Although time-independent nonlinear coupling forces between oscillators (characterized by nonlinear coupling terms of constant coefficients) has been studied extensively (see e.g. [149-151]), parametric resonance of coupled oscillators under periodically varying nonlinear coupling forces (characterized by nonlinear coupling terms of periodically-varying coefficients) has received much less attention [108-112]. For example, in the above-mentioned works on parametric resonance [102-105], the periodically varying coupling between any two adjacent microbeams is linearized and only elastic geometrical nonlinearity of the microbeams is taken into account. Also, most of previous works (except a few papers such as [108-112]) on parametric resonance of coupled oscillators, see e.g. [152-154], are limited to periodically varying coupling forces. No doubt, such a linearized coupling is reasonable for, say, the large array of doubly clamped microbeams studied in [102-104, 134] where the thickness (0.25 μm) of beams is much smaller than the gap (4 μm) between adjacent beams and therefore the elastic nonlinearity of the doubly clamped microbeams is much more relevant than the nonlinear effect of coupling. However, in some other cases, such as comb-drive microcantilever array, shown in Fig.6.1-1), with a gap between adjacent beams comparable to or even smaller than the thickness of microcantilevers [61-64, 66-70, 98-99, 101], elastic nonlinearity of microcantilevers is obviously much less relevant than the nonlinear dependency of the periodically varying coupling forces on the change in the gap between adjacent beams. In particular, in contrast to the elastic nonlinearity considered in [102-105] which leads to nonlinear terms of constant coefficients and has a stabilizing effect, the periodically varying coupling nonlinearity leads to nonlinear coupling terms of periodically-varying coefficients and has a destabilizing effect. This suggests that an oscillator system with periodically varying nonlinear coupling would more likely be parametrically excited than an oscillator system with elastic nonlinearity. Therefore, it is of great interest to study the effects of periodically varying nonlinear coupling on parametric resonance of coupled micromechanical oscillators.

The present work studies parametric resonance of nonlinearly coupled

micromechanical oscillators under periodically varying coupling forces. Here, motivated by comb-drive microcantilevers mentioned above and the fact that elastic geometrical nonlinearity is much relevant for doubly clamped beams than cantilevers, we neglect the elastic nonlinearity of oscillators and focus on the role of periodically varying nonlinear coupling between adjacent oscillators. As will be shown in the present work, the periodically varying nonlinear coupling leads to some new physical phenomena which have not appeared in linearly coupled oscillators studied previously [102-105] and also have not been studied in previous related works [108-112]. Actually, the periodically varying nonlinear coupling studied in this chapter allows the appearance of high-order subharmonic parametric resonance when the excitation frequency is a multiple or nearly a multiple ($\geq 3$) of one of the natural frequencies of the coupled oscillator system, although the conditions for the appearance of high-order subharmonic parametric resonance depend on the magnitude of linear damping.

## 6.2 Micromechanical linear oscillators with periodically varying nonlinear coupling

Let us consider a comb-drive microcantilever array, with the gap $d$ between two side-faces of adjacent beams which is comparable to the thickness of beams $H$, as shown in Fig.6.1-1). For simplicity, just like [102-105], we shall assume that the first and the last beams are fixed and stationary. As a result, the complex end-effects, such as those studied in [126-128] for static pull-in instability of a parallel array of mutually attracting microbeams, will not appear in the present analysis. Furthermore, also like [102-105], it is assumed that each individual beam oscillates in its fundamental mode, and the simple spring (oscillator) model shown in Fig.6.1-2) will capture essential characteristics of the comb-drive microcantilever array.

Therefore, let us consider ($N$+2) equally spaced oscillators of identical mass $m$ and spring constant $q$, arranged along a straight line from $k$=0 (fixed left end) to $k$=$N$+1 (fixed right end), as shown in Fig.6.1-2). Let the displacement of the $k$-th oscillator be $X_k$ (because the left and right end oscillators are fixed, $X_0 = X_{N+1} = 0$). Assume that any two adjacent oscillators are attracted to each other through microscale surface forces,

such as electrostatic, van der Waals or Casimir forces, given by $f = M / d^n$, where $M$

represents the amplitude of the attractive forces which can be periodically varying, $d$ is

the distance between the two adjacent oscillators, and the index $n$=2 (electrostatic force),

=3 (van der Waals force), or =4 (Casimir force) [51-59]. Here, it should be stated that

both van der Waals force and Casimir force share the same underlying physics, and thus

the former is actually the short distance limit whereas the latter is the long distance limit

of the same physical phenomenon. Thus, in the presence of a linear damping

characterized by a constant viscous coefficient $c$, dynamics of the $N$ mutually attracting

oscillators is governed by

$$\frac{d^2 x_k}{dt^2} + \frac{c}{m}\frac{dx_k}{dt} + \omega_0^2 x_k - \frac{M}{md_0^{n+1}}[\frac{1}{(1 + x_{k+1} - x_k)^n} - \frac{1}{(1 + x_k - x_{k-1})^n}] = 0 \,,(k=1,2,...,N) \quad (6.1)$$

where $x_k = \dfrac{X_k}{d_0}$ is dimensionless displacement of the $k$-th spring, $d_0$ is the initial

distance between adjacent springs, $t$ is the time, and $\omega_0 = \sqrt{\dfrac{q}{m}}$ is the frequency of a

single isolated spring in the absence of the spring-spring coupling with any other springs.

Apparently, the equilibrium position defined by zero displacements $x_k$ (or $X_k$)=0 ($k$= 1,

2,..., $N$) is a solution of (6.1), because two attraction forces from two opposite sides are

always equal and opposite for each of all intermediate oscillators ($k$= 1, 2,..., $N$).

However, non-zero solutions of (6.1) become possible when the coupling attractive forces

characterized by $M(t)$ meet some conditions. In particular, appearance of any stable

steady-state non-zero periodic solution in the neighborhood of the equilibrium position

(of zero-displacements), under periodically varying $M(t)$ of a certain frequency, defines

parametric resonance of the coupled oscillator system.

Natural frequencies of the coupled array of oscillators are determined by

infinitesimal linear vibration of the coupled oscillators in the neighborhood of their

equilibrium position $x_k$ (or $X_k$)=0 ($k$= 1, 2,..., $N$). For infinitesimal displacements around

the equilibrium position, linearized equation of (6.1) gives

$$\frac{d^2 x_k}{dt^2} + \frac{c}{m}\frac{dx_k}{dt} + \omega_0^2 x_k - nQ\omega_0^2 (2x_k - x_{k-1} - x_{k+1}) = 0, \ (k = 1, 2, \ldots, N) \qquad (6.2)$$

where $Q = \dfrac{M}{qd_0^{n+1}}$ is the periodically varying loading parameter, defined based on the

initial distance $d_0$. Thus, when $M$ is a reasonably small positive constant, there exist $N$

distinct natural frequencies of the linearized system (6.2) in the absence of the damping

($c=0$), given by $\omega_i = \sqrt{1 - 4nQ\sin^2 \dfrac{i\pi}{2(N+1)}}\,\omega_0$ ($i = 1, 2, \ldots, N$) [103]. For sufficiently

large $N$, the highest natural frequency, $\omega_N$, approaches $\omega_0$. On the other hand, the

lowest natural frequency, $\omega_1$, reduces to zero when $M$ increases gradually so that ($nQ$)

reaches ¼, which indicates the existence of stationary non-zero solution and static

instability of the coupled oscillator array, as studied in [126-128]. For example, for a

large coupled oscillator array with two end oscillators fixed, such a static instability

occurs when $Q=1/8$ for $n=2$, or $Q=1/12$ for $n=3$, or $Q=1/16$ for $n=4$.

Since comb-drive microcantilever arrays are usually electrostatically controlled, in

what follows, we shall focus on the behavior of the coupled oscillators controlled by

electrostatic forces ($n=2$). Thus, when only a constant dc voltage $V_{dc}$ is applied on the

coupled oscillators, the $N$ distinct natural frequencies of the linearized system are given

by

$$\omega_i = \sqrt{1 - 8Q\sin^2 \frac{i\pi}{2(N+1)}}\,\omega_0, \ (i = 1, 2, \ldots, N) \qquad (6.3)$$

where $Q = \dfrac{\varepsilon_0 S V_{dc}^2}{2d_0^3 q}$, $\varepsilon_0$ is the permittivity of the medium between the beams, and $S$ is

the side-face area of adjacent beams exposed to the electrostatic filed. On the other hand,

when a periodically varying ac voltage is added to the dc voltage, $V = V_{dc} + V_{ac}\cos(\Omega t)$,

where $V_{ac}$ and $\Omega$ are the amplitude and exciting frequency of the ac voltage, the

amplitude of the nonlinear electrostatic force $M$ will be periodically varying and given by

$$M = \frac{\varepsilon_0 S V^2}{2} = \frac{\varepsilon_0 S V_{dc}^2}{2}(1 + 2\frac{V_{ac}}{V_{dc}}\cos(\Omega t) + (\frac{V_{ac}}{V_{dc}})^2 \cos^2(\Omega t)) \tag{6.4}$$

Substituting (6.4) into (6.1), we obtain a dimensionless equation

$$\frac{d^2 x_k}{d\tau^2} + \frac{c}{m\omega_0}\frac{dx_k}{d\tau} + x_k$$
$$- Q[\frac{1}{(1 + x_{k+1} - x_k)^2} - \frac{1}{(1 + x_k - x_{k-1})^2}][1 + 2\frac{V_{ac}}{V_{dc}}\cos(\frac{\Omega}{\omega_0}\tau) + (\frac{V_{ac}}{V_{dc}})^2 \cos^2(\frac{\Omega}{\omega_0}\tau)] = 0 \tag{6.5}$$

where $\tau = \omega_0 t$.

When the periodically varying coupling terms in (6.5) are linearized, the theory of classic Mathieu equation predicts that parametric resonance occurs when the frequency of the parametric excitation $\Omega$ is close to $2\omega_i / j$, where $\omega_i$ is any one of the $N$ distinct natural frequencies defined in (6.3), and $j$ is a positive integer [123-124]. In this case, because $\omega_i < \omega_0$ ($i$=1, 2,..., $N$), all resonance frequencies for parametric excitation will be bounded from above by $2\omega_0$, and then there will be no parametric resonance when the excitation frequency $\Omega$ is much higher than $2\omega_0$ when the coupling between adjacent oscillators is linearized [102-105].

In this chapter, we study the effect of periodically varying nonlinear coupling on parametric resonance, with particular interest in whether high-order subharmonic parametric resonance exists when the excitation frequency is close to a multiple ($\geq 3$) of one of the natural frequencies $\omega_i$ ($i$= 1, 2,..., $N$). To this end, we shall seek, in the neighborhood of the equilibrium position, the lowest-order non-zero periodic solution of (6.5) with $\Omega / \lambda$ as the excited frequency, given by

$$x_k = a_k \cos(\frac{\Omega}{\lambda\omega_0}\tau) + b_k \sin(\frac{\Omega}{\lambda\omega_0}\tau) \tag{6.6}$$

where $\lambda$ is an integer or the inverse of an integer, and $a_k$ and $b_k$ are some undetermined constants ($k=$ 1, 2,..., $N$). Using the harmonic balance method [155-156], we substitute (6.6) into (6.5), and then multiplying Eqn. (6.5) by the functions $\cos(\frac{\Omega}{\lambda\omega_0}\tau)$ and $\sin(\frac{\Omega}{\lambda\omega_0}\tau)$ ($k=$ 1, 2,..., $N$), respectively, and integrating the resulting equation over [0, $2\pi$] lead to $2N$ nonlinear equations. The Newton iteration method is then employed to solve these equations for $2N$ unknown coefficients $a_k$ and $b_k$ ($k=$ 1, 2,..., $N$). In particular, the Newton iteration method with various initial values allows finding all possible solutions, and stability analysis of steady-state solutions [130] makes it possible to distinguish stable solutions from unstable ones. A non-zero stable solution of these nonlinear equations defines a parametric resonance characterized by a stable steady-state periodic solution of the form (6.6).

## 6.3 Parametric resonance of a single oscillator without damping

In order to clearly demonstrate essential features of parametric resonance of nonlinearly coupled oscillators, let us consider only three oscillators in which the middle one is nonlinearly coupled with two fixed end oscillators (thus $N=1$ and $X_0 = X_2 = 0$, see Fig.6.1-2)). Actually, our results showed that a coupled system of more than three oscillators (with $N>1$) exhibits essentially similar phenomena as the present simple system with $N=1$ (the details will be reported in next chapter). In this section, we first neglect the damping effect and consider $c = 0$. The effect of a linear damping will be studied in next section. In both sections, we take $Q=1/20$ and $\frac{V_{ac}}{V_{dc}}=0.1$ in Eqn. (6.5). It then follows from (6.3) that $\omega_1 =0.8944\,\omega_0$.

### 6.3.1 Parametric resonance with $\lambda \leq 2$

For the sake of comparison to previous related works with $\lambda \leq 2$ for linearly

coupled oscillators [102-105], we first study the parametric resonance with $\lambda \leq 2$. Based on the harmonic balance method, as described above, we shall seek a periodic solution of the form (6.6) by solving 2 nonlinear equations for the two unknowns $a_1$ and $b_1$. The existence of a non-zero solution $a_1$ and $b_1$ defines a periodic solution of the intermediate oscillator nonlinearly coupled with two fixed end oscillators, and the periodic solution can be expressed as $x_1 = A_m \cos(\dfrac{\Omega}{\lambda \omega_0 \tau} - \psi)$ (see Eqn. (6.6)), where the amplitude $A_m = \sqrt{a_1^2 + b_1^2}$, and the phase $\psi = arctg(b_1 / a_1)$.

Fig.6.2 shows the relationship between the amplitude of the excited resonance and the ac frequency $\Omega / \omega_0$ for parametric resonance defined by $\lambda = 0.5$, 1 or 2. In this figure and Figs6.3-6.6, the dash lines represent unstable steady-state solutions, while the solid lines represent stable steady-state solutions. Detailed stability analysis of steady-state solutions is explained in [130].

Here, it should be stated that any point on the solid or dashed line would represent more than one solution which have the same amplitude but with different phases. In Fig.6.2-1), curves $a$) and $b$) intersect with the $x$-coordinate axis at point $A$ ($\Omega / \omega_0 = 0.4451$) and $B$ ($\Omega / \omega_0 = 0.4489$), respectively, and point $C$ is the linear resonance frequency of $2\omega_1 / j$ with $j=4$, where $\omega_1 = 0.8944 \omega_0$. In Fig.6.2-2), the coordinate of point $A$ or $B$ is $\Omega / \omega_0 = 0.8936$ or 0.8942, respectively, and point $C$ is the linear resonance frequency of $2\omega_1 / j$ (=0.8944 $\omega_0$ with $j=2$). In Fig.6.2-3), the coordinate of point $A$ or $B$ is $\Omega / \omega_0 = 1.7654$ or 1.81, and point $C$ is the linear resonance frequency of $2\omega_1 / j$ (=1.7888 $\omega_0$ with $j=1$). In particular, our results show that points $A$ and $B$ will approach point $C$ when $\dfrac{V_{ac}}{V_{dc}}$ approaches zero.

Similar to the responses of a parametrically excited Duffing oscillator [155] and electrostatical microelectromechanical oscillators with cubic nonlinear coupling [108-112], the response of the present system (6.5) also exhibits hysteresis phenomenon. For example, it is seen from Fig.6.2 that when the ac frequency $\Omega / \omega_0$ is higher than the coordinate of point $B$ (say, 1.81 for $\lambda = 2$), only the (stable) trivial solution exists. When

the ac frequency is between the coordinates of points $A$ and $B$ (say, $1.7654 \leq \Omega/\omega_0 \leq 1.81$ for $\lambda = 2$), the trivial solution is unstable, and the only stable solution is the periodic solution shown by the solid line in Fig.6.2. When the ac frequency $\Omega/\omega_0$ is less than the coordinate of point $A$ (say, 1.7654 for $\lambda = 2$), two stable solutions exist, including the trivial solution and a stable steady-state solution shown by the solid line in Fig.6.2. Thus, when the ac frequency $\Omega/\omega_0$ decreased gradually from a bigger value (for example, more than 1.81), the amplitude of parametric resonance will increase along the solid line in Fig.6.2-3). On the other hand, when the ac frequency increased gradually from a smaller value (for example, less than 1.7654), there will be no parametric resonance until $\Omega/\omega_0$ reaches point $A$ (=1.7654) at which the response will jump abruptly to the solid line in Fig.6.2-3) and gradually decrease to zero along this solid line.

All of these results on the stable and unstable steady-state solutions shown in Fig.6.2 for parametric resonance with $\lambda \leq 2$ are qualitatively similar to those obtained in [102-105] based on linearly coupled oscillators and those obtained in [108-112] based on oscillators with a cubic nonlinear coupling, around the linear resonance frequencies $\Omega = 2\omega_1 / j$ ($j$=1, 2 or 4).


## 6.3.2 Parametric resonance with $\lambda \geq 3$

Different from the previous works [102-105] and [108-112] which only focused on parametric resonance with $\lambda \leq 2$, the present work is particularly interested in existence of high-order subharmonic parametric resonance with $\lambda \geq 3$, which is equivalent to a resonance frequency around $\Omega = 2\omega_1 / j$ with $0 < j < 1$.

Fig.6.3 shows the relationships between the amplitude of the excited resonance and the ac frequency for $\lambda = 3$, 4 or 8. In Fig.6.3-1), the solid line represents a stable steady-state solution, while an unstable steady-state solution also exists and is showed in Fig.6.3-1) by a dashed line which is almost coincident with the solid line and thus is covered by the solid line. Here, it should be stated that any point on the solid or dashed line would represent more than one solution which have the same amplitude but with different phases. The solution curves intersect with the $x$-coordinate axis at point $A$

($\Omega/\omega_0$ =2.6816) which approaches point $C$ when $\dfrac{V_{ac}}{V_{dc}}$ approaches zero, where the

coordinate of point $C$ is $\lambda\omega_1/\omega_0$ =2.6832 with $\lambda$ =3 (equivalent to $\Omega=2\omega_1/j$ with

$j$=2/3). In Fig.6.3-2), the two solution curves intersect with the x-coordinate axis at point

$A$ ($\Omega/\omega_0$ =3.5756) which approaches point $C$ when $\dfrac{V_{ac}}{V_{dc}}$ approaches zero, where the

coordinate of point $C$ is $\lambda\omega_1/\omega_0$ =3.5776 with $\lambda$ =4 (equivalent to $\Omega=2\omega_1/j$ with

$j$=1/2). Similar to Fig.6.3-1) for $\lambda=3$, the dashed line in Fig.6.3-3) for the unstable

solution with $\lambda=8$ is almost coincident with the solid line and thus is covered by the

solid one. The solution curves intersect the x-axis at point $A$ ($\Omega/\omega_0$ =7.1512) which

approaches point $C$ when $\dfrac{V_{ac}}{V_{dc}}$ approaches zero, where the coordinate of $C$

$=\lambda\omega_1/\omega_0$ =7.1552 with $\lambda$ =8 (equivalent to $\Omega=2\omega_1/j$ with $j$=1/4).

It is seen from Fig.6.3 that near point $A$, small-amplitude stable steady-state periodic solutions exist for $\lambda=3$, 4 or 8, in the neighborhood of the equilibrium position of the oscillators. Therefore, infinitesimal disturbances could lead to dynamic instability of the equilibrium position and the appearance of high-order subharmonic parametric resonance when the ac frequency is close to point $A$ at which $\Omega$ =2.6816$\omega_0$ for $\lambda=3$, or $\Omega$ =3.5756$\omega_0$ for $\lambda=4$, or $\Omega$ =7.1512$\omega_0$ for $\lambda=8$. These values of the resonance frequency $\Omega$ are very close to $\lambda\omega_1$, with a very small gap less than 0.1% for $\lambda=3$, 4 or 8. Furthermore, our results (the details are omitted here) showed that similar high-order subharmonic parametric resonance also occurs for $\lambda$ larger than 8. Therefore, in contrast to previous related works [102-105, 108-112] which showed the existence of lower-order subharmonic parametric resonance ($\lambda\leq2$), the present work shows that periodically varying nonlinear coupling in the nonlinearly coupled micromechanical oscillators does cause high-order subharmonic parametric resonance when the ac frequency is close to a multiple (say, 3, 4, 8 or more) of one of its natural frequencies.

In connection with this, we noticed that similar high-order subharmonic parametric resonance of specific order has been reported previously for a few damping-free nonlinear oscillators with periodically varying nonlinear powers of specific order

[157-158]. These previous works (such as [157-158]) indicated that if the periodically varying nonlinear term of the governing equation is a power of order ($\lambda$-1), then subharmonic parametric resonance of order $\lambda$ will exist while subharmonic parametric resonance of order higher than $\lambda$ will not exist. Since the present model includes a general periodically varying nonlinear term (see the fourth term on LHS of (6.5)) whose Taylor series contains all orders of powers, the system studied in this chapter is expected to exhibit subharmonic resonances of all orders (such as $\lambda$=3, 4, 8, or more), as shown by the above numerical results. In fact, our numerical results have confirmed that if the fourth term on LHS of (6.5) is expanded only up to the 7-th power, subharmonic parametric resonance of order 8 will exist while subharmonic parametric resonance of order 9 will not exist. On the other hand, if the fourth term on LHS of (6.5) is expanded up to the 9-th power, subharmonic parametric resonance of order 9 will exist. Therefore, our results are well consistent with the earlier works [157-158]. In particular, as stated in [157], theoretical results of [157] have been well confirmed experimentally.

## 6.4 Effects of the damping on parametric resonance of a single oscillator

Next, let us study the effect of a linear damping on parametric resonance of the coupled micromechanical oscillators under periodically varying coupling forces. The parameters used in this section are $Q$=1/20 and $\dfrac{V_{ac}}{V_{dc}} = 0.1$ (same as those in Section 6.3), but with a non-zero viscous coefficient $c > 0$.

### 6.4.1. Parametric resonance with $\lambda \leq 2$

Firstly, let us consider the parametric resonance with $\lambda \leq 2$, with increasing viscous coefficient $c$. It is found that for $\lambda \leq 2$, when the viscous coefficient is sufficiently small, there are still two different solution curves (one represents the stable steady-state solution, and the other represents the unstable one) which meet the $x$-coordinate axis at two distinct points, and these two solution curves change smoothly with increasing viscous coefficient. However, after the viscous coefficient reaches a certain critical value, the two solution

curves will originate from some points above the $x$-axis and no longer meet the $x$-axis. Hence, the critical viscous coefficient can be defined as the smallest viscous coefficient beyond which no more periodic solution with vanishingly small amplitude exists. The critical viscous coefficient defined in this way for $\lambda = 0.5$, 1, 2, 3, 4, or 8 is shown in Table 6.1. In particular, the critical viscous coefficient for $\lambda \geq 3$ is always zero, which could mean that high-order subharmonic parametric resonance with vanishing small amplitude will not exist in the presence of an even small linear damping.

For $\lambda = 2$, the relationship between the amplitude of the excited periodic solution and the ac frequency is shown in Fig.6.4 when the viscous coefficient is less than (or equal to) the critical value ($22.2 \times 10^{-3}$). In Fig.6.4, curve (1) represents the steady-state solutions without the damping effect (shown in Fig.6.2-3)), and curve (2) or (3) represents the solutions with the viscous coefficient $\dfrac{c}{m\omega_0} = 12 \times 10^{-3}$, or $22.2 \times 10^{-3}$

(the critical value). It is seen from Fig.6.4 that all stable solution curves originate from some points on the $x$-axis with zero-amplitude. Thus, when the viscous coefficient is less than (or equal to) the critical value, small-amplitude non-zero stable periodic solutions exist in the neighborhood of the equilibrium position, and infinitesimal disturbances can cause dynamic instability of the equilibrium position and parametric resonance of the coupled oscillators.

When the viscous coefficient is bigger than the critical value, the relationship between the amplitude of the excited periodic solution and the ac frequency for $\lambda = 2$ is shown in Fig.6.5. Different than Fig.6.4, the two solution curves shown in Fig.6.5 originate from a point $A$ which is above the $x$-axis and associated with non-zero amplitude. Since the stable solution curves do not intersect with the $x$-coordinate axis, instability of the equilibrium position will lead to a periodic oscillation of the oscillators with small but finite amplitude. If the smallest amplitude, which is determined by point $A$ in Fig.6.5, is defined as $a_{lowest}$, then the lowest amplitude $a_{lowest}$ increases with increasing viscous coefficient. For example, $a_{lowest}$ is $0.159\,d_0$ when the viscous coefficient $\dfrac{c}{m\omega_0}$ is $23 \times 10^{-3}$, while $a_{lowest}$ increases to $0.244\,d_0$ or $0.383\,d_0$ when

the viscous coefficient increases to $24 \times 10^{-3}$ or $27 \times 10^{-3}$. Our results show that the responses for $\lambda = 0.5$ and 1 are essentially similar to that shown in Fig. 6.4 or 6.5 for $\lambda = 2$, and therefore the details for $\lambda = 0.5$ and 1 are not shown here.

In summary, for $\lambda \le 2$, there exists a positive critical value for the viscous coefficient, as shown in Table 6.1. When the viscous coefficient is less than (or equal to) the critical value, stable periodic solutions with vanishingly small amplitude exist and parametric resonance exhibit similar phenomena as those discussed in Section 6.3 in the absence of damping. However, when the viscous coefficient is larger than the critical value, the amplitudes of possible stable periodic solutions are bounded from below by the smallest amplitude $a_{lowest}$ which increases with increasing viscous coefficient. In this case, periodic solutions with amplitude smaller than $a_{lowest}$ will not exist. In particular, because the critical viscous coefficient for $\lambda \ge 3$ is always zero (see Table 6.1), high-order subharmonic parametric resonance with vanishing small amplitude will not exist in the presence of any small linear damping.

Here, it should be stated that the damping effect on parametric resonance is a complicated issue. On one hand, Rhoads et. al [110-112] stated that the response is largely unaffected by damping and therefore these authors have limited their attention to linear damping only. On the other hand, Lifshitz and Cross [104] indicated that nonlinear damping is important for the amplitudes of steady-state solutions. In the present study, we only considered a linear damping, and how a nonlinear damping affect parametric resonance of nonlinearly coupled oscillators requests further research.

## 6.4.2 Parametric resonance with $\lambda \ge 3$

Let us now consider the damping effect on parametric resonance with $\lambda \ge 3$. It is found that the critical viscous coefficient for $\lambda \ge 3$ is constantly zero, as shown in Table 6.1, and there exists no periodic solution with vanishingly small amplitude for $\lambda \ge 3$ when the viscous coefficient is non-zero. In other words, for non-zero viscous coefficient, the amplitudes of all possible periodic solutions with $\lambda \ge 3$ are bounded from below by a positive number.

Fig.6.6 shows the relationship between the amplitude of the excited stable periodic

solution and the ac frequency with non-zero viscous coefficient for $\lambda = 8$. It is seen from Fig.6.6 that the lowest amplitude $a_{lowest}$ in the solution curve increases as the viscous coefficient increases. For example, the lowest amplitude $a_{lowest}$ is $0.156 d_0$ when the viscous coefficient $\dfrac{c}{m\omega_0}$ is $2 \times 10^{-8}$, while $a_{lowest}$ increases to $0.228 d_0$ or $0.334 d_0$ when the viscous coefficient increases to $2 \times 10^{-7}$ or $2 \times 10^{-6}$. Our results show that the responses for $\lambda = 3$ and 4 are essentially similar to that shown in Fig.6.6 for $\lambda = 8$, and therefore the details for $\lambda = 3$ and 4 are omitted here.

These results are consistent with the expected stabilizing effects of damping on parametric resonance. In fact, in the presence of a non-zero damping, it is expected that high-order subharmonic parametric resonance could occur only when the disturbances are large enough to bring the oscillator system to one stable steady-state state which is at a finite distance from the equilibrium position. Thus, roughly speaking, there are two conditions for the occurrence of high-order subharmonic parametric resonances with smaller disturbance. The first one is that the viscous coefficient should be reasonably lower, and the second one is that the excitation frequency should be sufficiently close to a multiple ($\geq 3$) of one of the natural frequencies of the system. In the presence of a sufficiently large damping, high-order subharmonic parametric resonance could occur only when the disturbances are large enough, to offer sufficient energy to drive the oscillator system to one steady-state periodic state which is at a finite distance from the equilibrium position.

Finally, it should be stated that the existence of stable high-order subharmonic parametric resonance also depends on the loading parameter $Q$ and the excitation parameter $\dfrac{V_{ac}}{V_{dc}}$. The domain of $Q$ and $\dfrac{V_{ac}}{V_{dc}}$ in which non-trivial stable steady-state solutions exist for high-order parametric resonance with $\lambda \geq 3$, in the absence of any damping, is shown in the shaded area in Fig.6.7. For example, when $\dfrac{V_{ac}}{V_{dc}} = 0.1$, the loading parameter $Q$ must be less than 0.248, in order to obtain the stable high-order

parametric resonance with $\lambda \geq 3$. When $\dfrac{V_{ac}}{V_{dc}}$ is 0, on the other hand, the problem becomes a static one and the system will become unstable when the loading parameter $Q$ is more than 1/4, consistent with the general results obtained in [126-128] for a large array of coupled springs.

# 6.5 Conclusions

Parametric resonance of comb-drive microcantilevers is studied based on a simplified model of nonlinearly coupled micromechanical oscillators. Different than most of previous related works, the present study focuses on the effects of periodically varying nonlinear coupling on parametric resonance, with a particular interest in the existence of high-order subharmonic parametric resonance. Indeed, our results show that the periodically varying nonlinear coupling leads to the occurrence of high-order subharmonic parametric resonance when the excitation frequency is equal or close to a multiple (say 3, 4, 8, or more) of one of the natural frequencies of the oscillator system. These results distinguish the present analysis from most previous related works based on a linearized coupling, and are well consistent with a few earlier theoretical and experimental works conducted for some specific forms of nonlinear coupling. Also, the effect of a linear damping on parametric resonance is investigated, and a critical viscous coefficient is defined as one of the conditions for the occurrence of parametric resonance.

Table 6.1 Critical viscous coefficient $\dfrac{c}{m\omega_0}$ when $Q = \dfrac{\varepsilon_0 S V_{dc}^2}{2 d_0^3 q} = 1/20$ and $\dfrac{V_{ac}}{V_{dc}} = 0.1$

| $\lambda$ | 0.5 | 1 | 2 | 3 | 4 | 8 |
|---|---|---|---|---|---|---|
| Critical viscous coefficient $\dfrac{c}{m\omega_0}$ | $7.6 \times 10^{-3}$ | $0.56 \times 10^{-3}$ | $22.2 \times 10^{-3}$ | 0 | 0 | 0 |
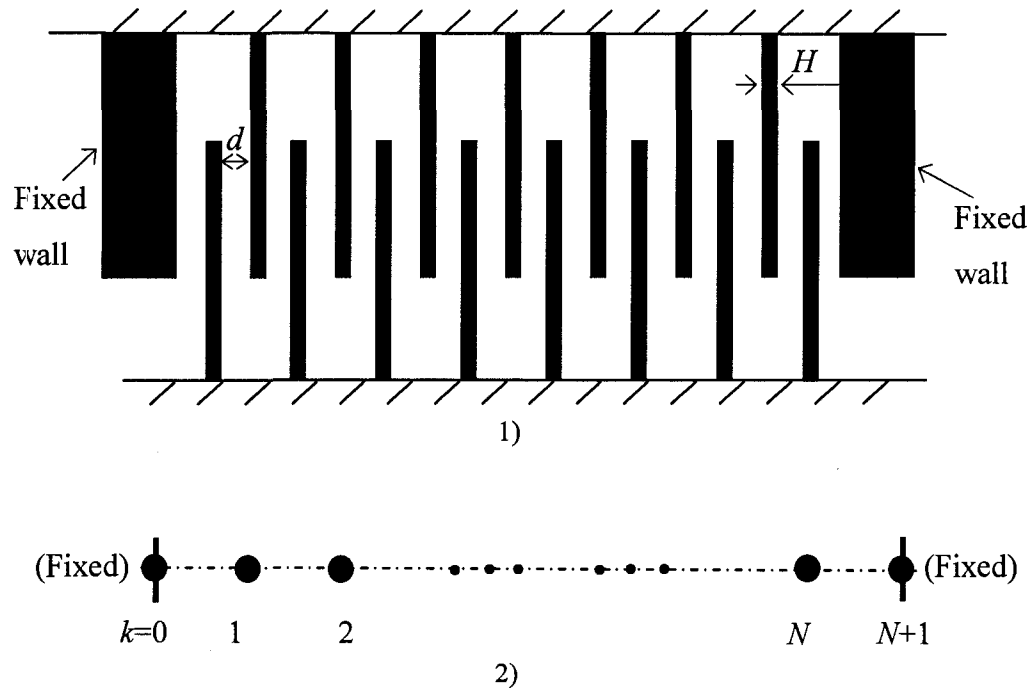
Fig.6.1 Comb-drive microcantilever array and simplified spring model.
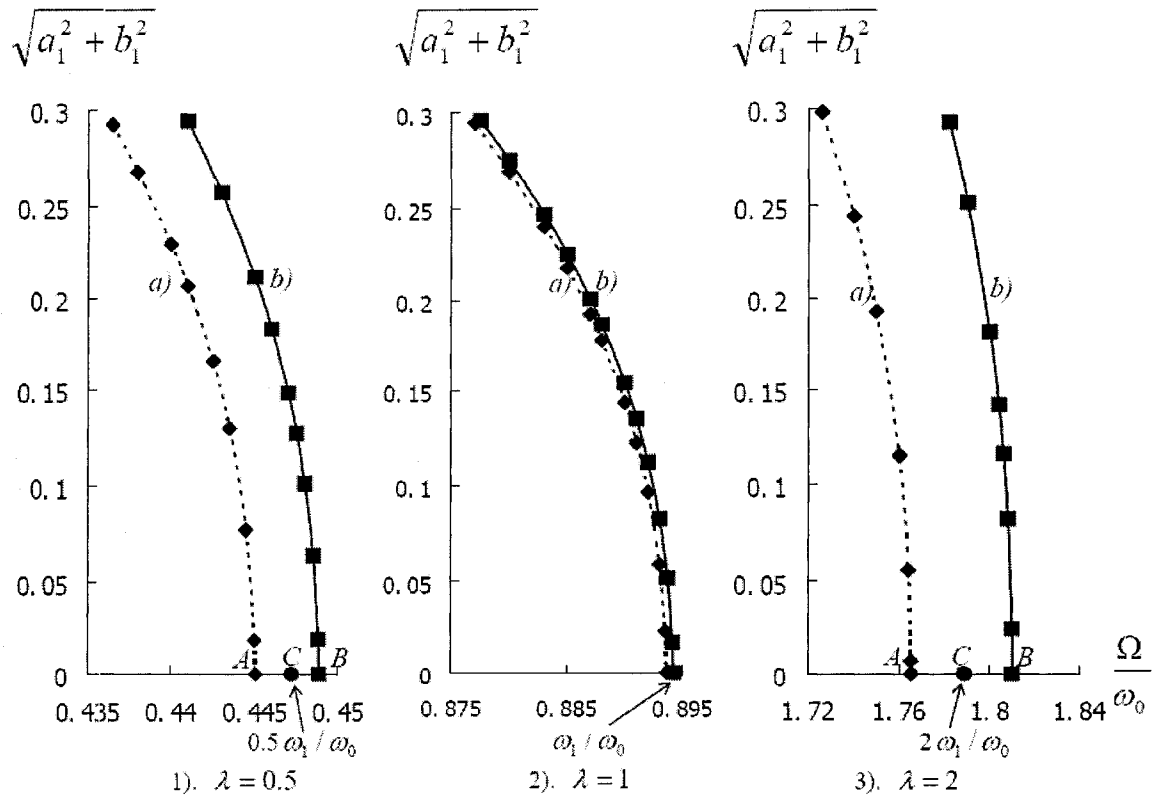
Fig.6.2 Parametric resonance for $\lambda \leq 2$ without the viscous effect when $Q = \dfrac{\varepsilon_0 S V_{dc}^2}{2 d_0^3 q} = 1/20$ and $\dfrac{V_{ac}}{V_{dc}} = 0.1$.
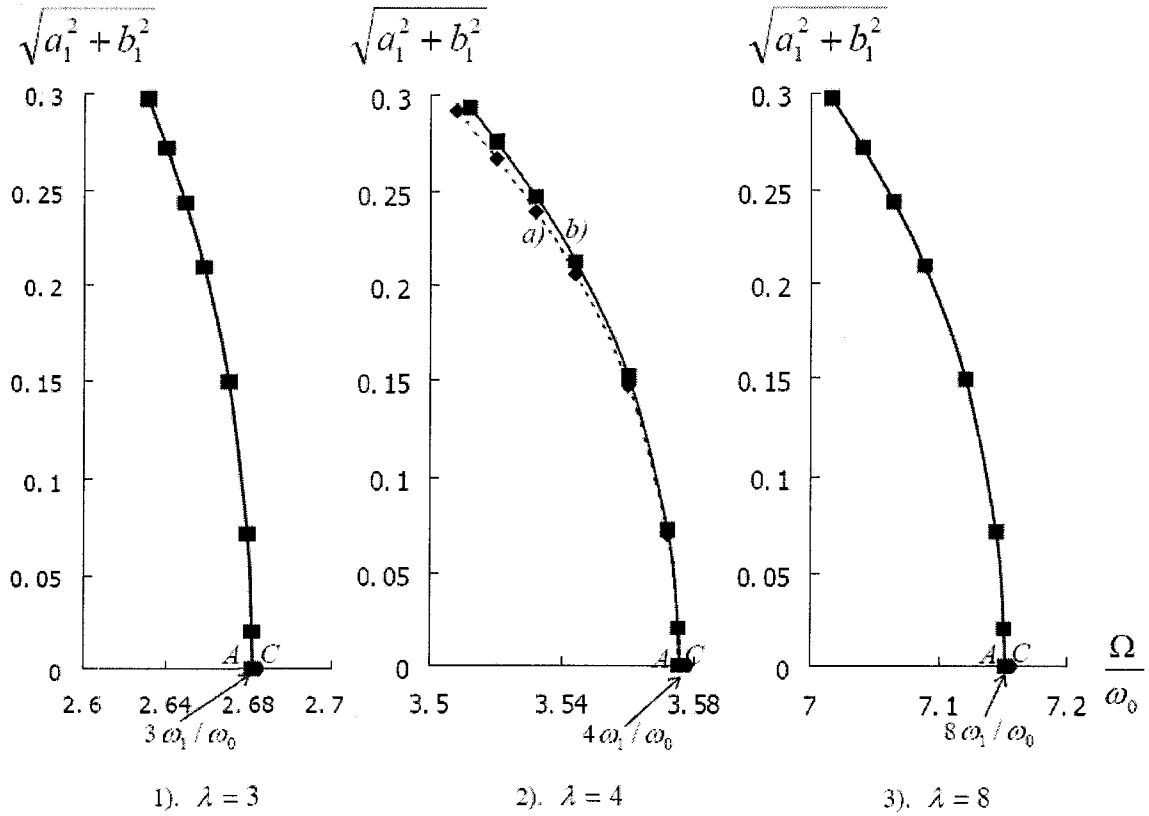
Fig.6.3 Parametric resonance for $\lambda \geq 2$ without the viscous effect when

$$Q = \frac{\varepsilon_0 S V_{dc}^2}{2 d_0^3 q} = 1/20 \text{ and } \frac{V_{ac}}{V_{dc}} = 0.1.$$
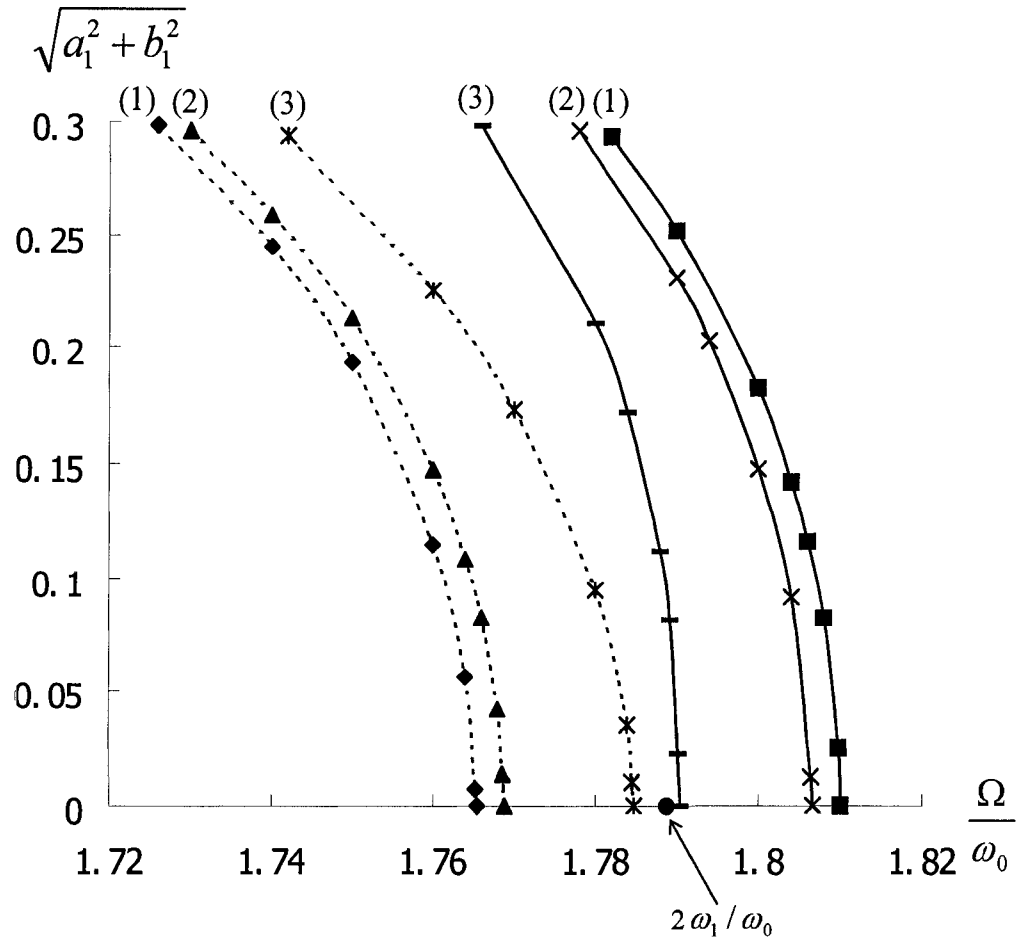
$$(1): \quad \frac{c}{m\omega_0}=0; \ (2): \quad \frac{c}{m\omega_0}=12\times10^{-3}; \ (3): \quad \frac{c}{m\omega_0}=22.2\times10^{-3}.$$

Fig.6.4 Parametric resonance for $\lambda = 2$ with the viscous coefficient

less than (or equal to) the critical value when $Q = \dfrac{\varepsilon_0 S V_{dc}^2}{2d_0^3 q}=1/20$ and

$\dfrac{V_{ac}}{V_{dc}}=0.1$, where the critical value is $\dfrac{c}{m\omega_0}=22.2\times10^{-3}$ for $\lambda=2$.
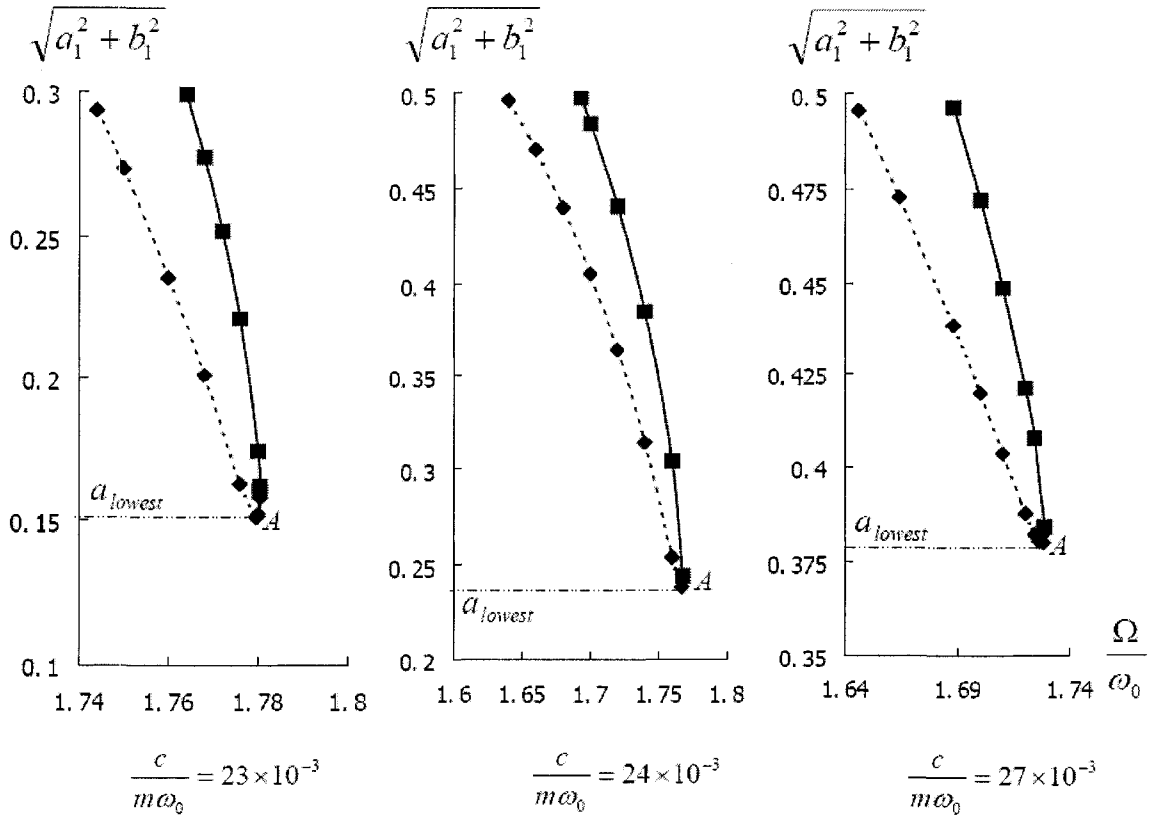
Fig.6.5 Parametric resonance for $\lambda = 2$ with the viscous coefficient more than

the critical value when $Q = \dfrac{\varepsilon_0 S V_{dc}^2}{2d_0^3 q} = 1/20$ and $\dfrac{V_{ac}}{V_{dc}} = 0.1$, where the critical value

is $\dfrac{c}{m\omega_0} = 22.2 \times 10^{-3}$ for $\lambda = 2$.
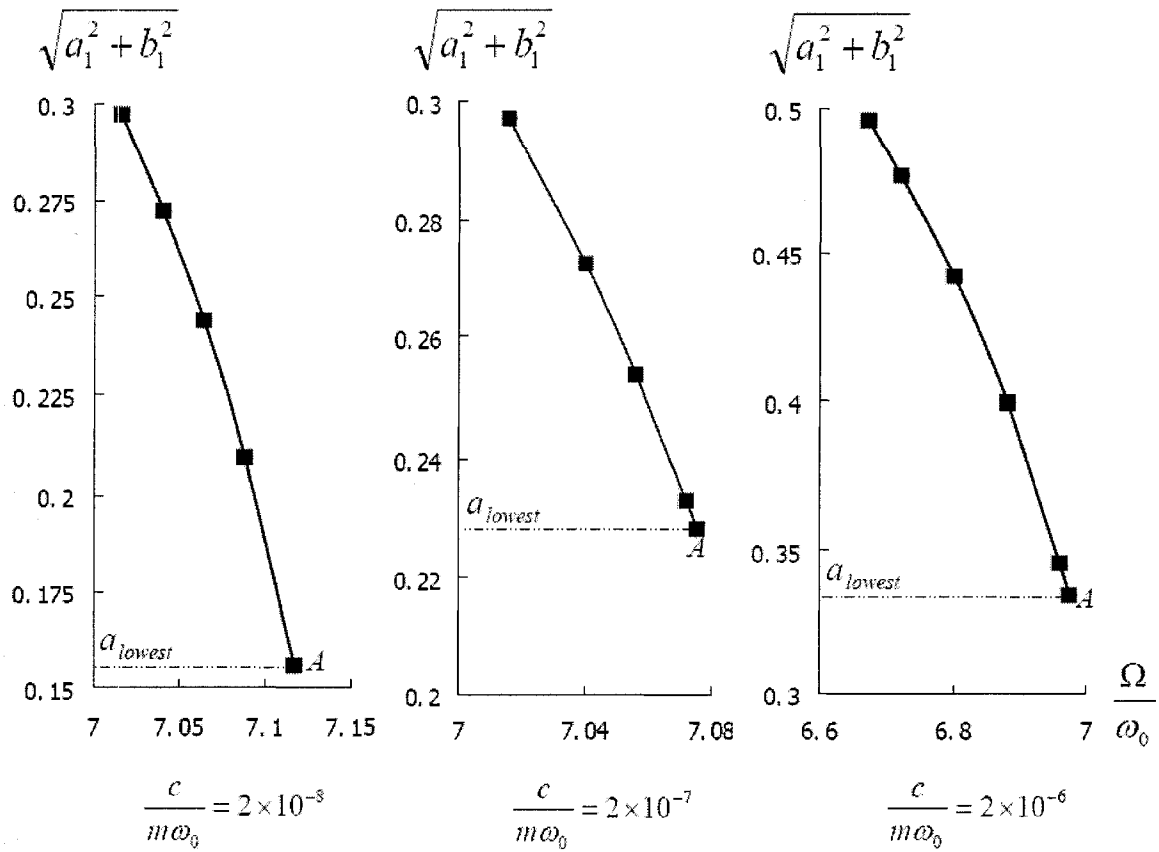
Fig. 6.6 Parametric resonance for $\lambda = 8$ with the viscous coefficient when

$$Q = \frac{\varepsilon_0 S V_{dc}^2}{2d_0^3 q} = 1/20 \text{ and } \frac{V_{ac}}{V_{dc}} = 0.1.$$

169
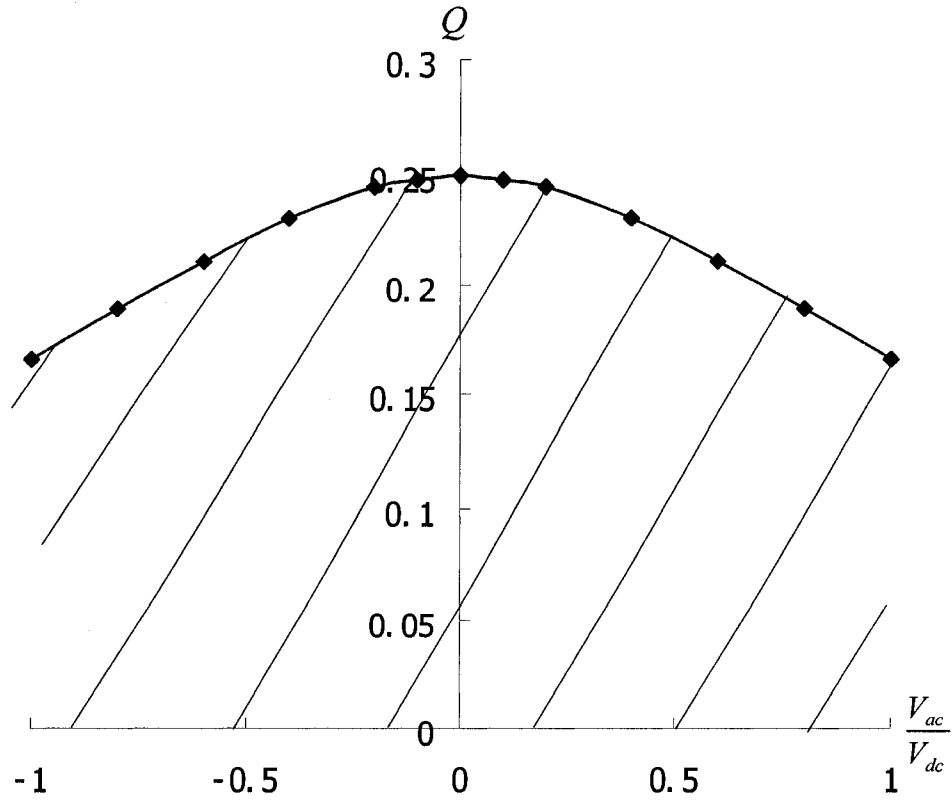
Fig.6.7 Domain of $Q$ and $\dfrac{V_{ac}}{V_{dc}}$ in which non-trivial stable periodic solutions can

be obtained for high-order parametric resonance with $\lambda \geq 3$ in the absence of

damping, where $Q = \dfrac{\varepsilon_0 S V_{dc}^2}{2 d_0^3 q}$.

# Chapter 7

# High-Order Subharmonic Parametric Resonance of a Nonlinearly Coupled Array of Micromechanical Nonlinear Oscillators

## 7.1 Introduction

In Chapter 6, we analyzed parametric resonance of a linear oscillator which is attracted by two fixed ends through periodically varying nonlinear coupling forces. In particular, high-order subharmonic parametric resonance is studied as a result of the nonlinear coupling. However, the results of Chapter 6 suffer two major limitations. First, the elastic nonlinearity is neglected and thus the oscillator is assumed to be linear. Second, only one single oscillator is studied and coupled dynamics of more than one oscillator is not addressed. Motivated by the two major limitations of Chapter 6, the present work studies parametric resonance of a coupled array of more than one nonlinear oscillator with nonlinear coupling between adjacent oscillators. Of particular interest is the effect of elastic nonlinearity on high-order subharmonic parametric resonance of coupled micromechanical oscillators.

In this chapter, a model is formulated for a nonlinearly coupled array of nonlinear oscillators in Section 7.2. Then we first discuss high-order subharmonic parametric resonance of a single nonlinear oscillator attracted by two fixed ends in Section 7.3, and further study high-order subharmonic parametric resonance of a coupled array of three nonlinear oscillators in Section 7.4. All results are finally summarized in Section 7.5.

171

## 7.2 The model for a nonlinearly coupled array of nonlinear oscillators

In this chapter, we still focus on the comb-drive microcantilever array shown in Fig.6.1-1), and the oscillator model shown in Fig.6.1-2) is employed to analyze essential characteristics of the comb-drive microcantilever array.

Assuming that a voltage $V$ is applied on any two adjacent oscillators, the electrostatic force applied on the $k$-th oscillator ($k=1, 2,..., N$) is (see (1.1))

$$F_{electric} = \frac{\varepsilon_0 S V^2}{2} [\frac{1}{(d_0 + X_{k+1} - X_k)^2} - \frac{1}{(d_0 + X_k - X_{k-1})^2}] \qquad (7.1)$$

where $\varepsilon_0$ is the permittivity of the medium between adjacent microbeams, $S$ is the area exposed to the electrostatic field, $d_0$ is the initial distance between two side-faces of adjacent microbeams, and $X_k$ is the displacement of the $k$-th oscillator. Different from Chapter 6, here, elastic nonlinearity of the oscillators is taken into account, and similar to [104, 108-112], all oscillators are assumed to be Duffing oscillators (the restoring force is symmetric, and nonlinear terms higher than the cubic-order are ignored). Thus, the elastic force acting on the $k$-th oscillator ($k=1, 2,..., N$) is

$$F_{elastic} = -m\omega_0^2 X_k - mbX_k^3 \qquad (7.2)$$

where $\omega_0 = \sqrt{\frac{q}{m}}$ is the frequency of a single isolated oscillator, $m$ is the mass, $q$ is the spring constant, and $b$ is the cubic nonlinear elasticity coefficient ($b>0$ for a hard oscillator, while $b<0$ for a soft oscillator). Thus, in the presence of a linear damping characterized by a constant viscous coefficient $c$, dynamics of the $k$-th oscillator ($k= 1, 2,..., N$) is governed by the dimensionless equation (see e.g. (6.1))

$$\frac{d^2 x_k}{d\tau^2} + \frac{c}{m\omega_0}\frac{dx_k}{d\tau} + x_k + \frac{b}{\omega_0^2}x_k^3 - \frac{\varepsilon_0 SV^2}{2d_0^3 q}[\frac{1}{(1+x_{k+1}-x_k)^2} - \frac{1}{(1+x_k-x_{k-1})^2}] = 0 \quad (7.3)$$

where $x_k = \dfrac{X_k}{d_0}$ is the dimensionless displacement of the $k$-th oscillator, and $\tau = \omega_0 t$ is the scaled time.

When there is only a dc voltage applied on the coupled oscillators ($V=V_{dc}$), the $N$ distinct natural frequencies of the oscillator system are given by (see (6.3))[103]

$$\omega_i = \sqrt{1 - 8Q\sin^2\frac{i\pi}{2(N+1)}}\,\omega_0, \quad (i=1,2,\ldots,N) \quad (7.4)$$

where $Q = \dfrac{\varepsilon_0 SV_{dc}^2}{2d_0^3 q}$ is defined based on the initial distance $d_0$.

When a periodically varying ac voltage is added to the dc voltage, $V = V_{dc} + V_{ac}\cos(\Omega t)$, where $V_{ac}$ and $\Omega$ are the amplitude and frequency of the ac voltage, Eqn (7.3) becomes

$$\frac{d^2 x_k}{d\tau^2} + \frac{c}{m\omega_0}\frac{dx_k}{d\tau} + x_k + \frac{b}{\omega_0^2}x_k^3$$

$$-Q[\frac{1}{(1+x_{k+1}-x_k)^n} - \frac{1}{(1+x_k-x_{k-1})^n}][1 + 2\frac{V_{ac}}{V_{dc}}\cos(\frac{\Omega}{\omega_0}\tau) + (\frac{V_{ac}}{V_{dc}})^2\cos^2(\frac{\Omega}{\omega_0}\tau)] = 0 \quad (7.5)$$

In this present analysis, we still focus on high-order subharmonic parametric resonance with the frequency $\omega = \Omega/\lambda$, where $\lambda$ is an integer and $\geq 3$ for high-order subharmonics, and the non-zero steady-state periodic solution of (7.5) is assumed to be

$$x_k = a_k + b_k\cos(\frac{\Omega}{\lambda\omega_0}\tau) + c_k\sin(\frac{\Omega}{\lambda\omega_0}\tau) \quad (7.6)$$

where $a_k$, $b_k$ and $c_k$ ($k=1, 2,..., N$) are some undetermined constants. In Eqn (7.6), we employ a constant term $a_k$, which defines the equilibrium position of the oscillation. Our results show that for a single oscillator, $a_1$ always equals to zero. For an oscillator array with more than one oscillator, $a_k$ is close to zero, and under the same conditions, the steady-state solution (7.6) is close to that given by (6.6). A non-zero stable solution of (7.5) defines a parametric resonance characterized by a stable steady-state periodic solution of the form (7.6).

In the next section, we shall first study the high-order subharmonic parametric resonance with $\lambda \geq 3$ for a single nonlinear oscillator. Then in Section 7.4, we will discuss the high-order subharmonic parametric resonance with $\lambda \geq 3$ for a coupled array of three nonlinear oscillators.

## 7.3 High-order subharmonic parametric resonance of a single nonlinear oscillator

Firstly, let us consider a single nonlinear oscillator which is attracted by two fixed ends (thus $N=1$ and $X_0 = X_2 = 0$, see Fig.6.1-2)). To be specific, we shall confine ourselves to the high-order subharmonic parametric resonance with $\lambda = 4$ and $\lambda = 6$. To this end, expanding the nonlinear coupling terms $\dfrac{1}{(1-x_1)^2}$ and $\dfrac{1}{(1+x_1)^2}$ in Eqn (7.5) into a Taylor series up to the 5-th power, we obtain

$$\frac{d^2 x_1}{d\tau^2} + \frac{c}{m\omega_0}\frac{dx_1}{d\tau} + x_1 + \frac{b}{\omega_0^2}x_1^3$$

$$-Q(4x_1 + 8x_1^3 + 12x_1^5)[1 + 2\frac{V_{ac}}{V_{dc}}\cos(\frac{\Omega}{\omega_0}\tau) + (\frac{V_{ac}}{V_{dc}})^2\cos^2(\frac{\Omega}{\omega_0}\tau)] = 0 \quad (7.7)$$

In this section, we will employ the method of slowly varying parameters, because this method is convenient in obtaining steady-state solutions of a single oscillator and discussing their instability [155-157]. Consider a subharmonic solution of order $1/\lambda$

around the equilibrium position $x_1 = 0$

$$x_1(\tau) = A_m(\tau)\cos[\frac{\Omega}{\lambda\omega_0}\tau - \psi(\tau)] \equiv A_m(\tau)\cos[\theta(\tau)] \qquad (7.8)$$

where $A_m(\tau)$ and $\psi(\tau)$ are the amplitude and phase functions of the subharmonic solution. For the steady-state solutions of a single oscillator, form (7.8) is same as form (7.6) with $a_1 = 0$, $A_m = \sqrt{b_1^2 + c_1^2}$, and $\psi = arctg(c_1 / b_1)$. Using the method of slowly varying parameters, we have

$$\frac{dA_m}{d\tau}\cos\theta + A_m\frac{d\psi}{d\tau}\sin\theta = 0 \qquad (7.9)$$

which ensures

$$\frac{dx_1(\tau)}{d\tau} = -A_m\frac{\Omega}{\lambda\omega_0}\sin\theta \qquad (7.10)$$

Substituting (7.8) into (7.7), we obtain

$$-\frac{dA_m}{d\tau}\sin\theta + A_m\frac{d\psi}{d\tau}\cos\theta - A_m\omega\cos\theta - \frac{c}{m\omega_0}A_m\sin\theta + \frac{A_m\cos\theta}{\omega} + \frac{bA_m^3\cos^3\theta}{\omega_0^2\omega}$$

$$-\frac{Q}{\omega}f(A_m\cos\theta,\tau) = 0 \qquad (7.11)$$

where $\omega = \dfrac{\Omega}{\lambda\omega_0}$ is the frequency of the subharmonic solution, and

$$f(A_m\cos\theta,\tau) = (4A_m\cos\theta + 8A_m^3\cos^3\theta + 12A_m^5\cos^5\theta)$$

$$[1 + 2\frac{V_{ac}}{V_{dc}}\cos(\frac{\Omega}{\omega_0}\tau) + (\frac{V_{ac}}{V_{dc}})^2\cos^2(\frac{\Omega}{\omega_0}\tau)] \qquad (7.12)$$

Multiplying (7.9) by $\cos\theta$ and (7.11) by $\sin\theta$, and subtracting, we obtain

$$\frac{dA_m}{d\tau} + A_m\omega\sin\theta\cos\theta + \frac{c}{m\omega_0}A_m\sin^2\theta - \frac{A_m\sin\theta\cos\theta}{\omega} - \frac{bA_m^3\cos^3\theta\sin\theta}{\omega_0^2\omega} + \frac{Q}{\omega}f\sin\theta = 0$$

(7.13)

Multiplying (7.9) by $\sin\theta$ and (7.11) by $\cos\theta$, and adding, we obtain

$$A_m\frac{d\psi}{d\tau} - A_m\omega\cos^2\theta - \frac{c}{m\omega_0}A_m\sin\theta\cos\theta + \frac{A_m\cos^2\theta}{\omega} + \frac{bA_m^3\cos^4\theta}{\omega_0^2\omega} - \frac{Q}{\omega}f\cos\theta = 0 \quad (7.14)$$

With the method of slowly varying parameters [155-157], $A_m(\tau)$ and $\psi(\tau)$ are considered constant over one cycle. Thus, integrating (7.13) and (7.14) with respect to $\theta$ from 0 to $2\pi$, we obtain

$$\frac{dA_m}{d\tau} + \frac{c}{2m\omega_0}A_m + \frac{Q}{2\pi\omega}\int_0^{2\pi}f\sin\theta d\theta = 0$$

(7.15)

$$A_m\frac{d\psi}{d\tau} - \frac{A_m\omega}{2} + \frac{A_m}{2\omega} + \frac{3bA_m^3}{8\omega_0^2\omega} - \frac{Q}{2\pi\omega}\int_0^{2\pi}f\cos\theta d\theta = 0$$

(7.16)

Let $\dfrac{dA_m}{d\tau} = 0$ and $\dfrac{d\psi}{d\tau} = 0$, and we can obtain the steady-state solutions of specific order $\lambda$. In the present analysis, we focus on the high-order subharmonics with $\lambda = 4$ and $\lambda = 6$. For example, for the high-order subharmonics with $\lambda = 4$ and $c=0$ (without damping), substituting $\dfrac{dA_m}{d\tau} = 0$, $\dfrac{d\psi}{d\tau} = 0$, $\lambda = 4$ and $c=0$ into Eqns (7.15-7.16), we obtain

$$\sin(4\psi) = 0$$

(7.17)

$$-\frac{\omega}{2}+\frac{1}{2\omega}+\frac{3bA_m^2}{8\omega_0^2\omega}-2\frac{Q}{\omega}(1+0.5\frac{V_{ac}^2}{V_{dc}^2})-3\frac{Q}{\omega}(1+0.5\frac{V_{ac}^2}{V_{dc}^2})A_m^2-3.75\frac{Q}{\omega}(1+0.5\frac{V_{ac}^2}{V_{dc}^2})A_m^4$$

$$-\frac{Q}{\omega}\frac{V_{ac}}{V_{dc}}\cos(4\psi)A_m^2-2.25\frac{Q}{\omega}\frac{V_{ac}}{V_{dc}}\cos(4\psi)A_m^4=0 \qquad (7.18)$$

With the given parameters such as the loading parameters $Q$ and $V_{ac}/V_{dc}$, the nonlinear elasticity coefficient $b/\omega_0^2$, and the excitation frequency $\Omega/\omega_0$ ($\omega=\Omega/(\lambda\omega_0)$), the steady amplitude $A_m$ and phase $\psi$ of the high-order subharmonics with $\lambda=4$ and $c=0$ can be obtained using Eqns (7.17-7.18). Fig.7.1 shows the high-order subharmonic parametric resonance with $\lambda=4$ of a nonlinearly coupled oscillator when $Q=1/100$, $V_{ac}/V_{dc}=0.1$, and $c=0$ (without damping). In Fig.7.1, Figs 7.3-7.6 and Figs 7.8-7.9, the solid lines represent stable steady-state solutions, while the dashed lines represent unstable steady-state solutions (the detailed stability analysis of the steady-state solutions will be shown for a single nonlinear oscillator). As shown in Fig.7.1, the high-order subharmonic response largely depends on the nonlinear elasticity coefficient $b$. For example, for the hard nonlinear oscillator with $b/\omega_0^2=1$, the two (stable/unstable) solution curves turn towards the right, while the two (stable/unstable) solution curves for the soft nonlinear oscillator with $b/\omega_0^2=-1$ turn towards the left. For the linear oscillator with $b/\omega_0^2=0$, the two (stable/unstable) solution curves lie between those with $b/\omega_0^2=1$ and those with $b/\omega_0^2=-1$. On the other hand, for all cases with $b/\omega_0^2=1$, 0 or $-1$, all of the solution curves start from the same point $A$ with the coordinate of $\Omega/\omega_0=3.9188$. It follows from Eqn (7.4) that the natural frequency of this single oscillator is $\omega_1/\omega_0=0.9798$, and the coordinate of point $C$ in Fig.7.1 is $4\omega_1/\omega_0=3.9192$. In particular, point $A$ approaches point $C$ when $V_{ac}/V_{dc}$ approaches zero.

It is seen from Fig.7.1 that near point $A$, small-amplitude stable steady-state solutions with $\lambda=4$ exist in the neighborhood of the equilibrium position $x_1=0$. Therefore, infinitesimal disturbances can lead to dynamic instability of the equilibrium position and the high-order subharmonics with $\lambda=4$ when the ac frequency is close to

point $A$ at which $\Omega = 3.9188\,\omega_0$. The high-order subharmonics are attributed to the nonlinear coupling between two adjacent oscillators. For example, if the nonlinear coupling terms $\dfrac{1}{(1-x_1)^2}$ and $\dfrac{1}{(1+x_1)^2}$ in Eqn (7.5) are linearized, it can be verified that high-order subharmonics with $\lambda \geq 3$ will not exist. These results are consistent with our previous results of high-order subharmonics for a nonlinearly coupled linear oscillator (with $b=0$) shown in Chapter 6.

Whether a steady-state solution defined by (7.17) and (7.18) is stable or not can be studied as follows. Firstly, with an infinitesimal disturbance, let

$$A_m = A_{m0} + \varepsilon, \quad \psi = \psi_0 + \eta \tag{7.19}$$

where $A_{m0}$ and $\psi_0$ are the solution of (7.17) and (7.18), and $\varepsilon$ and $\eta$ are the infinitesimal disturbance in the neighborhood of $(A_{m0}, \psi_0)$ in the $A_m$-$\psi$ phase plane. Substituting (7.19) into (7.15) and (7.16), noting $A_{m0}$ and $\psi_0$ satisfy (7.17) and (7.18), and retaining only the first powers of $\varepsilon$ and $\eta$, we obtain

$$\frac{d\varepsilon}{d\tau} = \frac{Q}{\omega}\frac{V_{ac}}{V_{dc}}\cos(4\psi_0)(4A_{m0}^3 + 6A_{m0}^5)\eta \tag{7.20}$$

$$\frac{d\eta}{d\tau} + \varepsilon[0.75\frac{b}{\omega_0^2\omega}A_{m0} - 6\frac{Q}{\omega}(1+0.5\frac{V_{ac}^2}{V_{dc}^2})A_{m0} - 15\frac{Q}{\omega}(1+0.5\frac{V_{ac}^2}{V_{dc}^2})A_{m0}^3$$

$$-2\frac{Q}{\omega}\frac{V_{ac}}{V_{dc}}\cos(4\psi_0)A_{m0} - 9\frac{Q}{\omega}\frac{V_{ac}}{V_{dc}}\cos(4\psi_0)A_{m0}^3] = 0 \tag{7.21}$$

Substituting (7.20) into (7.21), we obtain

$$\frac{d^2\eta}{d\tau^2} + g(A_{m0}, \psi_0)\eta = 0 \tag{7.22}$$

where

$$g(A_{m0},\psi_0) = \frac{Q}{\omega}\frac{V_{ac}}{V_{dc}}\cos(4\psi_0)(4A_{m0}^3 + 6A_{m0}^5)\,[0.75\frac{b}{\omega_0^2\omega}A_{m0} - 6\frac{Q}{\omega}(1+0.5\frac{V_{ac}^2}{V_{dc}^2})A_{m0}$$

$$-15\frac{Q}{\omega}(1+0.5\frac{V_{ac}^2}{V_{dc}^2})A_{m0}^3 - 2\frac{Q}{\omega}\frac{V_{ac}}{V_{dc}}\cos(4\psi_0)A_{m0} - 9\frac{Q}{\omega}\frac{V_{ac}}{V_{dc}}\cos(4\psi_0)A_{m0}^3] \quad (7.23)$$

Let $\eta = e^{\mu}$, substituting it into (7.22), we obtain $\mu^2 = -g(A_{m0},\psi_0)$. If $g(A_{m0},\psi_0)>0$, $\mu^2<0$, and both $\varepsilon$ and $\eta$ are bounded, indicating that the solution is stable. On the other hand, if $g(A_{m0},\psi_0)<0$, $\mu$ is real, and $\varepsilon$ and $\eta$ are unbounded, indicating that this solution is unstable. For example, for the solution curves turning to the right (when $b/\omega_0^2=1$), the solid line representing stable steady-state solutions has $\cos(4\psi_0)=1$ (and $g(A_{m0},\psi_0)>0$), while the dashed line representing unstable steady-state solutions has $\cos(4\psi_0)=-1$ (and $g(A_{m0},\psi_0)<0$). On the other hand, for the solution curves turning to the left (when $b/\omega_0^2=0$ or $-1$), the solid line has $\cos(4\psi_0)=-1$ (and $g(A_{m0},\psi_0)>0$), while the dashed line has $\cos(4\psi_0)=1$ (and $g(A_{m0},\psi_0)<0$).

For large disturbances, stability of steady-state solutions can be analyzed based on Eqns (7.15-7.16). For example, for $\lambda=4$ and $c=0$, Eqns (7.15-7.16) can be combined as

$$\frac{dA_m}{d\psi} = \frac{f_1(A_m,\psi)}{f_2(A_m,\psi)} \quad (7.24)$$

where

$$f_1(A_m,\psi) = \frac{Q}{\omega}\frac{V_{ac}}{V_{dc}}\sin(4\psi)A_m^4 + 1.5\frac{Q}{\omega}\frac{V_{ac}}{V_{dc}}\sin(4\psi)A_m^6 \quad (7.25)$$

$$f_2(A_m,\psi) = [\frac{\omega}{2} - \frac{1}{2\omega} + 2(1+0.5\frac{V_{ac}^2}{V_{dc}^2})\frac{Q}{\omega}]A_m - \frac{3b}{8\omega_0^2\omega}A_m^3 + 3(1+0.5\frac{V_{ac}^2}{V_{dc}^2})\frac{Q}{\omega}A_m^3$$

$$+3.75(1+0.5\frac{V_{ac}^2}{V_{dc}^2})\frac{Q}{\omega}A_m^5 + \frac{Q}{\omega}\frac{V_{ac}}{V_{dc}}\cos(4\psi)A_m^3 + 2.25\frac{Q}{\omega}\frac{V_{ac}}{V_{dc}}\cos(4\psi)A_m^5 \quad (7.26)$$

179

The first integral of (7.24) is

$$[\frac{\omega}{4} - \frac{1}{4\omega} + (1 + 0.5\frac{V_{ac}^2}{V_{dc}^2})\frac{Q}{\omega}]A_m^2 - \frac{3b}{32\omega_0^2\omega}A_m^4 + 0.75(1 + 0.5\frac{V_{ac}^2}{V_{dc}^2})\frac{Q}{\omega}A_m^4$$

$$+ 0.625(1 + 0.5\frac{V_{ac}^2}{V_{dc}^2})\frac{Q}{\omega}A_m^6 + 0.25\frac{Q}{\omega}\frac{V_{ac}}{V_{dc}}\cos(4\psi)A_m^4 + 0.375\frac{Q}{\omega}\frac{V_{ac}}{V_{dc}}\cos(4\psi)A_m^6 = K \quad (7.27)$$

where $K$ is a constant of integration, depending on the amplitude and phase of the initial disturbance. For each value of $K$, Eqn (7.24) defines a trajectory in the $A_m$-$\psi$ phase plane. Similar to the stability analysis of steady-state solution described in [157], we use $A_m$ as the polar coordinate from the origin and $\phi(\equiv \lambda\psi)$ as the polar angle (because it is convenient to plot $A_m$ against $\phi$, instead of $A_m$ against $\psi$). The phase-plane diagram is shown in Fig.7.2 for the high-order subharmonic parametric resonance with $\lambda = 4$ when $Q = 1/100$, $V_{ac}/V_{dc} = 0.1$, $b/\omega_0^2 = 1$, $c = 0$, and $\Omega/\omega_0 = 4.0$. It is seen from Fig.7.2 that the amplitude $A_m$ is stable in all regions, however, the phase $\phi \equiv 4\psi$ is stable only in the shaded regions. The net change of $\phi$ in such shaded regions after one cycle is zero, while the net change is $2\pi$ in the unshaded regions. In addition, it is also found from Fig.7.2 that when the initial motion lies in the shaded regions, the steady-state solution related to $\cos(4\psi_0) = 1$ (or $4\psi_0 = 2n\pi$, where $n$ is an integer) is stable, while the steady-state solution related to $\cos(4\psi_0) = -1$ (or $4\psi_0 = 2n\pi + \pi$) is unstable.

In a similar way, we can obtain stable and unstable steady-state solutions for the high-order subharmonic parametric resonance with $\lambda = 6$ of a nonlinearly coupled oscillator, which are similar to Fig.7.1 for $\lambda = 4$ and omitted here. In the next section, we will focus on the high-order subharmonics with $\lambda = 4$ and 6 of a nonlinearly coupled array of three nonlinear oscillators.

# 7.4 High-order subharmonic parametric resonance of a nonlinearly coupled array of three nonlinear oscillators

In this section, we will consider a nonlinearly coupled array of three nonlinear

oscillators (thus $N$=3 and $X_0 = X_4$ =0, see Fig.6.1-2)). Our results (omitted here) showed that a coupled system of more than three oscillators (with $N$>3) exhibits essentially similar phenomena as the present system with $N$=3.


## 7.4.1 Steady-state solutions of high-order subharmonic parametric resonance

Since the method of slowly varying parameters is not convenient in solving the equations (7.5) for an array of three nonlinear oscillators, in this section, we will employ the harmonic balance method [155-156] and Newton iteration method to seek steady-state solutions of the form (7.6).

With the harmonic balance method, we substitute (7.6) into (7.5), in which the nonlinear coupling terms $\dfrac{1}{(1+x_{k+1}-x_k)^2}$ and $\dfrac{1}{(1+x_k-x_{k-1})^2}$ ($k$=1, 2 and 3) are expanded into a Taylor series up to the 5-th power (similar to Section 7.3, here, we still confine ourselves to the high-order subharmonic resonance with $\lambda = 4$ and $\lambda = 6$). Then, we multiply Eqn (7.5) by the functions of 1, $\cos(\dfrac{\Omega}{\lambda\omega_0}\tau)$, and $\sin(\dfrac{\Omega}{\lambda\omega_0}\tau)$ ($k$= 1, 2, 3), respectively, and integrate the resulting equations over [0, $2\pi$], in order to obtain 9 nonlinear equations. Finally, Newton iteration method is used to solve these nonlinear equations for 9 unknown coefficients $a_k$, $b_k$ and $c_k$ ($k$= 1, 2, 3). High-order subharmonic parametric resonance of a nonlinearly coupled oscillator array is defined by a non-zero stable steady-state periodic solution of the form (7.6) with $\lambda \geq 3$ (say, $\lambda$=4 or 6).

Fig.7.3 shows the high-order subharmonic parametric resonance with $\lambda = 4$ of three nonlinearly coupled oscillators when $Q$=1/100, $V_{ac}/V_{dc} = 0.1$, $b/\omega_0^2 = 1$, and $c$=0 (without damping), where $A_{m1} = \sqrt{b_1^2 + c_1^2}$, $A_{m2} = \sqrt{b_2^2 + c_2^2}$, and $A_{m3} = \sqrt{b_3^2 + c_3^2}$ are the amplitudes of the first, second, and third oscillators, respectively. In addition, it follows from Eqn (7.4) that three natural frequencies of this coupled oscillator array are $\omega_1/\omega_0$=0.9653, $\omega_2/\omega_0$=0.9798, and $\omega_3/\omega_0$=0.9941, and the coordinate of point $C_1$,

$C_2$ or $C_3$ in Fig.7.3 is $4\omega_1/\omega_0 = 3.8612$, $4\omega_2/\omega_0 = 3.9192$, or $4\omega_3/\omega_0 = 3.9764$, respectively. It is seen from Fig.7.3 that there are three resonance domains with the excitation frequencies close to $4\omega_1$, $4\omega_2$ and $4\omega_3$. In each resonance domain, both the stable and unstable solution curves intersect with the $x$-coordinate axis at point $A_1$ ($\Omega/\omega_0 = 3.8603$), $A_2$ ($\Omega/\omega_0 = 3.9188$), or $A_3$ ($\Omega/\omega_0 = 3.97636$), close to point $C_1$, $C_2$ or $C_3$, respectively (with the relative error in $x$-coordinate less than 0.02%). In particular, point $A_1$, $A_2$, or $A_3$ approaches point $C_1$, $C_2$ or $C_3$, respectively, when $V_{ac}/V_{dc}$ approaches zero.

It is seen from Fig.7.3 that near point $A_1$, $A_2$, or $A_3$, small-amplitude stable steady-state solutions with $\lambda = 4$ exist in the neighborhood of the equilibrium position $x_1 = 0$. Therefore, infinitesimal disturbances can lead to dynamic instability of the equilibrium position and the high-order subharmonics with $\lambda = 4$ when the ac frequency is close to point $A_1$ at which $\Omega/\omega_0 = 3.8603$, $A_2$ at which $\Omega/\omega_0 = 3.9188$, or $A_3$ at which $\Omega/\omega_0 = 3.97636$.

In the following Sections 7.4.2-7.4.5, we will study the respective effects of the parameters such as the loading parameter $Q$, the ac voltage $V_{ac}$, the damping coefficient $c$, and the nonlinear elasticity coefficient $b$, on high-order subharmonic parametric resonance. Our results show that the effects of these parameters on the high-order subharmonic parametric resonance in the first, second or third resonance domain are essentially similar to each other. Thus in Figs 7.4-7.8, we will mainly focus on the high-order subharmonics in the first resonance domain only, and those in the second and third resonance domains are omitted.

## 7.4.2 Effects of the loading parameter $Q$

Firstly, let us consider the effects of the loading parameter $Q$, which is defined as $\dfrac{\varepsilon_0 S V_{dc}^2}{2d_0^3 q}$ (see Section 7.2) and depends on the dc voltage $V_{dc}$ and the initial gap $d_0$.

Fig.7.4 shows the high-order subharmonic parametric resonance with $\lambda = 4$ in the first

resonance domain for some specific values of $Q$ when $V_{ac}/V_{dc} = 0.1$, $b/\omega_0^2 = 1$, and

$c$=0 (without damping). It is found that when $Q$ is small as $1/10^6$, the two solution curves turn towards the right, while the two solution curves turn towards the left when $Q$ increases to be 1/20. When $Q$=1/100, the two solution curves turn towards the right, however, compared to the two solution curves with $Q = 1/10^6$, they become steeper with bigger slopes. This phenomenon for high-order subharmonics with varying loading parameter $Q$ is qualitatively similar to that for the low-order subharmonics with $\lambda = 2$ of a nonlinearly coupled oscillator array [110-111]. As shown in figure 7 of [110], when $V_{dc}$ is small as 5$V$, both stable and unstable solution curves turn towards the right. As shown in figure 9 of [110], When $V_{dc}$ increases to be 40$V$, the two solution curves turn towards the left. The experimental results in [111] also confirm this phenomenon. For example, when the applied voltage is 7.6$V$, the stable solution curve turns towards the right, as shown in figure 33 of [111], while the stable solution curve turns towards the left when the voltage increases to be 33.0$V$, as shown in figure 35 of [111].

Here, let us examine the solution curves with a very small $Q$ (say, $Q = 1/10^6$). Since $Q$ is inversely proportional to $d_0^3$ and becomes small for large $d_0$, the case with a small $Q$ is associated with the comb-drive microbeam array with large initial gap $d_0$. Thus, the results in Fig.7.4 show that high-order subharmonic parametric resonance exists not only in the comb-drive arrays with a smaller gap (or bigger $Q$) as shown in Fig.6.1-1) [61-64, 66-70, 98-99, 101], but also in the arrays with a bigger gap (or smaller $Q$), such as those shown in [102-104, 134].

## 7.4.3 Effects of the ac voltage $V_{ac}$

Next, let us consider the effects of the ac voltage $V_{ac}$. Fig.7.5 shows the high-order subharmonic parametric resonance with $\lambda = 4$ in the first resonance domain for some specific values of $V_{ac}/V_{dc}$ when $Q$=1/100, $b/\omega_0^2 = 1$, and $c$=0 (without damping). It is found that the effects of increasing the ac voltage $V_{ac}$ are similar to those of increasing the loading parameter $Q$. For example, when $V_{ac}/V_{dc}$=0.1, the two solution curves turn

towards the right, while the two solution curves turn towards the left when $V_{ac}/V_{dc}$ increase to be 2. When $V_{ac}/V_{dc}$=0.5, the two solution curves lie between those with $V_{ac}/V_{dc}$=0.1 and those with $V_{ac}/V_{dc}$=2.

In addition, it is also seen from Fig.7.5 that with increasing $V_{ac}$, the distance between point $C$ ($4\omega_1/\omega_0$=3.8612, where $\omega_1$ is given by Eqn (7.4)) and the intersection point (at which the two solution curves meet the $x$-coordinate axis) will increase. In addition, the intersection point will approach point $C$ when $V_{ac}/V_{dc}$ approaches zero.

## 7.4.4 Effects of the linear damping coefficient $c$

Furthermore, let us consider the effect of the linear damping coefficient $c$. Fig.7.6 shows the high-order subharmonic parametric resonance with $\lambda = 4$ in the first resonance domain for some specific values of $\dfrac{c}{m\omega_0}$ when $Q$=1/100, $V_{ac}/V_{dc} = 0.1$, and $b/\omega_0^2$=1. With the damping effect, the amplitudes of all possible periodic solutions of high-order subharmonics are found to be bounded from below by a positive number. For example, the lowest amplitude $a_{lowest}$ is $0.0821\,d_0$, $0.1797\,d_0$ or $0.2519\,d_0$ when the viscous coefficient $\dfrac{c}{m\omega_0}$ is $1\times10^{-5}$, $5\times10^{-5}$ or $1\times10^{-4}$ respectively. Fig.7.7 shows the relationship between $a_{lowest}$ and $\dfrac{c}{m\omega_0}$ for some specific values of $b/\omega_0^2$ in the first resonance domain of high-order subharmonic parametric resonance with $\lambda = 4$ when $Q$=1/100 and $V_{ac}/V_{dc} = 0.1$. It is seen from Fig.7.7 that for any hard, linear, or soft oscillator with $b/\omega_0^2$=1, 0, or -1, $a_{lowest}$ increases with the increase of the damping coefficient. For example, for the soft oscillator with $b/\omega_0^2$=-1, the lowest amplitude $a_{lowest}$ is $0.0801\,d_0$ when the viscous coefficient $\dfrac{c}{m\omega_0}$ is $1\times10^{-5}$, while $a_{lowest}$ increases to $0.1755\,d_0$ or $0.2423\,d_0$ when the viscous coefficient increases to $5\times10^{-5}$ or $1\times10^{-4}$.

These results are consistent with the expected stabilizing effects of damping on parametric resonance. In fact, in the presence of the damping effect, it is expected that high-order subharmonic parametric resonance could occur only when the disturbances are large enough to bring the oscillator system to one steady state which is at a finite distance from the equilibrium position.

## 7.4.5 Effects of the nonlinear elasticity coefficient $b$

Finally, let us consider the effects of the nonlinear elasticity coefficient $b$. Fig.7.8 shows the high-order subharmonic parametric resonance with $\lambda = 4$ in the first resonance domain for some specific $b/\omega_0^2$ when $Q=1/100$, $V_{ac}/V_{dc} = 0.1$, and $c=0$ (without damping). It is seen from Fig.7.8 that the effect of decreasing the nonlinear elasticity coefficient $b$ is similar to that of increasing the loading parameter $Q$ or the ac voltage $V_{ac}$. For example, when $b/\omega_0^2=1$ (hard nonlinear oscillator), the two solution curves turn towards the right, while the two solution curves turn towards the left when $b/\omega_0^2 = -1$ (soft nonlinear oscillator). When $b/\omega_0^2=0$ (linear oscillator), the two solution curves lie between those with $b/\omega_0^2=1$ and those with $b/\omega_0^2=-1$. In addition, it is seen from Fig.7.8 (and Fig.7.1 for a single oscillator) that the location of intersection point (between the solution curves and the $x$-coordinate axis) is not affected by varying nonlinear elasticity coefficient $b$. However, the intersection point largely depends on the loading parameter $Q$ or the ac voltage $V_{ac}$, as shown in Figs 7.4-7.5.

As discussed in Section 7.4.4, the amplitudes of steady-state solutions with the damping effect are bounded from below by a positive number $a_{lowest}$. For varying coefficient $b/\omega_0^2$, it is found from Fig.7.7 that the lowest amplitude $a_{lowest}$ increases with the increase of $b/\omega_0^2$, when the damping coefficient is fixed. For example, with the damping coefficient $\dfrac{c}{m\omega_0} = 1\times10^{-4}$, as shown in Fig.7.7, $a_{lowest}$ is $0.2423\,d_0$ when $b/\omega_0^2=-1$, while $a_{lowest}$ increases to $0.2471\,d_0$ or $0.2519\,d_0$ when $b/\omega_0^2$ increases to 0 or 1. These results show that the positive nonlinear elasticity coefficient has a stabilizing effect on parametric resonance, while the negative one has an unstabilizing effect.

Thus, when the damping coefficient is reasonably low and the oscillators are reasonably soft, a small disturbance can cause high-order subharmonics of a nonlinearly coupled array of nonlinear oscillators. However, if the damping is sufficiently large or the oscillators are very hard, high-order subharmonics could occur only when the disturbances are large enough, to drive the oscillator system to a steady-state periodic state with the lowest amplitude $a_{lowest}$.

Our results shown in this chapter are consistent with some earlier works [157-158], which indicated that subharmonic parametric resonance of order $\lambda$ will exist while subharmonics of order higher than $\lambda$ will not exist if the periodically varying nonlinear term is a power of order ($\lambda$-1). In the present analysis, our numerical results confirm that if the fourth term on LHS of (7.5) is expanded only up to the 5-th power, subharmonic parametric resonance of order 6 will exist (see e.g. Fig.7.9), while subharmonic parametric resonance of order 7 will not exist. On the other hand, if the fourth term on LHS of (7.5) is expanded up to the 6 or 7-th power, subharmonic parametric resonance of order 7 or 8 will exist, while subharmonic parametric resonance of order 8 or 9 will not exist. Our present results show that the range of the excitation resonance frequencies of a micromechanical oscillator array could be expanded to $3\omega_0$, $4\omega_0$, ..., not bounded from above by $2\omega_0$ as predicted by the previous related works based on linearized coupling [102-105].

# 7.5 Conclusions

This chapter studies high-order subharmonic parametric resonance of an array of micromechanical nonlinear oscillators. We focus on the effects of nonlinear coupling between adjacent oscillators, and take into account the elastic nonlinearity of oscillators. It is found that high-order subharmonic parametric resonance is attributed to nonlinear coupling between adjacent oscillators, and its details depend on the dc and ac voltages, the nonlinear elasticity coefficient, and the linear damping coefficient. For example, with the damping effect, the amplitudes of all high-order subharmonic steady-state solutions are found to be bounded from below by a positive number, and the lowest amplitude increases as the nonlinear elasticity coefficient or the damping coefficient increases. The

present model suggests that the range of the excitation frequencies for parametric resonance of a nonlinearly coupled micromechanical nonlinear oscillator array could be expanded as compared to the range predicted by the previous models based on linearized coupling. It is believed that the results obtained here offer new and useful insights into the ongoing research on nonlinear dynamics of coupled microbeams or nanobeams in MEMS or NEMS.
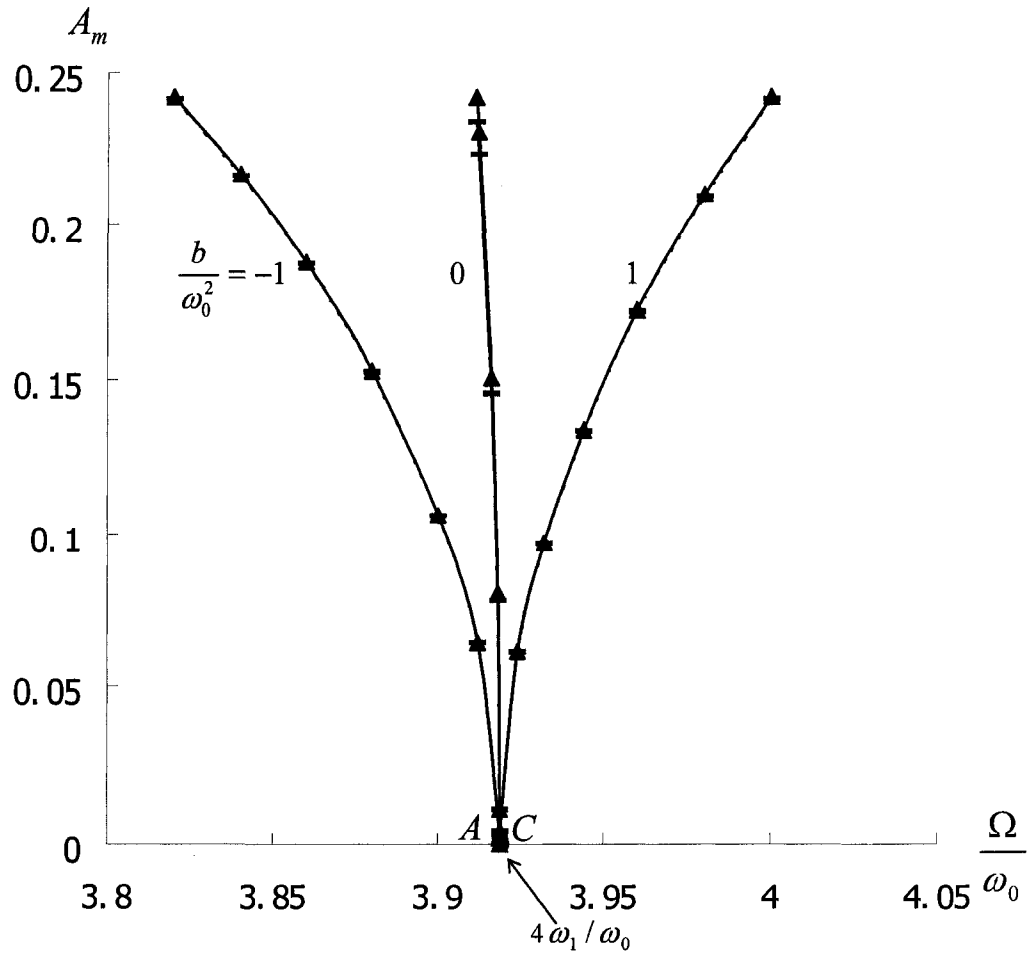
Fig.7.1 High-order subharmonic parametric resonance with $\lambda = 4$ of a nonlinearly coupled oscillator for some specific values of $b/\omega_0^2$ when $Q=1/100$, $V_{ac}/V_{dc} = 0.1$, and $c=0$ (without damping).

Fig.7.2 Phase-plane diagram for high-order subharmonic parametric resonance with $\lambda = 4$ of a nonlinearly coupled oscillator when $Q=1/100$, $V_{ac}/V_{dc} = 0.1$, $b/\omega_0^2 = 1$, $c=0$, and $\Omega/\omega_0 = 4.0$.

1) 1st resonance domain    2) 2nd resonance domain    3) 3rd resonance domain

Fig.7.3 High-order subharmonic parametric resonance with $\lambda = 4$ of three nonlinearly coupled oscillators when $Q$=1/100, $V_{ac}/V_{dc} = 0.1$, $b/\omega_0^2 = 1$, and $c$=0 (without damping).

$$A_{m1} + A_{m2} + A_{m3}$$
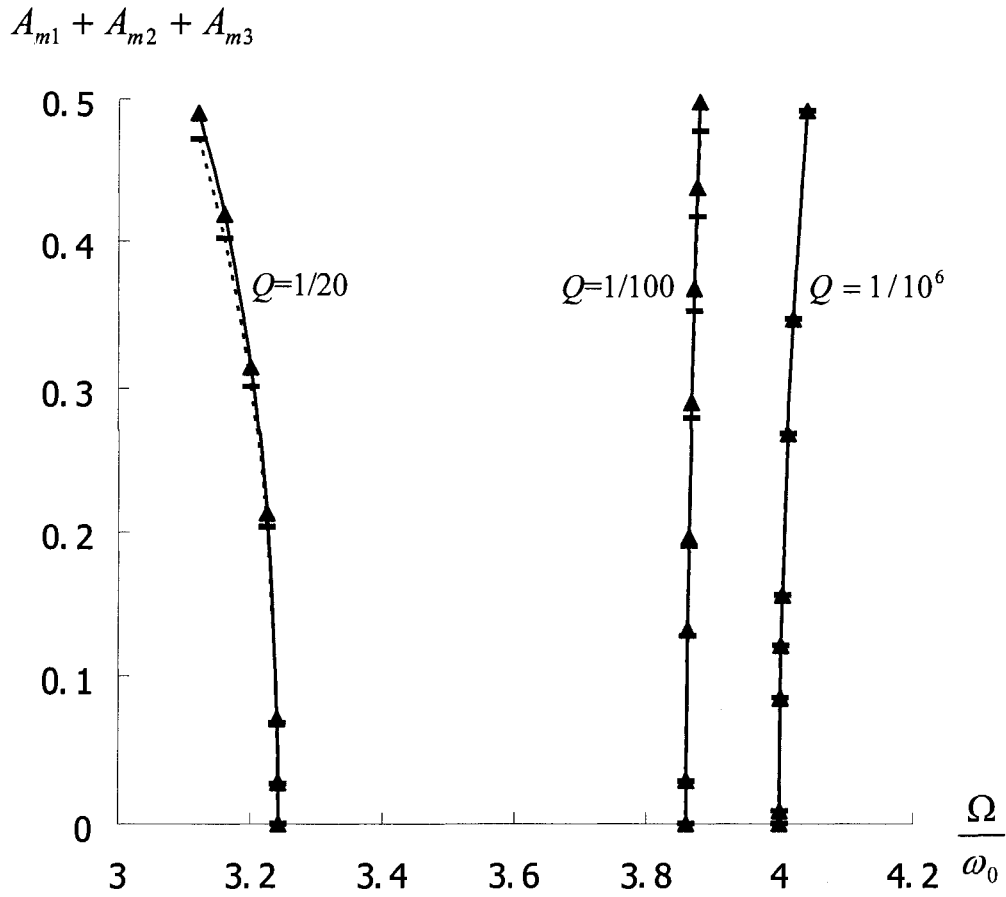


Fig.7.4 High-order subharmonic parametric resonance with $\lambda = 4$ in the first resonance domain for some specific values of $Q$ when $V_{ac}/V_{dc} = 0.1$, $b/\omega_0^2 = 1$, and $c=0$ (without damping).

191
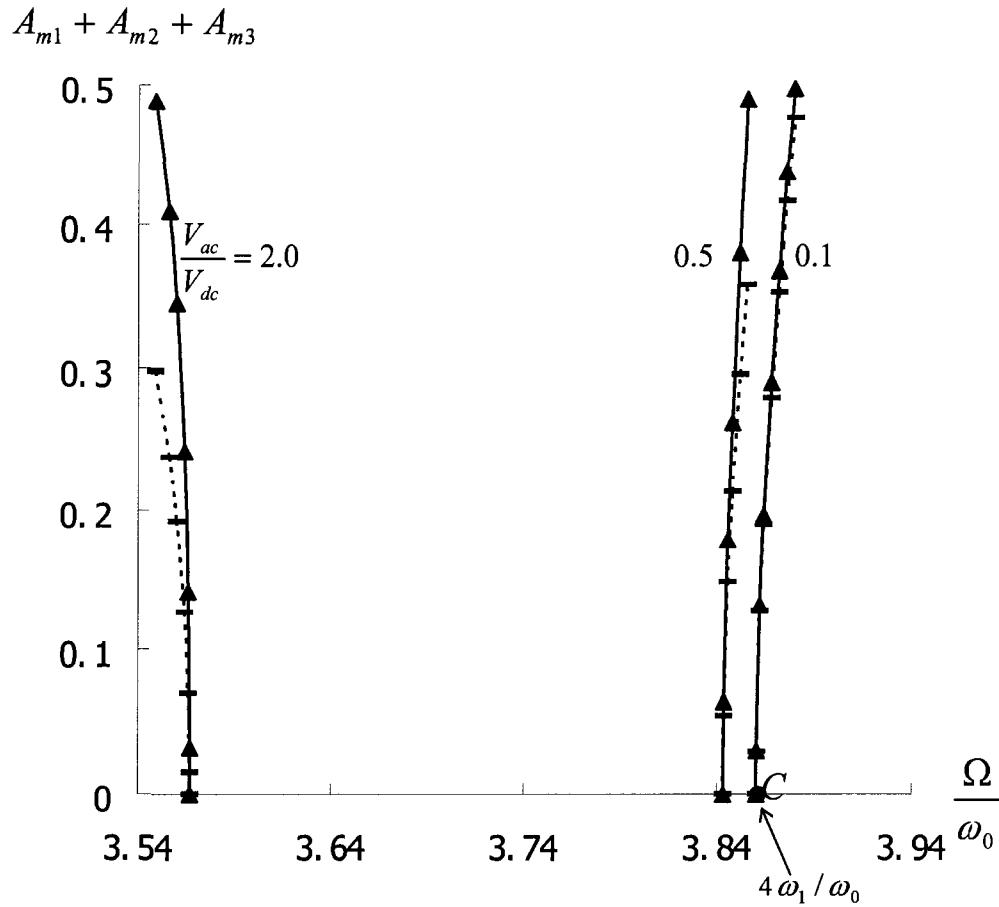
Fig.7.5 High-order subharmonic parametric resonance with $\lambda = 4$ in the first resonance domain for some specific values of $V_{ac}/V_{dc}$ when $Q=1/100$, $b/\omega_0^2 = 1$, and $c=0$ (without damping).
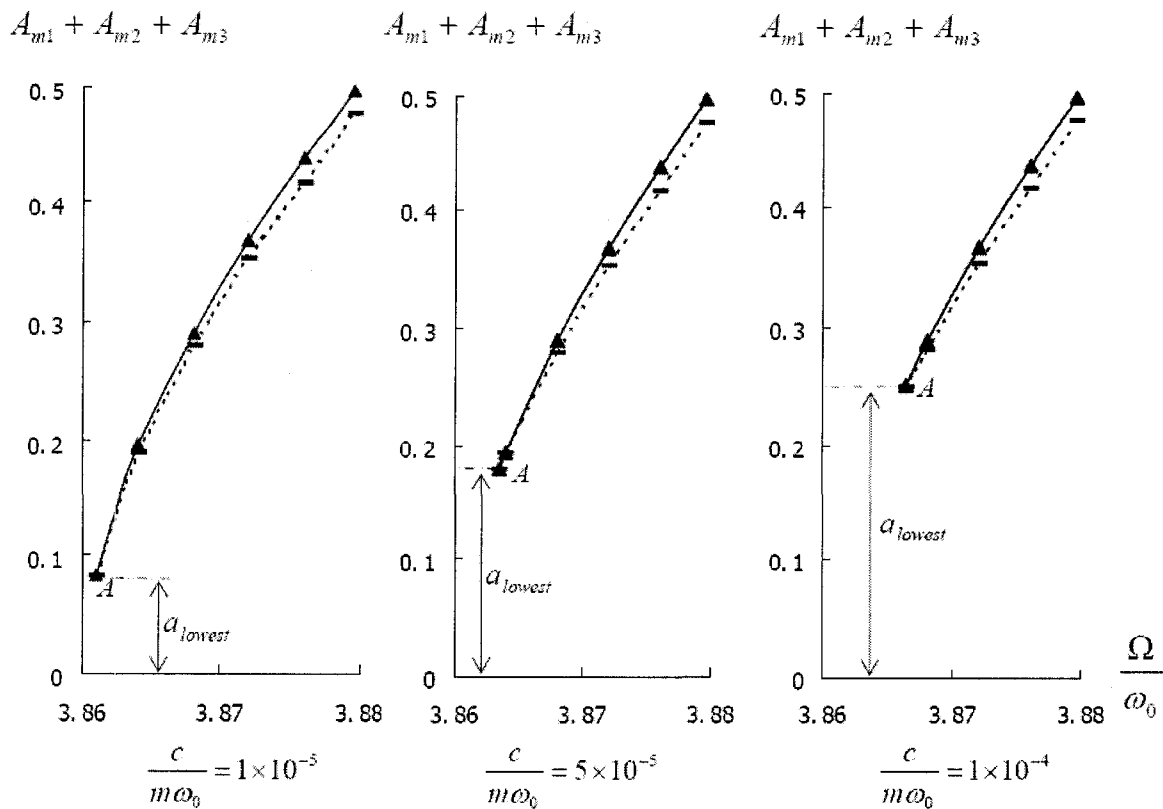
Fig.7.6 High-order subharmonic parametric resonance with $\lambda = 4$ in the first resonance domain for some specific values of $\dfrac{c}{m\omega_0}$ when $Q$=1/100, $V_{ac} / V_{dc} = 0.1$, and $b / \omega_0^2$=1.
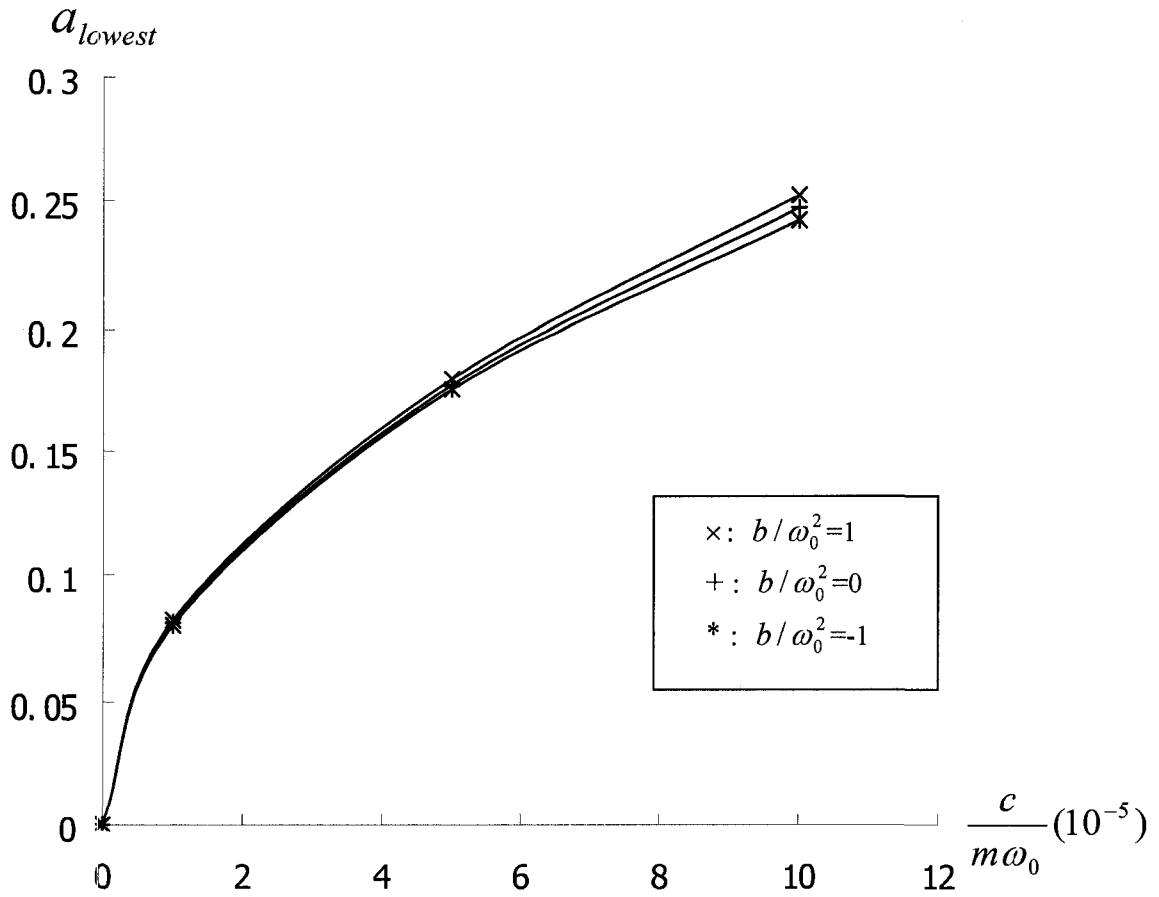
Fig. 7.7 Relationship between $a_{lowest}$ and $\dfrac{c}{m\omega_0}$ for some specific values of

$b/\omega_0^2$ in the first resonance domain of high-order subharmonic parametric

resonance with $\lambda = 4$ when $Q=1/100$ and $V_{ac}/V_{dc} = 0.1$.

Fig.7.8 High-order subharmonic parametric resonance with $\lambda = 4$ in the first resonance domain for some specific values of $b / \omega_0^2$ when $Q=1/100$, $V_{ac} / V_{dc} = 0.1$, and $c=0$ (without damping).
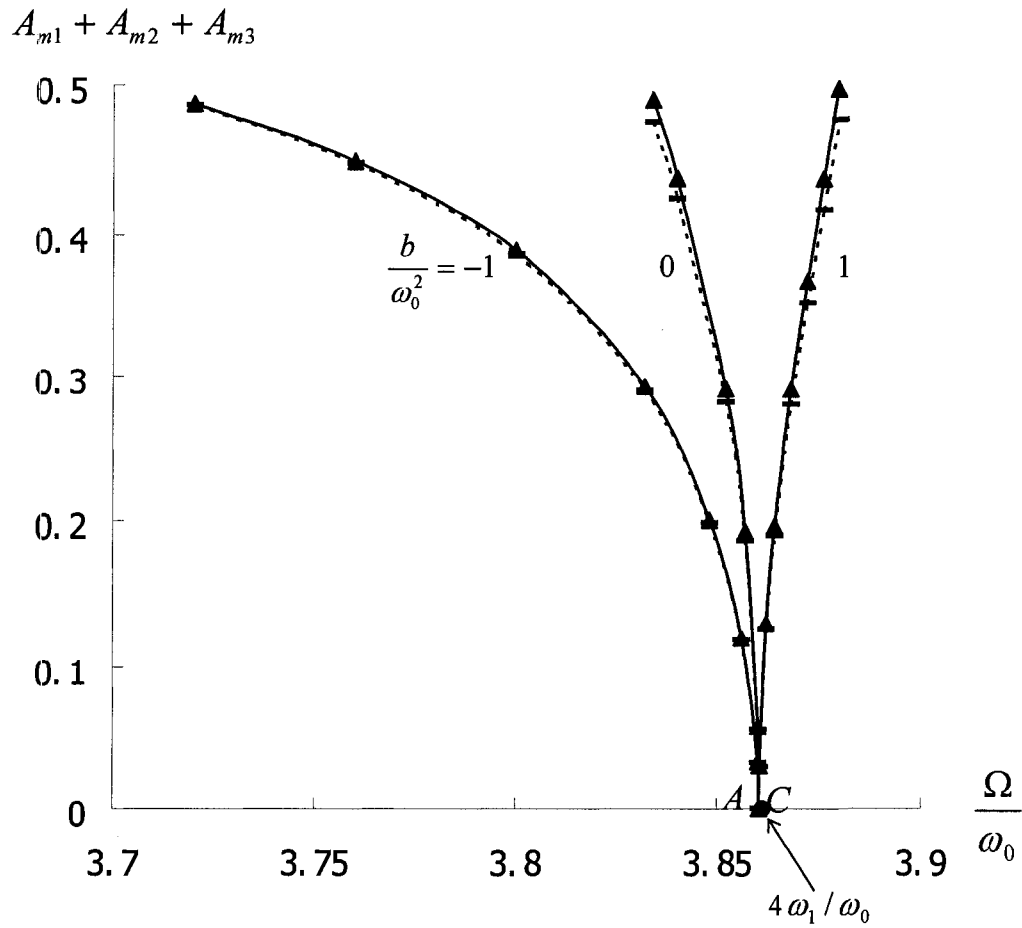
1) 1st resonance domain    2) 2nd resonance domain    3) 3rd resonance domain
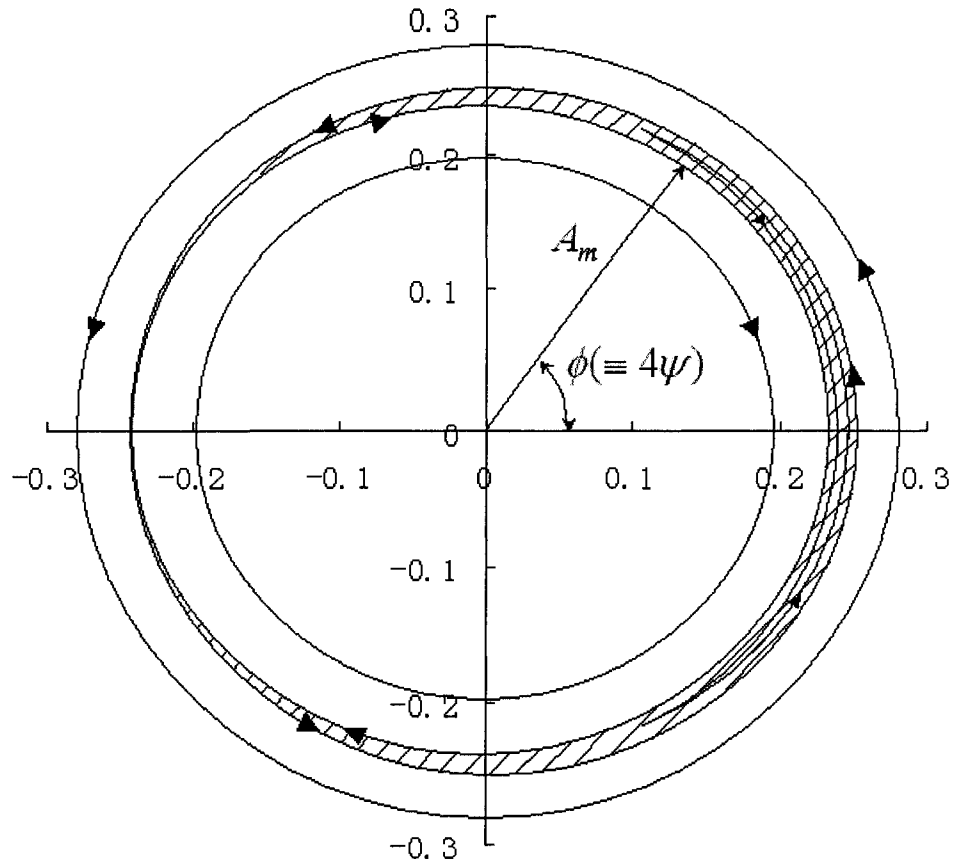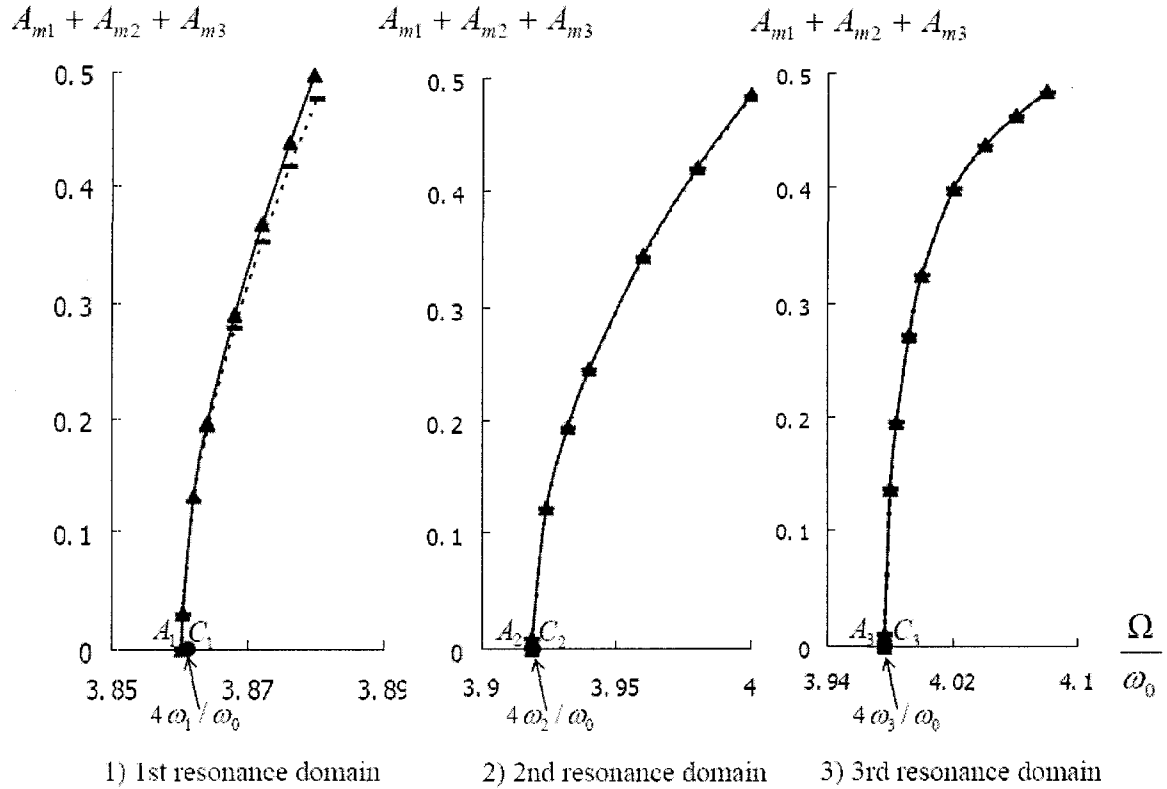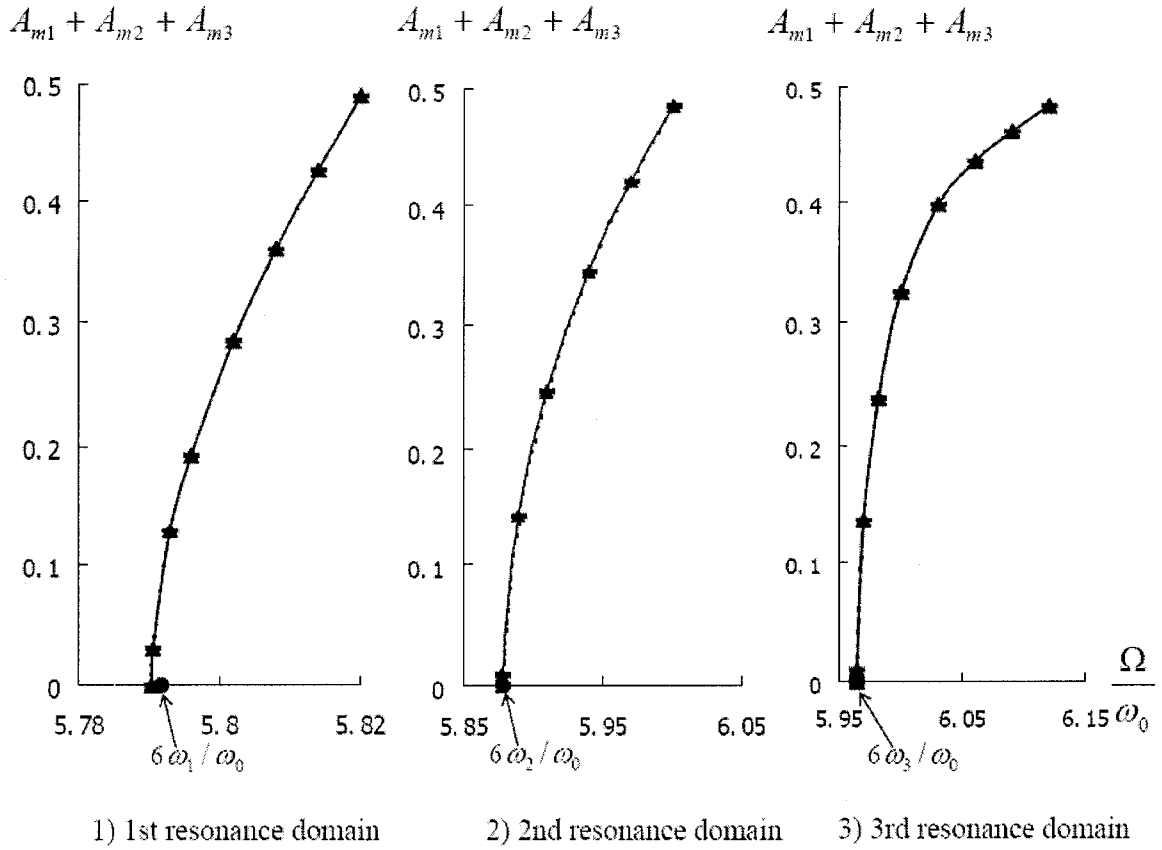
Fig.7.9 High-order subharmonic parametric resonance with $\lambda = 6$ of three nonlinearly coupled oscillators when $Q=1/100$, $V_{ac}/V_{dc} = 0.1$, $b/\omega_0^2 = 1$, and $c=0$ (without damping).

# Chapter 8

# Conclusions and Future Plans

## 8.1 Conclusions

In this thesis, we focus on some unexplored important mechanics issues in MEMS, such as adhesion, structural instability, and parametric resonance of mutually attracting microbeam arrays. First, an analytic model is developed by considering elastic strain energy and surface energy of microbeams to study adhesion of two adjacent opposing microcantilevers in comb drive structures. Then we analyze structural instability of mutually attracting microbeam arrays, with an emphasis on the end-effect of the end beams on instability of the microbeam arrays. Finally, we investigate parametric resonance of comb drive microbeam arrays based on a model of nonlinearly coupled oscillators, which confirms the existence of high-order subharmonic parametric resonance due to nonlinear coupling between adjacent oscillators.

The major conclusions of this thesis are summarized as follows.

### (1) Adhesion of two opposing microcantilevers

i) The critical values of surface energy for initial adhesion and full adhesion of two opposing microcantilevers increase monotonically with increasing overlap length. This is attributed to the fact that increasing overlap length leads to a decrease in the unattached suspended length of the cantilevers and then an increases in the release rate of the strain energy, which requires a higher surface energy for adhesion of the two cantilevers. Therefore, the strength of two opposing cantilevers against adhesion can be enhanced by

increasing (rather than decreasing) the overlap length.

ii) The adhesion of two beams of large overlap length occurs at higher surface energy and has larger maximum attached length, thus it can have a lower total energy than an attached state of two beams of small or moderate overlap length as the full adhesion is approached. In particular, the former can be energetically stable while the latter is usually only metastable before the full adhesion is reached.

iii) The critical values of surface energy for adhesion of two opposing microcantilevers are much lower than the critical values of surface energy for adhesion of a single microcantilever attracted by a rigid substrate which is popularly studied in the literature. This confirms that, compared to a single cantilever attracted by a rigid substrate under otherwise similar conditions, two opposing cantilevers not only request a much lower critical value of surface energy for adhesion, but also have an energetically more stable attached equilibrium state.

## (2) Structural instability of a parallel array of mutually attracting identical microbeams

i) The equilibrium deflections of the intermediate beams (except the two beams at the two ends) in the parallel array are negligible because two attractions from two neighboring beams are almost equal but opposite. Because the end beams are attracted by their adjacent beams from one side only, they have large non-zero deflections, which can cause a significant end-effect on structural instability of the parallel microbeam array.

ii) When the end-effect is neglected, the critical value of the beam-beam interaction coefficient for instability of the parallel array, defined based on initial separation between adjacent beams, is exactly a half of the critical value of the interaction coefficient for

instability of two mutually attracting beams, or equivalently a quarter of the critical value of the interaction coefficient for instability of a single beam attracted by a rigid body.

iii) The end-effect lowers the critical value about 20%-35% when the number of beams is sufficiently large, irrespective of the boundary conditions of beams.

iv) Structural instability of a large parallel array of mutually attracting identical microbeams can be analyzed by a substitution method, based on instability analysis of a small array of only a few microbeams at the ends of the original large array with its innermost microbeam fixed. This substitution method can predict the critical value for instability of the original large array of microbeams with reasonable relative errors (typically less than 5%), even when a small array of only 4 or 5 microbeams at the ends of the original large array are considered.

## (3) Structural instability of mutually attracting comb drive microcantilevers

i) When the end-effect is neglected, the critical value of the beam-beam interaction coefficient for instability of the array is exactly a half of the critical value for instability of two mutually attracting opposing cantilevers. This conclusion is valid for all combinations of the geometrical and material parameters of the microcantilevers.

ii) For comb drive microcantilevers with identical bending rigidities, the end-effect lowers the critical value about 25%-35% when the number of beams is sufficiently large, irrespective of the overlap length. The critical value for instability with (or without) the end-effect is a non-monotonic function of the overlap depth and attains its minimum when the overlap depth is close to half of the length of the microcantilevers.

iii) For comb drive microcantilevers with different bending rigidities, the end-effect lowers the critical interaction coefficient for instability by how much, and the reduction in the critical value for instability increases as bending rigidities of the end beams decrease when the lengths of the microcantilevers are given. This conclusion confirms that end design could have a significant influence on instability of comb drive microcantilevers.

iv) Structural instability of a large array of mutually attracting comb drive microcantilevers can be analyzed by a substitution method, based on instability analysis of a small array of only a few microcantilevers at the ends of the original large array with its innermost microcantilevers fixed. This substitution method can predict the critical value for instability of the original large array with reasonable relative errors (typically less than 5%), even when a small array of only 4 or 5 microcantilevers at the ends of the original large array are considered.

## (4) High-order subharmonic parametric resonance of nonlinearly coupled oscillators

i) The periodically varying nonlinear coupling does lead to the appearance of high-order subharmonic parametric resonance when the external excitation frequency is a multiple or nearly a multiple ($\geq 3$) of one of the natural frequencies of the oscillator system. This interesting new phenomenon does not appear in previous studies on linearly coupled micromechanical oscillators.

ii) High-order subharmonic response depends on the dc and ac voltages, the nonlinear elasticity coefficient, and the linear damping coefficient. For example, with the damping effect, the amplitudes of all high-order subharmonic steady-state solutions are found to be bounded from below by a positive number, and the lowest amplitude increases as the

nonlinear elasticity coefficient or the damping coefficient increases.

iii) In general, there are two conditions for the occurrence of high-order subharmonic parametric resonances with smaller disturbance. The first one is that the damping coefficient should be reasonably lower, and the second one is that the excitation frequency should be sufficiently close to a multiple ($\geq 3$) of one of the natural frequencies of the system. In the presence of a sufficiently large damping, high-order subharmonic parametric resonance could occur only when the disturbances are large enough, to offer sufficient energy to drive the oscillator system to one steady-state periodic state which is at a finite distance from the equilibrium position.

iv) Our results on high-order subharmonics suggest that the range of the excitation frequencies for parametric resonance of nonlinearly coupled oscillators can be much more expanded as compared to the range predicted by the previous models with linearized coupling. It is believed that the results obtained in this thesis offer new and useful insights into the ongoing research on nonlinear dynamics of coupled microbeams or nanobeams in MEMS or NEMS.

## 8.1 Future plans

Following this thesis, the future plans are as follows.

## (1) Parametric resonance of comb drive microbeam arrays based on elastic beam/cantilever models

In this thesis, we employ a simple model of nonlinearly coupled oscillators to analyze parametric resonance of comb drive microbeam arrays. Actually, similar oscillator models (with linear or nonlinear coupling) are widely used in recent studies to

201

simplify the analysis [102-112, 146-149]. All of these simplified models have assumed that each individual beam oscillates in its fundamental mode, and they can be treated as oscillators of one degree of freedom. However, compared to these simplified oscillator models, the elastic beam/cantilever model can provide more realistic and reliable results for comb drive microbeam arrays, although it also involves much more complicated analysis. At the next step I will try to use the elastic beam/cantilever model to analyze parametric resonance of comb drive microbeam arrays. All of these results will be compared to those based on the simplified oscillator model in our previous works [130-131] and the known related data reported in the literature [102-105, 108-112].

## (2) End-effect on parametric resonance of comb drive microbeam arrays

In the present studies, just like previous related works [102-105], we assume that the first and last oscillators in the oscillator array are fixed and stationary (see Fig.6.1-2)). Consequently, the end-effect of the end beams on parametric resonance of microbeam arrays has been neglected. However, in some practical problems, the end microbeams can be flexible, and then the end-effects can have a significant effect on static and dynamic behaviors of the large microbeam array. For example, our research results on pull-in instability of comb drive microcantilevers show that this end-effect can lower the critical value of interaction coefficient for instability by 25%-35% when the microcantilevers have the same lengths and bending rigidities [127]. How the end-effect affects parametric resonance of a large coupled microbeam array will be studied with both the simplified oscillator model and elastic beam model.

## (3) Nonlinear damping effects on parametric resonance of comb drive microbeam arrays

In this thesis, we consider the effects of a linear damping on parametric resonance, and discuss the condition for existence of high-order subharmonics with a linear damping coefficient. However, nonlinear damping is thought to play an important role in parametric resonance of coupled oscillators [102-105]. For example, Lifshitz and Cross took into account a cubic nonlinear damping (see Eqn (1.10)), and found that the amplitudes of steady-state solutions of parametric resonance are much affected by this nonlinear damping [104]. At the next step, I will investigate the effects of nonlinear damping on high-order subharmonic parametric resonance of nonlinearly coupled oscillators, and these results will be compared to our previous results with a linear damping [130-131] and the related results on low-order subharmonic parametric resonance [104].

## (4) Experimental work or finite element work to verify our mechanics models and analytic methods

Experiments or finite element work can be carried out to study adhesion, structural instability and parametric resonance of microbeam arrays. These results will be compared to our numerical results shown in this thesis to examine the accuracy of our mechanics models. Finally, our analytic methods can be adjusted and improved based on experimental observation or finite element analysis.

# References

[1] Quake SR, Scherer A, From micro- to nanofabrication with soft materials, Science 290: 1536-1540, 2000.

[2] Kleckner D, Marshall W, de Dood MJA, Dinyari KN, Pors BJ, Irvine WTM, Bouwmeester D, High finesse opto-mechanical cavity with a movable thirty-micron -size mirror, Physical Review Letters 96: 173901, 2006.

[3] Srinivasan S, Hiller J, Kabius B, Auciello O, Piezoelectric/ultrananocrystalline diamond heterostructures for high-performance multifunctional micro/nanoelectromechanical systems, Applied Physics Letters 90: 134101, 2007.

[4] Berggren KK, Bard A, Wilbur JL, Gillaspy JD, Helg AG, Mcclelland JJ, Rolston SL, Phillips WD, Prentiss M, Whitesides GM, Microlithography by using neutral metastable atoms and self-assembled monolayers, Science 269: 1255-1257, 1995.

[5] Kobayashi J, Mori Y, Okamoto K, Akiyama R, Ueno M, Kitamori T, Kobayashi S, A microfluidic device for conducting gas-liquid-solid hydrogenation reactions, Science 304: 1305-1308, 2004.

[6] Cumpston BH, Ananthavel SP, Barlow S, Dyer DL, Ehrlich JE, Erskine LL, Heikal AA, Kuebler SM, Lee IYS, McCord-Maughon D, Qin JQ, Rockel H, Rumi M, Wu XL, Marder SR, Perry JW, Two-photon polymerization initiators for three-dimensional optical data storage and microfabrication, Nature 398: 51-54, 1999.

[7] Ishigami N, Ago H, Motoyama Y, Takasaki M, Shinagawa M, Takahashi K, Ikuta T, Tsuji M, Microreactor utilizing a vertically-aligned carbon nanotube array grown inside the channels, Chemical Communications 16: 1626-1628, 2007.

[8] Jackman RJ, Brittain ST, Adams A, Prentiss MG, Whitesides GM, Design and fabrication of topologically complex, three-dimensional microstructures, Science 280: 2089-2091, 1998.

[9] Gao PX, Mai WJ, Wang ZL, Superelasticity and nanofracture mechanics of ZnO nanohelices, Nano Letters 6: 2536-2543, 2006.

[10] Boyce BL, Grazier JM, Buchheit TE, Shaw MJ, Strength distributions in

polycrystalline silicon MEMS, Journal of Microelectromechanical Systems 16:179-190, 2007

[11] Wolf B, Brischwein M, Baumann W, Ehret R, Kraus M, Monitoring of cellular signalling and metabolism with modular sensor-technique: The PhysioControl-Microsystem (PCM (R)), Biosensors & Bioelectronics 13:501-509, 1998.

[12] Dufour I, Heinrich SM, Josse F, Theoretical analysis of strong-axis bending mode vibrations for resonant microcantilever (bio)chemical sensors in gas or liquid phase, Journal of Microelectromechanical Systems 16: 44-49, 2007.

[13] Maluf N, An introduction to microelectromechanical systems engineering, Artech House, Boston, 1999.

[14] Elwenspoek M, Wiegerink R, Mechanical microsensors, Springer, Berlin, 2001.

[15] Feynman RP, There is plenty of room at the bottom, Journal of Microelectromechanical Systems 1: 60-66, 1992.

[16] Regis E, Nano: the emerging science of nanotechnology, Little Brown and Company, Boston, 1995.

[17] Senturia SD, Microsystem design, Kluwer Academic Publishers, Boston, 2001.

[18] Gardner JW, Microsensors, Wiley, Chichester UK, 1994.

[19] Lyshevski SE, MEMS and NEMS systems, devices, and structures, CRC Press, Boca Raton, 2002.

[20] Lyshevski SE, Micro- and nano-electromechanical systems: fundamental of micro- and nano- engineering, CRC Press, Boca Raton, 2000.

[21] Roukes ML, Nanoelectromechanical systems face the future, Physics World 14: 25-31, 2001.

[22] Campbell SA, The science and engineering of microelectronic fabrication. Oxford University Press, New York, 1996.

[23] Fairchild Corporation, Semiconductor & integrated circuit fabrication techniques. Reston, VA, 1979.

[24] Madou M, Fundamentals of microfabrication, CRC Press, New York,1997.

[25] Sze SM, Semiconductor devices: physics and technology, Wiley, New York, 1985.

[26] Kovacs GTA, Micromachined transducers sourcebook, WCB McGraw-Hill, New

York, 1998.

[27] Wolf S, Tauber RN, Silicon processing for the VLSI era, vol. 1: process technology, Lattice Press, Sunset Beach, CA, 2000.

[28] Kovacs GTA, Maluf NI, Petersen KE, Bulk micromachining of silicon, Proceedings of the IEEE 86: 1536-1551, 1998.

[29] Bustillo JM, Howe RT, Muller RS: Surface micromachining for microelectromechanical systems, Proceedings of the IEEE 86:1552-1574, 1998.

[30] Miller DC, Boyce BL, Dugger MT, Buchheit TE, Gall K, Characteristics of a commercially available silicon-on-insulator MEMS material, Sensors and Actuators A 138: 130-144, 2007.

[31] Ma RH, Ho MC, Lee CY, Wang YH, Fu LM, Micromachined silicon cantilever paddle for high-flow-rate sensing, Sensors and Materials 18: 405-417, 2006.

[32] Sharpe WN, Pulskamp J, Gianola DS, Eberl C, Polcawich RG, Thompson RJ, Strain measurements of silicon dioxide microspecimens by digital imaging processing, Experimental Mechanics 47: 649-658, 2007.

[33] Bhatt V, Chandra S, Silicon dioxide films by RF sputtering for microelectronic and MEMS applications, Journal of Micromechanics and Microengineering 17: 1066-1077, 2007.

[34] Cianci E, Coppa A, Foglietti V, Young's modulus and residual stress of DF PECVD silicon nitride for MEMS free-standing membranes, Microelectronic Engineering 84: 1296-1299, 2007.

[35] Griffith G, Haji-Saeed B, Sengupta SK, Goodhue WD, Khoury J, Woods CL, Kierstead J, Patterned multipixel membrane mirror MEMS optically addressed spatial light modulator with megahertz response, IEEE Photonics Technology Letters 19: 173-175, 2007.

[36] Reddy A, Kahn H, Heuer AH, A MEMS-based evaluation of the mechanical properties of metallic thin films, Journal of Microelectromechanical Systems 16: 650-658, 2007.

[37] Scharf TW, Prasad SV, Dugger MT, Kotula PG, Goeke RS, Grubbs RK, Growth, structure, and tribological behavior of atomic layer-deposited tungsten disulphide solid lubricant coatings with applications to MEMS , Acta Materialia 54: 4731-4743,

2006.

[38] Sayah A, Parashar VK, Gijs MAM, LF55GN photosensitive flexopolymer: A new material for ultrathick and high-aspect-ratio MEMS fabrication, Journal of Microelectromechanical Systems 16: 564-570, 2007.

[39] Modafe A, Ghalichechian N, Frey A, Lang JH, Ghodssi R, Microball-bearing-supported electrostatic micromachines with polymer dielectric films for electromechanical power conversion, Journal of Micromechanics and Microengineering 16: S182-S190, 2006.

[40] Ahn JH, Kim HS, Lee KJ, Jeon S, Kang SJ, Sun YG, Nuzzo RG, Rogers JA, Heterogeneous three-dimensional electronics by use of printed semiconductor nanomaterials, Science 314: 1754-1757, 2006.

[41] Panhorst DW, Lefevre V, Rider LK, Micro Electro-Mechanical Systems (MEMS), Inertial Measurements Unit (IMU) common guidance program, Ferroelectrics 342: 205+, 2006.

[42] Vogel D, Gollhardt A, Michel B, Micro- and nanomaterials characterization by image correlation methods, Sensors and Actuators A 99: 165-171, 2002.

[43] Brennan D, Alderman J, Sattler L, Walshe J, Huang J, O'Connor B, O'Mathuna C, Development of a micro-spectrometer system for process control application, Infrared Physics & Technology 43: 69-76, 2002.

[44] Polla DL, Erdman AG, Robbins WP, Markus DT, Diaz-Diaz J, Rizq R, Nam Y, Brickner HT, Wang A, Krulevitch P, Microdevices in medicine, Annual Review of Biomedical Engineering 2: 551-576, 2000.

[45] Kim B, Schmittdiel MC, Degertekin FL, Kurfess TR, Scanning grating microinterferometer for MEMS metrology, Journal of Manufacturing Science and Engineering – Transactions of the ASME 126: 807-812, 2004.

[46] Core TA, Tsang WK, Sherman SJ, Fabrication technology for an integrated surface-micromechined sensor, Solid State Technology 36: 39-47, 1993.

[47] Bishop D, Gammel P, Giles CR, The little machines that are making it big, Physics Today 54: 38-44, 2001.

[48] Van Kessel PF, Hornbeck LJ, Meier RE, Douglass MR, MEMS-based projection display, Proceedings of the IEEE 86: 1687-1704, 1998.

## REFERENCES

[49] Bassous E, Taub HH, Kuhn L, Ink jet printing nozzle arrays etched in silicon, Applied Physics Letters 31: 135-137, 1977.

[50] Young DJ, Micromachining for rf communications, MRS Bulletin 26: 331-332, 2001.

[51] Maboudian R, Howe RT, Critical review: adhesion in surface micromechanical structures, Journal of Vacuum Science & Technology B 15: 1-20, 1997.

[52] Komvopoulos K, Adhesion and friction forces in MEMS, Journal of Adhesion Science and Technology 17: 477-517, 2003.

[53] Mastrangelo CH, Adhesion-related failure mechanisms in micromechanical devices. Tribology Letters 3: 223-238, 1997.

[54] Krupp H, Particle adhesion, Advances in Colloid and Interface Science 1: 111-239, 1967.

[55] Bhushan B, Adhesion and stiction: mechanism, measurement techniques, and methods for reduction, Journal of Vacuum Science & Technology B 21: 2262-96, 2003.

[56] Zhou SA, On forces in microelectromechanical systems, International Journal of Engineering Science 41: 313-335, 2003.

[57] Zhao YP, Wang LS, Yu TX, Mechanics of adhesion in MEMS: a Review, Journal of Adhesion Science and Technology 17: 519-546, 2003.

[58] Bostrom M, Sernelius BE, Retardation-enhanced van der Waals force between thin metal films, Physical Review B 62: 7523-7526, 2000.

[59] Tas N, Sonnenberg T, Jansen H, Legtenberg R, Elwenspoek M, Stiction in surface micromachining, Journal of Micromechanics and Microengineering 6: 385-97, 1996.

[60] Israelachvili JN, Intermolecular and surface forces, Academic, London, 1992.

[61] Pelesko JA, Bernstein DH, Modeling MEMS and NEMS, Chapman & Hill/CRC, Boca Raton, 2003.

[62] Korvink JG, Paul O, MEMS: a practical guide to design, analysis and applications, William Andrew Publishing, NY, 2006.

[63] McMillan JA, High frequency mechanical resonant devices, Ph.D dissertation, Cornell University, NY, 1993.

[64] Chu LL, Gianchandani YB, A micromachined 2D positioner with electrothermal

actuation and sub-nanometer capacitive sensing, Journal of Micromechanics and Microengineering 13: 279-285, 2003.

[65] Bollee B, Electrostatic motors, Philips Technical Review 30: 178-194, 1969.

[66] Tang WC, Nguyen T, Howe RT, Laterally driven polysilicon resonant microstructures, Sensors and Actuators 20: 25-32, 1989.

[67] Tang WC, Nguyen T, Judy MW, Howe RT, Electrostatic comb drive of lateral polysilicon resonators, Sensors and Actuators 21: 328-331, 1990.

[68] Tang WC, Lim MG, Howe RT, Electrostatic comb drive levitation and control method, Journal of Microelectromechanical Systems 1: 170-178, 1992.

[69] Garcia EJ, Sniegowski JJ, Surface micromeachined microengine, Sensors and Actuators 48: 203-214, 1995.

[70] Sniegowski JJ, Garcia EJ, Surface-micromachined gear trains driven by an on-chip electrostatic microengine, IEEE Electron Device Letters 17: 366-368, 1996.

[71] Judy MW, Howe RT, Polysilicon hollow beam lateral resonators, Proceedings of the IEEE Micro-Electro-Mechanical Systems Workshop: 265-271, 1993.

[72] Lin L, Howe RT, Pisano AP, Microelectromechanical filters for signal processing, Journal of Microelectromechanical Systems 7: 286-294, 1998.

[73] Jaecklin VP, Linder C, de Rooij NF, Moret JM, Vuilleumier R, Optical microshutters and torsional micromirrors for light modulator arrays, Proceedings of the IEEE Micro-Electro-Mechanical Systems Workshop: 124-127, 1993.

[74] Kim CJ, Pisano AP, Muller RS, Overhung electrostatic micro gripper, Journal of Microelectromechanical Systems 1: 31-36, 1992.

[75] Loconto DP, Muller RS, High-sensitive micromechanical electrostatic voltmeter, Proceedings of the 7th International Conference on Solid-State Sensors and Actuators (Transducers): 878-881, 1993.

[76] Daneman MJ, Tien NC, Solgaard O, Pisano AP, Lau KY, Muller RS, Linear microvibromotor for positioning optical components, Journal of Microelectromechanical Systems 5: 159-165, 1996.

[77] Garcia EJ, Sniegowski JJ, Surface micromachined microengine as the driver for micromechanical gears, Proceedings of the 8th International Conference on Solid-State Sensors and Actuators (Transducers): 365-368, 1995.

## REFERENCES

[78] Alley RL, Cuan G.J, Howe RT, Komvopoulos K, The effect of release-etch processing on surface microstructure stiction, Proceedings of the IEEE Solid State Sensor and Actuator Workshop: 202–207, 1992.

[79] Wang RX, Shayganpur A, Sareskani S, Spelt JK, Analytical peel load prediction as a function of adhesive stress concentration, Journal of Adhesion 82: 39-61, 2006.

[80] Wang RX, Cui J, Sinclair AN, Spelt JK, Strength of adhesive joints with adherend yielding: I. Analytical model, Journal of Adhesion 79: 23-48, 2003

[81] Wang RX, Sinclair AN, Spelt JK, Strength of adhesive joints with adherend yielding: II. Peel experiments and failure criteria , Journal of Adhesion 79: 49-66, 2003.

[82] Mastrangelo CH, Hsu CH, Mechanical stability and adhesion of microstructures under capillary forces – part I: basic theory, Journal of Microelectromechanical Systems 2: 33-43, 1993.

[83] Mastrangelo CH, Hsu CH, Mechanical stability and adhesion of microstructures under capillary forces – part II: experiments, Journal of Microelectromechanical Systems 2: 44-55, 1993.

[84] Knapp JA, de Boer MP, Mechanics of microcantilever beams subject to combined electrostatic and adhesive forces, Journal of Microelectromechanical Systems 11: 754-764, 2002.

[85] Jones EE, Begley MR, Murphy KD, Adhesion of micro-cantilevers subjected to mechanical point loading: modelling and experiments, Journal of the Mechanics and Physics of Solids 51: 1601-1622, 2003.

[86] Johnstone RW, Parameswaran M, Theroretical limits on the freestanding length of cantilever produced by surface micromachining technology, Journal of Micomechanics and Microengineering 12: 855-861, 2002.

[87] Wu D, Fang N, Sun C, Zhang X, Adhesion force of polymeric three-dimensional microstructures fabricated by microstereolithography, Applied Physics Letters 81: 3963-3965, 2002.

[88] Spengen WM, Puers R, Wolf ID, A physical model to predict stiction in MEMS, Journal of Micomechanics and Microengineering 12: 702-713, 2002.

[89] Meng Q, Mehregany M, Mullen RL, Theroretical modeling of microfabricated beams with elastically restrained supports, Journal of Microelectromechanical

Systems 2: 128-137, 1993.

[90] Bhushan B (Editor), Springer handbook of nanotechnology, Springer, Berlin, 2004.

[91] Houston MR, Howe RT, Maboudian R, Effect of hydrogen termination on the work of adhesion between rough polycrystalline silicon surfaces, Journal of Applied Physics 81: 3474-3483, 1997.

[92] De Boer MP, Knapp JA, Michalske TA, Srinivasan U, Maboudian R, Adhesion hysteresis of silane coated microcantilevers, Acta Materialia 48: 4531-4541 2000.

[93] Yang FQ, Contact deformation of a micromechanical structure, Journal of Micomechanics and Microengineering 14: 263-268, 2004.

[94] Rogers JW, Mackin TJ, Phinney LM, A thermomechanical model for adhesion reduction of MEMS cantilevers, Journal of Microelectromechanical Systems 11: 512-520, 2002.

[95] Boer MP, Michalske TA, Accurate methods for determining adhesion of cantilever beams, Journal of Applied Physics 86: 817-827, 1999.

[96] Pamidighantam S, Puers R, Baert K, Tilmans HAC, Pull-in voltage analysis of electrostatically actuated beam structures with fixed-fixed and fixed-free end conditions, Journal of Micromechanics and Microengineering 12: 458-464, 2002.

[97] Chowdhury S, Ahmadi M, Miller WC, A closed-form model for the pull-in voltage of electrostatically actuated cantilever beams, Journal of Micomechanics and Microengineering 15: 756-763, 2005.

[98] Hirano T, Furuhata T, Gabriel KJ, Fujita H, Design, fabrication, and operation of submicron gap comb-drive microactuators, Journal of Microelectromechanical Systems 1: 52-59, 1992.

[99] Zhou GY, Dowd P, Tilted folded-beam suspension for extending the stable travel range of comb-drive actuators, Journal of Micomechanics and Microengineering 13: 178-183, 2003.

[100] Younis MI, Abdel-Rahman EM, Nayfeh A, A reduced-order model for electrically actuated microbeam-based MEMS, Journal of Microelectromechanical Systems 12: 672-680, 2003.

[101] Legtenberg R, Groeneveld AW, Elwenspoek M, Comb-drive actuators for large displacements, Journal of Micomechanics and Microengineering 6: 320-329, 1996.

REFERENCES

[102] Buks E, Roukes ML, Metastability and the Casimir effect in micromechanical systems, Europhysics Letters 54: 220-226, 2001.

[103] Buks E, Roukes ML, Electrically tunable collective response in a coupled micromechanical array, Journal of Microelectromechanical Systems 11: 802-807, 2002.

[104] Lifshitz R, Cross MC, Response of parametrically driven nonlinear coupled oscillators with application to micromechanical and nanomechanical resonator arrays, Physical Review B 67: 134302, 2003.

[105] Bromberg Y, Cross MC, Lifshitz R, Response of discrete nonlinear systems with many degrees of freedom, Physical Review E 73: 016214, 2006.

[106] Turner KL, Miller SA, Hartwell PG, MacDonald NC, Strogatz SH, Adams SG, Five parametric resonances in a microelectromechanical system, Nature 396: 149-152, 1998.

[107] Miller SA, Turner KL, MacDonald NC, Microelectromechanical scanning probe instruments for array architectures, Review of Scicentific Instruments 68: 4155-4162, 1997.

[108] Zhang WH, Baskaran R, Turner KL, Tuning the dynamic behavior of parametric resonance in a micromechanical oscillator, Appliced Physics Letters 82: 130-132, 2003.

[109] Zhang WH, Baskaran R, Turner KL, Effect of cubic nonlinearity on auto-parametrically amplified resonant MEMS mass sensor, Sensors and Actuators A 102: 139-150, 2002.

[110] Rhoads JF, Shaw SW, Turner KL, The nonlinear response of resonant microbeam systems with purely-parametric electrostatic actuation, Journal of Micromechanics and Microengineering 16: 890-899, 2006.

[111] Rhoads JF, Shaw SW, Turner KL, Moehlis J, DeMartini BE, Zhang WH, Generalized parametric resonance in electrostatically actuated microelectromechanical oscillators, Journal of Sound and Vibration 296: 797-829, 2006.

[112] Rhoads JF, Shaw SW, Turner KL, Baskaran R, Tunable microelectromechanical filters that exploit parametric resonance, Journal of Vibration and Acoustics-

Transaction of the ASME 127: 423-430, 2005.

[113] Shim SB, Imboden M, Mohanty P, Synchronized oscillation in coupled nanomechanical oscillators, Science 316: 95-99, 2007.

[114] Zhang WM, Meng G, Nonlinear dynamic analysis of electrostatically actuated resonant MEMS sensors under parametric excitation, IEEE Sensors Journal 7: 370-380, 2007.

[115] Requa MV, Turner KL, Electromechanically driven and sensed parametric resonance in silicon microcantilevers, Applied Physics Letters 88: 263508, 2006.

[116] De SK, Aluru NR, Complex nonlinear oscillations in electrostatically actuated microstructures, Journal of Microelectromechanical Systems 15: 355-369, 2006.

[117] Nayfeh AH, Younis MI, Dynamics of MEMS resonators under superharmonic and subharmonic excitations, Journal of Micromechanics and Microengineering 15: 1840-1847, 2005.

[118] Krylov S, Harari I, Cohen Y, Stabilization of electrostatically actuated microstructures using parametric excitation, Journal of Micromechanics and Microengineering 15: 1188-1204, 2005.

[119] Davis WO, O'Reilly OM, Pisano AP, On the nonlinear dynamics of tether suspensions for MEMS, Journal of Vibration and Acoustics- Transaction of the ASME 126: 326-331, 2004.

[120] Jensen BD, Mutlu S, Miller S, Kurabayashi K, Allen JJ, Shaped comb fingers for tailored electromechanical restoring force, Journal of Microelectromechanical Systems 12: 373-383, 2003.

[121] Kraus A, Erbe A, Blick RH, Corso G, Richter K, Parametric frequency tuning of phase-locked nanoelectromechanical resonators, Applied Physics Letters 79: 3521-3523, 2001.

[122] Turner K, Baskaran R, Zhang WH, Micro-scale sensors and filters utilizing non-linear dynamic response of single and coupled oscillators, Lecture Notes in Control and Information Sciences 289: 101-112, 2003.

[123] Mclachlan, NW, Theory and Application of Mathieu Functions, Dover, New York, 1964.

[124] Landau LD, Lifshitz, EM, Mechanics, Butterworth-Heinemann, Oxford, 1976.

[125] Zhu J, Ru CQ, Mioduchowski A, Surface energy-driven adhesion of two opposing microcantilevers, Acta Mechanica 184: 33-45, 2006.

[126] Zhu J, Ru CQ, Mioduchowski A, Structural instability of a parallel array of mutually attracting identical microbeams, Journal of Micromechanics and Microengineering 16: 2220-2229, 2006.

[127] Zhu J, Ru CQ, Mioduchowski A, Surface-forces-driven instability of comb-drive microcantilevers in MEMS, Journal of Adhesion Science and Technology 20: 1125-1146, 2006.

[128] Zhu J, Pull-in instability of two opposing microcantilever arrays with different bending rigidities, International Journal of Mechanical Sciences 50: 55-68, 2008.

[129] Zhu J, Ru CQ, Mioduchowski A, Instability of a large coupled microbeam array initialized at its two ends, Journal of Adhesion 83: 195-221, 2007.

[130] Zhu J, Ru CQ, Mioduchowski A, High-order subharmonic parametric resonance of nonlinearly coupled micromechanical oscillators, European Physical Journal B 58: 411-421, 2007.

[131] Zhu J, Ru CQ, Mioduchowski A, High-order subharmonic parametric resonance of a nonlinearly coupled array of micromechanical nonlinear oscillators, in preparation.

[132] Johnson KL, Kendall K, Roberts AD, Surface energy and the contact of elastic bodies, Proceedings of the Royal Society of London Series A 324: 301-313, 1971.

[133] Craighead HC, Nanoelectromechanical Systems, Science 290: 1532-1535, 2000.

[134] Ekinci KL, Roukes ML, Nanoelectromechanical Systems, Review of Scientific Instruments 76: 061101, 2005.

[135] Treacy MM, Ebbesen TW, Gibson JM, Exceptionally high Young's modulus observed for individual carbon nanotubes, Nature 381: 678-680, 1996.

[136] Wong EW, Sheehan PE, Lieber CM, Nanobeam mechanics: elasticity, strength, and toughness of nanorods and nanotubes, Science 277: 1971-1975, 1997.

[137] Poncharal P, Wang ZL, Ugarte D, de Heer WA, Electrostatic deflections and electromechanical resonances of carbon nanotubes, Science 283: 1513-1516, 1999.

[138] Dequesnes M, Rotkin SV, Aluru NR, Calculation of pull-in voltages for carbon-nanotube-based nanoelectromechanical switches, Nanotechnology 13:

120-131, 2002.

[139] Ru CQ, Elastic models for carbon nanotubes, In: Nalwa HS (Ed.), Encyclopedia of Nanoscience and Nanotechnology, American Scientific Publishers, Vol. 2: 731-744. 2004.

[140] Timoshenko SP, Theory of elastic stability, McGraw-Hill, New York, 1961.

[141] Chajes A, Principles of structural stability theory, Prentice-Hall, Englewood Cliffs, NJ, 1974.

[142] Grade JD, Jerman H, Kenny TW, Design of large deflection electrostatic actuators, Journal of Microelectromechanical Systems 12: 335-343, 2003.

[143] Osterberg PM, Senturia SD, M-TEST: A test chip for MEMS material property measurement using electrostatically actuated test structures, Journal of Microelectromechanical Systems 6: 107–118, 1997.

[144] Zhang LX, Zhao YP, Electromechanical model of RF MEMS switches, Microsystem Technologies 9: 420 – 426, 2003.

[145] Sounart TL, Michalske TA, Zavadil KR, Frequency-dependent electrostatic actuation in microfluidic MEMS, Journal of Microelectromechanical Systems 14: 125-133, 2005.

[146] Zalalutdinov M, Ilic B, Czaplewski D, Zehnder A, Craighead HG, Parpia JM, Frequency-tunable micromechanical oscillator, Applied Physics Letters 77: 3287-3289, 2000.

[147] Sato M, Hubbard BE, Sievers AJ, Ilic B, Czaplewski DA, Craighead HG, Observation of locked intrinsic localized vibrational modes in a micromechanical oscillator array, Physical Review Letters 90: 044102, 2003.

[148] Sato M, Hubbard BE, English LQ, Sievers AJ, Ilic B, Czaplewski DA, Craighead HG, Study of intrinsic localized vibrational modes in micromechanical oscillator arrays, Chaos 13: 702-715, 2003.

[149] Sato M, Hubbard BE, Sievers AJ, Colloquium: Nonlinear energy localization and its manipulation in micromechanical oscillator arrays, Reviews of Modern Physics 78: 137-157, 2006.

[150 Sato M, Hubbard BE, Sievers AJ, Ilic B, Craighead HG, Optical manipulation of intrinsic localized vibrational energy in cantilever arrays, Europhysics Letters 66:

318-323, 2004.

[151] Flach S, Willis CR, Discrete breathers, Physics Reports 295: 181-264, 1998.

[152] Bena I, Broeck CVD, Coupled parametric oscillators, Europhysics Letters 48: 498-504, 1999.

[153] Goldobin D, Pikovsky A, Collective modes in parametrically excited oscillator arrays, Europhysics Letters 59: 193-198, 2002.

[154] Bobryk RV, Chrzeszczyk A, Parametric resonance in coupled oscillators driven by colored noise, Europhysics Letters 68: 344-349, 2004.

[155] Nayfeh AH, Mook DT, Nonlinear Oscillation, Wiley, New York, 1979.

[156] Bobylev NA, Burman YM, Korovin SK, Approximate procedures in nonlinear oscillation theory, Walter de Gruyter, Berlin, 1994.

[157] Tso WK, Caughey TK, Parametric excitation of a nonlinear system, Journal of Applied Mechanics – Transactions of the ASME 32: 899-902, 1965.

[158] Mond M, Cederbaum G, Khan PB, Zarmi Y, Stability analysis of the nonlinear Mathieu equation, Journal of Sound and Vibration 167: 77-89, 1993.